MODELLING THE GEOMETRIC STRUCTURE OF THE MAGNETIC FIELD IN THE NIGHTSIDE MAGNETOSPHERE

A Thesis Submitted to the College of

Graduate Studies and Research

In Partial Fulfillment of the Requirements

For the Degree of Master of Science

In the Department of Physics and Engineering Physics

University of Saskatchewan

Saskatoon

By

SARAH NOEL TODERIAN

Permission to Use

In presenting this thesis in partial fulfillment of the requirements for the degree of Master of Science from the University of Saskatchewan, I agree that the Libraries from this University many make it freely available for inspection. I further agree that permission for copying of this thesis/dissertation in any manner, in whole or in part, for scholarly purposes may be granted by the professor or professors who supervised my thesis work or, in their absence, by the Head of the Department or the Dean of the College in which my thesis work was done. It is understood that any copying or publication or use of this thesis/dissertation or parts thereof for financial gain shall not be allowed without my written permission. It is also understood that due recognition shall be given to me and to the University of Saskatchewan in any scholarly use which many be made of any material in my thesis.

Requests for permission to copy or to make other uses of materials in this thesis in whole or part should be addressed to:

Head of the Department of Physics and Engineering Physics
University of Saskatchewan
Saskatoon, Saskatchewan S7N 5E2

OR

Dean
College of Graduate Studies and Research
University of Saskatchewan
107 Administration Place
Saskatoon, Saskatchewan S7N 5A2

Abstract

In this thesis, a simple model of the stretched magnetic field lines in the nightside magnetotail was created. The nightside magnetosphere model contains four main regions: plasmasphere, plasma sheet, magnetic lobes, and low latitude boundary layers. The plasma sheet is split into three regions based on the shape of the closed field lines present: dipole plasma sheet, transition plasma sheet, and stretched plasma sheet (SPS). The SPS, the focus of this thesis, is split into two regions: disruption zones (DZs) and a central neutral sheet (NS). The shape of the stretched field lines in the SPS determines the boundaries for the DZ and NS regions. The stretched field lines contain four inflection points. The convex curvature regions form the DZs and the central concave curvature region forms the NS. The NS is split into two regions: outer neutral sheet (ONS) and inner neutral sheet (INS). Due to the reversal of the x-component of the magnetic field at the center line of the NS, the protons are magnetized in the ONS and "unmagnetized" in the INS.

There are two main current systems in the SPS. The first is a double vortex current system consisting of eastward current in the DZs that closes westward in the NS. The second system is the NS field-aligned current (FAC) system. It is generated in the INS mainly by the earthward convective drift of the electrons while the "unmagnetized" protons have little convective drift and remain tailward of the electrons. This FAC system produces the pre-onset electron auroral arc during the growth phase of the substorm.

A simple model of the stretched magnetic field lines was created in order to calculate the current systems present in the SPS. The simple model was based entirely upon the shape of the stretched field lines. It passed two physical tests, divergence of the magnetic field and limits at infinity, so it was used to calculate currents. The total current using Ampere's law and the curvature current was found. Both results agreed with the double vortex current system.

Acknowledgements

First, I would like to acknowledge my supervisors Dr. George Sofko and Dr. Glenn Hussey. This thesis would not have been possible without the guidance and support they provided. In particular, I want to thank Dr. George Sofko for inspiring me with his enthusiasm and dedication to science.

Second, I would like to acknowledge my advisory committee Dr. Sasha Koustov and Dr. Tom Steele. I would like to thank Dr. Tom Steele for guiding me through the analysis presented in Chapter 5 and introducing me to Mathematica. I would also like to acknowledge the help of Associate Professor Colin Waters from the School of Mathematical and Physical Sciences at the University of Newcastle Australia who provided an alternate solution for my project at the SuperDARN 2013 Workshop after the analysis presented in Chapter 5 failed.

Third, I would like to acknowledge the SuperDARN community. Specifically, for Dr. Jean-Pierre St. Maurice and Dr. Pasha Ponomarenko for keeping me on my toes with their questions during group meetings. I would like to acknowledge Dr. Kathryn McWilliams for creating Figure 2.23 and allowing me to use it in my thesis. Also, I would like to thank Kevin Kreiger, Gareth Perry, Ashton Reimer, Grant Scoular, and Matthew Wessel for being there whenever I had a silly question, needed to bounce an idea off someone, or just needed to chat.

Finally, I would like to acknowledge my family and partner Cory. I want to thank my family for supporting me through this challenging time in my life and for “willingly” listening to my science rants. I want to also thank Cory for always being there for me and keeping me on track. I would not have been able to finish this thesis without him.

Table of Contents

List of Tables

List of Figures

List of Abbreviations

AM LLBL	Dawn Low Latitude Boundary Layer
DPS	Dipole Plasma Sheet
DTNL	Distant Tail Neutral Line
DZ	Disruption Zone
DZN	Disruption Zone North
DZS	Disruption Zone South
FAC	Field-Aligned Current
GSE	Geocentric Solar Ecliptic
GSM	Geocentric Solar Magnetospheric
IGRF	International Geomagnetic Reference Field
IMF	Interplanetary Magnetic Field
INS	Inner Neutral Sheet
LLBL	Low Latitude Boundary Layer
NS	Neutral Sheet
ONS	Outer Neutral Sheet
PM LLBL	Dusk Low Latitude Boundary Layer
PS	Plasma Sheet
PSBL	Plasma Sheet Boundary Layer
SPS	Stretched Plasma Sheet
TPS	Transition Plasma Sheet
VNENL	Very Near Earth Neutral Line

Chapter 1

Introduction

The Earth's magnetic field is commonly assumed for simplicity to be a dipole magnetic field. However, numerical models such as the International Geomagnetic Reference Field (IGRF) that are based upon satellite and land measurements clearly show that the Earth's magnetic field is not simply dipolar. The IGRF uses time dependent Gauss coefficients and Schmidt semi-normalized associated Legendre functions to describe the Earth's magnetic field (Finlay et al., 2010). The IGRF needs to be updated every five years in order to account for the slight changes over time. The eleventh generation of the IGRF has coefficients that are dependent on the maximum spherical harmonic degree of 13 (Finlay et al., 2010). The dipole terms in the IGRF could dominate at specific areas, but other higher order terms are needed in order to describe the Earth's magnetic field accurately. For the purposes of this thesis, the near-Earth portion of the magnetic field will be assumed to be dipolar.

The magnetosphere consists of the extension of Earth's magnetic field above the Earth with its low-altitude base being the ionosphere. The shape of the magnetosphere is determined largely by its interaction with the interplanetary magnetic field (IMF) that originates from the sun. A common picture of the magnetosphere is shown in Figure 1.1. The typical axis system consists of the positive x-axis pointing towards the sun, the positive y-axis pointing duskward, and the positive z-axis pointing northward. The IMF is carried by the solar wind, which is traveling radially outward from the sun. The solar wind and IMF collide with the Earth's field to produce a shock front called the bow shock. It is depicted in Figure 1.2. The shocked solar wind that flows around the magnetosphere makes up a region called the magnetosheath. The boundary between the magnetosphere and the magnetosheath is called the magnetopause. In simplistic terms, the magnetopause is recognized as a boundary between a vacuum magnetic

field (magnetosphere) and plasma (magnetosheath) (Kivelson and Russell, page 228). The bow shock, magnetosheath, and magnetopause comprise the major elements that surround the magnetosphere.

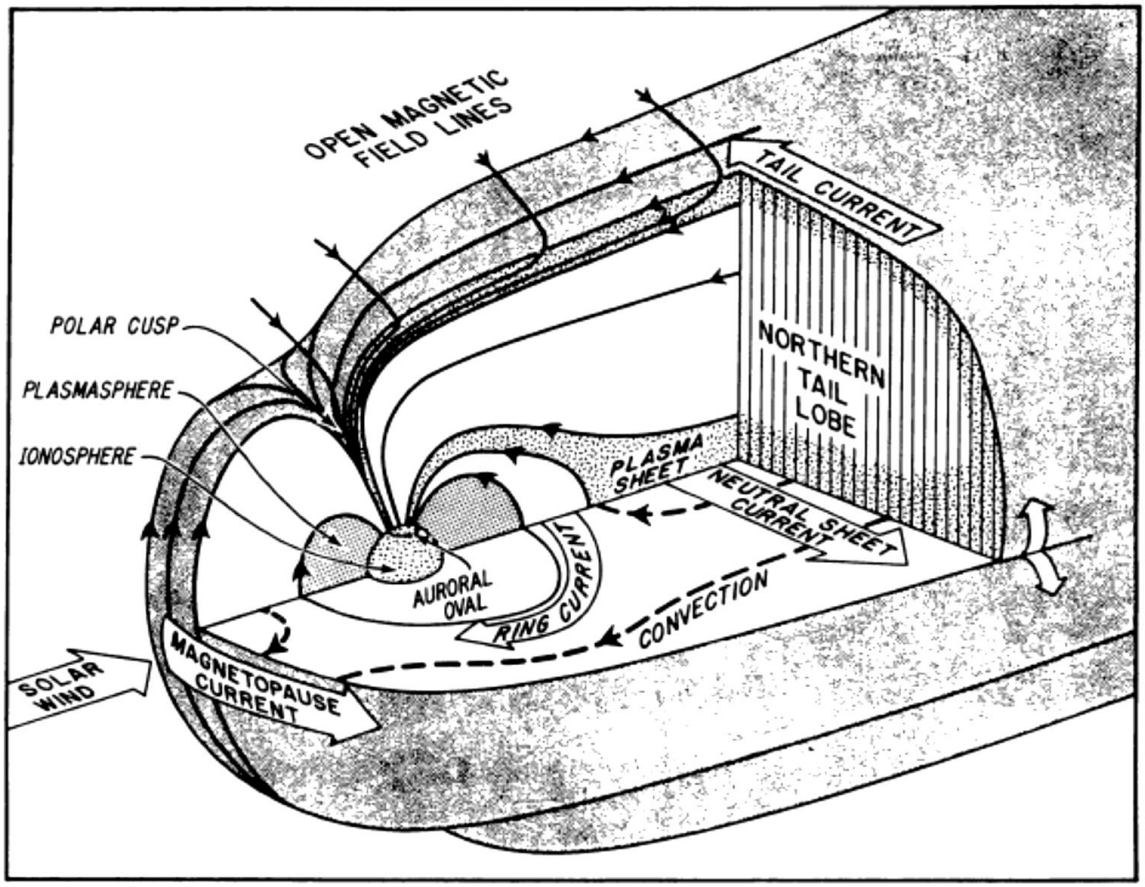

Figure 1.1 Earth's magnetosphere with various currents (magnetopause current, ring current, neutral sheet current, and tail current) and plasma regions (plasmasphere, plasma sheet, lobe, and ionosphere) outlined (Lopez and Baker, 1994).

The interaction of the solar wind and IMF with the Earth's magnetic field causes it to change its shape. The magnetic field lines are compressed in on the dayside of the Earth and are elongated on the nightside of the Earth. The magnetosphere is split into different regions depending on the type of field line present. Some of the basic regions of the magnetosphere are shown in Figure 1.1, Figure 1.2, and Figure 1.3. These regions include the north and south lobes, plasmasphere, and plasma sheet. The north and south lobes contain "open" field lines; the plasmasphere contains dipole field lines; and the plasma sheet contains closed field lines that

vary from slightly stretched dipole shape to a higher stretched shape. These regions are discussed in more detail in the following paragraphs. Another region that is not depicted in the figures presented here is called the low latitude boundary layer (LLBL). The LLBL is a boundary between the magnetopause and the magnetosphere in low latitude regions. It is only a few thousand kilometers thick and is recognized by plasma flow that is very similar to that in the magnetosheath but with a reduced particle density and velocity (Hones et al., 1972).

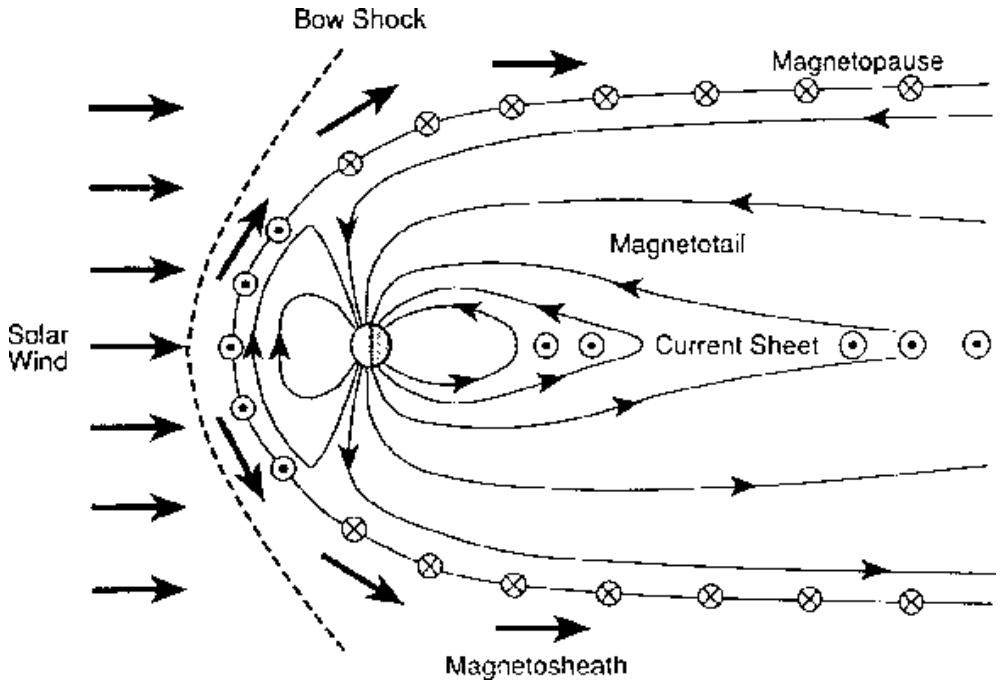

Figure 1.2 Cross-section view of the magnetosphere (Kivelson and Russell, page 229) highlighting the solar wind, bow shock, magnetopause, and magnetosheath.

The magnetic lobes are regions of the magnetosphere that contain "open" field lines. These field lines are called "open" because they are connected to both the Earth and the IMF. They are created by dayside reconnection through the IMF interacting with the Earth's magnetic field. The IMF flows anti-sunward, so it carries the lobe field lines from the dayside to the nightside of the magnetosphere. The shape of these field lines is highly influenced by the IMF. On the nightside, the open field lines will be very long and almost parallel to the x-y or equatorial plane. If they are pressed together, the north and south lobe field lines in the magnetotail will undergo nightside reconnection, which creates closed stretched field lines. This process will be discussed in more detail in Section 2.3.2.

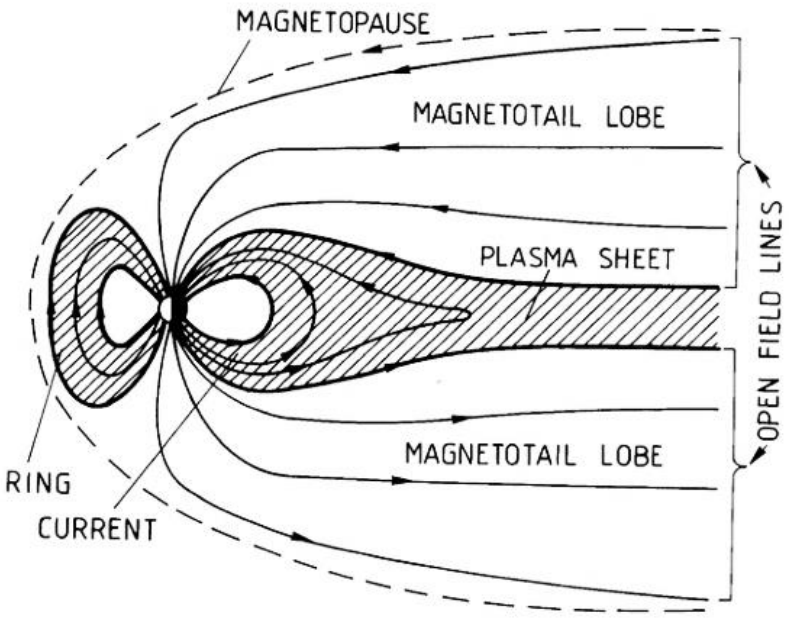

Figure 1.3 Cross-section view of magnetosphere (Vasyliunas, 1981) highlights the lobes and plasma sheet.

The plasmasphere consists of the area of magnetosphere that immediately surrounds the Earth. Initially, the plasmasphere was thought to be a region of pure dipole field lines that corotates with the Earth (Carpenter, 1966). However, recent studies show that the plasmasphere is subcorotational with a rotational speed approximately 88% to 95% of the Earth's rotational speed (Galvan et al., 2010). The boundary between the plasmasphere and the rest of the magnetosphere is called the plasmapause. The plasmapause is the mean location of a sharp drop in plasma density. The plasmapause location is influenced by solar activity. During quiet times, the plasmapause location is farther away from the Earth, around six to seven Earth radii (Carpenter, 1966). During more active times, the plasmapause location is closer to the Earth (Kivelson and Russell, page 299). The plasmapause location for moderate, steady solar activity is represented in Figure 1.4 as the solid black line. The location of the plasmapause is based on experimental measurements of whistlers (Carpenter, 1966). As is seen in Figure 1.4, the plasmapause location is not uniform in all sectors of time. The whistler measurements show that there is a bulge in the plasmasphere in the dusk sector. Also, the plasmapause location ranges from around three to five Earth radii (R_E) in the magnetotail.

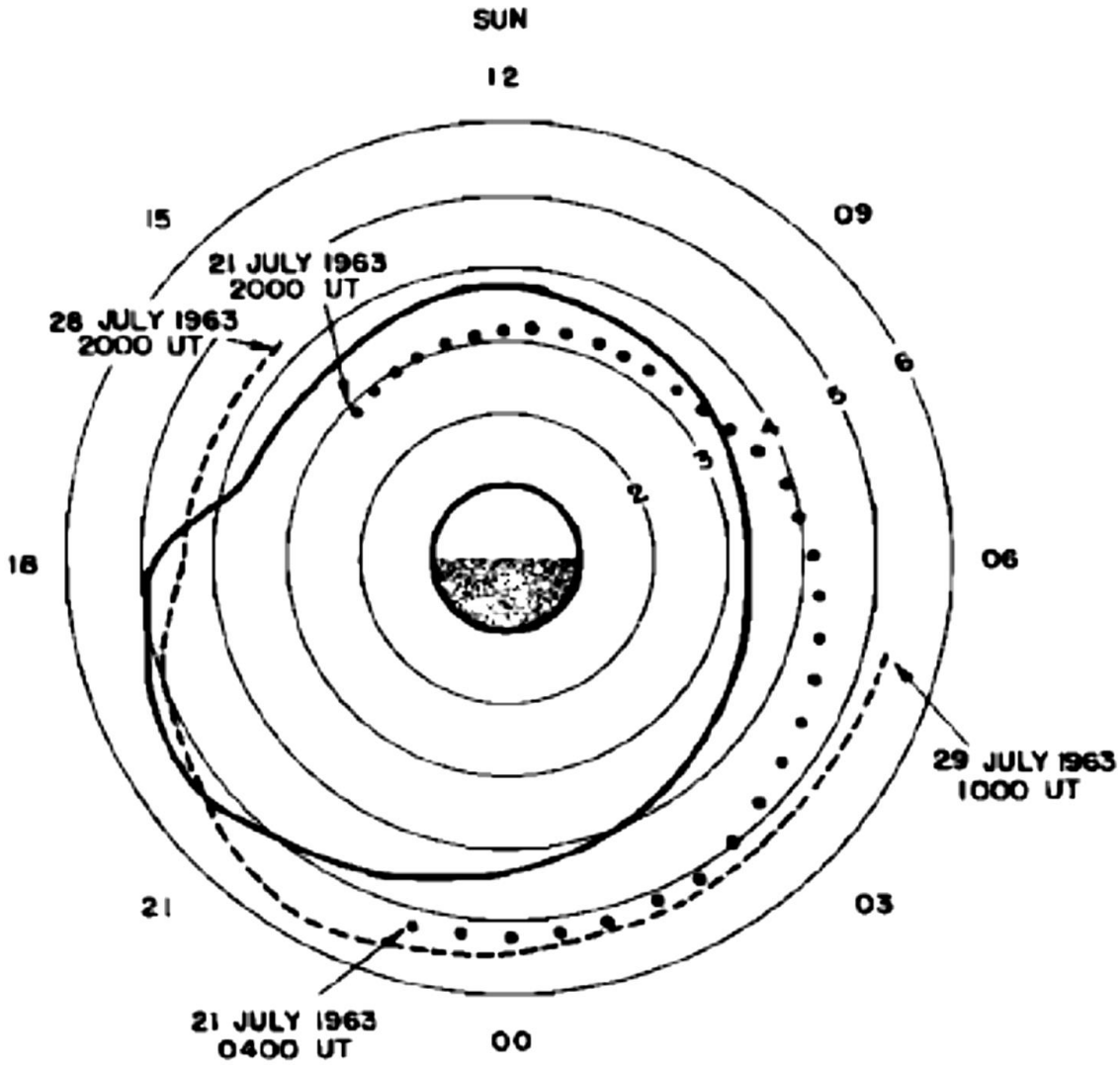

Figure 1.4 Plasmapause location in the equatorial plane based on whistler measurements for moderate, steady solar conditions (Carpenter, 1966).

The plasma sheet (PS) is the area in the magnetotail that contains plasma on closed magnetic field lines, which can range in shape from almost dipolar to the elongated, stretched shape seen in Figure 1.2 and Figure 1.3. The boundary between the PS and the north and south lobes is called the plasma sheet boundary layer (PSBL). In the center of the PS, there is a region called the neutral sheet (NS). The NS contains a current sheet in order to be consistent with the stretched magnetic field lines present in the PS. Above the NS, the magnetic field is directed earthward; below the NS, the magnetic field is directed anti-earthward.

There are multiple current systems occurring in the magnetosphere. Some of these are shown in Figure 1.5. They consist of the magnetopause or Chapman-Ferraro current, the cross tail current, and the ring current. The magnetopause current is a dayside eastward boundary current flowing on the magnetopause between the magnetosheath and the magnetosphere. The crosstail current is a westward current that crosses the tail from dawn to dusk and then closes along the magnetopause. The ring current flows westward around the Earth, roughly centered on the equatorial plane. The ring current is associated with magnetic storms and substorms and produces a depression of the northward magnetic field at the equator of the Earth. During substorms, other currents can arise including a partial ring current, which is located in the nightside portion of the ring current, and field-aligned or Birkeland currents, which are currents that flow along magnetic field lines and connect regions of the magnetosphere to the ionosphere.

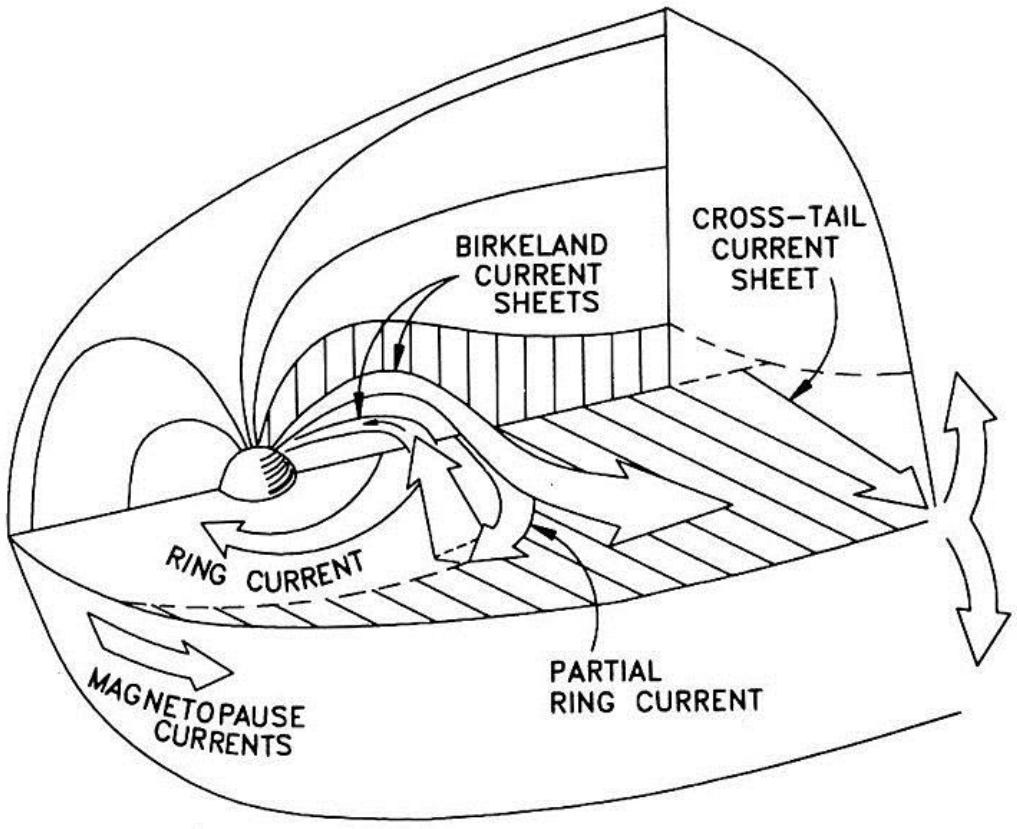

Figure 1.5 Three dimensional view of the magnetosphere with magnetopause current, crosstail current, ring and partial ring current, and the Birkeland currents labelled.

In the past, many models of the magnetosphere have been developed. Ness (1969) completed a thorough review of all the past experimental and theoretical models that specifically look at the magnetotail. In this era, the magnetotail was known to exist and was recognized as a stretched region of magnetic field behind the Earth. Also, a plasmasheet was thought to be embedded between the regions of opposite magnetic field. The tail was known to play an important role during substorms, but the exact role was not known. Also, how the stretched field lines were formed was heavily debated. Models of the magnetotail were mainly theoretical models since there was not much satellite data collected from the magnetotail at this time. Ness (1969) recognized many outstanding problems with the understanding of the magnetotail that he believed could only be answered by further analysis of satellite data when it became available.

Roederer (1969) also completed a review of magnetospheric models. In his review, he focused on models that were valid in the region between 4 and 15 Earth radii away from the Earth. As previously stated, models at that point in time were based mainly upon theory rather than satellite data. Models were created by assuming the total field to be the sum of an internal magnetic field, typically the dipole field from the Earth, and an external magnetic field. The external magnetic field was the sum of the IMF carried by the solar wind and the field sources in the magnetosphere such as the magnetopause current and the cross tail current. Two computational methods used for the external fields are boundary surface and image dipole models. The boundary surface models involved using an expansion in spherical harmonics to find the surface currents on the magnetopause due to a solar wind perpendicular to the Earth's dipole field (Roederer, 1969). The current in the NS was simulated by adding an infinitely thin current sheet in the equatorial plane in the magnetotail (Roederer, 1969). The boundary surface models were first presented in papers by Mead (1964) and Williams and Mead (1965). The image dipole models involved modeling the currents in the magnetopause "by a large image dipole placed between the earth and the sun" (Roederer, 1969). In order to simulate the currents in the magnetotail, a current sheet of thickness of 0.5 Earth radii was added (Roederer, 1969). The image dipole models were first presented in papers by Hones (1963) and Taylor and Hones (1965). Both of these models, while enlightening, suffered from deficiencies, the main one concerning this thesis being improper modeling of the magnetotail.

Walker (1976) completed a review of the more recent models being developed. This included more complicated image dipole and boundary surface models, as well as defined magnetopause models and empirical models. A new image dipole model was presented in papers by Willis and Pratt (1972) and Thomas et al. (1974). However, Walker (1976) advised exercising caution when using these models in the context of the magnetotail, especially in the equatorial plane. Choe et al. (1973) and Choe and Beard (1974a, 1974b) created the most "precise calculation of the self-consistent magnetopause" (Walker, 1976) in terms of a boundary surface model of the magnetosphere. However, the spherical harmonic expansion they used to create the tail current is only valid until out to ten Earth radii in the negative x-direction (Walker, 1976). Therefore, it is not useful to use for studying the magnetotail in the range of 10 to 60 R_E downtail, from which substorm activity is strongly driven. Next, the boundary surface models evolved to include not just the magnetopause and tail currents, but also the ring current. The first of this type of model was presented by Sugiura and Poros (1973) and the second presented by Olson (1974) and Olson and Pfitzer (1974). The ring current that was added was only for quiet time, so there was no partial ring current. Therefore, these models are once again not suited for analyzing the magnetotail in terms of substorms since not only would the ring current be more intense, but also there would be a partial ring current. Next, two models were developed where the magnetopause was assumed to be a certain shape. "The magnetic field was assumed to be derivable from a scalar potential and to be tangential to the boundary. The scalar potential was then found by solving Laplace's equation with Neumann's boundary condition" (Walker, 1976). The first of this kind of model was presented by Alekseev and Shabansky (1972) and the second was presented by Voigt (1972). Both models assumed an infinitesimally thin neutral sheet and are simpler alternatives to the boundary surface models (Walker, 1976). The final type of magnetospheric model to emerge was an empirical model. Mead and Fairfield (1975) constructed a 17-coefficient model using a least-squares fit on satellite data. What is different about this model is that it does not assume that the magnetic field is curl-free, like the other models present at this time. However, it still does not accurately measure the magnetotail past 12-14 Earth radii and cannot describe the neutral sheet current (Mead and Fairfield, 1975). In summary, by the 1970s, the models were becoming more intricate and complicated, but the magnetotail was not accurately modeled, especially during non-quiet times.

Table 1.1 Comparison of empirical magnetosphere models (Jordan, 1994)

Model	*Magnetopause*	*Main Field*	*Ring Current*	*Tail Current*	*Input Parameters*	*General Remarks*
Hilmer-Voigt	Hemisphere and cylinder Shielding currents for dipole only	Vacuum dipole	Vector potential (eastward and westward)	Segments of magnetic filaments	Tilt Standoff distance *Dst* Midnight equatorward boundary	Flexible model for various conditions 1–350 R_E
Mean-Fairfield	No explicit representation	None	No explicit representation	No explicit representation	Tilt *Kp*	**B** components from data fit to power series expansion Total current from curl of **B** 5–15 R_E Four *Kp* level Fit to Explorer 33, 34, 41, and 43
Olson-Pfitzer tilt dependent (1977)	Empirical shape Fixed R_0 Empirical shielding	None	Wire loops (eastward and westward)	Wire loops	Tilt	Quiet model only 2.5–15.0 R_E Fit to OGO 3 and 5 and Explorer 33 and 35
Olson-Pfitzer dynamic (1988)	Empirical shape Variable R_0 Empirical shielding	None	Wire loops (eastward and westward)	Wire loops	Standoff distance *Dst*	Scalable model 2.5–60 R_E No tilt
Tsyganenko-Usmanov	No explicit shape, R_0, or shielding Products of polynomials and decaying exponentials Empirical fit to data	None	Vector potential (westward only)	Current filaments Central sheet only Finite extent downtail	Tilt *Kp*	11 *Kp* levels 5–20 R_E Fit to Explorer 33, 34, 41, and 43, plus HEOS 1 and 2
Tsyganenko 1987	No explicit shape, R_0, or shielding Products of polynomials and decaying exponentials Empirical fit to data	None	Vector potential (westward only)	Current filaments Central and return current sheets Infinite extent downtail	Tilt *Kp*	Two versions: Long: 5–70 R_E 6 *Kp* levels Short: 5–30 R_E 8 *Kp* levels Fit to eight IMP and two HEOS data sets
Tsyganenko 1989	No explicit shape, R_0, or shielding Products of polynomials and decaying exponentials Empirical fit to data	None	Vector potential (westward only)	Vector potential	Tilt *Kp*	Six *Kp* levels 5–70 R_E Fit to eight IMP and two HEOS data sets

Tsyganenko (1990) published a very thorough review of empirical modeling techniques and results from the existing empirical magnetosphere models. He discussed in detail many of the models presented in the last paragraph, as well as the updated versions of these models. Jordan (1994) completed his own review of empirical models, many of which were also discussed by Tsyganenko. A table from Jordan (1994) summarizing the prominent empirical

models at the time is shown in Table 1.1. The reviewed models include the Mead and Fairfield model (1975) previously discussed, the Olson and Pfitzer tilt-dependent model (1977), the Tsyganenko and Usmanov model (1982), two other Tsyganenko models (1987 and 1989), the Olson and Pfitzer dynamic model (1982), and the Hilmer-Voigt model (1995). As seen in Table 1.1, all of the models include the magnetopause, ring, and tail current with each model implementing these currents in a different way. The Olson and Pfitzer tilt-dependent model is designed for only quiet times while the others have the ability to adjust to varying conditions, usually by setting the Kp level. The Kp index indicates the level of activity occurring in the magnetosphere with lower numbers representing a quiet magnetosphere and higher numbers representing an active magnetosphere. Also, each model is valid for certain ranges in space, with most being valid in the vicinity of the magnetotail. Models were finally being developed with the ability to study the magnetotail in more disturbed conditions. However, there are some issues in using these models to analyze the magnetotail in more disturbed conditions. The empirical models are created by taking an average over relevant satellite data. Therefore, regarding substorms, "an empirical model tends to have a thicker current sheet than is present in the real magnetotail since the real magnetotail may move up and down in the *Z* direction. Such tail "flapping" broadens the apparent observed thickness obtained by averaging or binning the satellite data" (Wanliss et al., 2000). Thus, the empirical models showed the average formation of the magnetotail, but were still not able to describe intricate details occurring in the magnetotail.

The Tsyganenko models mentioned in the last paragraph are among the more popular models that are used. Over the years, they have changed and developed substantially (see Tsyganenko and Usmanov, 1982; Tsyganenko, 1987; Tsyganenko, 1989; Tsyganenko, 1995; Tsyganenko, 1996; Tsyganenko, 2002a; Tsyganenko, 2002b; Tsyganenko et al., 2003; Tsyganenko and Sitnov, 2005; and Tsyganenko and Sitnov, 2007). As mentioned previously, one of the criticisms of the early Tsyganenko models is that since the model is an average, it will not properly model things like current sheets in the magnetotail. It will make the current sheet too large, which is not useful for studying the conditions during substorms. However, these models provide a good basis for overall magnetospheric behavior and therefore can be slightly tweaked in order to be useful for studying different aspects of the magnetotail. For example,

Pulkkinen et al. (1991, 1992, and 1994) took the 1989 Tsyganenko model and tweaked it in order to study the growth phase of substorms. They needed to "include a localized thinning of the crosstail current sheet so that the stretching of the near-Earth magnetic field during the substorm growth phase was reasonable" (Wanliss et al., 2000). Lu et al. (1999) took the 1996 Tsyganenko model and "incorporat[ed] an adjustment to the intensity and thickness of the near-tail current sheet and a contribution from the substorm current wedge" (Wanliss et al., 2000). The latest Tsyganenko models (Tsyganenko et al., 2003; and Tsyganenko and Sitnov, 2005) are specifically built to model substorms. This is done by taking data only from substorm events in order to create their empirical model. Thus, empirical models have improved greatly to the point of being able to show details of the changing magnetosphere during substorm events. The other latest models (Tsyganenko and Sitnov, 2007; and Sitnov et al., 2008) focus on using high resolution to see more details of the dynamics occurring in the magnetosphere. Modeling has advanced so far that teams like Tóth et al. (2005) are combining models of all parts of the Sun-Earth system to create an overall space weather simulation with the hope of one day being able to predict space weather events. Impressive as these models are, they are not practical to use in some studies of the magnetotail due to the complexity. Instead, some researchers create simple models of the magnetic field lines in order to study the magnetotail. Past simple models are discussed in the next paragraphs.

Harris (1962) produced one of the first and simplest models of the current sheet in the magnetotail. It consists of a one-dimensional current sheet that is based on the balance of magnetic field and plasma pressures. In the Harris model, the magnetic field $\vec{B}$ is given by (Kivelson and Russell, page 251)

$$\vec{B}(z) = B_0 \tanh\left(\frac{z}{h}\right)\hat{x} \qquad 1.1$$

where B_0 is the ambient magnetic field strength at an infinite distance away and h is the half-width of the current sheet in the z-direction. A picture of the Harris magnetic field is shown in Figure 1.6.

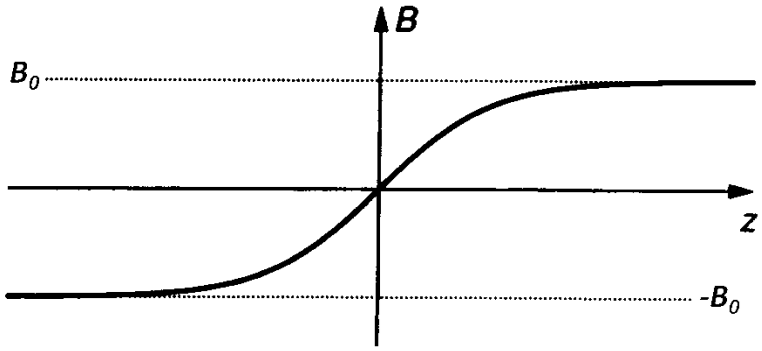

Figure 1.6 Graphical representation of the magnetic field in the Harris current sheet model showing that the field eventually reaches the constant value of B_0.

The plasma pressure p in the Harris model is given by (Kivelson and Russell, page 251)

$$p(z) = p_0 \text{sech}^2\left(\frac{z}{h}\right) \tag{1.2}$$

where p_0 is the pressure at the center of the current sheet. The total pressure consists of the sum of the magnetic and the particle pressure (Kivelson and Russell, page 251). This is mathematically represented as

$$p_{total} = \frac{B^2}{2\mu_0} + p \tag{1.3}$$

where μ_0 is the permeability of free space $\left(\mu_0 = 4\pi \times 10^{-7}\text{NA}^{-2}\right)$. Inserting equation 1.1 and equation 1.2 into the above equation gives the total pressure of the Harris model as

$$p_{total} = \frac{B_0^2}{2\mu_0}\tanh^2\left(\frac{z}{h}\right) + p_0\text{sech}^2\left(\frac{z}{h}\right) . \tag{1.4}$$

The total pressure can be simplified to

$$p_{total} = 2p_0 \tag{1.5}$$

if it is assumed that the pressure at the center of the current sheet is the same as the purely magnetic pressure at the outside, namely

$$p_0 = \frac{B_0^2}{2\mu_0} \,. \qquad 1.6$$

Therefore, the total pressure inside the current sheet is constant in the Harris model, making it very simple to implement into theoretical models, like the ones discussed in the previous paragraphs. Simple models of the whole magnetosphere are discussed in the following paragraphs.

Luhmann and Friesen (1979) developed a simple model of the magnetosphere as an alternative to the more complex quantitative models that were emerging at that time. "The basic model is constructed from a dipole field and a uniform field directed sunward in the northern hemisphere and anti-sunward in the southern hemisphere" (Luhmann and Friesen, 1979). They simply added a constant in the x-direction to the dipole field in order to create the stretched field lines. A picture of the field lines created by this model is shown in **Error! Reference source not found.**. "[I]t is superior for simulating effects related to the tail configuration" (Luhmann and Friesen, 1979).

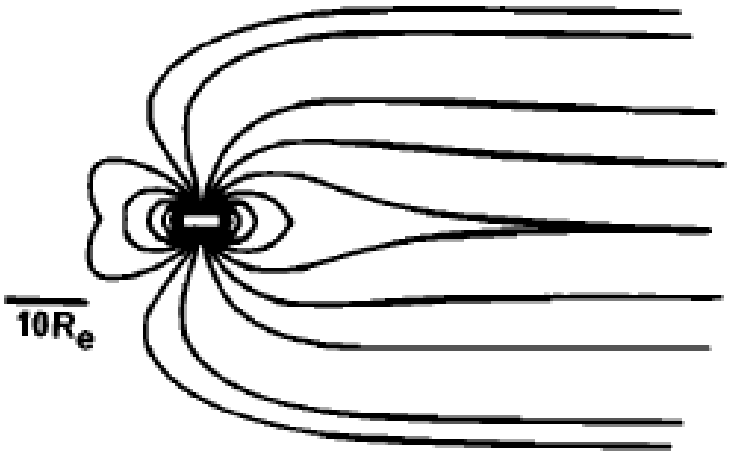

Figure 1.7 Field lines from the simple Luhmann and Friesen model (1979) in the noon-midnight meridian plane.

Wanliss et al. (2000) created a simple model of the magnetotail in order to study the current sheet during the growth phase of substorms. "The model comprises a dipole field, an equilibrium tail component, and an azimuthally and radially confined weak magnetic field region" (Wanliss et al., 2000). The model is more complicated than Luhmann and Friesen's model, but this is necessary to create the conditions in the tail appropriate to the growth phase of a substorm. The central region of weak magnetic field is necessary for this phase of a substorm, and the reason for this will be discussed in greater detail in chapter 2. The field lines produced by this simple model are shown in **Error! Reference source not found.**. The shape of the field lines is influenced by the strength of the lobe magnetic field and the magnetotail current sheet half thickness (Wanliss et al., 2000). **Error! Reference source not found.** shows two different combinations of these parameters. Specifying these parameters made it very easy for them to analyze the current sheet during substorms compared to using an empirical model.

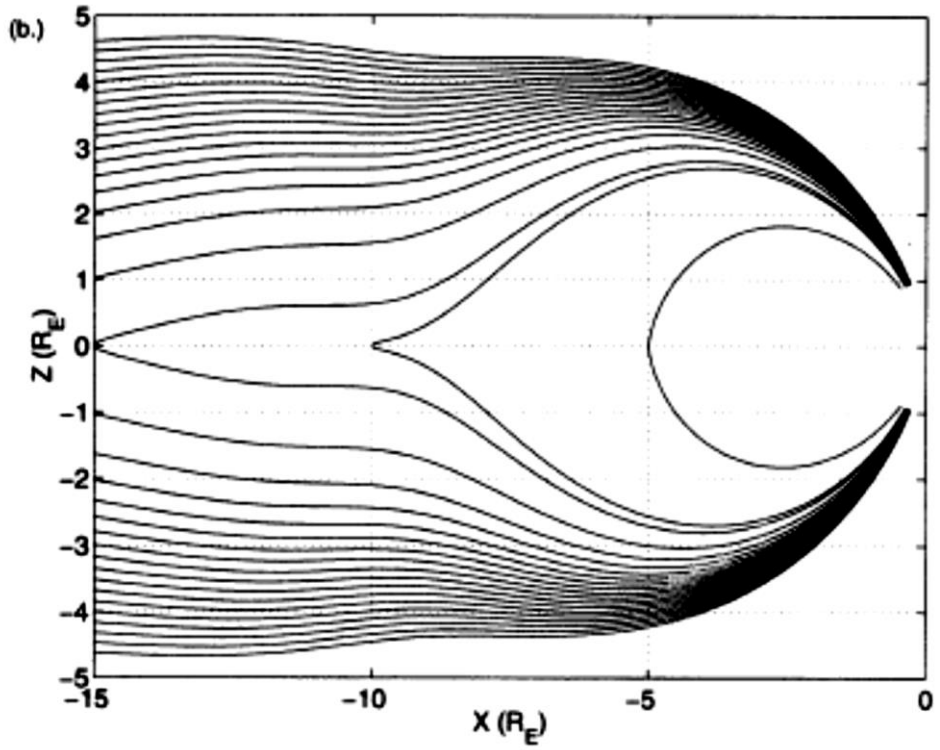

Figure 1.8 Field lines from the Wanliss et al. model (2000) in the noon-midnight meridian plane.

Kabin et al. (2011) also created a simple model in order to analyze dispersionless injections that occur during substorms. Their model is made by adding a tail field component to

the dipole magnetic field (Kabin et al., 2011). Their model is dependent on the thickness of the magnetotail, the strength of the cross tail current, and "the location and sharpness of the transition from dipole-like to tail-like fields" (Kabin et al., 2011). The field lines produced by this model are shown in Figure 1.9. Figure 1.9 shows two different combinations of these parameters. Specifying these parameters made it very easy for them to analyze the current sheet during substorms compared to using an empirical model.

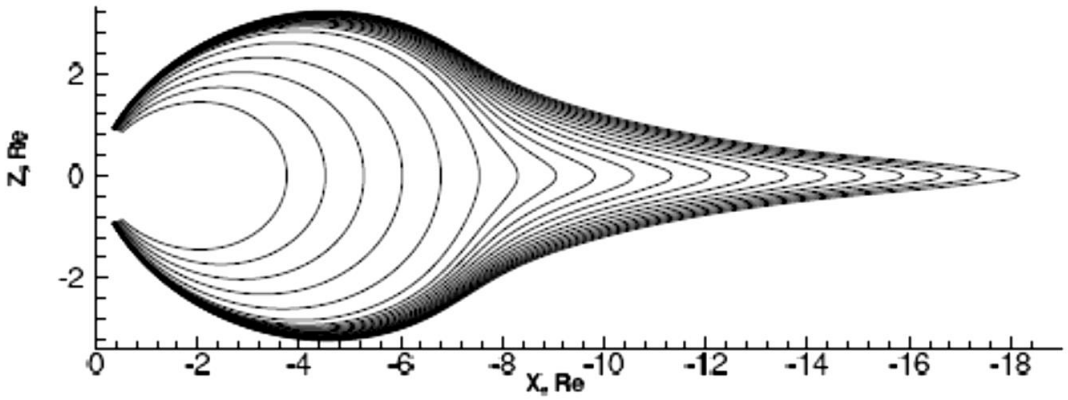

Figure 1.9 Field lines from the Kabin et al. model (2011) in the noon-midnight meridian plane.

Main Objectives and Outline of Thesis

In this thesis, a simple model of the magnetotail based on the shape of the stretched field lines was created in order to analyze the currents occurring in the magnetotail. The shape used for the stretched field lines contains four inflection points. Sofko et al. (2013) believe this field line shape leads to a double vortex current system in the magnetotail that is centered on the NS. The simple model of the magnetotail presented in this thesis can be used to test the validity of the double vortex current system by analyze the currents produced by the model.

This thesis contains six chapters. The second chapter will present the necessary background information and the criteria for the simple model. This includes defining a model of the nightside magnetosphere and the shape of the stretched field lines, explaining the role of stretched field lines in substorms, deriving an overall current formula for the magnetotail, and

justifying the double vortex current system by analyzing the overall current formula. The third chapter will present the simple model of the magnetotail. It will go in depth into the design of the model. Also, the physicality is tested by checking the divergence of the magnetic field and limits at infinity. The fourth chapter will present results found from using the simple model. The results include the current that is found directly from the magnetic field model by using Ampere's law, the pitch angle and gyroradius of the particles at every point in the magnetotail, and the current produced by the first term in the overall current formula that will be derived in Chapter 2. The fifth chapter will present an alternative solution to creating a divergence free magnetic field that was attempted for this thesis. It involves numerically solving Poisson's equation. The attempt was not successful because it required more computing power than was anticipated, but the method is presented in Chapter 5. Finally, the sixth chapter will summarize the results from the model, and future steps for this project will be outlined.

Chapter 2

Theory and Criteria for Simple Model

In this chapter, the physics occurring in the magnetotail is presented. Before the physics can be analyzed, some basic definitions are needed. The coordinate system used in this thesis is described in Section 2.1 and a brief overview of the sections of the magnetotail is given in Section 2.2. Next, one of the regions of the magnetotail, the stretched plasma sheet, will be described further by defining the shape of the field lines present in this region and its role during a substorm. Finally, some pertinent physics occurring in the magnetotail will be analyzed, namely the particle drifts and the current in the magnetotail. The important particle drifts, which include the convective drift, the curvature drift, and the gradient drift, are derived in Section 2.4. The general current formula is derived in Section 2.5 and the direction of the current in the magnetotail is found in Section 2.6.

2.1 Coordinate System

Two coordinate systems frequently used in space physics are the geocentric solar magnetospheric (GSM) coordinate system and the geocentric solar ecliptic (GSE) coordinate system. The GSM coordinate system is based upon the magnetic field of the Earth and the GSE coordinate system based upon to the orbit of the Earth. In both coordinate systems, the center of the Earth is the origin and the x-axis points towards the sun. In the GSM coordinate system, the x-z plane contains the dipole axis of the Earth's magnetic field. The dipole axis is directed towards the South Pole and changes location with the daily rotation of the Earth. The y-axis is defined as the cross product between the x-axis direction and Earth's dipole. The z-direction completes the right handed system with it being directed towards the North Pole. The GSM

coordinate system is dependent on the time of day through the rotation of the Earth's dipole axis. This leads to more complicated analysis and, therefore, this coordinate system will not be used in this thesis. In the GSE coordinate system, the x-y plane is the ecliptic plane. The y-axis points towards dusk or westward in the magnetotail and the z-axis is perpendicular to the ecliptic plane and in the direction of the ecliptic north pole. This coordinate system is much simpler to use since it does not include time dependencies. However, the GSE coordinate system does not explicitly contain any information about the Earth's magnetic field. Therefore, for this thesis, a more simplified version of the GSE coordinate system is used. Since this thesis is not concerned with any seasonal or diurnal effects, it can be assumed that the Earth's dipole axis and the ecliptic plane are perpendicular to each other. Therefore, the simplified coordinate system consists of the x-axis pointing towards the sun; the y-axis is in the dusk or westward in the magnetotail; and the z-axis is antiparallel to the dipole axis of the Earth's magnetic field. This coordinate system is depicted in Figure 2.1 and is given the name of simplified geocentric solar ecliptic coordinates.

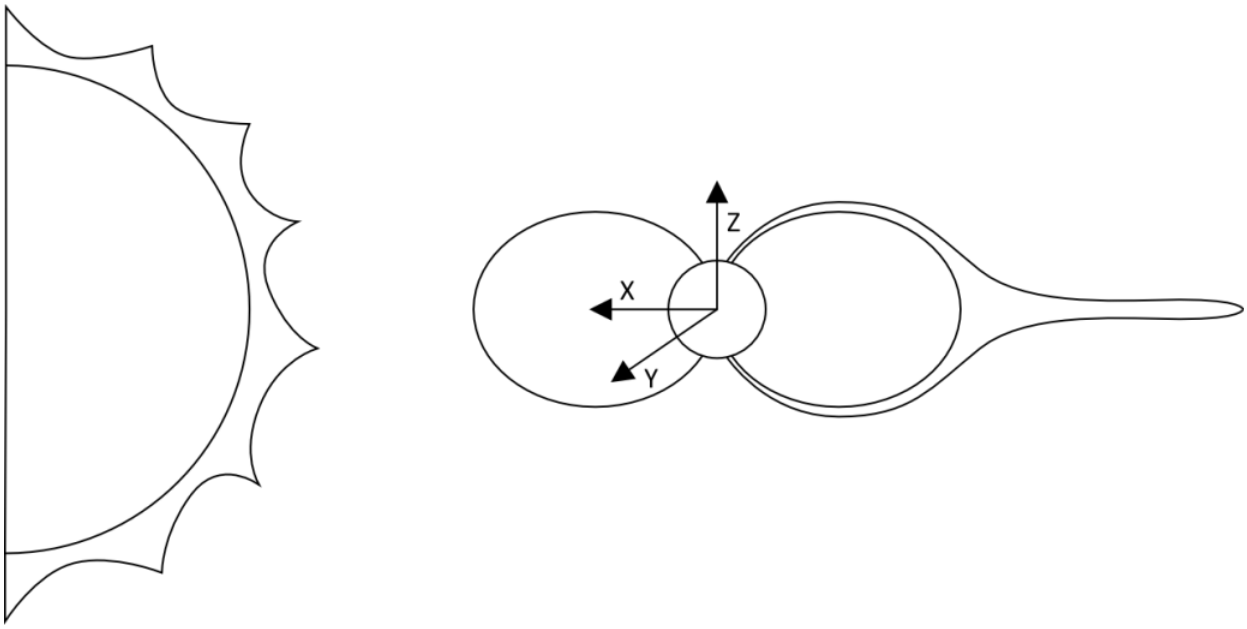

Figure 2.1 Simplified geocentric solar ecliptic coordinates where the x-axis points towards the sun, the y-axis points towards west, and the z-axis is assumed to be antiparallel to the dipole axis of the Earth's magnetic field.

2.2 Regions of the Magnetotail

Chapter 1 presented a brief overview of the different regions in the magnetosphere. This section will highlight the regions that are specifically in the magnetotail and describe the PS region in more detail. Two dimensional slices of the magnetotail are shown in Figure 2.2 and Figure 2.3. The first figure shows the magnetosphere in the x-y or equatorial plane. The second figure shows the magnetosphere in the x-z plane or the noon-midnight meridian plane. There are six main areas in the magnetotail: LLBL (blue), lobes (red), plasmasphere (teal), dipole plasma sheet (yellow), transition plasma sheet (green), and stretched plasma sheet (orange). The first three regions were already discussed in detail in Chapter 1. The last three regions are located in the PS. Sofko et al. (2013) splits the PS into these three different regions based on the different types of closed magnetic field lines that exist within the PS.

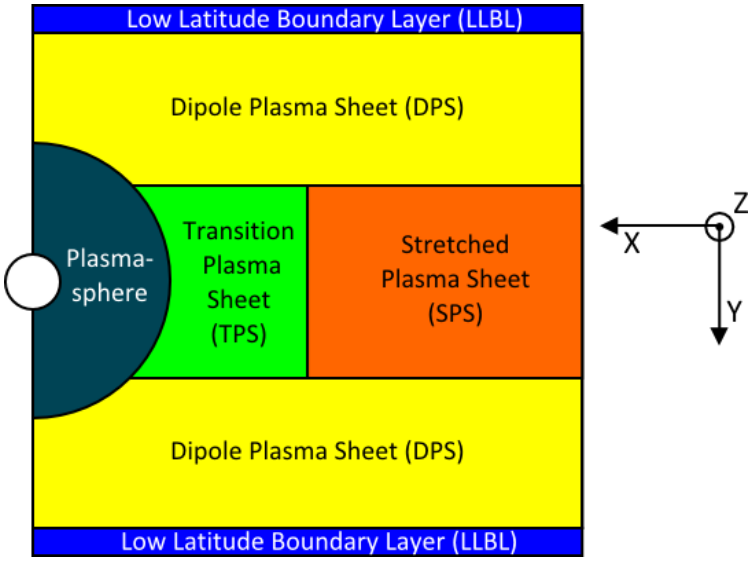

Figure 2.2 The x-y slice of the magnetosphere contains the LLBL, plasmasphere, and the three sections of the PS (DPS, TPS, and SPS).

The first region in the PS is the dipole plasma sheet (DPS). It contains quasi-dipolar field lines. The field lines are quasi-dipolar due to the activity occurring in the magnetosphere. For the purposes of this thesis, the field lines are assumed to behave like dipole field lines in terms of how the magnetic field affects the plasma. The DPS is the assumed default state of the PS, meaning if there were no outside forces on the magnetic field lines in the PS, it would only

consist of quasi-dipolar field lines. The second region in the PS is the transition plasma sheet (TPS). It contains field lines that are transitioning between dipole and stretched shape. This is a very dynamic region during substorms. The TPS is not the focus of this thesis, but Sofko et al. (2013) discuss some of the physics occurring in this region during substorms. The last region in the PS is the stretched plasma sheet (SPS). It contains stretched field lines. The SPS is split into three different regions based on the direction of the current. The first region is the NS. In the NS, there is a strong westward current, which is compatible with the crosstail current that was mentioned in Chapter 1. The other two regions are unique to the new substorm model presented by Sofko et al. (2013). They are called the disruption zones (DZs). They consist of regions of eastward current. The NS occupies the center of the SPS and the DZs occupy the regions above and below the NS. The overall current formation in the magnetotail consists of a double solenoid with the current following eastward in the DZs and then closing westward in the NS. The justification behind the direction of this magnetotail current configuration is presented in Section 2.6 with the basis of the argument derived from the shape of the field lines in the SPS. A detailed discussion of the shape of the stretched field lines in the SPS is presented in the next section. Also, the growth and decay of substorms are essentially linked to the growth and decay of the SPS. Furthermore, it is the SPS that maps to the nightside auroral zone. The role of the SPS in substorms will also be presented in the next section.

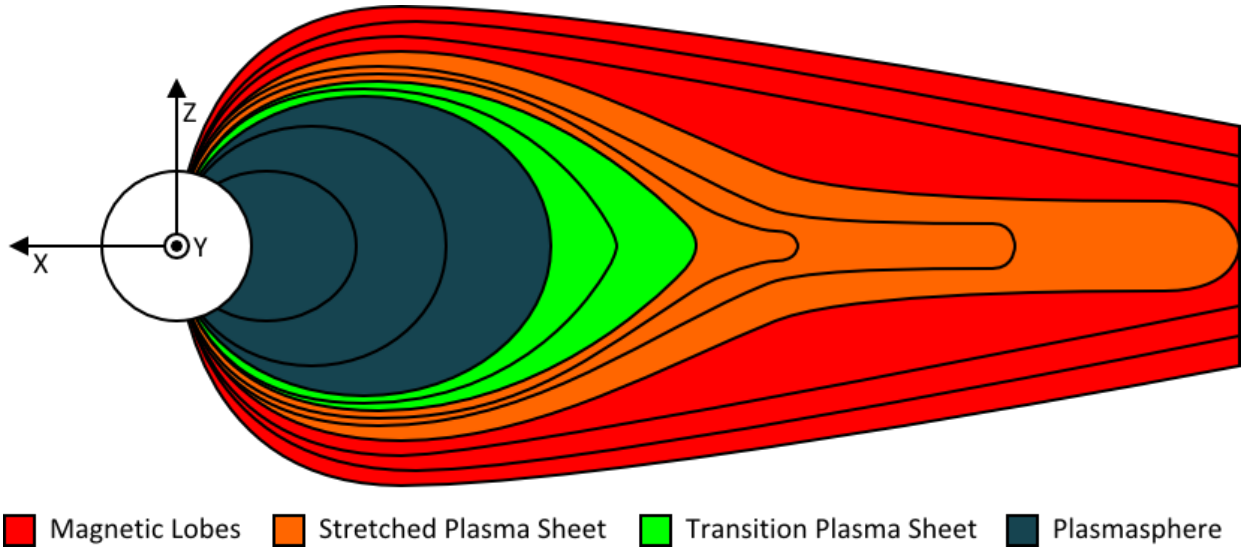

Figure 2.3 The x-z slice of the magnetosphere contains the plasmasphere, north and south lobes, TPS and SPS.

2.3 Stretched Plasma Sheet

2.3.1 Shape of Stretched Field Lines

There is no agreement on the shape of the stretched field lines in the SPS within the space physics community. One commonly used shape, and the shape that will be used in this thesis, is shown in Figure 2.4 taken from a recent paper by Haerendel (2010). The shape is shown by the closed field line located in the plasma sheet. The stretched field line he presents drapes over the field lines in the plasmasphere and TPS, creating inflection points that separate regions of concave and convex curvature in the field line, and has a thin, elongated section in the magnetotail. The other common depiction of stretched field lines retains a stretched dipole shape without the inflection. However, Sofko et al. (2013) have found that the geometry with inflection points is consistent with the observed sequence of substorm events.

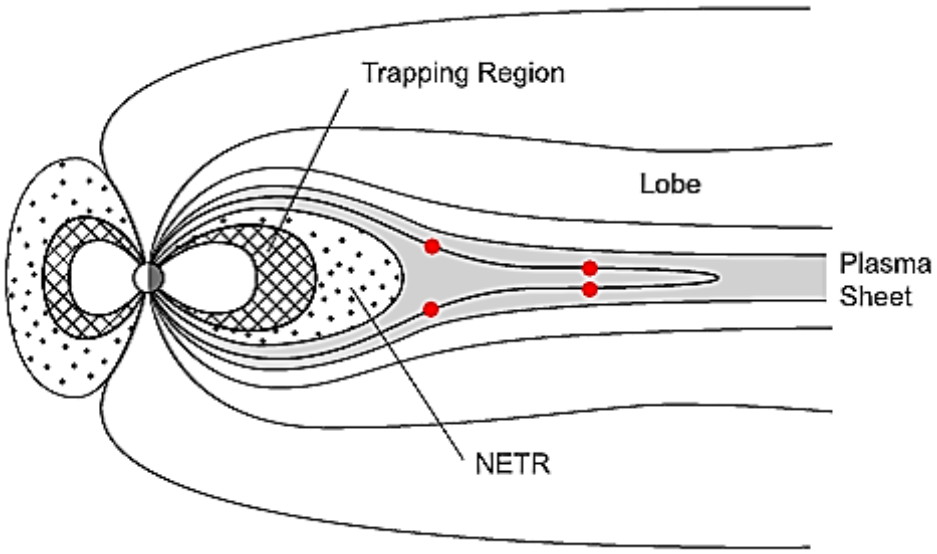

Figure 2.4 Noon-midnight meridian plane view of the magnetosphere (Haerendel, 2010). The inflection points are represented by red circles.

One reason for the curvature in the stretched field lines is that the lobe lines have to drape over the plasmasphere. If the plasmapause is located 5 R_E away from the Earth in the negative *x*-direction, the dipole field lines in the plasmasphere will reach z values of approximately ±2 R_E if

the plasmasphere is viewed in the x-z or noon-midnight meridian plane (calculation is shown in Appendix A). This is demonstrated in Figure 2.5. The plasmapause boundary comes closer to Earth with increased magnetic activity, but the plasmasphere region will always be present with its roughly dipole field lines.

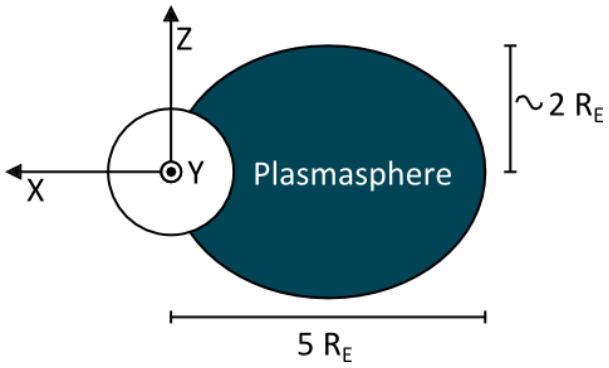

Figure 2.5 The plasmasphere has a maximum height of approximately ±2 R_E in the z direction if it goes out to 5 R_E in the negative x direction.

As will be discussed more in the next subsection, stretched field lines are created and destroyed by antiparallel reconnection. In simplistic terms, antiparallel reconnection is a process where, when two field lines with antiparallel directions are pressed together, a strong current sheet that separates the lines becomes a region in which a new magnetic formation can occur. Therefore, antiparallel reconnection can only occur when the field lines are in very close proximity to each other. Thus, if the elongated section of the stretched field line needs to be very thin (much less than two Earth radii) to facilitate antiparallel reconnection, then the field lines must drape over the plasmasphere in order to create the thin, elongated section. This is demonstrated in Figure 2.6. This creates curvature in the field lines.

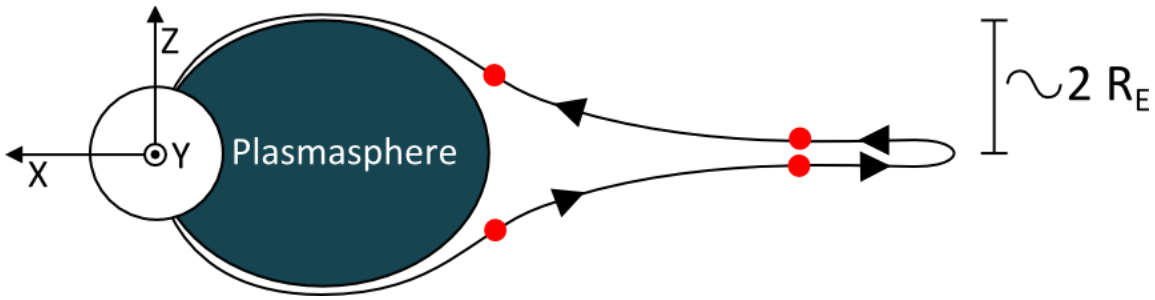

Figure 2.6 The stretched field lines drape over the plasmasphere creating inflection points.

Shen et al. (2003) used Cluster measurements in order to investigate the curvature of the field lines in the magnetotail. Their observations concerning the curvature radius of the field lines are summarized in Figure 2.7. Based on their observations, the curvature in the NS points earthward, the shape is concave and the radius of curvature is less than two Earth radii (Shen et al., 2003). They also found that the NS is very thin during the growth and expansion phase of substorms (thinnest region less than 0.5 Earth radii) and thicker during the recovery phase (thinnest region greater than 0.8 Earth radii) (Shen et al., 2003). In the DZs, they found that the curvature vector points northward in the north lobe and southward in the south lobe, or convex, and the radius of curvature is between five and ten Earth radii (Shen et al., 2003). As seen in Figure 2.7, the boundary between the DZs and the NS, if this boundary was based entirely on curvature, corresponds to a very large radius of curvature meaning that the field lines are almost straight in this region. The boundaries between the DZs and the lobes were arbitrarily placed as it is difficult to distinguish between the two field lines since the field line could potentially close very far downtail.

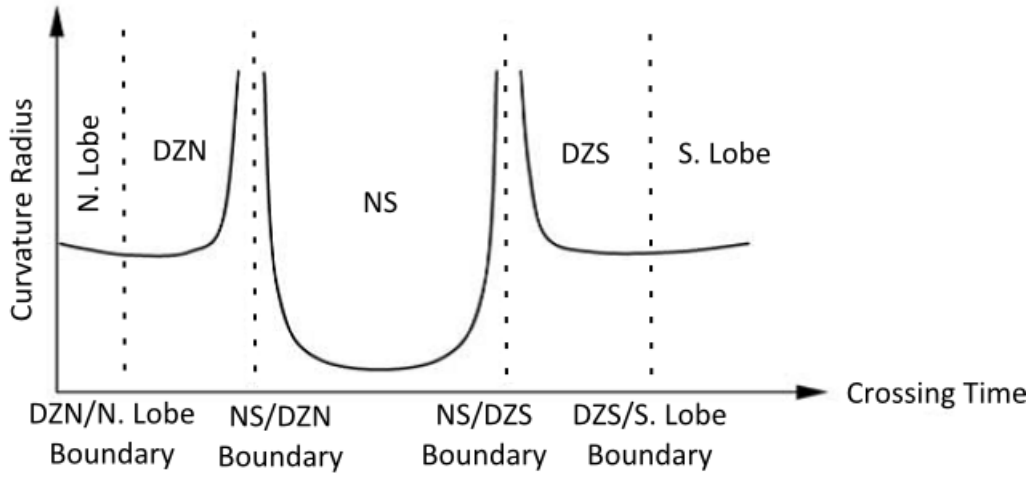

Figure 2.7 Curvature radius in the magnetotail computed from Cluster measurements (Shen et al., 2003) with labels adapted.

The proposed field line shape in the magnetotail by Shen et al. (2003) is shown in Figure 2.8. However, Shen et al. (2003) assumed that many of the lines on which the inflection points occurred were lobe lines, and Sofko et al. (2013) argue that a substantial fraction of them are closed stretched field lines. This geometry of the stretched field lines with inflection points plays

a very important role in the substorms according to Sofko et al. (2013) and will be discussed in detail when analyzing the direction of the current in Section 2.6.

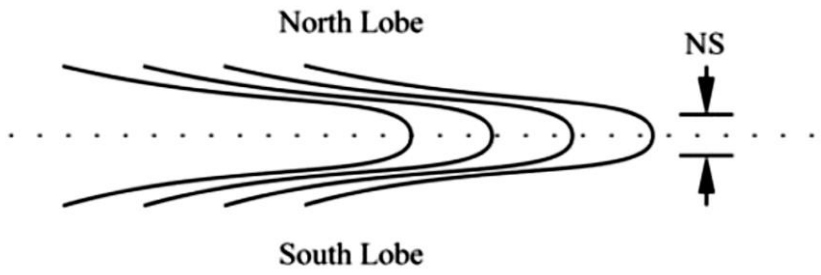

Figure 2.8 Proposed field line geometry in magnetotail based from Cluster measurements (Shen et al., 2003).

Other arguments that support this shape of stretched field lines include the convective drift of the plasma in the magnetotail, a minimum in the magnetic field on the earthward side of the SPS, and a double vortex current system proposed by Sofko et al. (2013) in the magnetotail. These aspects and the reasons why they support the shape of the field stretched field lines will be discussed in later sections of this chapter.

2.3.2 Evolution of Stretched Plasma Sheet

The growth and decay of the SPS follows the three phases of a substorm. The three phases consist of the growth phase, the onset phase, and the recovery phase. These phases relative to the SPS are shown in Figure 2.9. The shape of the stretched field lines used is the shape discussed in the previous subsection.

Figure 2.10 shows the changes in the magnetotail during a substorm as presented by Hones (1984). Even though he draws his stretched field lines without inflection points, the evolution of the SPS is very similar as can be seen by comparing the following two figures. The plasmoid that forms in panel 3 and is eventually ejected downward in panel 6 is a very important feature of the Hones magnetic geometry.

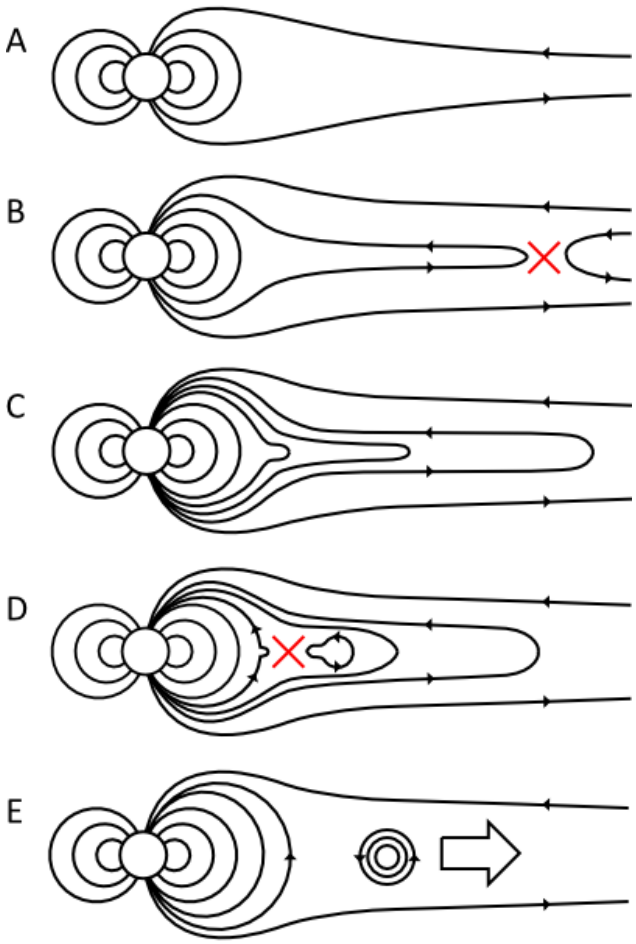

Figure 2.9 Panels A through E represent the development and decay of the SPS. Panel A shows the idealistic time zero, where there are no stretched closed field lines in the magnetotail. Panel B shows the first stretched closed field line created through antiparallel reconnection between two lobe field lines. Panel C shows the SPS filling up as more lobe lines reconnect. Panel D represents the onset of the substorm where the innermost stretched field line reconnects. Panel E represents the time after all the stretched field lines have reconnected.

Panel A in Figure 2.9 represents the idealistic time zero, where there are no stretched closed field lines present in the magnetotail. The only field lines that are present are the field lines in the plasmasphere and the magnetic lobes. The lobe field lines either come out of the South Pole or go into the North Pole. The reconnection of the north lobe and south lobe field lines produces the stretched closed field lines in the SPS. The reconnection occurs at the distant tail neutral line (DNTL), which is represent by the red X in panel B in Figure 2.9, and is a key feature of substorm growth.

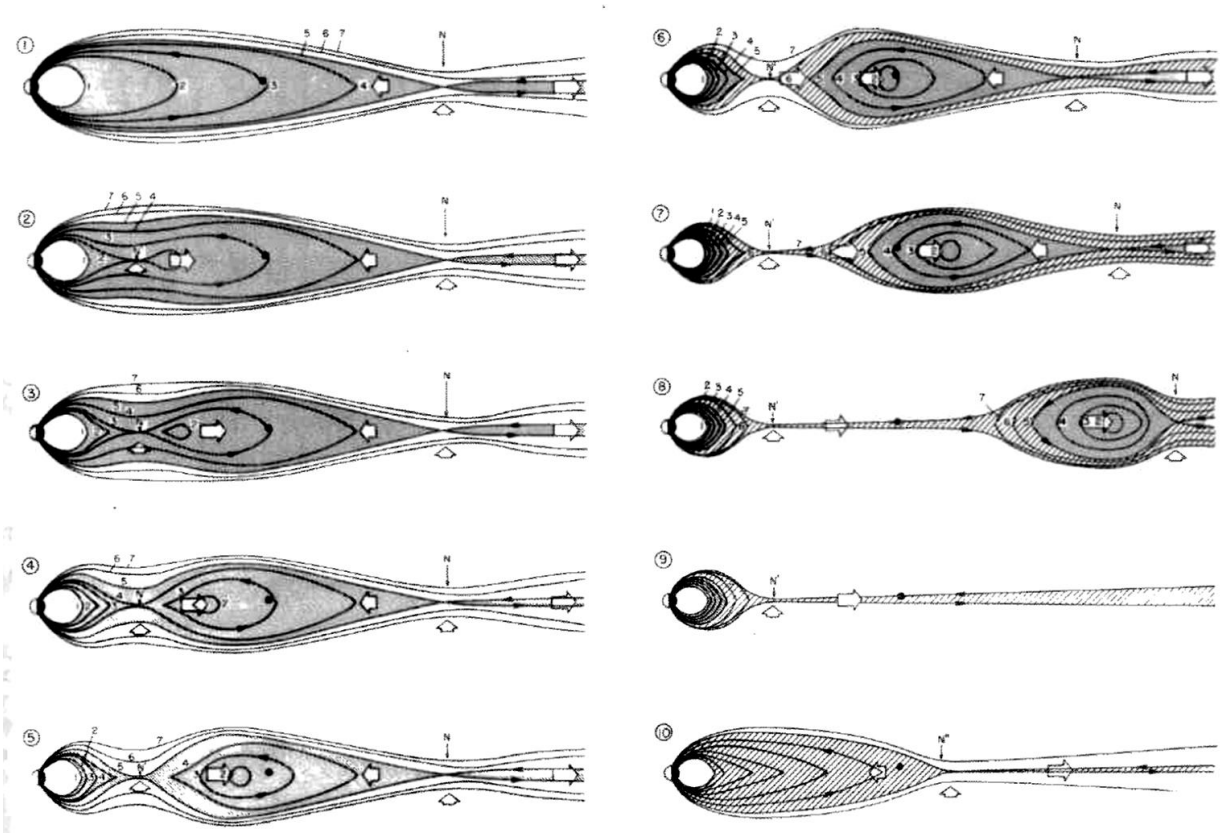

Figure 2.10 Changes in the magnetotail plasma sheet during substorms (Hones, 1984).

The creation of the first stretched field lines is shown in panel B in Figure 2.9. Dungey (1961), while describing overall convection in the magnetosphere, was the first to propose reconnection occurring in the tail between the north and south magnetic lobes in order to create stretched field lines. He theorized that this could only happen when the IMF had a z-component, in order to create reconnection on the dayside. However, newer results show that reconnection events also can happen when the IMF is purely in the y-direction, purely in the z-direction, or has all three components (Crooker et al., 1998; Watanabe et al., 2007; Watanabe and Sofko, 2008; Watanabe and Sofko, 2009a; Watanabe and Sofko, 2009b). This is because there are locations in the three dimensional magnetic topology of the Earth where the Earth's field is antiparallel to a given IMF orientation. Reconnection also can occur between nonantiparallel magnetic fields (Cowley, 1973) and this is called component merging. However, in the case of the magnetotail, it is usual to assume that reconnection tends to be purely between antiparallel magnetic fields (eg. Kivelson and Russell, page 277).

In general, reconnection can take place only in conditions where the frozen-in-flux theorem breaks down. The frozen-in-flux theorem states that if there is high conductivity, the plasma is frozen into the magnetic field (Kivelson and Russell, page 237). In other words, plasma can move freely along magnetic field lines, but not across magnetic field lines. During reconnection, however, plasma must flow between magnetic field lines in order to create a new magnetic configuration. In the case of antiparallel reconnection, the frozen-in-flux theorem breaks down when two magnetic field lines of opposite directions are pressed together. In the magnetotail, this is accomplished by the innermost north lobe and south lobe field lines being pressed together by pressure in the magnetic lobes. As stated before, this occurs at the DTNL, which is located approximately 100 Earth radii away from the Earth in the tail (Baker et al., 1984; Watanabe et al., 1998). When these field lines are pressed together, an intense current develops between them in order to compensate for the curl in the magnetic field. This current creates a diffusion region where the frozen-in-flux theorem breaks down (Kivelson and Russell, page 241). The intense current creates a region that takes away "the plasma's ability to conduct electricity, which allows an electric field to build up and the magnetic field lines to move through the plasma and reconnect" (Miller, 2013). A three dimensional and two dimensional picture of this process are shown in Figure 2.11. Panels 1a and 1b represent the field lines before the reconnection event. As the antiparallel field lines are pressed together, an intense current appears that is directed in the positive y-direction. This forms a guide field along the y-direction in the diffusion zone. The guide field causes the particles to flow in the y-direction, which separates the x-line, as seen in Panel 1a. In the diffusion region, the plasma can easily form a new configuration, leading to reconnection. The field lines after the reconnection event are shown in Panels 2a and 2b. The field line configuration has changed from L_{IN}-L_{OUT} and R_{IN}-R_{OUT} to L_{IN}-R_{OUT} and R_{IN}-L_{OUT}. Figure 2.11 also shows the particle flow during reconnection. Initially, the plasma is flowing towards the center, causing the antiparallel magnetic field lines to come in close proximity, creating the intense current and the diffusion zone. Since the current and electric field are in the same direction in the diffusion zone, energy is dissipated and transferred to the particles. This causes the particles to travel away from the reconnection site in what is known as the reconnection jet. In terms of the magnetotail, reconnection between the north and south lobe field lines creates a stretched field line earthward of the reconnection event and an IMF field line anti-earthward of the reconnection event. The reconnection jet causes the

stretched field line to travel earthward and the IMF field line to travel anti-earthward. The creation of the first stretched field line in the magnetotail is the beginning of the growth phase of the substorm.

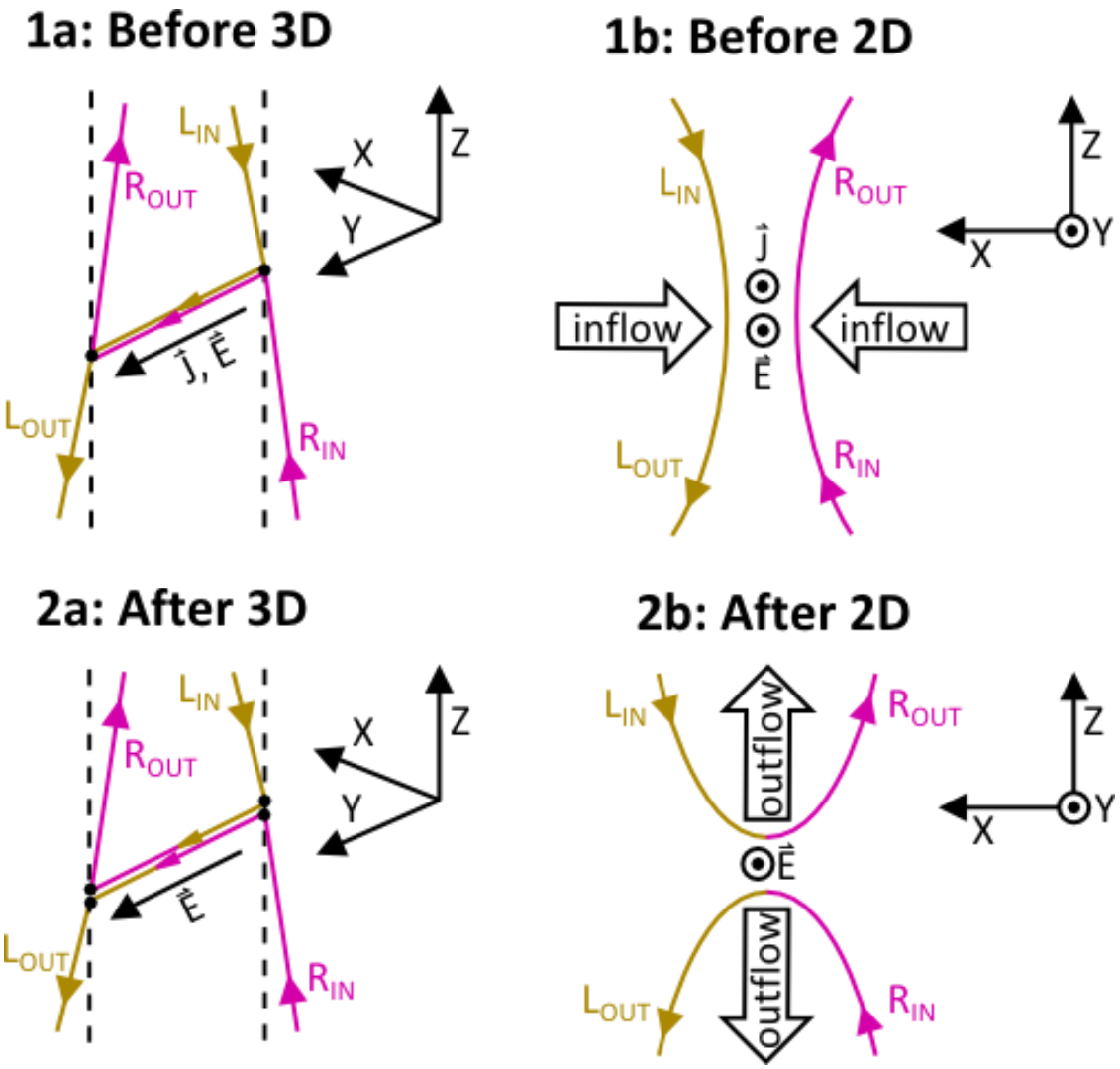

Figure 2.11 Panels 1a and 1b represent the field lines before the reconnection event. Panels 2a and 2b represent the field lines after the reconnection event with the field lines in their new configuration. The arrows on the 2D pictures represent the particle flow during reconnection.

Panel C in Figure 2.9 is a continuation of the growth phase. During the growth phase, lobe field lines are continuously converted to stretched field lines due to reconnection. The growth of the SPS leads to the growth of the NS. This is important for the next phase of the substorm, namely the onset phase. However, the growth of the SPS does correspond to

magnetotail convection in steady state. It is true that this can lead to substorm conditions, however the changes are smooth and gradual up until onset. Zhou and Tsurutani (2001) found that even if the SPS builds up, onset can only occur if there is some sort of trigger. Therefore, the SPS will continually build up in the magnetotail, even if a substorm does not occur.

Panel D in Figure 2.9 shows the onset of the substorm. Onset is trigged by reconnection in the most earthward stretched field line. One possible explanation for reconnection occurring in the magnetotail is the Kelvin-Helmholtz instability. As will be discussed in more detail in Section 2.6, the shape of the stretched field lines creates a westward current in the NS and eastward currents in the DZs. The opposing ion directions create a momentum shear between the two different regions, which leads to the Kelvin-Helmholtz instability. The ions create the momentum shear since they are much more massive than the electrons. Both Lee et al. (1988) and Nakagawa and Nishida (1989) have studied the Kelvin-Helmholtz instability in the magnetotail. The velocity shear creates waves at the two DZ/NS boundaries. These two sets of waves can be present in two modes: the sausage mode and the kink mode. These modes are depicted in Figure 2.12. With respect to the center line of the NS, the kink mode represents the two sets of waves being out of phase and the sausage mode represents them being in phase. The velocity threshold for the kink mode is much lower than the velocity threshold for the sausage mode (Nakagawa and Nishida, 1989). Therefore, the waves occurring in the magnetotail will be in kink mode until the velocity difference in the shear region surpasses the Alfvén velocity. Mathematically, the Alfvén velocity v_A is given by (Kivelson and Russell, page 337)

$$v_A = \frac{B}{\sqrt{\mu_0 \rho}} \tag{2.1}$$

where B is the magnitude of the magnetic field and ρ is the particle density. In the NS, the magnetic field is low and the particle pressure is high. Therefore, the Alfvén velocity will have a low value, making it an easy threshold to surpass. Substorm onset occurs when the velocity shear between the particles drifting in the DZs and NS surpasses this Alfvén velocity threshold. The sausage mode waves provide the antiparallel field line condition for reconnection. The most earthward stretched magnetic field line will have the highest curvature and hence also the highest

current, so it will be the first to reconnect. Sofko et al. (2013) call this the very near Earth neutral line (VNENL), and its location is around eight to nine Earth radii away from the Earth. These reconnection events are the cause of enhanced aurora on the Earth during the substorm. Each reconnection event causes an earthward injection of particles, which travel to and from the ionosphere as field-aligned currents (FACs). The FACs that flow upwards from the ionosphere are due to precipitating energetic electrons. These electrons excite the ionospheric atoms upon impact. When these excited atoms return to a less-excited energy level, the auroral photon luminosity results.

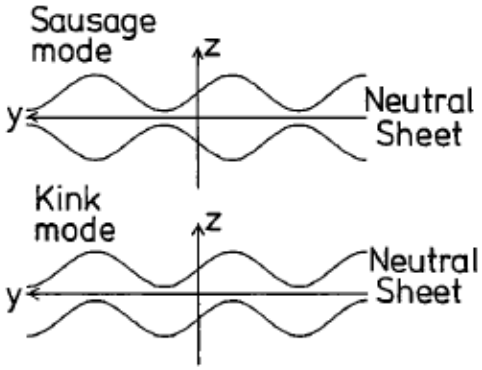

Figure 2.12 The sausage and kink mode that result from the velocity shear between the NS and DZs (Nakagawa and Nishida, 1989).

On the earthward side of the x-line, these reconnection events create a roughly dipolar field. On the tailward side, a plasmoid (Hones, 1984) is created, as shown in Figure 2.10. A plasmoid is a completely self-contained region of closed field. Once the first stretched field line reconnects, the plasmoid starts moving anti-earthward, causing the next field lines to stretch even more. The enhancement of the stretching of the field line causes an increase in the current in the DZs due to the increase of curvature. Eventually, the velocity threshold from kink mode to sausage mode will be surpassed, and reconnection will occur again. The plasmoid will continue moving downtail, causing each successive stretched field line to subsequently reconnect. After the last stretched field line reconnects, the plasmoid is not constrained by the closed lines of the SPS anymore. It is free to continue travelling anti-earthward into space. Plasmoids have been observed by satellites moving away from the Earth at around 100 to 200 Earth radii away (Moldwin and Hughes, 1992). The plasmoid is recognized by its "bipolar signature in the B_z

direction" (Moldwin and Hughes, 1992). Once the plasmoid has traveled away from the Earth, the magnetotail is at substorm time zero again (panel A in Figure 2.9). This is the life cycle of the SPS is the controlling influence on the substorm.

The particle drifts occurring in the magnetotail play an important role in SPS during substorms from the currents they create. In the next section, the equations for the particle drifts are derived. In Section 2.5, the currents due to the drifts are derived and the direction of the current is discussed in Section 2.6.

2.4 Single Particle Magnetic Drift Equations

In space, charged particles will be influenced by various forces causing them to drift. The drifts can be analyzed using Newton's second law, which is given as

$$\sum \vec{F} = m\vec{a} = m\frac{d\vec{v}}{dt} \tag{2.2}$$

where $\vec{F}$ is the force vector, m is the mass, $\vec{a}$ is the acceleration vector, and $\vec{v}$ is the velocity vector. There are two cases to analyze, the first being drifts that have no variations in time and the second being drifts that do have variations in time. First, the case with no variations in time will be analyzed. The second case will be analyzed in Section 2.4.4.

With the assumption that the drift of the particle has no variation in time, the right-hand side of equation 2.2 goes to zero. Now, the forces acting on charged particles in the magnetotail need to be defined. The most basic force is the force on a charged particle due to a magnetic field. This force is called the Lorentz force $\vec{F}_{mag}$ and is given by

$$\vec{F}_{mag} = q\vec{v} \times \vec{B} \tag{2.3}$$

where q is the charge of the particle. The other forces present in the magnetotail acting on charged particles consist of the Coulomb force due to an electric field, the centrifugal force due to curved magnetic field lines, and the gradient force due to gradients in the magnetic field. For simplicity sake, these forces will be grouped together for now. Inserting the above equation into equation 2.2 and accounting for the other forces gives

$$q\vec{v} \times \vec{B} + \sum \vec{F}_{other} = 0 \,. \tag{2.4}$$

Next, cross the magnetic field unit vector $\hat{b}$ with the above equation giving

$$q\left(\vec{v} \times \vec{B}\right) \times \hat{b} + \sum \vec{F}_{other} \times \hat{b} = 0 \,. \tag{2.5}$$

The first term can be expanded using the following vector identity (Huba, page 4)

$$\vec{A} \times \left(\vec{B} \times \vec{C}\right) = \left(\vec{C} \times \vec{B}\right) \times \vec{A} = \left(\vec{A} \cdot \vec{C}\right)\vec{B} - \left(\vec{A} \cdot \vec{B}\right)\vec{C} \,. \tag{2.6}$$

Therefore, equation 2.5 becomes

$$q\left(\left(\hat{b} \cdot \vec{v}\right)\vec{B} - B\vec{v}\right) + \sum \vec{F}_{other} \times \hat{b} = 0 \,. \tag{2.7}$$

This can be simplified further by splitting the velocity vector into components that are parallel and perpendicular to the magnetic field, which is given as

$$\vec{v} = \vec{v}_{\parallel} + \vec{v}_{\perp} = v_{\parallel}\hat{b} + \vec{v}_{\perp} \tag{2.8}$$

where $\vec{v}_{\parallel}$ is the parallel velocity vector, $\vec{v}_{\perp}$ is the perpendicular velocity vector, and $v_{\parallel}$ is the magnitude of the parallel velocity. Therefore, equation 2.7 becomes

$$q\left(Bv_{\parallel}\hat{b} - Bv_{\parallel}\hat{b} - B\vec{v}_{\perp}\right) + \sum \vec{F}_{other} \times \hat{b} = 0\,, \tag{2.9a}$$

which reduces to

$$-qB\vec{v}_{\perp} + \sum \vec{F}_{other} \times \hat{b} = 0\,. \tag{2.9b}$$

Solving for the perpendicular velocity gives the general drift formula for a particle in a magnetic field with no time variations as

$$\vec{v}_{\perp} = \frac{\sum \vec{F}_{other} \times \hat{b}}{qB}\,. \tag{2.10}$$

The overall drift will be given by the drift terms derived from the other forces present in the magnetotail. As stated previously, these other forces consist of the Coulomb force, centrifugal force, and gradient force. The drifts due to these forces are derived in sections 2.4.1, 2.4.2, and 2.4.3 respectively. The second case of equation 2.2 is analyzed in Section 2.4.4.

2.4.1 Convective Drift

The first drift in the magnetotail is due to the Coulomb force, also known as the electric force. The Coulomb force $\vec{F}_E$ is given by

$$\vec{F}_E = q\vec{E} \tag{2.11}$$

where $\vec{E}$ is the electric field vector. Inserting the above equation into the general drift equation due to a force (equation 2.10) gives the formula for the convective drift as

$$\vec{v}_{conv} = \frac{\vec{E} \times \hat{b}}{B}\,. \tag{2.12}$$

The convective drift only occurs in the presence of an electric field. The convective drift is the same for both ions and electrons because it does not depend on the charge or on the mass of the particle.

2.4.2 Curvature Drift

The second drift in the magnetotail is due to the centrifugal force that acts on a particle as it moves along a curved magnetic field. The centrifugal force is the force experienced by a particle as it travels around a curved path. The centripetal force is the force that acts toward the center of the osculating circle and that keeps the object on a curved path. Therefore, the relation between the centrifugal and centripetal force when there are no time variations is given as

$$\vec{F}_{centrifugal} = -\vec{F}_{centripetal}. \tag{2.13}$$

The magnitude of the centripetal force is given as

$$F_{centripetal} = \frac{mv^2}{\rho_c} \tag{2.14}$$

where v is the tangential velocity and ρ_c is the radius of the osculating circle, which is the circle tangential to the curved path. The direction of the centripetal force is given by the direction of the centripetal acceleration. This can be found by analyzing Figure 2.13. The centripetal acceleration and the radius of the osculating circle have antiparallel directions. The tangential velocity is the component of the velocity vector that is parallel to the magnetic field vector. Using this information, the centripetal force vector can be defined as

$$\vec{F}_{centripetal} = -\frac{mv_{\parallel}^2}{\rho_c}\hat{\rho}_c \tag{2.15}$$

where $\hat{\rho}_c$ is the unit vector of the radius of the osculating circle. The curvature of a path can be described by the curvature vector $\vec{K}$ by

$$\vec{K} = -\frac{1}{\rho_c}\hat{\rho}_c \,. \tag{2.16}$$

It represents the degree of curvature of a path. If the radius of the osculating circle is large, the curvature of the path is small, and vice versa. Inserting the above equation into equation 2.15 gives the final result for the centripetal force as

$$\vec{F}_{centripetal} = mv_{\parallel}^2\vec{K} \,. \tag{2.17}$$

Therefore, the centrifugal force, which is the force felt by the particle, is given by

$$\vec{F}_{centrifugal} = -mv_{\parallel}^2\vec{K} \,. \tag{2.18}$$

The above formula can be simplified by defining the parallel energy $W_{\parallel}$ of the particle as

$$W_{\parallel} = \frac{1}{2}mv_{\parallel}^2 \,. \tag{2.19}$$

Therefore, the final form of the centrifugal force is given as

$$\vec{F}_{centrifugal} = -2W_{\parallel}\vec{K} \,. \tag{2.20}$$

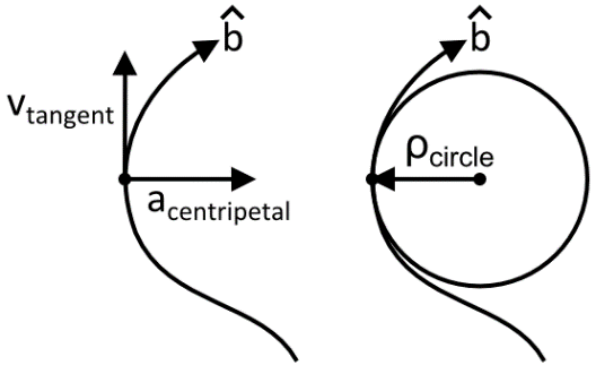

Figure 2.13 The directions the tangential velocity, centripetal acceleration, and radius of the osculating circle.

The curvature drift can now be found by inserting the centrifugal force equation into the general drift formula (equation 2.10). The curvature drift $\vec{v}_{curv}$ is found to be

$$\vec{v}_{curv} = -\frac{2W_{\parallel}}{qB}\vec{K} \times \hat{b} \,. \tag{2.21}$$

If the cross product order is flipped, the final form of the curvature drift is

$$\vec{v}_{curv} = \frac{2W_{\parallel}}{qB}\hat{b} \times \vec{K} \,. \tag{2.22}$$

The curvature drift depends on the charge of the particle. Therefore, the electrons will go in the opposite direction to the ions causing a current. The current caused by the curvature drift will be discussed in Section 2.5.1.

2.3.3 Gradient Drift

The third drift occurring in the magnetotail is the gradient drift. It is due to the presence of a gradient in the magnetic field, or, in other words, the presence of a constant but non-uniform magnetic field. The gradient force $\vec{F}_{grad}$ is given by (Baumjohann and Treumann, page 21)

$$\vec{F}_{grad} = -\mu\vec{\nabla}B \tag{2.23}$$

where μ represents the magnetic moment and $\vec{\nabla}$ represents the Del operator. The magnetic moment for a particle in the magnetosphere is given by (Baumjoham and Treumann, page 20)

$$\mu = \frac{W_{\perp}}{B} \tag{2.24}$$

where $W_{\perp}$ is the perpendicular energy. Therefore, the final form of the gradient force is

$$\vec{F}_{grad} = -\frac{W_{\perp}}{B}\vec{\nabla}B \,. \tag{2.25}$$

The gradient drift can be found by inserting the equation for the gradient force into the general drift equation (equation 2.10). The gradient drift $\vec{v}_{grad}$ is then

$$\vec{v}_{grad} = -\frac{W_{\perp}}{qB^2}\vec{\nabla}B \times \hat{b} \,. \tag{2.26}$$

The negative sign can be removed by reversing the order of the cross product in the above formula. Therefore, the gradient drift is given as

$$\vec{v}_{grad} = \frac{W_{\perp}}{qB^2}\hat{b} \times \vec{\nabla}B \,. \tag{2.27}$$

Like the curvature drift, the gradient force is dependent on the charge of the particle so it will also create a current. The current due to the gradient drift will be discussed in Section 2.5.1.

The total time independent drift of the charged particles in the magnetotail is the summation of the convective, curvature, and gradient drift. Mathematically, this is given as:

$$\vec{v}_{total} = \frac{1}{B}\vec{E} \times \hat{b} + \frac{2W_{\parallel}}{qB}\hat{b} \times \vec{K} + \frac{W_{\perp}}{qB^2}\hat{b} \times \vec{\nabla}B \,. \tag{2.28}$$

2.4.4 Polarization Drift

The last three drifts were found by assuming there were no time variations in the drift of the charged particles. However, if it is assumed that there are no time variations in the magnetic field, but there are time variations in the electric field, a drift called the polarization drift can be derived. It is derived by using equation 2.2 and inserting the Lorentz force (equation 2.3) in place of the sum of forces gives

$$q\vec{v} \times \vec{B} = m\frac{d\vec{v}}{dt} \,. \tag{2.29}$$

Crossing both sides with the magnetic field unit vector gives

$$q\left(\vec{v} \times \vec{B}\right) \times \hat{b} = m\frac{d\vec{v}}{dt} \times \hat{b} \,. \tag{2.30}$$

The left hand side of equation 2.30 was simplified at the beginning of this section. Therefore, the it becomes

$$-qB\vec{v}_{\perp} = m\frac{d\vec{v}}{dt} \times \hat{b} \,. \tag{2.31}$$

Since the magnetic field does not vary in time, it can be moved into the time derivative on the right hand side of the above equation, which gives

$$-qB\vec{v}_{\perp} = m\frac{d\left(\vec{v} \times \hat{b}\right)}{dt} \,. \tag{2.32}$$

If the electric field is varying in time, the only particle drift that will be affected is the convective drift, since it is the only drift that is dependent on the electric field. Therefore, the convective drift (equation 2.12) can be inserted into the above equation in place of the velocity vector giving

$$-qB\vec{v}_{\perp} = m\frac{d}{dt}\left(\frac{\left(\vec{E} \times \hat{b}\right) \times \hat{b}}{B}\right) \,. \tag{2.33}$$

The triple cross product can be expanded using the vector identity given in equation 2.6. It expands to

$$\left(\vec{E} \times \hat{b}\right) \times \hat{b} = \left(\hat{b} \cdot \vec{E}\right)\hat{b} - \left(\hat{b} \cdot \hat{b}\right)\vec{E} = \left(\hat{b} \cdot \vec{E}\right)\hat{b} - \vec{E} \,. \tag{2.34}$$

Assuming the electric field is perpendicular to the magnetic field simplifies the above equation to

$$\left(\vec{E} \times \hat{b}\right) \times \hat{b} = -\vec{E}_{\perp} . \tag{2.35}$$

Inserting the above equation into equation 2.33 gives

$$-qB\vec{v}_{\perp} = \frac{m}{B}\frac{d}{dt}\left(-\vec{E}_{\perp}\right) = -\frac{m}{B}\frac{d\vec{E}_{\perp}}{dt} . \tag{2.36}$$

Simplifying and solving for the perpendicular velocity gives the polarization drift $\vec{v}_{pol}$ as

$$\vec{v}_{pol} = \frac{m}{qB^2}\frac{d\vec{E}_{\perp}}{dt} . \tag{2.37}$$

This drift is time dependent. The simple model created and used in this thesis is a time-independent model. It represents the magnetic field line configuration at a point in time and does not show how the field lines evolve with time. Therefore, the polarization drift will not be examined in the context of this simple model.

2.5 Current Equations

In electrodynamics, currents are usually discussed in terms of current density. The current density is the current per unit area. Therefore, the current and current density vectors have the same direction. In general, the current density $\vec{J}$ can be defined as four separate parts

$$\vec{J} = \vec{J}_F + \vec{\nabla} \times \vec{M} + \frac{\delta \vec{P}}{\delta t} + \varepsilon_0 \frac{\delta \vec{E}}{\delta t} \tag{2.38}$$

where $\vec{J}_F$ represents the current density due to the free charges, the second term represents the bound current or the magnetization current with $\vec{M}$ being the magnetization vector, the third term

represents the polarization current with $\vec{P}$ being the polarization vector for a dielectric, and the last term represents the displacement current where ϵ_0 is the permittivity of free space. The polarization current is present in a dielectric material. Since the magnetosphere is a conductor, this term will be zero. The displacement current is dependent on the time derivative of the electric field. As discussed in Section 2.4.4, the model created in this thesis is time independent. Therefore, the displacement current cannot be tested with this model. The formula of the total current that pertains to this time independent model is given by

$$\vec{J} = \vec{J}_F + \vec{\nabla} \times \vec{M} \,. \tag{2.39}$$

The current due to free charges will be derived in Section 2.5.1 and the magnetization current will be derived in Section 2.5.2.

2.5.1 Current due to Free Charges

The free charges in the magnetosphere are a collection of various ions and electrons. The different ion species found in the magnetotail include H^+ or protons, He^+, He^{2+}, and O^+ (Kivelson and Russell, page 277). The mixture includes particles that were initially in the solar wind (He^{2+}) and the ionosphere (He^+ and O^+). However, for this analysis, only the motion of protons and electrons will be considered because these are the majority of particles in the magnetotail (Baumjohann and Treumann, page 7). Also, being a plasma, there is an assumption that there is an equal number of positive and negative charges, making the plasma overall neutral (Baumjohann and Treumann, page 1). Now, after all these assumptions are taken into consideration, the current due to freely floating protons and electrons in the magnetotail is given by (Baumjohann and Treumann, page 12)

$$\vec{J}_F = q_p n_p \vec{v}_p + q_e n_e \vec{v}_e = en\left(\vec{v}_p - \vec{v}_e\right) \tag{2.40}$$

where e is the elementary charge ($e = 1.6022 \times 10^{-19}\text{C}$), n is the particle density, $\vec{v}_p$ is the velocity of the protons, and $\vec{v}_e$ is the velocity of the electrons. The protons and electrons will be

both curvature and gradient drifting in the magnetotail. Therefore, the velocities in the above formula will be split into two terms giving

$$\vec{J}_F = en\left(\vec{v}_{p,curv} - \vec{v}_{e,curv}\right) + en\left(\vec{v}_{p,grad} - \vec{v}_{e,grad}\right). \tag{2.41}$$

The curvature and gradient drift equations are given in equations 2.22 and 2.27 respectively. Inserting these equations into the above formula gives

$$\vec{J}_F = en\left(\frac{2W_{\parallel}^{+}}{eB}\hat{b}\times\vec{K} + \frac{2W_{\parallel}^{-}}{eB}\hat{b}\times\vec{K}\right) + en\left(\frac{W_{\perp}^{+}}{eB^2}\hat{b}\times\vec{\nabla}B + \frac{W_{\perp}^{-}}{eB^2}\hat{b}\times\vec{\nabla}B\right), \tag{2.42}$$

which simplifies to

$$\vec{J}_F = \frac{2n\left(W_{\parallel}^{+} + W_{\parallel}^{-}\right)}{B}\hat{b}\times\vec{K} + \frac{n(W_{\perp}^{+} + W_{\perp}^{-})}{B^2}\hat{b}\times\vec{\nabla}B. \tag{2.43}$$

The total parallel and perpendicular energy can be defined as

$$W_{\parallel} = W_{\parallel}^{+} + W_{\parallel}^{-} \tag{2.44a}$$

and

$$W_{\perp} = W_{\perp}^{+} + W_{\perp}^{-}. \tag{2.44b}$$

Therefore, the final result for the current due to free charges is given as

$$\vec{J}_F = \frac{2nW_{\parallel}}{B}\hat{b}\times\vec{K} + \frac{nW_{\perp}}{B^2}\hat{b}\times\vec{\nabla}B. \tag{2.45}$$

2.5.2 Magnetization Current

The magnetization current is the second term in equation 2.39. It is found by taking the cross product between the Del operator and the magnetization vector. Magnetization is the product of a group of charged particles exposed to a magnetic field producing tiny dipoles that overall have a net direction. Therefore, the magnetization vector is defined as

$$\vec{M} \equiv magnetic\ dipole\ moment\ per\ unit\ volume\ . \tag{2.46}$$

In mathematical terms, the magnetization vector for plasma consisting of protons and electrons is given as

$$\vec{M} = n^{+}\vec{\mu}^{+} + n^{-}\vec{\mu}^{-} \tag{2.47}$$

where n^{+} represents the number of protons per unit volume, n^{-} represents the number of electrons per unit volume, $\vec{\mu}^{+}$ represents the magnetic dipole moment for one proton, and $\vec{\mu}^{-}$ represents the magnetic dipole moment for one electron. Assuming neutral plasma, the above equation can be simplified to

$$\vec{M} = n(\vec{\mu}^{+} + \vec{\mu}^{-})\ . \tag{2.48}$$

The magnetic moment vector for a charged particle is given as

$$\vec{\mu} = -\frac{W_{\perp}}{B}\hat{b} \tag{2.49}$$

where the negative sign indicates that the gyration of the particles causes them to be diamagnetic. Inserting this result into equation 2.48 gives

$$\vec{M} = n\left(-\frac{W_{\perp}^{+}}{B} - \frac{W_{\perp}^{-}}{B}\right)\hat{b} = -\frac{n(W_{\perp}^{+} + W_{\perp}^{-})}{B}\hat{b}\ . \tag{2.50}$$

Using the definition of the total perpendicular energy (equation 2.44b) gives the final result for the magnetization vector as

$$\vec{M} = -\frac{nW_{\perp}}{B}\hat{b}\,. \tag{2.51}$$

Now the magnetization current can be found.

The magnetization current is given as the cross product between the Del operator and the magnetization vector. Inserting equation 2.51 in place of the magnetization vector gives

$$\vec{\nabla} \times \vec{M} = -\vec{\nabla} \times \left(\frac{nW_{\perp}}{B}\hat{b}\right)\,. \tag{2.52}$$

The cross product in the above equation can be expanded using a vector identity, which is given as (Huba, page 4)

$$\vec{\nabla} \times \left(f\vec{A}\right) = f\vec{\nabla} \times \vec{A} + \vec{\nabla}f \times \vec{A}\,. \tag{2.53}$$

This changes equation 2.52 to

$$\vec{\nabla} \times \vec{M} = -\frac{nW_{\perp}}{B}\vec{\nabla} \times \hat{b} - \vec{\nabla}\left(\frac{nW_{\perp}}{B}\right) \times \hat{b} \tag{2.54}$$

The second term in the above equation can be expanded using another vector identity (Huba, page 4), which is given as

$$\vec{\nabla}(fg) = g\vec{\nabla}f + f\vec{\nabla}g\,. \tag{2.55}$$

After this expansion, equation 2.54 now becomes

$$\vec{\nabla} \times \vec{M} = -\frac{nW_{\perp}}{B}\vec{\nabla} \times \hat{b} - \frac{\vec{\nabla}(nW_{\perp}) \times \hat{b}}{B} - nW_{\perp}\vec{\nabla}\left(\frac{1}{B}\right) \times \hat{b}\,. \tag{2.56}$$

The last term in the above equation can be simplified giving

$$\vec{\nabla} \times \vec{M} = -\frac{nW_{\perp}}{B}\vec{\nabla} \times \hat{b} - \frac{\vec{\nabla}(nW_{\perp}) \times \hat{b}}{B} + \frac{nW_{\perp}}{B^2}\vec{\nabla}B \times \hat{b}\,. \tag{2.57}$$

The cross product in the first term in the above equation can be represented by another cross product, which is

$$\vec{\nabla} \times \hat{b} = \hat{b} \times \vec{K}\,. \tag{2.58}$$

The proof is shown in Appendix C. Therefore, inserting the above equation into equation 2.57 and reversing the order of the cross products gives the final form of the magnetization current as

$$\vec{\nabla} \times \vec{M} = -\frac{nW_{\perp}}{B}\hat{b} \times \vec{K} + \frac{1}{B}\hat{b} \times \vec{\nabla}(nW_{\perp}) - \frac{nW_{\perp}}{B^2}\hat{b} \times \vec{\nabla}B\,. \tag{2.59}$$

2.5.3 Total Current

Inserting the results for the current due to free charges (equation 2.45) and magnetization current (equation 2.59) into the total current formula (equation 2.39) gives

$$\vec{J} = \frac{2nW_{\parallel}}{B}\hat{b} \times \vec{K} + \frac{nW_{\perp}}{B^2}\hat{b} \times \vec{\nabla}B - \frac{nW_{\perp}}{B}\hat{b} \times \vec{K} + \frac{1}{B}\hat{b} \times \vec{\nabla}(nW_{\perp}) - \frac{nW_{\perp}}{B^2}\hat{b} \times \vec{\nabla}B\,. \tag{2.60}$$

Cancelling and combining like terms gives the general result for the current in the magnetotail in terms of energy as

2.61

$$\vec{J} = \frac{n(2W_{\parallel} - W_{\perp})}{B}\hat{b} \times \vec{K} + \frac{1}{B}\hat{b} \times \vec{\nabla}(nW_{\perp}) \, .$$

The current can be defined in terms of pressures by using the following relations between pressure and energy (derivations are in Appendix D):

$$p_{\parallel} = 2nW_{\parallel} \qquad 2.62a$$

and

$$p_{\perp} = nW_{\perp} \, . \qquad 2.62b$$

Converting the energy variables to pressure in equation 2.61 gives the general result for the current in the magnetotail in terms of pressure as

$$\vec{J} = \frac{p_{\parallel} - p_{\perp}}{B}\hat{b} \times \vec{K} + \frac{1}{B}\hat{b} \times \vec{\nabla}p_{\perp} \, . \qquad 2.63$$

Equations 2.61 and 2.63 represent the standard current formulas found in most textbook (e.g. Parks, 2004 see Chapter 7). However, in the case of the magnetotail, two terms need to be added in order to describe special cases. These terms include a current due to the convective drift and a current due to "unmagnetized" protons. These extra terms are derived in the following paragraphs.

In general, the convective drift will not cause a current because it causes the protons and electrons to flow in the same direction. If there are an equal number of electrons and protons, then there will not be an overall current due to the convective drift. A current can only happen when there are either more protons than electrons or vice versa. In other words, there has to be a pool of excess positive or negative charge. In this case, it is useful to define the particle density of the protons and electrons in terms of the base density plus the amount of extra particles that offsets the neutrality of the plasma. Mathematically, this is represented as

$$n_p = n + n_{p,excess} \tag{2.64a}$$

for the protons and

$$n_e = n + n_{e,excess} \tag{2.64b}$$

for the electrons. In a neutral plasma, both $n_{p,excess}$ and $n_{e,excess}$ will be zero. In certain places in the magnetotail, either $n_{p,excess}$ or $n_{e,excess}$ will be nonzero, which will lead to a convective current. The convective current can be mathematically found using the same method used for finding the currents due to the curvature and gradient drift. Therefore, the convective current $\vec{J}_{conv}$ is given as

$$\vec{J}_{conv} = en_p\vec{v}_{conv} - en_e\vec{v}_{conv} = e\big(n_p - n_e\big)\vec{v}_{conv}\,. \tag{2.65}$$

Inserting the equations for the proton and electrons density (equations 2.64a and 2.64b) and the equation for the convective drift (equation 2.12) into the above equation gives

$$\vec{J}_{conv} = e\big(n + n_{p,excess} - n - n_{e,excess}\big)\left(\frac{\vec{E}\times\hat{b}}{B}\right) = \frac{e\big(n_{p,excess} - n_{e,excess}\big)}{B}\vec{E}\times\hat{b}\,. \tag{2.66}$$

This describes the convective current due to excess positive or negative charge in the plasma.

In the magnetotail, there is an area in the center of the NS called the inner neutral sheet (INS) where the protons are "unmagnetized". The NS geometry is such that at the center, there is a reversal of the x-component of the magnetic field from negative on the south side to positive on the north side. At the center, where the x-component is zero, the field is purely northward. The reversal of the x-component causes the proton gyration sense to change, which causes them to have "serpentine orbits" (Speiser, 1965). In simplistic terms, the protons can be deemed unmagnetized and therefore they do not respond to the magnetic field at all. The electrons remain magnetized because their gyroradius is much smaller than the protons' gyroradius and thus are not affected by the reversal in the x-component. When the protons are unmagnetized,

they do not have convective, curvature, or gradient drift. Instead, they will be accelerated due to the Coulomb force since an electric field called the dawn to dusk electric field is present in the magnetotail. As the unmagnetized protons travel through the electric field, some work is done on them. The protons will start traveling in the direction of the dawn to dusk electric field, which is the positive y-direction (this will be shown in Section 2.6.3). Mathematically, the work that the protons undergo is given by

$$W = F_E \Delta y \tag{2.67}$$

where Δy is the distance that the unmagnetized protons travel in the y-direction. Inserting the definition of the Coulomb force (equation 2.11) into the above equation gives

$$W = qE\Delta y = eE_{DD}\Delta y \tag{2.68}$$

where E_{DD} is the dawn to dusk electric field. Setting the work to equal the kinetic energy, the associated speed can be found. This gives

$$\frac{1}{2} m_p v_{y,un}^2 = eE_{DD}\Delta y \tag{2.69}$$

where m_p is the mass of the proton and $v_{y,un}$ is the speed of the unmagnetized protons. Solving the above equation for speed gives

$$v_{y,un} = \sqrt{\frac{2eE_{DD}\Delta y}{m_p}} \, . \tag{2.70}$$

The y-velocity increase due to this work will be in the direction of the dawn to dusk electric field. This gives the final result for the velocity due to the unmagnetized protons as

$$\vec{v}_{y,un} = \sqrt{\frac{2eE_{DD}\Delta y}{m_p}}\,\hat{y}\,. \tag{2.71}$$

The current due to these energized unmagnetized protons can be found using the current due to free charges method. Therefore, the unmagnetized current $\vec{J}_{un}$ is given as

$$\vec{J}_{un} = en_{p,un}\vec{v}_{y.un} \tag{2.72}$$

where $n_{p,un}$ represents the number of protons that are unmagnetized. Inserting the equation for the unmagnetized velocity (equation 2.71) into the above equation gives

$$\vec{J}_{un} = en_{p,un}\sqrt{\frac{2eE_{DD}\Delta y}{m_p}}\,\hat{y}\,. \tag{2.73}$$

This represents the current due to unmagnetized protons in the magnetotail. As stated before, the protons in the thinned down region of the NS will have serpentine orbits instead of the normal gyration motion. This represents the protons acting as both magnetized and unmagnetized because they are attempting to respond to the magnetic field but are getting confused due to the changing magnetic field in their gyration. Therefore, the protons will not respond as purely unmagnetized in this region, but only partially (Speiser, 1965). A factor f needs to be added to equation 2.73 in order to account for only a fraction of the motion of the protons behaving as unmagnetized. Equation 2.73 becomes

$$\vec{J}_{un} = fen_{p,un}\sqrt{\frac{2eE_{DD}\Delta y}{m_p}}\,\hat{y} \tag{2.74}$$

where f is a value that is less than or equal to one that represents the fraction of proton motion that is behaving as unmagnetized.

Adding the results for the convective current (equation 2.66) and the current due to the unmagnetized protons (equation 2.74) to the general current formula (equation 2.63) gives the total current in the magnetotail as

$$\vec{J}_{total} = \frac{p_{\parallel} - p_{\perp}}{B}\hat{b} \times \vec{K} + \frac{1}{B}\hat{b} \times \vec{\nabla} p_{\perp} + \frac{e\left(n_{p,excess} - n_{e,excess}\right)}{B}\vec{E} \times \hat{b} + fen_{p,un}\sqrt{\frac{2eE_{DD}\Delta y}{m_p}}\hat{y}\,. \tag{2.75}$$

Now that equation for the current in the magnetotail has been found, the direction of the current can be theoretically analyzed. This is done in the next section.

2.6 Current Direction in the Magnetotail

The direction of the current in the magnetotail is dependent on the combination of the four terms presented in equation 2.75: the first term is dependent on the difference between parallel and perpendicular pressure and the cross product between the magnetic field unit vector and the curvature vector; the second term is dependent on the cross product between the magnetic field unit vector and the gradient of the perpendicular particle pressure; the third term is dependent on an excess of either positive or negative charge and the cross product between the electric field vector and the magnetic field unit vector; and the fourth term is dependent on the direction of the electric field vector, which is the positive y-direction. The direction of the current produced by these terms will be analyzed in subsections 2.6.1, 2.6.2, and 2.6.3 respectively and the overall current direction in the magnetotail will be analyzed in Subsection 2.6.4.

2.6.1 Direction of the Cross Product between the Magnetic Field Unit Vector and the Curvature Vector in the Magnetotail

As shown in Section 2.3.1, the stretched field lines in the SPS have inflection points. In other words, the curvature can change from concave to convex along a stretched field line. The direction of the cross product between the magnetic field unit vector and the curvature vector on a stretched field line in the noon-midnight meridian plane is shown in Figure 2.14. In the equatorial concave region of a stretched field line, the cross product $\hat{b} \times \vec{K}_{NS}$ produces a current in the positive y or westward direction. However, in the convex DZ regions above and below the NS, the cross product $\hat{b} \times \vec{K}_{DZ}$ produces a current in the negative y or eastward direction. The first term in the current equation is also dependent on the difference between the parallel and perpendicular pressure. Therefore, if the overall parallel pressure is greater than the perpendicular pressure, the current produced by the first term in equation 2.75 will be westward in the NS and eastward in the DZs.

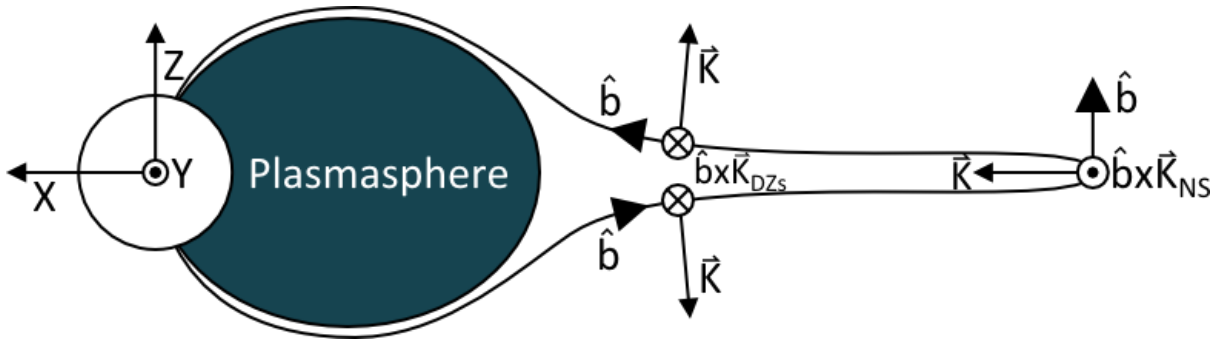

Figure 2.14 Cross product between the magnetic field unit vector and the curvature vector has a westward direction in the NS and an eastward direction in the DZs in the noon-midnight meridian plane.

2.6.2 Direction of the Cross Product between the Magnetic Field Unit Vector and the Gradient of the Perpendicular Particle Pressure in the Magnetotail

As shown in equation 2.62b, the perpendicular particle pressure is dependent on the number of particles as well as the perpendicular energy of the particles. The behavior of the

perpendicular pressure in the magnetotail can be determined by analyzing the deep minimum in the magnetotail that occurs in the NS. This deep minimum was first inferred by Erickson (1984). It was confirmed theoretically by Hau et al. (1989) after they analyzed a two-dimensional force-balanced magnetic field model they created in order to study convection in the magnetotail. They found that a steady state in magnetotail convection can only be achieved if there is a deep minimum in magnetic field at the inner edge of the plasma sheet. They also found that there was a maximum in the particle pressure in the same location as the deep minimum in the magnetic field. This location corresponds to the earthward edge of the NS in the stretched magnetic field configuration presented in this thesis. In 2010, Saito et al. presented satellite data that verified this deep minimum at the center of the plasma sheet in the magnetotail. They found a minimum in the z-component of the magnetic field that began around 20 to 30 minutes prior to onset of a substorm. In the center of the NS, the x-component of the magnetic field is zero. Therefore, the minimum in the magnetic field would be represented by a minimum in the z-component of the magnetic field. Saito et al. (2010) proposed a profile of the z-component of the magnetic field based upon their satellite measurements. It is shown in the second panel in Figure 2.15.

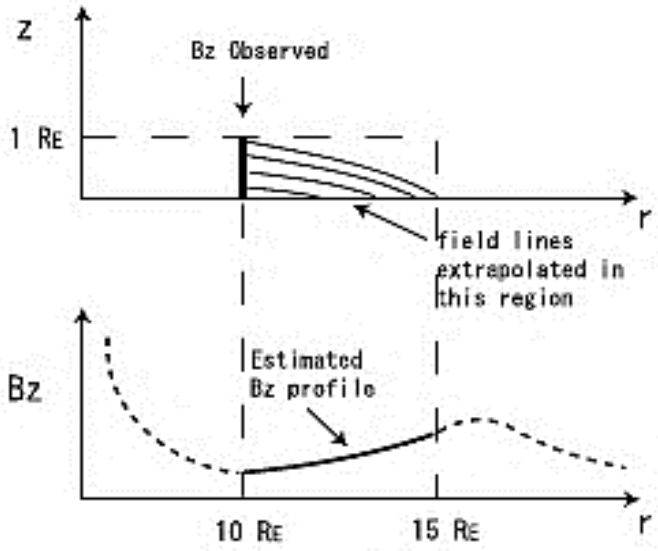

Figure 2.15 Proposed profile of the z-component of the magnetic field for the center of the NS based upon satellite measurements (Saito et al., 2010).

The first panel shows the shape of the field lines (without the dipole part) in the magnetotail. This was the first physical evidence of the deep minimum in the magnetic field and, therefore, supportsthe steady state magnetotail convection proposed in a model by Hau et al. (1989). Therefore, the results from Saito et al. also confirm a maximum in the particle pressure in the NS. It will be assumed that this means there is specifically a maximum in the perpendicular particle pressure in the NS. This assumption will be justified in Section 2.6.4.

Gradient vectors point from lower to higher values. Therefore, the gradient of the perpendicular particle pressure in the SPS will point toward the maximum that is present in the NS. The direction of the cross product between the magnetic field unit vector and the gradient of the perpendicular particle pressure in the noon-midnight meridian plane is shown in Figure 2.16. The maximum of perpendicular particle pressure in the NS causes the current dependent on this cross product to be in the westward direction in all sections of the magnetotail (both NS and DZs). This current represents the current produced by the second term in equation 2.75.

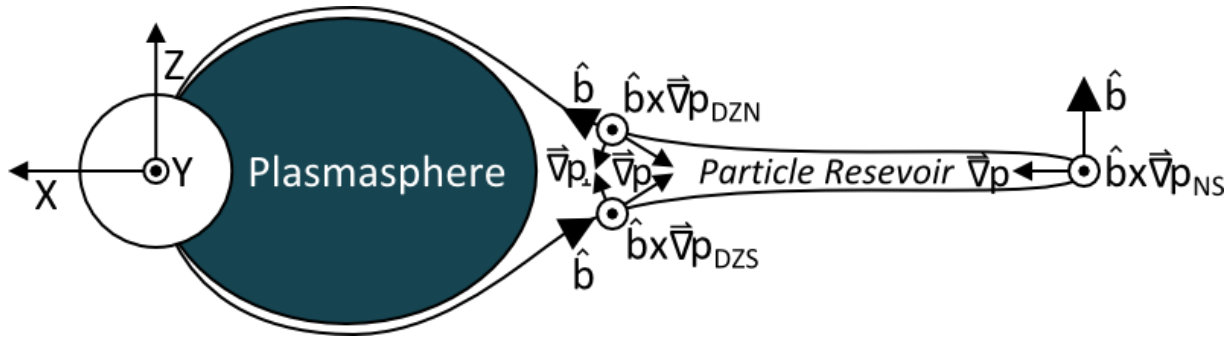

Figure 2.16 Cross product between the magnetic field unit vector and the gradient of the perpendicular particle pressure has a westward direction in both the NS and DZs in the noon-midnight meridian plane.

2.6.3 Direction of the Cross Product between the Electric Field Vector and the Magnetic Field Unit Vector in the Magnetotail

In the magnetotail, it is commonly accepted that an electric field is present that is directed from the dawn side to the dusk side. It is called the dawn to dusk electric field $(\vec{E}_{DD})$. One

explanation for the dawn to dusk electric field is the transfer of plasma, momentum, and energy from the solar wind into the magnetosphere (Eastman et al., 1976). Eastman et al. based this theory upon experimental findings of Baker and Hammel (1965) and summarized the results from the experiment as "a plasma stream can traverse a magnetic field region by becoming electrically polarized, its polarization field, $\vec{E}$, opposing the Lorentz force on the plasma particles" (Eastman et al., 1976). The shocked solar wind in the magnetosheath acts as the plasma stream and the LLBL acts as the magnetic field region. The Lorentz force is given in equation 2.3. It causes protons to go one way and the electrons to go the other. In the LLBLs, this sets up the dawn to dusk electric field across the magnetotail. The situation in the equatorial plane is depicted for the dawn LLBL in Figure 2.17. This figure depicts a zoomed in region on the dawn side of the LLBL with the magnetosphere being below the layer and the magnetosheath being above. As shown in Figure 2.2, the region next to the LLBL is the DPS, which contains a quasi-dipolar magnetic field. This magnetic field in the equatorial plane will be directed in the positive *z*-direction, as shown in Figure 2.17.

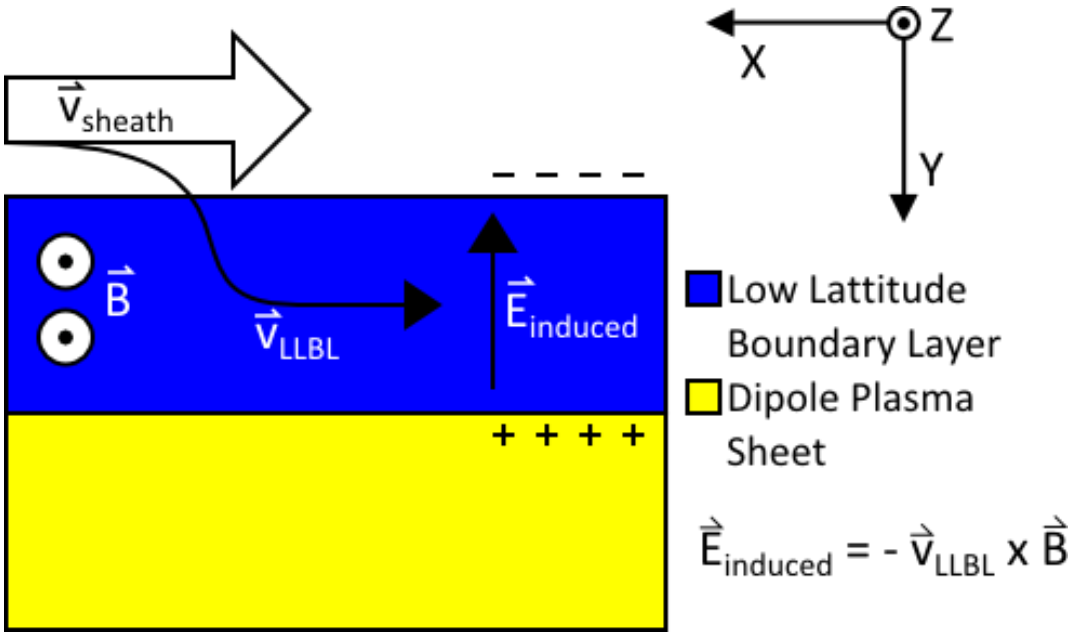

Figure 2.17 In the dawn LLBL, the Lorentz force creates a buildup of positive charge on the DPS/LLBL boundary.

The shocked solar wind inside the magnetosheath is moving anti-earthward. Some of this momentum and plasma gets transferred into the LLBL. This produces an electric field in both the dawn and dusk portions of the LLBL. On the dawn side, the Lorentz force creates an excess of positive charge on the edge of the LLBL connected to the plasma sheet. On the dusk side, the induced electric field creates an excess of negative charge on the edge of the LLBL connected to the plasma sheet. This creates an overall electric field in the magnetotail pointing from dawn to dusk, as shown in Figure 2.18.

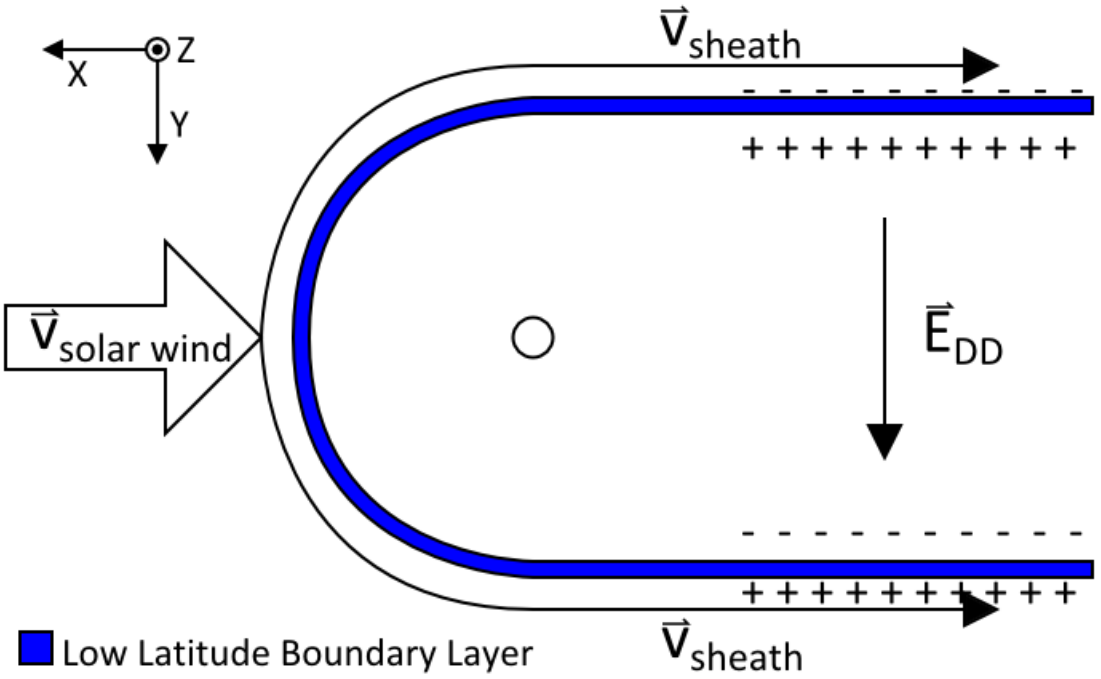

Figure 2.18 The dawn to dusk electric field is created by the excess positive charge on the dawn side inner LLBL edge and negative charge on the dusk side inner LLBL edge.

The excess of charge in the magnetopause will try to restore neutrality. It can do this by traveling along the magnetopause to the other pool of excess charge. This is the source of the magnetopause current. The electrons on the dawn side will travel to the protons on the dusk side and vice versa causing a current from the dusk side of the magnetopause to the dawn side. This is shown in Figure 2.19.

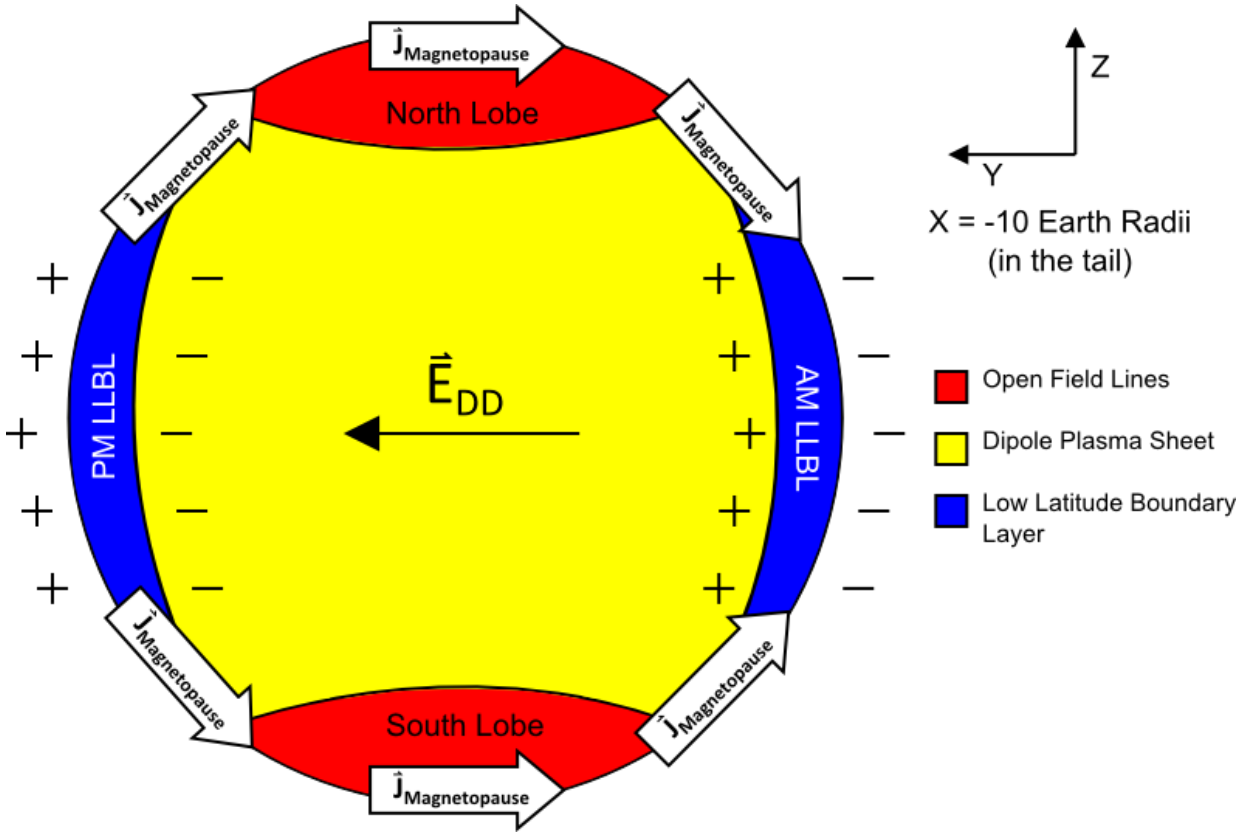

Figure 2.19 The magnetopause current flows along the magnetopause from the dusk side to the dawn side.

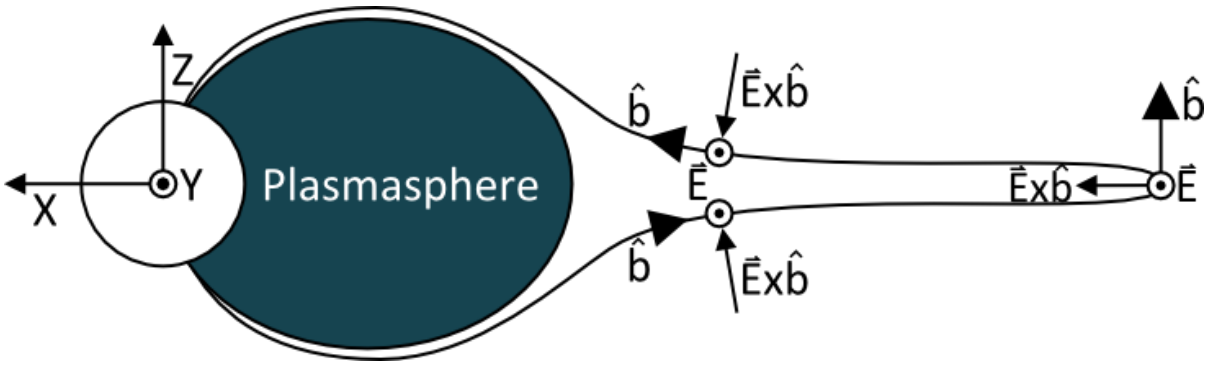

Figure 2.20 Direction of the cross product between the dawn to dusk electric field and the magnetic field unit vector is directed towards the NS in the DZs and earthward in the NS.

The cross product between the dawn to dusk electric field and the magnetic field unit vector will lead insight into the direction of the current produced by the third term in the overall current formula (equation 2.75). The direction of this cross product in the noon-midnight

meridian plane is shown in Figure 2.20. This represents the direction that both the protons and electrons will travel due to the convective drift. The convective drift in the DZs will cause the plasma to drift towards the NS. This will fill the NS will plasma over time. The convective drift in the NS will cause the electrons to travel earthward. The protons will not convective drift in the NS because they are unmagnetized in the INS. The specific currents produced by this drift will be analyzed in the next section.

As a brief side note, Figure 2.20 shows how the convective drift supports the shape of stretched field lines that was presented in Section 2.3.1. Since the plasma is "frozen" into the magnetic field, as discussed in Section 2.3.2, the shape of the field lines will change as the plasma convective drifts. The convective drift will cause both the protons and electrons to flow towards the NS in the DZs and earthward in the NS. Therefore, the field lines will naturally drift into the shape that contains four inflection points. The field lines also drift earthward and become shorter in length over time to relieve the magnetic stress associated with stretching of the field lines (a dipole line being the state of lowest energy and least stress). This is physically expected as the field lines are created at the DTNL due to the earthward motion of the plasma in the reconnection jet. This earthward motion of the field lines is an important factor in determining the overall current in the magnetotail, which is discussed in the next section.

2.6.4 Total Current Direction in the Magnetotail

Each term in equation 2.75 plays a different role in the magnetotail. Before the total current direction can be discussed, the state of the charged particles in the magnetotail needs to be defined. As stated before, the magnetotail is mainly made up of electrons and protons. These charged particles do not simply travel along a magnetic field line, they gyrate around it. The gyroradius or radius of this motion is given by (Baumjohann and Treumann, page 14)

$$r_g = \frac{mv_\perp}{qB} \,. \tag{2.76}$$

Since electrons have a much smaller mass than protons, the electrons will have a much smaller gyroradius than protons.

The charged particles in the magnetotail abide by two adiabatic invariants if adiabatic conditions are met. The first invariant states that the magnetic moment of a particle stays constant. This is mathematically represented as

$$\mu = \frac{W_\perp}{B} = \text{constant}\,. \tag{2.77}$$

The characteristic time scale for this invariant is the gyroperiod, so adiabatic conditions apply for changes that occur slower than this time. The second adiabatic states that the momentum along one bounce (or how long it takes the particle to travel from one bounce point to the opposite point and back to the original point) stays constant. Mathematically, it is represented as

$$J = \oint m v_\parallel ds_\parallel = m\langle v_\parallel \rangle \oint ds_\parallel = m\langle v_\parallel \rangle l_\parallel = \text{constant} \tag{2.78}$$

where the triangle brackets represent the average parallel speed along the bounce motion and $l_\parallel$ represents the length of bounce motion. The characteristic time for the second invariant is the time for a complete bounce cycle. For protons, this can be about ten minutes in the magnetotail so changes in the magnetic field faster than this can occur and lead to the second adiabatic invariant being not valid. For electrons, the time to complete a bounce cycle is on the order of seconds. Therefore, the second adiabatic invariant typically holds for electrons in the magnetotail.

Each particle will also have a pitch angle, which is the angle between its velocity vector and the magnetic field. If a particle has a low pitch angle, it is basically parallel to a magnetic field and if it has a pitch angle of 90°, its motion is perpendicular to the magnetic field. The pitch angle of a particle will change as it moves along the field line. The lowest pitch angle value is at the equator. As it travels away from the equator along the magnetic field line, the pitch angle will increase until 90° or it gets absorbed into the atmosphere if it makes it all the

way there. After hitting 90°, the particle reverses its motion and continues travelling along the magnetic field line. An isotropic distribution of particles means that there are particles with equatorial pitch angles ranging from 0° to 90°. An anisotropic distribution of particles means that there are particles with equatorial pitch angles only around one value.

The model of the nightside magnetosphere presented in this thesis contains a thin NS in the center of the magnetotail. According to Cowley (1978), this configuration is only possible when parallel pressure (and therefore energy) is greater than the perpendicular pressure/energy. For this case, "a thin, non-adiabatic current layer will in general form at the sheet center, usually embedded within a much broader adiabatic current distribution" (Cowley, 1978). Therefore, the NS is split into two regions: the inner neutral sheet (INS) and the outer neutral sheet (ONS). The INS is the center of the NS and the ONS is the rest of the NS that surrounds the INS. Non-adiabatic conditions are created when the protons become unmagnetized in the INS. However, the electrons remain magnetized because they have a much smaller gyroradius than the protons and therefore are not affected by the reversal in the x-component of the magnetic field at the center of the NS. In summary, the ONS is a region of the NS where the protons remain adiabatic and magnetized and the INS is a region of the NS where the protons are unmagnetized and therefore non-adiabatic. The protons in the INS will be scrambled and scattered, eventually returning them to an isotropic distribution (Cowley, 1978). The electrons remaining magnetized during this will continually be in the anisotropic state around 0° pitch angles.

The adiabatic invariants also support an anisotropic distribution of pitch angles in the magnetotail. After the closed stretched field lines are created at the DTNL, they start moving earthward. The field line becomes shorter as it gets closer to the Earth. As the field line changes length, the second adiabatic invariant describes how the average parallel speed will change. Comparing a field line at two different points in time where it has different lengths gives

$$m\langle v_{\parallel}\rangle_1 l_{\parallel,1} = m\langle v_{\parallel}\rangle_2 l_{\parallel,2}\,, \tag{2.79a}$$

which can be rearranged to

$$\frac{l_{\parallel,1}}{l_{\parallel,2}} = \frac{\langle v_{\parallel} \rangle_2}{\langle v_{\parallel} \rangle_1} \,. \tag{2.79b}$$

If point 1 describes a point in time where the field line is longer than point 2, then the average parallel speed at point 2 must be greater than the average parallel speed at point 1. Therefore, the field line gains parallel speed, and thus parallel energy, as it travels towards the Earth from the DTNL. The definition of parallel speed is given as

$$v_{\parallel} = v \cos \alpha \tag{2.80}$$

where v is the total speed of a charged particle that stays constant along a field line and α is the pitch angle of a charged particle. Therefore, in order to gain parallel speed as the field line moves earthward, either the total speed needs to go up or the pitch angle of the particle needs to go down. In order to determine which one, the first adiabatic invariant needs to be analyzed. By using the first adiabatic invariant, the perpendicular energy and the magnetic field can be compared at different points in the magnetotail. Comparing the equatorial value of the two previous points in time of a field line using the first adiabatic invariant gives

$$\frac{W_{\perp,1}}{B_{01}} = \frac{W_{\perp,2}}{B_{02}} \,, \tag{2.81a}$$

which can be rearranged to

$$\frac{B_{02}}{B_{01}} = \frac{W_{\perp,2}}{W_{\perp,1}} \tag{2.81b}$$

where B_{01} is the magnetic field value at the center of the NS when the field line is farther away from the Earth and B_{02} is the magnetic field value at the center of the NS when the field line is closer to the Earth. The magnetic field inside the NS remains very low throughout the SPS. There is a deep minimum in the magnetic field at the most earthward edge of the NS, but the difference between this and other places in the NS is still relatively close especially when comparing to the change in the length of the field line. Therefore, as the magnetic field line

moves closer to the Earth, the particle does not gain a lot of perpendicular energy. If anything, the particle loses perpendicular energy because the equatorial magnetic field goes down as the field line gets closer to the Earth because it enters the deep minimum region. The perpendicular energy can be described in terms of pitch angle as

$$W_{\perp} = \frac{1}{2} m v_{\perp}^2 = \frac{1}{2} m v^2 \sin^2 \alpha \tag{2.82}$$

The perpendicular energy is dependent on the sine of the pitch angle, thus it will have a lower value if there is a lower pitch angle. Therefore, if the perpendicular energy of the particle goes down and the parallel energy of the particle goes up as the field line travels towards the Earth, then the pitch angle of the particle must go down. Thus, particles are expected to have a low equatorial pitch angle giving an anisotropic distribution in the magnetotail, as discussed in the previous paragraph.

In terms of the current, this makes each term in equation 2.75 play a role in different parts of the magnetotail. The first term depends on the difference between the parallel and perpendicular energies and the cross product between the magnetic field unit vector and the curvature vector. This current will only be carried by the electrons, since they are anisotropic. The overall current produced by the protons will essentially be zero because of their isotropic distribution. Therefore, the protons will not contribute any curvature current. Since the parallel energy will definitely be greater than the perpendicular energy, the direction of the current produced by this term will follow what is presented in Figure 2.14. Therefore, there will be an eastward current in the DZs and a westward current in the NS.

The second term in equation 2.75 is dependent on the perpendicular energy. The electrons will not produce a very strong current from this term because they are mainly travelling in the parallel direction. However, the protons will contribute some current due to this term since they have an isotropic distribution. The current produced by this term with the protons will not be that strong compared to the curvature current produced by the electrons. In Section 2.6.2, the direction of the current produced by this term was found under the assumption that since

there is a particle pressure maximum in the center of the NS then there is a perpendicular particle pressure maximum as well. This assumption is justified because the perpendicular particle pressure depends on both the number density as well as perpendicular current. As discussed previously, the perpendicular energy does not change greatly along the center of the NS. Therefore, there will not be a very significant gradient in the perpendicular energy. However, it is well established that the NS is filling up with particles, meaning that it is a highly dense region compared to other areas in the magnetotail. Therefore, the gradient in the perpendicular particle pressure will mainly be determined by the gradient in the number density. Thus, the direction of the current shown in Figure 2.16 will describe the second term in equation 2.75. Therefore, the second term will produce a westward current in both the NS and DZs. This current will enhance the westward current in the NS produced by the curvature current of the electrons but will only dampen the eastward current in the DZs that is produced by the curvature current of the electrons.

The third term in equation 2.75 is dependent on the charge of the particle and the cross product between the electric field vector and the magnetic field unit vector. This current is only present when there is an excess of either positive or negative charge. In the magnetotail, this occurs in five locations. In the INS, the ions are unmagnetized and thus are not convective drifting along with the electrons anymore. As the electrons move earthward due to the convective drift, there will be an overall current that will be directed anti-earthward. Also, the electrons are separating from the protons, creating an electron reservoir at the earthward end of the INS and a proton reservoir at the other end of the INS. This current and these reservoirs are an important generator current and source of particles for auroral activity come onset. The other four locations are in the DZs, two in the DZS and two in the DZN. The eastward current in the DZs runs into problems when it hits the edge of the SPS. Outside the SPS in the DPS, there is a westward current. Therefore, there is a pile up of negative charges on the dusk edge of the SPS and a pile up of positive charges on the dawn edge of the SPS. The convective drift causes both particles to travel towards the NS, creating a current towards the NS on the dawn edge of the SPS and a current away from the NS on the dusk edge of the SPS. These currents close the current loop systems in the magnetotail, creating a double vortex current system. This will be discussed in more detail later in this section.

The fourth term in equation 2.75 describes the unmagnetized protons in the INS. The protons are travelling in response to the westward dawn to dusk electric field. This creates a westward current in the INS, which will just enhance the westward current that is already there due to the curvature current of the electrons. Once the protons become unmagnetized, they still carry their forward momentum. This will cause them to travel towards the anti-earthward end of the NS, enhancing the proton reservoir discussed in the previous paragraph.

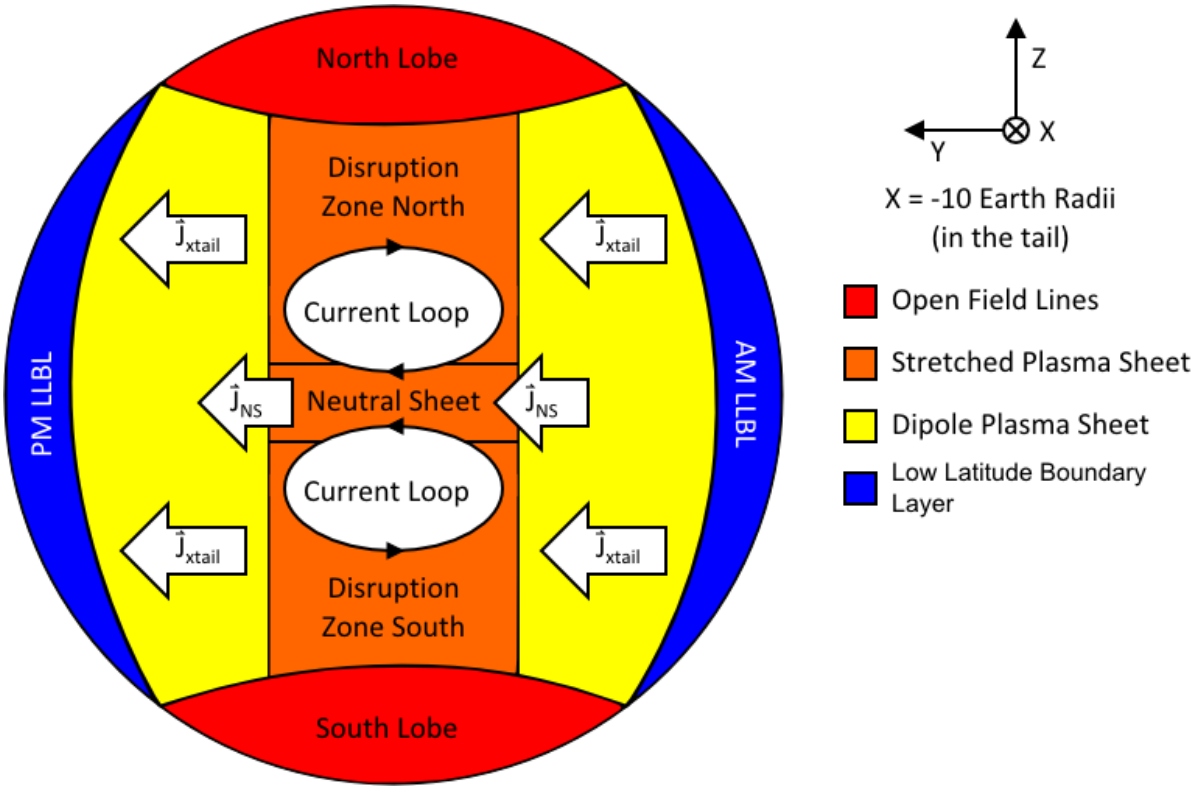

Figure 2.21 Double vortex current system in the SPS consists of an eastward current in the DZs that closes westward in the NS.

After taking the directions of all four terms into consideration, the overall current system in the magnetotail is shown in Figure 2.21. The current travels eastward in the DZs and westward in the NS. The convective current closes the current loop creating the double vortex configuration shown in Figure 2.21. The two current loops intensify the stretching of the closed stretched field with the magnetic field they create (into the page for DZN and out of the page for DZS). This proposed current system supports the findings of Mitchell et al. (1990) and Williams et al. (1990). Mitchell et al. (1990) claims throughout most of the growth phase, the current is

provided by the curvature current due to the electrons. Just prior to onset, the most intense current is carried by the unmagnetized protons in the INS (Mitchell et al., 1990). The protons take over the current prior to onset because as they are accelerated through the INS due to the Coulomb force, they gain energy (Williams et al., 1990). This intense current in the INS creates the velocity shear that is needed in order to change the Kelvin-Helmholtz instability from kink mode to sausage mode.

The cross tail current travelling in the DPS, which is generated by the LLBLS, cannot travel through the DZ transition. It has two available paths: it can either travel through the NS or divert around the SPS into the TPS. This is the first disruption presented in the double disruption substorm theory by Sofko et al. (2013). The second disruption, after enough conductivity has built up in the ionosphere, is the crosstail current diverted down into the ionosphere through FACs. This creates a make shift substorm current wedge. McPherron et al. (1973) proposed that a portion of the crosstail current is diverted down magnetic field lines to the ionosphere, crosses westward through the auroral zone, and then travels back to the magnetotail through magnetic field lines. This process is shown in Figure 2.22.

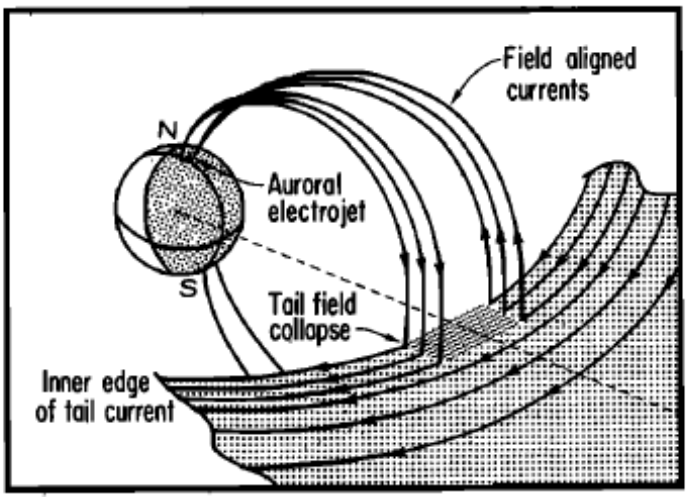

Figure 2.22 The cross tail current is diverted during the growth phase of a substorm (McPherron et al., 1973). It is diverted down to the ionosphere, crosses from the dawn to dusk auroral electrojet, and then returns to the magnetotail.

Even though this was proposed many years ago, the reason for the disruption of the crosstail current has been a source of contention. The nightside magnetosphere model presented here provides an explanation, namely the crosstail current is diverted around the SPS. Thus, the geometry of the stretched magnetic field lines presented in Section 2.3.1 leads to a current system in the magnetotail that explains the disruption of the crosstail current.

Another FAC current system that is present in the magnetotail originates from the SPS. The double vortex current system is the first main current system in the SPS and the NS FAC system is the second. It is represented in Figure 2.23.

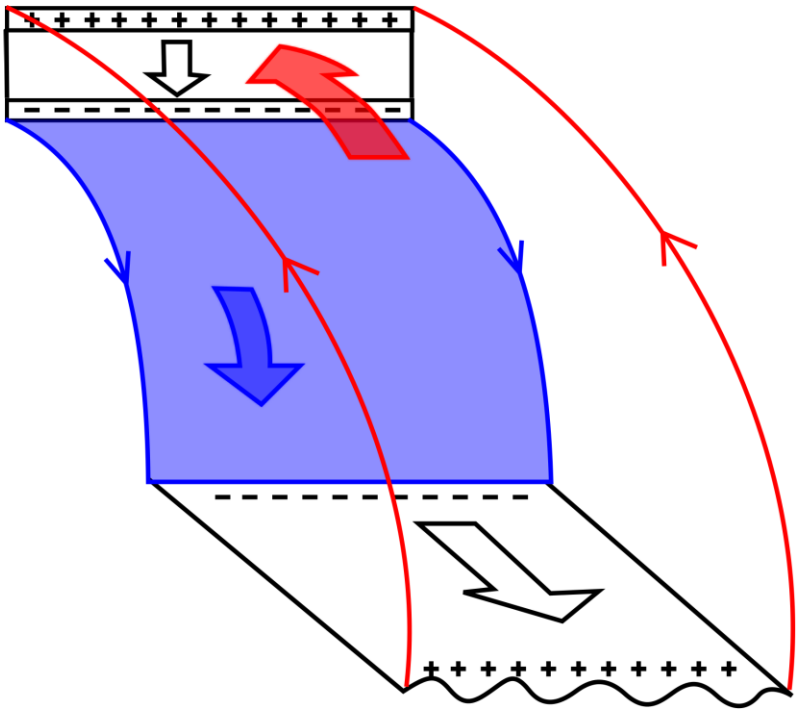

Figure 2.23 NS FAC system is created by the anti-earthward generator current present in the INS (bottom horizontal white plane). The electron reservoir maps down to low latitudes in the ionosphere (top vertical white plane) through an upward FAC (blue). The proton reservoir maps down to high latitudes in the ionosphere through a downward FAC (red). The system closes in the ionosphere through an equatorward Pedersen current (Provided by Dr. Kathryn McWilliams).

As mentioned previously, there is an anti-earthward generator current present in the INS with an electron reservoir on the earthward end of the INS and a proton reservoir on the anti-earthward

end of the INS. This is the source of the NS FAC system. The two particle reservoirs are created by the electrons convective drifting earthward while the protons do not because they are unmagnetized in the INS. The proton reservoir maps down to the ionosphere through a downward FAC at high latitudes and it is shown by the red path in Figure 2.23; the electron reservoir maps down to the ionosphere through an upward FAC at lower latitudes and it is shown by the blue path in Figure 2.23. The system closes equatorward in the ionosphere through a Pedersen current where energy can be dissipated through Joule heating. This FAC system is responsible for the pre-onset electron auroral arc that is a critical element in the growth phase of substorms. However, this topic is beyond the scope of this thesis as geometry is the focus rather than substorms. But, it is important to define this current system as it results directly from the geometry of the stretched magnetic field lines.

2.7 Summary

In this chapter, a model of the nightside magnetosphere was presented where the shape of the stretched field lines creates a double vortex current system in the magnetotail. The magnetotail consists of four major regions: plasmasphere, magnetic lobes, LBLL, and PS. The PS is split into three different regions based on the shape of the closed field lines: the first region is the DPS, which contains quasi-dipolar field lines; the second region is the TPS, which contains field lines that are transitioning between dipole and stretched; and the last region is the SPS, which contains stretched field lines. The SPS further splits into three regions based on the direction of the current present. The NS is the central region of the stretched field lines and contains a westward current. The DZs are the regions above and below the NS and contain eastward currents. Overall, the current system is a double solenoid with the current flowing eastward in the DZs and closing westward in the NS, as shown in Figure 2.21.

The oppositely directed currents occur in the SPS due to the shape of the field lines. The stretched field lines have inflection points that separate regions of concave and convex curvature in the field lines. The DZs are regions of convex curvature and the NS is a region of concave curvature. The stretched field lines have these inflection points because they need to drape over the plasmasphere and TPS in order to facilitate antiparallel reconnection and the convective drift

of the plasma naturally moves the plasma into this field line formation. As the NS fills with plasma, a deep minimum in the magnetic field is formed on the earthward end of the NS. This creates intense curvature in the most earthward stretched field lines. The double vortex current system also supports this shape of field line because the current loops enhance the stretching of the magnetic field lines. Furthermore, Shen et al. (2003) show from Cluster measurements that there is a change of curvature sense in the magnetotail, which supports the field line shape presented in this thesis.

The growth and decay of the SPS follows the three phases of a substorm. In the growth phase, the stretched field lines are created by two lobe field lines antiparallel reconnecting. Newly created stretched field lines move earthward. During the growth phase, the SPS begins to fill with stretched field lines and the NS begins to thin. The thinly stretched region of the field line facilitates onset of the substorm by antiparallel reconnection, creating bursts of plasma down to the ionosphere. A plasmoid is created as a consequence of this reconnection, which is a ball of magnetic field that is completely independent from the Earth's magnetic field, and travels anti-earthward. Each subsequent stretched field line reconnects until there are no more closed stretched field lines and the plasmoid is free to travel away from the Earth. In the recovery phase, there are no stretched field lines present in the magnetotail and the whole process can now be repeated.

Four magnetic drifts considered in this chapter include the convective, curvature, gradient and polarization drift. The polarization drift is dependent on the time derivative of the electric field. The model that will be presented in the next chapter is time independent. Therefore, the polarization drift cannot be found in this thesis. The convective, curvature, and gradient drifts are needed to find the overall current in the magnetotail. The total current is dependent on four terms: current due to free charges, magnetization current, polarization current, and displacement current. The polarization current refers to a dielectric material so it does not pertain to the magnetosphere. The displacement current cannot be found since it is dependent on the time derivative of the electric field vector. The current due to free charges is found by analyzing the drifts the charged particles have in the magnetotail. The curvature and gradient drifts are charge separating drifts. Therefore, they will create a current in neutral plasma because they will cause

the protons and electrons to travel in opposite directions. The convective drift causes the protons and electrons to travel in the same direction; therefore, it will not cause a current in neutral plasma. The convective drift will only cause a current if there is a group of plasma with an excess of either positive or negative charge. This does occur in certain places in the magnetotail. Finally, the last current occurring in the magnetotail is the current of the unmagnetized protons. In the center of the NS, the protons become confused by the reversal of the x-component of the magnetic field and become unmagnetized. They will not respond to the magnetic field anymore but instead be pushed along by the Coulomb force due to the dawn to dusk electric field. This splits the NS into two regions: INS and ONS. The electrons remain magnetized in both regions whereas the protons are magnetized in the ONS and unmagnetized in the INS. The magnetization current consists of two terms, one that exactly cancels the current due to the gradient drift and another that is dependent on the cross product between the magnetic field unit vector and the gradient of the perpendicular particle pressure. Adding the terms due to the free charges and the magnetization gives the total time-independent current in the magnetotail (equation 2.75). It consists of four terms. The direction and effect the currents have in the three regions in the SPS (DZ, ONS, and INS) are summarized in Table 2.1. As previously stated, there are two main current systems occurring in the SPS: the double vortex current system and the NS FAC system. The double vortex current system consists of an eastward current in the DZs that closes westward in the NS. This current is mainly composed of the anisotropic electrons curvature drifting in the magnetotail, which is the first term in equation 2.75. The current produced by the second term in equation 2.75, which is mainly carried by the isotropic protons, enhances the westward current in the ONS and slightly dampens the eastward current in the DZs. The convective current (third term in equation 2.75) is important for two reasons. First, it closes the current loops creating the double vortex system in the magnetotail. Second, it causes the electrons to drift away from the unmagnetized protons in the INS, creating an anti-earthward current and an electron reservoir on the earthward end of the INS. This creates a proton reservoir on the anti-earthward end of the INS. The anti-earthward current in the INS is the generator current for the NS FAC system. The proton reservoir maps down to high latitudes in the ionosphere through a downward FAC; the electron reservoir maps down to lower latitudes in the ionosphere through an upward FAC. The system closes in the ionosphere through a Pedersen current. This FAC system is a critical part of the growth phase of substorms and is responsible

for the electron pre-onset arc. Lastly, the current due to the unmagnetized protons supports the double vortex current system. It is westward in the INS, which enhances the westward current in the NS created by the curvature current of the electrons. The protons also gain energy, which intensifies this westward current. This is also necessary for onset of the substorm.

Table 2.1 The directions and effects of the terms in the total current formula

	Current Direction and Location in Magnetotail
$\frac{n(2W_{\parallel} - W_{\perp})}{B}\hat{b} \times \vec{K}$	• Eastward direction in DZs and westward direction in NS (INS and ONS) • Very strong from anisotropic electrons • Zero from isotropic protons
$\frac{1}{B}\hat{b} \times \vec{\nabla} p_{\perp}$	• Westward direction in the DZs and ONS • Basically zero from anisotropic electrons • Moderate current from isotropic protons
$\frac{e\left(n_{i,excess} - n_{e,excess}\right)}{B}\vec{E} \times \hat{b}$	• Toward (protons) or away from (electrons) the NS in DZs and anti-earthward (electrons) in the INS • Closes the current loops by creating a current toward the NS on the dawn side of the SPS and a current away from the NS on the dusk side of the SPS • Causes the electrons to travel earthward in the INS, creating an anti-earthward current that will be the generator for auroral activities
$en_{i,unmag}\sqrt{\frac{2eE_{DD}\Delta y}{m_p}}\hat{y}$	• Westward (unmagnetized protons) in the INS • Enhances the westward current that is already present due to electron curvature current • Intensifies over time since the unmagnetized protons gain energy as they travel through the INS

The next chapter will present a model of the closed stretched magnetic field lines in the magnetotail that was developed over the course of this Masters project. The model contains the field lines in both the TPS and the SPS. In Chapter 4, this model is used to calculate some

physical properties in the magnetotail including the pitch angle and gyroradius of the charged particles, as well as the direction of the overall current. This will show that the shape of the stretched field lines presented in this chapter naturally leads to the double vortex current system in the magnetotail.

Chapter 3

Simple Model of Stretched Magnetic Field Lines

In this chapter, the equations for the magnetic field in the magnetotail are presented. There are two different sets of equations: the dipole equations and the stretched equations. The dipole equations are well known and are defined for the Earth's dipole field. In the magnetotail, the dipole equations are used to represent the plasmasphere. The stretched equations are not known and therefore must be designed. The stretched equations are used to represent both the outer TPS and the SPS in the magnetotail. The stretched model is restricted to the noon-midnight meridian plane; then the stretched magnetic field equations are put under two tests of physical validity: divergence and limits in the extremes. It is found that the stretched magnetic field equations pass both of these physical tests. Therefore, they can be used to calculate parameters such as the pitch angle and gyroradius of a particle as well as the overall current in the magnetotail, which will be discussed in the next chapter.

3.1 Earth's Dipole Magnetic Field

The Earth's field can be simplified to a bar magnet where the South Pole is the positive end and the North Pole is the negative end. Thus, for the Earth's dipole field, the field lines will travel out of the South Pole and into the North Pole. The dipole equations are well known and easily derivable (see Kivelson and Russell, page 165). The component equations in relative Cartesian coordinates are given as

$$B_x = -\frac{3XZB_{eq,s}}{(X^2 + Y^2 + Z^2)^{5/2}}\,, \tag{3.1a}$$

$$B_y = -\frac{3XYB_{eq,s}}{(X^2+Y^2+Z^2)^{5/2}}\,, \tag{3.1b}$$

and

$$B_z = \frac{(X^2+Y^2-2Z^2)B_{eq,s}}{(X^2+Y^2+Z^2)^{5/2}}\,. \tag{3.1c}$$

where $B_{eq,s}$ is the magnetic field at the equator on the surface of the Earth ($B_{eq,s} = 3.1 \times 10^{-4}$T) and (X, Y, Z) represent Cartesian coordinates relative to the radius of the Earth a ($a = 6.378 \times 10^6$m). Mathematically, these relative Cartesian coordinates are given by

$$(X, Y, Z) = \left(\frac{x}{a}, \frac{y}{a}, \frac{z}{a}\right)\,. \tag{3.2}$$

Equations 3.1a to 3.1c represent the Earth's dipole magnetic field in three dimensions. However, since the model is only defined in the noon-midnight meridian plane, Y can be set to zero. Therefore, the component equations in the noon-midnight meridian plane are given as

$$B_x = -\frac{3XZB_{eq,s}}{(X^2+Z^2)^{5/2}}\,, \tag{3.3a}$$

$$B_y = 0\,, \tag{3.3b}$$

and

$$B_z = \frac{(X^2-2Z^2)B_{eq,s}}{(X^2+Z^2)^{5/2}}\,. \tag{3.3c}$$

As discussed in Chapter 1, the plasmasphere is assumed to be dipolar field that immediately surrounds the Earth. The plasmapause location varies under different solar parameters. For this model, it is assumed that the plasmapause location is five Earth radii away

from the Earth along the negative x-axis. Equations 3.3a and 3.3c can be used to model the magnetic field in the plasmasphere in the noon-midnight meridian plane. In Figure 3.1, a representation of the shape of the field lines in the plasmasphere in the noon-midnight meridian plane is shown where the circle centered on the origin represents the Earth. This figure only depicts the shape of the field lines in the plasmasphere. It does not represent the typical method of plotting field lines where the field lines are separated so that the magnetic flux is constant between them.

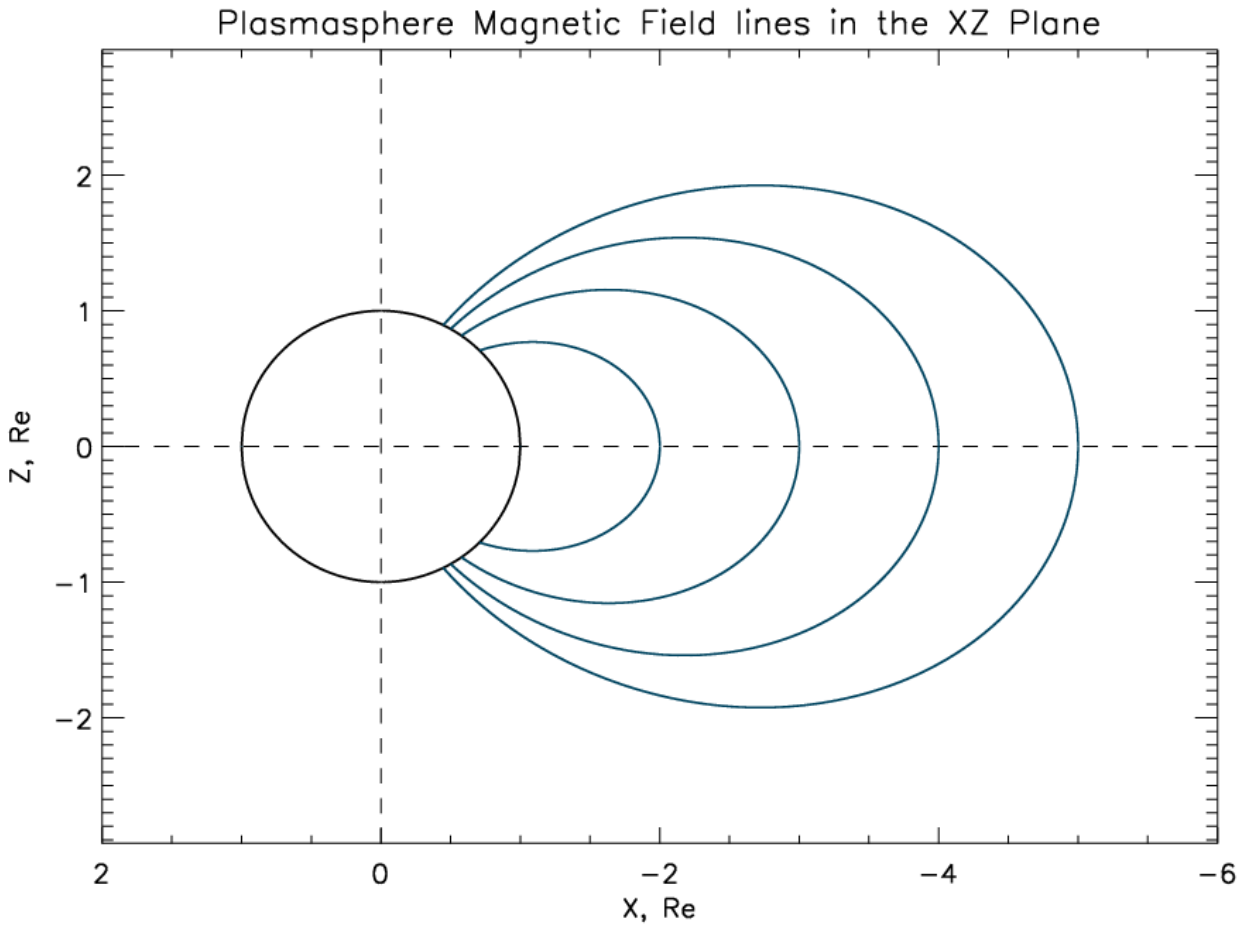

Figure 3.1 Modeled dipole field lines that show the shape of the field lines in the plasmasphere (teal) in the noon-midnight meridian plane.

3.2 Stretched Magnetic Field

3.2.1 Stretched Magnetic Field Equations

The main goal of this thesis work was to develop equations for the stretched magnetic field in the magnetotail. Section 2.3.1 outlined the desired shape for the stretched magnetic field lines. It consists of a dipole-like shape near Earth, then an elongated section in the magnetotail where there is a change from convex to concave curvature in the field lines. The design of the stretched magnetic field equations includes allowing the dipole field to decay in the negative x-direction and adding a stretched field that creates the elongated section in the tail. The specifics of how the stretching is obtained will be discussed in Section 3.2.2 and Section 3.2.3. Below are the proposed equations for the stretched magnetic field in the noon-midnight meridian plane in relative Cartesian coordinates:

$$B_x = -\frac{3XZB_{eq,s}}{(X^2+Z^2)^{5/2}} e^{\frac{X}{\Delta X_D}} - \frac{XZ}{X^2+Z^2} X_{extra} e^{-Z}\,, \tag{3.4a}$$

$$B_y = 0\,, \tag{3.4b}$$

and

$$B_z = \frac{(X^2-2Z^2)B_{eq,s}}{(X^2+Z^2)^{5/2}} e^{\frac{X}{\Delta X_D}} - Z_{extra} e^{\left(-\frac{(X-X_{min})^2}{X_{scale}} - \frac{Z^2}{Z_{scale}}\right)} \tag{3.4c}$$

where ΔX_D is the e-folding distance for decay of the dipole term ($\Delta X_D = 10$), X_{extra} is a scaling term for the stretch of the x-component ($X_{extra} = 3 \times 10^{-7}$ T), Z_{extra} is a scaling term for the stretch of the z-component ($Z_{extra} = 1.5 \times 10^{-7}$ T), and X_{min}, X_{scale}, and Z_{scale} are variables specific to a Gaussian that will be discussed in more detail in Section 3.2.3.

Equations 3.4a-3.4c describe two sections in the model: TPS and SPS. As discussed in Section 2.2, the SPS contains the stretched magnetic field lines and the TPS contains the field

lines that transition between dipole and stretched lines. The final region, the plasmasphere, was discussed in the previous section. The picture of the shape of the magnetic field lines in the magnetotail in the noon-midnight meridian plane is shown in Figure 3.2. Again, this figure represents the shape of the field lines in the different regions and is not designed to show the spacing of field lines with constant flux between them. The field lines are numbered from 2 to 12. Field lines 2 to 5 comprise the dipole field lines in the plasmasphere; field lines 6 to 7 comprise the TPS; and field lines 8 to 12 comprise the SPS. The field line number represents the location where the field line would cross the x-axis if it was a dipole field line. In the plasmasphere, the field lines cross the x-axis at the line number location showing they are dipole field lines. In the TPS, the field lines are slightly stretched, so they cross the x-axis farther in the negative direction than if they were dipole. In the SPS, a large amount of stretching occurs which can be easily seen in field line 12, which crosses the x-axis at -21.8 instead of -12 if it was a dipole field line. Thus, the lengths of the stretched field lines are quite significant compared to their dipole counterparts. Therefore, as stated in Chapter 2, the particles will gain a significant amount of parallel energy as the field lines move earthward and become shorter.

Both the TPS and SPS contain stretched forms of dipole field lines. However, the SPS field lines contain inflection points and the TPS field lines do not. The inflection points are represented in Figure 3.2 as red squares. They represent a change in the sense of curvature. There are two senses of curvature present: concave and convex. Concave curvature describes the curvature of the dipole and transition field lines as well as the central region of the stretched field lines. Convex curvature describes the regions between inflection points that are in the same quadrant in Figure 3.2. These different regions of curvature separate the stretched field lines into three areas: DZN, NS, and DZS. The DZs are defined as the regions of convex curvature and the NS is defined as the central region of concave curvature. The inflection points, if extended out into the y-direction, represent surfaces that are the boundaries of these three different regions in the stretched magnetic field lines. The inflection points that are highest and lowest in Z in Figure 3.2 represent the boundary surface of the DZN and DZS respectively and two sets of inflection points that are closest to the x-axis represent the boundary surfaces between the NS and the DZs. The inflection points give a mathematical basis for the boundaries between the different regions in the magnetotail, which is not present anywhere in the current literature. The method behind

how the shape of the field lines in the TPS and SPS were achieved is discussed in the next two subsections.

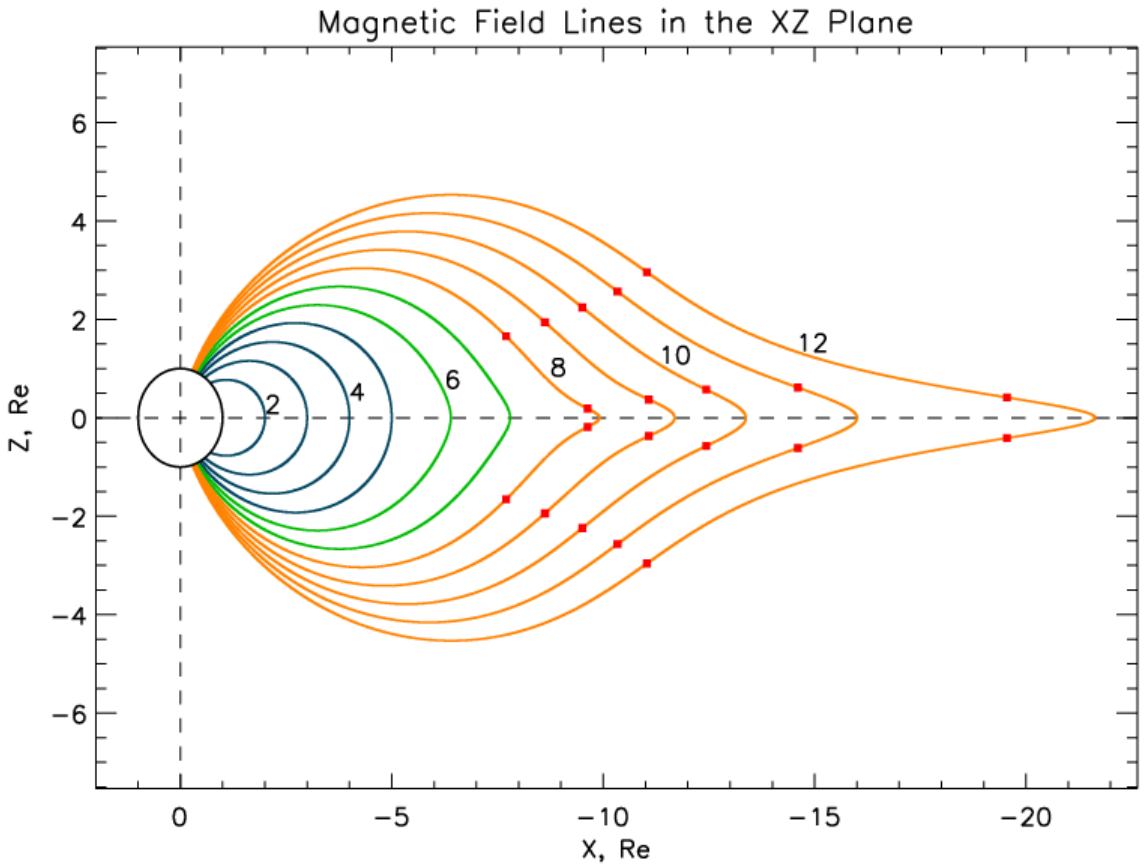

Figure 3.2 Model of the shape of the field lines in the magnetotail in the noon-midnight meridian plane that contains the dipole field lines in the plasmasphere (teal), the transitioning field lines in the TPS (green), and the stretched field lines in the SPS (orange). The inflection points of the stretched field lines are shown by red squares.

3.2.2 X-Component of Stretched Magnetic Field Equations

The x-component for the stretched magnetic field is equation 3.4a. The first term is the x-component of the dipole magnetic field multiplied by an exponential decay in the X direction. This means that the farther out in the negative X direction, the less influence the dipole field will have on the field line shape. The second term is responsible for creating the large amount of stretching in the X direction, as seen in Figure 3.2. It is accomplished by having a larger x-

component than z-component in the area where stretching is needed. Physically, the stretching should occur at low values of Z because the stretched part of the field is centered about the x-axis. Therefore, the x-component needs to increase to a maximum at a low value of Z in order to create the stretching. Also, for physical validity, the term needs to be zero either when X equals zero or Z equals zero. The second term in the x-component of the stretched magnetic field namely,

$$B_{x,term\,2} = -\frac{XZ}{X^2 + Z^2} X_{extra} e^{-Z} \tag{3.5}$$

has maxima in both X and Z. For X, the maximum is found to be at (derivation in Appendix F.1)

$$X_{max} = \pm Z\,. \tag{3.6}$$

The case that applies to this model is when the right side of the equation is negative, since the magnetotail is along the negative X-axis. For the purposes of this model, the highest Z value that will be used is around Z equal to four, which can be clearly seen in Figure 3.2. Therefore, the lowest X value that a maximum will occur in the scope of this model will be negative four. Thus, the maxima described in equation 3.6 will all occur in the area where the dipole field dominates. In the stretched field region, equation 3.5 will be decreasing in the negative X direction since the maxima have already occurred. This is what is physically expected because the Earth's magnetic field should decrease in the tailward direction.

The maximum in the Z direction is found to be at (derivation in Appendix F.2)

$$Z_{max}^3 + Z_{max}^2 + X^2 Z_{max} - X^2 = 0\,. \tag{3.7}$$

The above equation needs to be solved numerically. Table 3.1 summarizes the solutions for Z_{max} for various values of X. As can be seen, all maxima occur under a value of Z equaling one. Therefore, the maximum stretching will occur at a small Z value, which is one of the conditions

previously stated. After the function peaks at Z_{max}, it will decrease as it goes farther in the positive Z direction, which is what is physically expected.

Table 3.1 Solutions of equation 3.12 for various X values

X	Z_{max}
-2	0.752172
-4	0.903014
-6	0.950988
-8	0.970966
-10	0.980939
-12	0.986572
-14	0.990048
-16	0.992336
-18	0.993921
-20	0.995062

As stated before, the stretched magnetic field formulas are designed in a way that the dipole magnetic field dominates close to the Earth and the stretched magnetic field dominates farther away from the Earth. Also, there are the transition field lines between the dipole field and the stretched magnetic field. How this transition between dipole and stretched field is accomplished is shown in Figure 3.3, Figure 3.4, and Figure 3.5. Essentially, it is achieved by having either the first or the second terms in equation 3.4a dominate.

Figure 3.3 shows how the x-component varies with respect to Z at $X = -7$. The yellow curve represents the decaying dipole in equation 3.4a and the purple curve represents the stretching term in equation 3.4a. As seen in Figure 3.2, this slice corresponds to dipole field lines with slight stretching at low values of Z. The dipole term of the x-component dominates at this X value. Therefore, the field line will be mainly dipolar in shape. At low values of Z, the stretched term slightly skews the curve, creating the slight stretch in the field line that is necessary for the TPS.

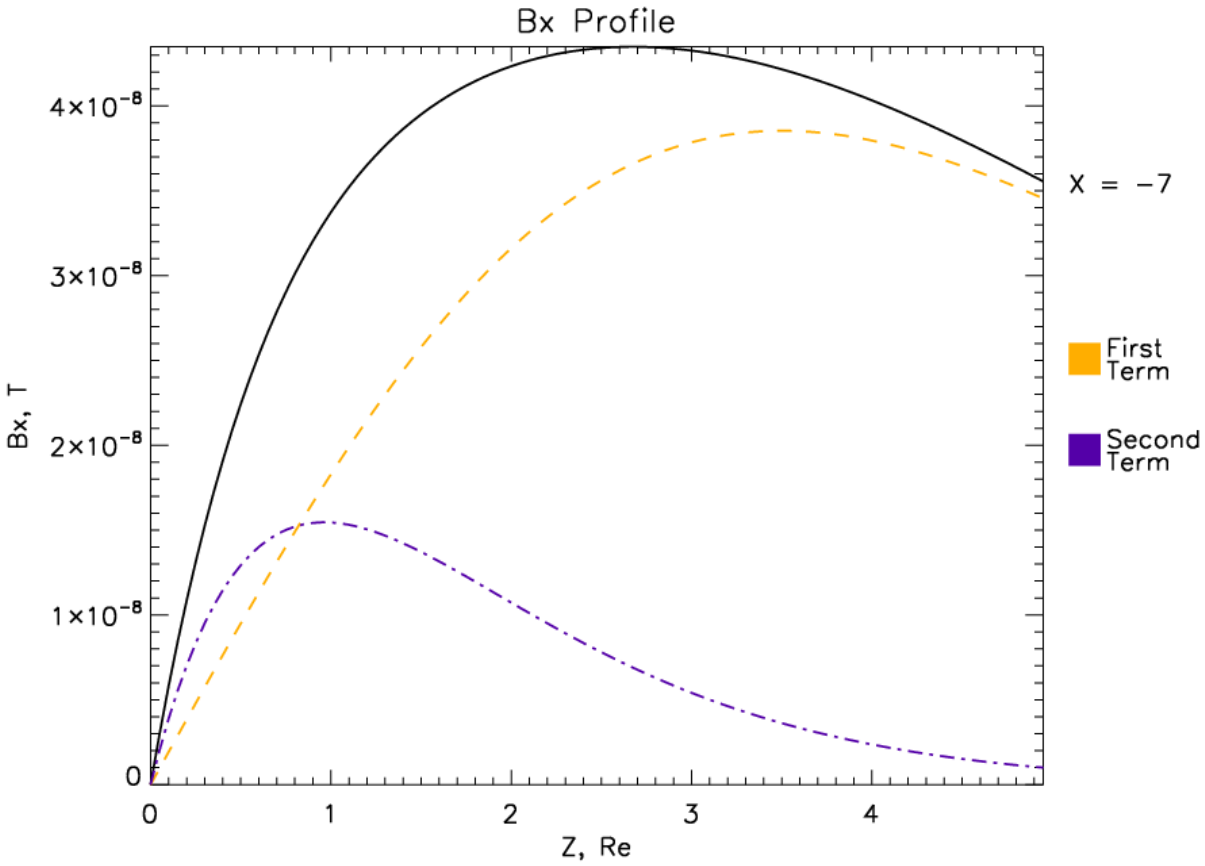

Figure 3.3 Profile of the x-component for the stretched magnetic field at a slice at $X = -7$.

Figure 3.4 shows how the x-component varies with respect to Z at $X = -10$, which roughly corresponds to the location where field line 8 intersects with the x-axis. Therefore, this slice consists of the first stretched field lines with field lines above that are still mainly dipolar in shape. As seen in Figure 3.4, the dipole and stretched terms of the x-component dominate in different ranges of Z. The stretched term dominates at low value of Z. This creates the most earthward stretched field lines. The dipole term dominates at higher values of Z. This creates the field lines above the first stretched field lines to still have a mainly dipolar shape. Overall, this represents the first stretched field lines in the SPS that have a very thin NS and substantial convex curvature.

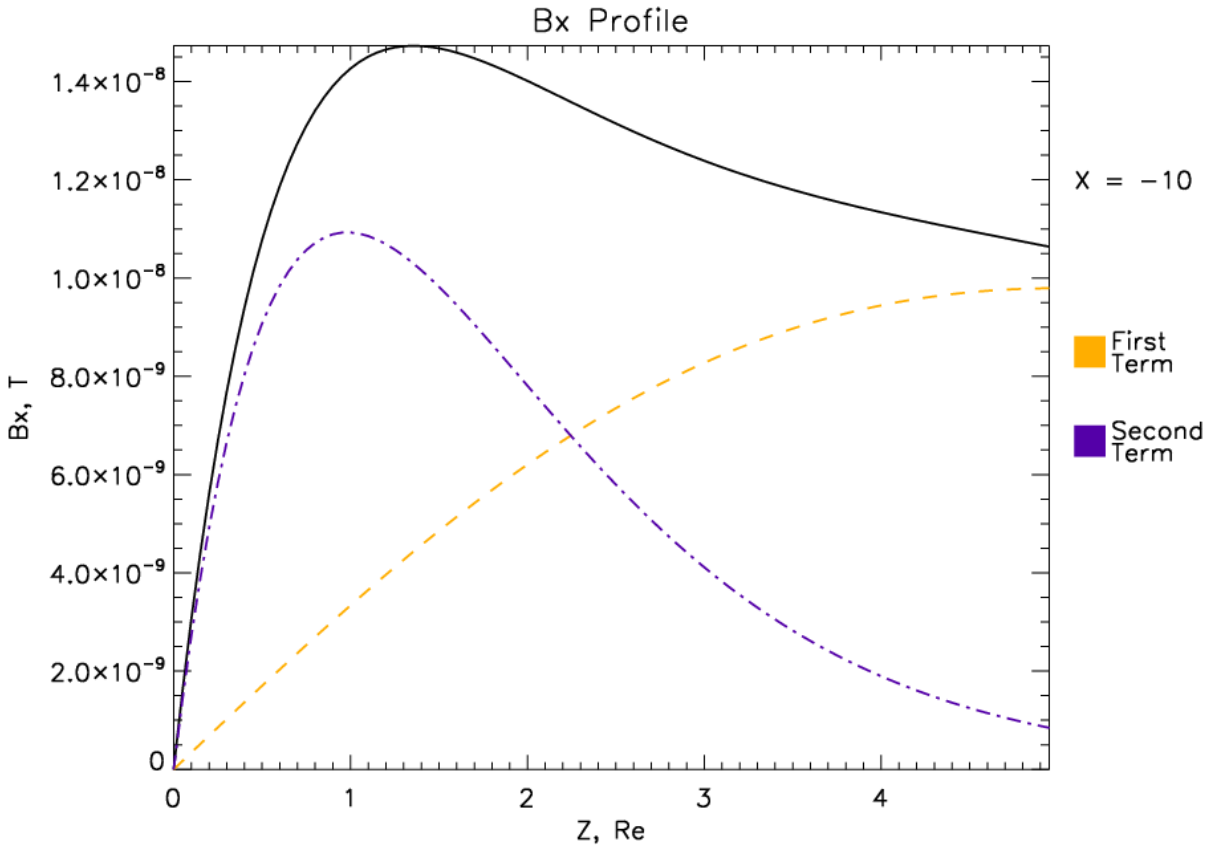

Figure 3.4 Profile of the x-component for the stretched magnetic field at a slice at $X = -10$.

Figure 3.5 shows how the x-component varies with respect to Z at $X = -19$. As seen in Figure 3.2, this region corresponds to the very stretched region of the magnetotail where the field lines are basically parallel to the x-axis. Figure 3.5 shows that the stretched term dominates in this slice of the magnetotail. This far away from the Earth, the field lines are either stretched (closed) or lobe (open) field lines. The dipole field should not be present, which is shown in Figure 3.5. Also, note that the maximum value of the x-component between Figure 3.4 and Figure 3.5 has dropped dramatically. This is due to the decrease in the total magnetic field value with distance from the Earth.

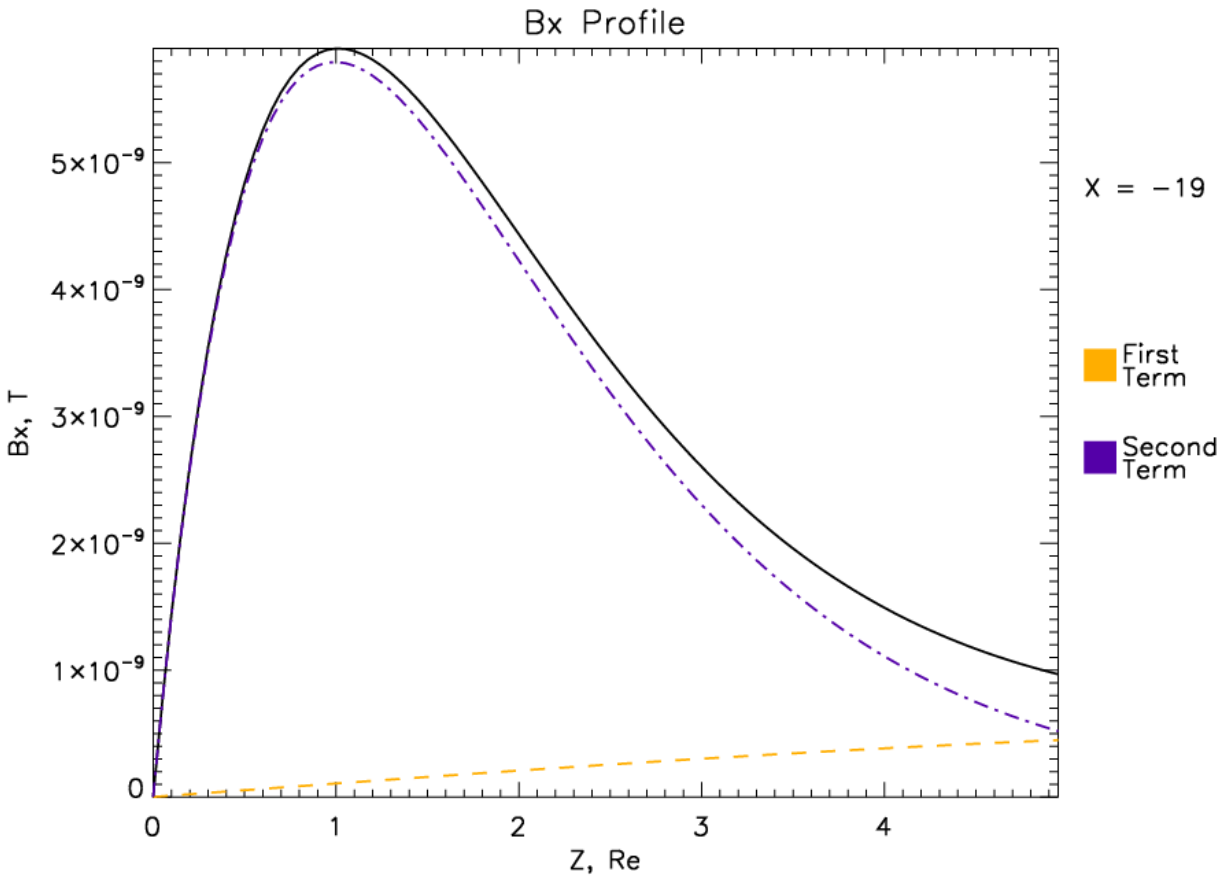

Figure 3.5 Profile of the x-component of the stretched magnetic field at a slice at $X = -19$.

3.2.3 Z-Component of Stretched Magnetic Field Equations

The z-component of the stretched magnetic field is equation 3.4c. It consists of two terms. The first term is the z-component dipole term multiplied by an exponential decay in the negative X direction. As stated before, this allows the dipole field to decay away and the stretched field to take over. The second term represents a Gaussian. This term is needed in order to create the deep minimum in the magnetic field that was described in Section 2.6.2. The deep minimum is implemented into the model by subtracting the Gaussian term from the decaying dipole term along the negative x-axis or where the NS would be located. The Gaussian term is given by

$$B_{z,term\,2} = -X_{extra} e^{\left(-\frac{(X-X_{min})^2}{X_{scale}} - \frac{Z^2}{Z_{scale}}\right)}. \qquad 3.8$$

The variables X_{min}, X_{scale}, and Z_{scale} are the parameters of the Gaussian. The Gaussian is centered about the point $(X_{min,}, 0)$. For this model, X_{min} is set to a value of negative eight. The Gaussian is chosen to be centered about that point in the XZ plane because it represents the location where the increased stretching occurs to create the slight stretching in the TPS and the extreme curvature at the inner edge of the SPS. The variables X_{scale} and Z_{scale} define the sharpness of the Gaussian in either direction. For this model, X_{scale} is set to ten and Z_{scale} is set to one half. This means there is a very sharp Gaussian in the Z direction and a more gradual Gaussian in the X direction. Once again, this represents thinning of the NS, particularly at the earthward end of the SPS, because it occurs over a very small range of Z.

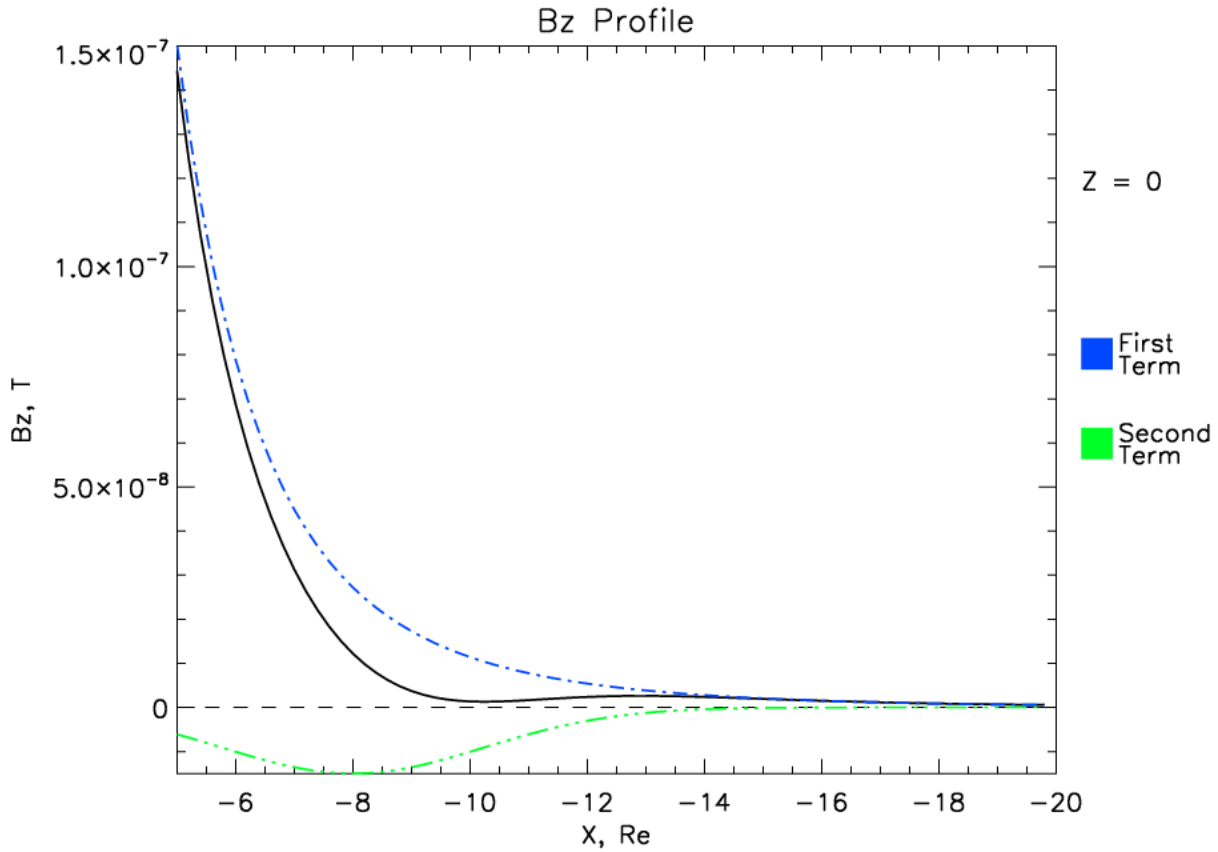

Figure 3.6 Profile of the z-component of the stretched magnetic field at a slice at $Z = 0$.

Figure 3.6 shows how the z-component varies with respect to X at $Z = 0$, which is the center of the NS. The blue curve represents the decaying dipole term in equation 3.4c and the green curve represents the Gaussian term in equation 3.4c. The Gaussian is at its maximum at this point in order to create the absolute minimum in the magnetic field at about $X = -10$, where there is also the greatest convex curvature between the inflection points. Subtracting the Gaussian from the decaying dipole curve gives a clear drop in the value of the magnetic field that increases back to a maximum at around $X = -13$. The minimum in the z-component in this x-range contributes to the maximum in convex curvature that is present at the earthward side of the SPS. Since the x-component has a maximum at this point, as was shown in the previous section, and the z-component has a minimum at this point, the conditions are ideal for intense stretching, as seen in Figure 3.2. As the value of Z increases from zero, the Gaussian will get smaller and thus have less effect on the decaying dipole term.

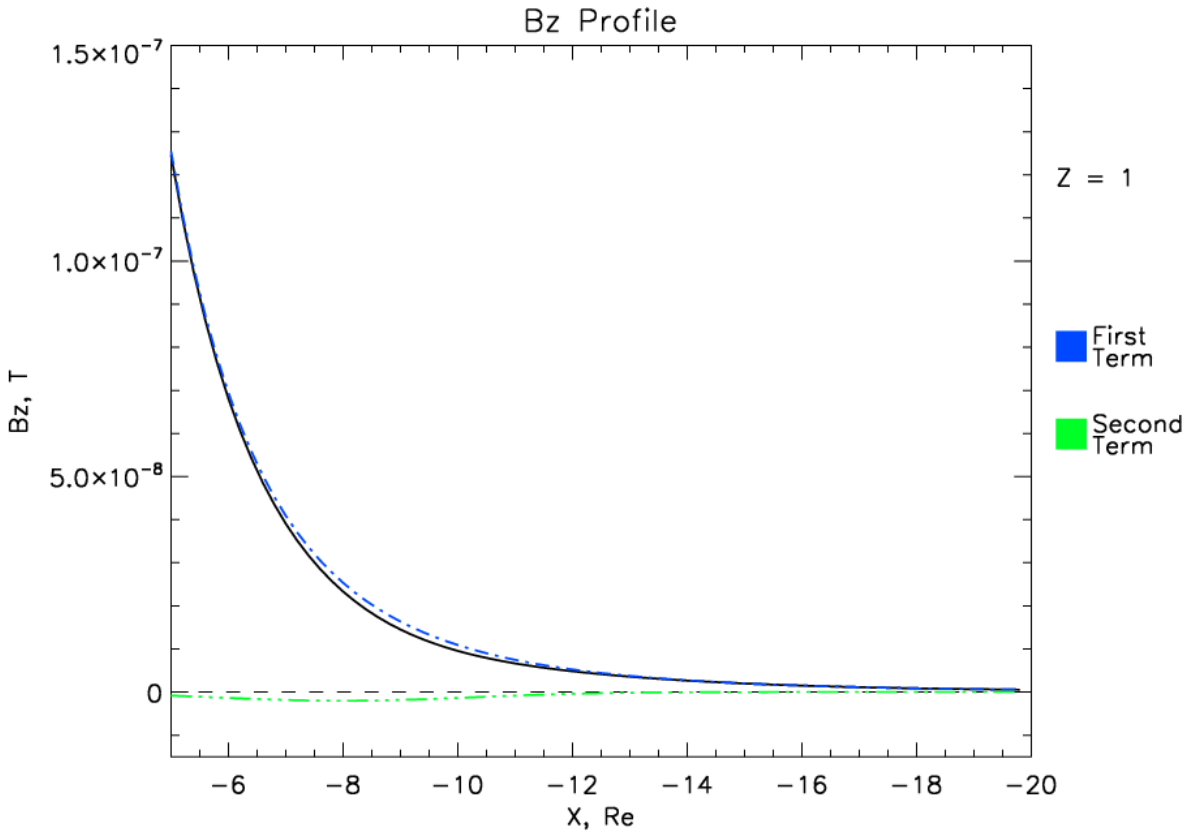

Figure 3.7 Profile of the z-component of the stretched magnetic field at a slice at $Z = 1$.

Figure 3.7 shows how the z-component varies with respect to X at $Z = 1$. This represents the area inside the DZN. The Gaussian term or green curve is basically zero at this point. Therefore, the actual value of the z-component does not stray very far from the decaying dipole curve or the blue curve. Since this is now in the DZN, the magnetic field does not need to lessen to allow for a growing particle pressure as is needed in the NS. Therefore, the minimum in the z-component does not need to be present anymore. Finally, it is also worthwhile to note that in both Figure 3.6 and Figure 3.7, the value of the z-component of the stretched magnetic field decays basically to zero as X increases in the negative direction, in keeping with the decrease of the Earth's magnetic field.

Now that a magnetic field has been defined for the TPS and SPS, there are two tests that can be done in order to check the validity of the model. Firstly, Maxwell's equations state that the divergence of the magnetic field must be zero. Secondly, as was mentioned in this section, the magnetic field should equal zero at infinity. Using the equations designed for the stretched field, both of these physical tests can be checked. The divergence is analyzed in the next section and the limit at infinity is tested in Section 3.4.

3.3 Divergence of the Magnetic Field

Maxwell's equations state that the divergence of a magnetic field must be zero. Mathematically, this is represented as

$$\vec{\nabla} \cdot \vec{B} = 0 \tag{3.9}$$

where the Del operator defined in relative Cartesian coordinates is

$$\vec{\nabla} = \frac{1}{a}\frac{\delta}{\delta X}\hat{x} + \frac{1}{a}\frac{\delta}{\delta Y}\hat{y} + \frac{1}{a}\frac{\delta}{\delta Z}\hat{z}\,. \tag{3.10}$$

As seen in the above equation, the divergence of the magnetic field is inherently a three dimensional entity. Therefore, there is a problem with the equations defined in Section 3.2

because they are defined only in the noon-midnight meridian plane. There is no y-component defined for the stretched magnetic field. However, one can be assigned to the stretched magnetic field by analyzing the divergence. If the x-component and the z-components of the stretched magnetic field have nonzero divergences, a y-component can be found in order to force the divergence of the three dimensional magnetic field to be zero. Firstly, the equations for the stretched magnetic field need be changed to three dimensions instead of two dimensions. The result is

$$B_x = -\frac{3XZB_{eq,s}}{(X^2+Y^2+Z^2)^{5/2}} e^{\frac{X}{\Delta X_D}} - \frac{XZ}{X^2+Y^2+Z^2} X_{extra} e^{-Z} \qquad 3.11a$$

and

$$B_z = \frac{(X^2+Y^2-2Z^2)B_{eq,s}}{(X^2+Y^2+Z^2)^{5/2}} e^{\frac{X}{\Delta X_D}} - Z_{extra} e^{\left(-\frac{(X-X_{min})^2}{X_{scale}} - Y^2 - \frac{Z^2}{Z_{scale}}\right)} \qquad 3.11b$$

The changes that have been made are including the Y variable to the dipole parts of the equations, including the Y term to the part of the second term in the x-component so that it represents a radial distance, and including a Y term to the Gaussian in the z-component.

3.3.1 Derivation of the Y-Component for the Stretched Magnetic Field

In order to find the necessary y-component of the stretched magnetic field, the divergence needs to be calculated in relative Cartesian coordinates. It is given as

$$\vec{\nabla} \cdot \vec{B} = \left(\frac{1}{a}\frac{\delta}{\delta X}\hat{x} + \frac{1}{a}\frac{\delta}{\delta Y}\hat{y} + \frac{1}{a}\frac{\delta}{\delta Z}\hat{z}\right) \cdot \left(B_x\,\hat{x} + B_y\,\hat{y} + B_z\,\hat{z}\right) = \frac{1}{a}\frac{\delta B_x}{\delta X} + \frac{1}{a}\frac{\delta B_y}{\delta Y} + \frac{1}{a}\frac{\delta B_z}{\delta Z}\,. \qquad 3.12$$

As stated before, Maxwell's equations state that the divergence of the magnetic field must be zero. Therefore, equation 3.12 becomes

$$0 = \frac{\delta B_x}{\delta X} + \frac{\delta B_y}{\delta Y} + \frac{\delta B_z}{\delta Z} \ . \tag{3.13}$$

Rearranging to solve for the y-component gives

$$\frac{\delta B_y}{\delta Y} = -\frac{\delta B_x}{\delta X} - \frac{\delta B_z}{\delta Z} \tag{3.14a}$$

where the y-component can be isolated by taking the derivative with respect to Y giving

$$B_y = -\int \frac{\delta B_x}{\delta X} dY - \int \frac{\delta B_z}{\delta Z} dY \ . \tag{3.14b}$$

Now the y-component of the magnetic field can be found through calculations using the x and z components of the stretched magnetic field.

First, the derivative of the x-component with respect to X needs to be found. It is calculated in Appendix G.1 (equation G.2). Using this solution, the integral with respect to Y is found to be

$$\int \frac{\delta B_x}{\delta X} dY = -3ZB_{eq,s}\, e^{\frac{X}{\Delta X_D}} \left(\int \frac{-4X^2 + Y^2 + Z^2}{(X^2 + Y^2 + Z^2)^{7/2}} dY + \frac{X}{\Delta X_D} \int \frac{dY}{(X^2 + Y^2 + Z^2)^{5/2}} \right) - ZX_{extra} e^{-Z} \int \frac{-X^2 + Y^2 + Z^2}{(X^2 + Y^2 + Z^2)^2} dY \ . \tag{3.15}$$

Calculating the integrals gives the result of

$$\int \frac{\delta B_x}{\delta X} dY = -\frac{XYZB_{eq,s}(3X^2 + 2Y^2 + 3Z^2)}{\Delta X_D (X^2 + Z^2)^2 (X^2 + Y^2 + Z^2)^{3/2}}\, e^{\frac{X}{\Delta X_D}} + \frac{YZB_{eq,s}}{(X^2 + Z^2)^3 (X^2 + Y^2 + Z^2)^{5/2}}\, e^{\frac{X}{\Delta X_D}} (12X^6 + 15X^4Y^2 + 6X^2Y^4 + 21X^4Z^2 + 10X^2Y^2Z^2 - 2Y^4Z^2 + 6X^2Z^4 - 5Y^2Z^4 - 3Z^6) \tag{3.16}$$

$$+\frac{Z}{X^2+Z^2}X_{extra}e^{-Z}\left(\frac{X^2Y}{X^2+Y^2+Z^2}-\frac{Z^2}{\sqrt{X^2+Z^2}}\tan^{-1}\left(\frac{Y}{\sqrt{X^2+Z^2}}\right)\right).$$

Now, the z-component term needs to be found. It is calculated in Appendix G.3 (equation G.25). Using this solution, the integral with respect to Y is found to be

$$\int\frac{\delta B_z}{\delta Z}dY = 3ZB_{eq,s}\,e^{\frac{X}{\Delta X_D}}\int\frac{(-3X^2-3Y^2+2Z^2)}{(X^2+Y^2+Z^2)^{7/2}}dY + \frac{2Z}{Z_{scale}}Z_{extra}\int e^{\left(-\frac{(X-X_{min})^2}{X_{scale}}-Y^2-\frac{Z^2}{Z_{scale}}\right)}dY\ . \tag{3.17}$$

Calculating the integrals give the result of

$$\begin{aligned}\int\frac{\delta B_z}{\delta Z}dY = &-\frac{YZB_{eq,s}}{(X^2+Z^2)^3(X^2+Y^2+Z^2)^{5/2}}\,e^{\frac{X}{\Delta X_D}}(9X^6+15X^4Y^2+6X^2Y^4\\&+12X^4Z^2+10X^2Y^2Z^2-2Y^4Z^2-3X^2Z^4-5Y^2Z^4-6Z^6)\\&+\frac{2Z}{Z_{scale}}Z_{extra}e^{\left(-\frac{(X-X_{min})^2}{X_{scale}}-\frac{Z^2}{Z_{scale}}\right)}\mathrm{erf}(Y)\,.\end{aligned} \tag{3.18}$$

Finally, the y-component of the stretched magnetic field can be found by substituting equations 3.18 and 3.16 into equation 3.14b. The result is given as

$$\begin{aligned}B_y = &\frac{YZB_{eq,s}(-3X^2-9X^4Z^2-9X^2Z^4-3Z^6)}{(X^2+Z^2)^3(X^2+Y^2+Z^2)^{3/2}}\,e^{\frac{X}{\Delta X_D}}\\&+\frac{XYZB_{eq,s}(3X^2+2Y^2+3Z^2)}{\Delta X_D(X^2+Z^2)^2(X^2+Y^2+Z^2)^{3/2}}\,e^{\frac{X}{\Delta X_D}}\\&-\frac{Z}{X^2+Z^2}X_{extra}e^{-Z}\left(\frac{X^2Y}{X^2+Y^2+Z^2}-\frac{Z^2}{\sqrt{X^2+Z^2}}\tan^{-1}\left(\frac{Y}{\sqrt{X^2+Z^2}}\right)\right)\\&-\frac{2Z}{Z_{scale}}Z_{extra}e^{\left(-\frac{(X-X_{min})^2}{X_{scale}}-\frac{Z^2}{Z_{scale}}\right)}\mathrm{erf}(Y)\,,\end{aligned} \tag{3.19a}$$

which can be simplified to

$$B_y = -\frac{3YZB_{eq,s}}{(X^2+Y^2+Z^2)^{5/2}}e^{\frac{X}{\Delta X_D}} + \frac{XYZ(3X^2+2Y^2+3Z^2)B_{eq,s}}{\Delta X_D(X^2+Z^2)^2(X^2+Y^2+Z^2)^{3/2}}e^{\frac{X}{\Delta X_D}} \quad 3.19b$$
$$+\frac{Z}{X^2+Z^2}X_{extra}e^{-Z}\left(-\frac{X^2Y}{X^2+Y^2+Z^2}\right.$$
$$\left.+\frac{Z^2}{\sqrt{X^2+Z^2}}\tan^{-1}\left(\frac{Y}{\sqrt{X^2+Z^2}}\right)\right)$$
$$-\frac{2Z}{Z_{scale}}Z_{extra}e^{\left(-\frac{(X-X_{min})^2}{X_{scale}}-\frac{Z^2}{Z_{scale}}\right)}\text{erf}(Y)\,.$$

Therefore, the stretched magnetic field components in three dimensions are given as

$$B_x = -\frac{3XZB_{eq,s}}{(X^2+Y^2+Z^2)^{5/2}}e^{\frac{X}{\Delta X_D}} - \frac{XZ}{X^2+Y^2+Z^2}X_{extra}e^{-Z}, \quad 3.20a$$

$$B_y = -\frac{3YZB_{eq,s}}{(X^2+Y^2+Z^2)^{5/2}}e^{\frac{X}{\Delta X_D}} + \frac{XYZ(3X^2+2Y^2+3Z^2)B_{eq,s}}{\Delta X_D(X^2+Z^2)^2(X^2+Y^2+Z^2)^{3/2}}e^{\frac{X}{\Delta X_D}} \quad 3.20b$$
$$+\frac{Z}{X^2+Z^2}X_{extra}e^{-Z}\left(-\frac{X^2Y}{X^2+Y^2+Z^2}\right.$$
$$\left.+\frac{Z^2}{\sqrt{X^2+Z^2}}\tan^{-1}\left(\frac{Y}{\sqrt{X^2+Z^2}}\right)\right)$$
$$-\frac{2Z}{Z_{scale}}Z_{extra}e^{\left(-\frac{(X-X_{min})^2}{X_{scale}}-\frac{Z^2}{Z_{scale}}\right)}\text{erf}(Y)\,,$$

and

$$B_z = \frac{(X^2+Y^2-2Z^2)B_{eq,s}}{(X^2+Y^2+Z^2)^{5/2}}e^{\frac{X}{\Delta X_D}} - Z_{extra}e^{\left(-\frac{(X-X_{min})^2}{X_{scale}}-Y^2-\frac{Z^2}{Z_{scale}}\right)}\,. \quad 3.20c$$

The three dimensional equations (equations 3.20a through 3.20c) of the stretched magnetic field are valid for this simple model of the magnetotail for two reasons. Firstly, the divergence of the magnetic field (in three dimensions) equals zero. This can be easily shown by

adding the three derivatives together. The derivative of the y-component with respect to Y is calculated in Appendix G.2 (equation G.14). Adding together the three derivatives gives

$$\vec{\nabla}\cdot\vec{B}=\frac{1}{a}\Bigg(-\frac{3ZB_{eq,s}(-4X^2+Y^2+Z^2)}{(X^2+Y^2+Z^2)^{\frac{7}{2}}}e^{\frac{X}{\Delta X_D}}-\frac{3XZB_{eq,s}}{\Delta X_D(X^2+Y^2+Z^2)^{\frac{5}{2}}}e^{\frac{X}{\Delta X_D}}$$
$$-\frac{Z(-X^2+Y^2+Z^2)}{(X^2+Y^2+Z^2)^2}X_{extra}e^{-Z}-\frac{3ZB_{eq,s}(X^2-4Y^2+Z^2)}{(X^2+Y^2+Z^2)^{\frac{7}{2}}}e^{\frac{X}{\Delta X_D}}$$
$$+\frac{3XZB_{eq,s}}{\Delta X_D(X^2+Y^2+Z^2)^{\frac{5}{2}}}e^{\frac{X}{\Delta X_D}}+\frac{Z(-X^2+Y^2+Z^2)}{(X^2+Y^2+Z^2)^2}X_{extra}e^{-Z}$$
$$-\frac{2Z}{Z_{scale}}Z_{extra}e^{\left(-\frac{(X-X_{min})^2}{X_{scale}}-Y^2-\frac{Z^2}{Z_{scale}}\right)}-\frac{3ZB_{eq,s}(3X^2+3Y^2-2Z^2)}{(X^2+Y^2+Z^2)^{\frac{7}{2}}}$$
$$+\frac{2Z}{Z_{scale}}Z_{extra}e^{\left(-\frac{(X-X_{min})^2}{X_{scale}}-Y^2-\frac{Z^2}{Z_{scale}}\right)}\Bigg), \tag{3.21a}$$

which gives the desired result of

$$\vec{\nabla}\cdot\vec{B}=0\,. \tag{3.21b}$$

Therefore, the three dimensional stretched magnetic field equations presented in this thesis are divergence free. Secondly, the y-component of the stretched magnetic field is zero in the noon-midnight meridian plane. This also can be simply shown by setting Y to zero in the equation for the y-component of the stretched magnetic field, which is given as

$$B_y(X,0,Z)=-\frac{3(0)ZB_{eq,s}}{(X^2+0+Z^2)^{5/2}}e^{\frac{X}{\Delta X_D}}+\frac{X(0)Z(3X^2+2Y^2+3Z^2)B_{eq,s}}{\Delta X_D(X^2+Z^2)^2(X^2+Y^2+Z^2)^{3/2}}e^{\frac{X}{\Delta X_D}}$$
$$+\frac{Z}{X^2+Z^2}X_{extra}e^{-Z}\left(-\frac{X^2(0)}{X^2+0+Z^2}+\frac{Z^2}{\sqrt{X^2+Z^2}}\tan^{-1}\left(\frac{0}{\sqrt{X^2+Z^2}}\right)\right)$$
$$-\frac{2Z}{Z_{scale}}Z_{extra}e^{\left(-\frac{(X-X_{min})^2}{X_{scale}}-\frac{(Z-Z_{min})^2}{Z_{scale}}\right)}\mathrm{erf}(Y) \tag{3.22a}$$

and simplifies to

$$B_y(X, 0, Z) = 0\,. \qquad 3.22b$$

Thus, the y-component of the stretched magnetic field is zero in the noon-midnight meridian plane. The final physical test, limits in the extremes, is discussed in the next section.

3.4 Limit at Infinity

Physically, the Earth's magnetic field at a distance of infinity should have a value of zero. Therefore, the model should abide by this physical restriction. The equations designed for the stretched magnetic field are defined in the negative X, positive Z quadrant. Thus, the extremes that need to be checked are:

1. Negative infinity in the X-direction;
2. Positive and negative infinity in the Y-direction;
3. Positive Infinity in the Z-direction.

Since the model has not been checked for physical validity in other quadrants, the other extremes do not need to be checked. The computation of all of these limits is shown in Appendix H. Table 3.2 summarizes the results.

Overall, the stretched magnetic field equations behave physically in the extremes. The only exception is the y-component of the stretched magnetic field with the limit of either positive or negative infinity in the Y direction. However, since this model of the stretched magnetic field lines is going to be used only in the noon-midnight meridian plane, the y-component of the magnetic field will have no effect on the shape of the field lines. Also, if the limit is either taken in the X or Z direction afterwards, a solution of zero is obtained. Therefore, for the purposes of using the stretched magnetic field model in the noon-midnight meridian plane, the model is

deemed physical since the y-component of the magnetic field has no effect on the magnetic field in this plane.

Table 3.2 Limits at infinity for all components of the stretched magnetic field in all directions

	X-Component	**Y-Component**	**Z-Component**
$\lim_{X\to-\infty}$	Zero	Zero	Zero
$\lim_{Y\to\pm\infty}$	Zero	• Finite answer but if the limit is taken in either the x or z direction, then an answer of zero is obtained	Zero
$\lim_{Z\to\infty}$	Zero	Zero	Zero

3.5 Summary

In this chapter, equations that represent the stretched magnetic field in the magnetotail were presented. The equations were designed in the noon-midnight meridian plane to create the shape of the field lines in the magnetotail outlined in Section 2.3.1. Figure 3.2 shows the shape of the field lines in the magnetotail. The field lines in the plasmasphere have a dipolar shape. The field lines in the TPS are slightly stretched but contain no inflection points. They entirely have concave curvature. The stretched field lines have quite a significant length compared to the field lines in the plasmasphere and TPS. The field line that would intersect the x-axis at -12 if it was dipole in shape stretches all the way to -21.8. This means that as the stretched field lines move earthward due to the convective drift, they will gain a considerable amount of parallel energy as shown by the second adiabatic invariant. The stretched field lines also contain four inflection points. The inflection points represent boundary surfaces for three different regions in the magnetotail. The two regions of convex curvature are labelled as the DZs. The central region of concave curvature is labelled as the NS. The inflection points provide a mathematical basis for defining these regions in the magnetotail.

The field line shapes presented in Figure 3.2 are created by an x and z component of the stretched magnetic field. The x-component and z-component each contain two terms. The first

term is a dipole field term that is designed to decay farther away from the Earth. The second term is a stretching term that is designed to create the large amount of stretching in the tail. For the x-component, the stretching is accomplished by having a maximum. This maximum occurs in the DZs in order to create the long, almost horizontal field in the stretched field lines. For the z-component, the stretching is accomplished by having a minimum. This minimum occurs in the center of the NS in order to create the deep minimum in the magnetic field that was discussed in Section 2.6.2. The y-component of the stretched magnetic field was not needed for the noon-midnight meridian plane as it has no effect on the magnetic field in this plane.

After the stretched magnetic field equations were defined, they needed to be tested for physical validity. The first test is the zero divergence of the magnetic field. Divergence is a three dimensional problem. Therefore, the y-component of the stretched magnetic field is needed in order to find the divergence of the total magnetic field. In this case, the divergence equation was used to solve for a y-component for the stretched magnetic field, making the divergence of the total field automatically zero. The second physical test for the stretched magnetic field is the limit at infinity. Physically, the Earth's magnetic field should be zero at an infinite distance away from the Earth. It was found that all components of the stretched magnetic field are zero at infinity expect for the y-component at a limit of positive or negative infinity in the Y direction. However, since the y-component has no effect on the magnetic field in the noon-midnight meridian plane, the stretched magnetic field is deemed physical for the purposes of this thesis. The next chapter will use the stretched magnetic field equations to find some physical results such as the particle behavior in the SPS as well as the direction and intensity of the overall current in the stretched magnetotail.

Chapter 4

Preliminary Results from Simple Model

In this chapter, parameters in the magnetotail are calculated using the stretched magnetic field model that was presented in the previous chapter. The parameters that are calculated consist of the pitch angle and gyroradius of a charged particle and the direction of the current in the magnetotail. Firstly, the current created by a magnetic field can be directly found using Ampere's Law. The current produced by the stretched magnetic field presented in the previous chapter is calculated in Section 4.1. Secondly, a particle's pitch angle and gyroradius change as it travels along a magnetic field line. The stretched magnetic field equations presented in the previous chapter can be used to find the value of these parameters at all points in the magnetotail. The pitch angle is calculated in Section 4.2 and the gyroradius is calculated in Section 4.3. Lastly, the current direction can be inferred by analyzing the terms in the overall current formula that was presented in Section 2.6 (equation 2.75). The direction of the current produced by the first term can be found by using the stretched magnetic field equations and is calculated in Section 4.4. Calculating the direction of this individual term provides insight into the direction of the total current. This can be compared to the direction of the overall current found in Section 4.1. The pitch angle, proton unmagnetized regions, and direction of the current in the magnetotail calculated in this chapter can be used to support the model presented in Chapter 2.

4.1 Current Calculated Directly from Stretched Magnetic Field Model using Ampere's Law

The current produced by a specific magnetic field can be found using Ampere's law, which is Maxwell's fourth equation. The full form of this equation is given as

$$\vec{\nabla} \times \vec{B} = \mu_0 \vec{J}_{total} \tag{4.1}$$

where $\vec{J}_{total}$ is the total current density, which is given in equation 2.38. The total current density is composed of the summation of the current due to free charges, the magnetization current, the polarization current, and the displacement current. Expanding the total current density term in equation 4.1 gives

$$\vec{\nabla} \times \vec{B} = \mu_0 \left(\vec{J}_F + \vec{\nabla} \times \vec{M} + \frac{\delta \vec{P}}{\delta t} + \epsilon_0 \frac{\delta \vec{E}}{\delta t} \right) . \tag{4.2}$$

The model of the stretched magnetic field presented in Chapter 3 is time independent. Therefore, two terms in the above formula go to zero giving the time-independent form of Ampere's law as

$$\vec{\nabla} \times \vec{B} = \mu_0 \left(\vec{J}_F + \vec{\nabla} \times \vec{M} \right) = \mu_0 \vec{J} \tag{4.3}$$

where $\vec{J}$ is the total time-independent current density. Now, the current density in the magnetotail can be analyzed. The total time-independent current density can be found by calculating the curl of the stretched magnetic field model. This will show whether the shape of the stretched field lines that was presented in Section 2.3.1 supports the double vortex current system that was presented in Section 2.6.4. This analysis is completed in this section. The double vortex system was justified by analyzing the individual terms that were derived for the current due to free charges and the magnetization current. The total time-independent current density consists of four terms and is given in equation 2.75. The first term describes the curvature current that is likely dominated by the electrons. This current is dependent on the cross product between the magnetic field unit vector and the curvature vector and the difference between the parallel and perpendicular pressures. The direction of this current can be found by using the stretched magnetic field model that was presented in the previous chapter. This is done in Section 4.4. The second term in equation 2.75 is mainly carried by the protons and is dependent on the cross product between the magnetic field unit vector and the gradient of the perpendicular pressure. The magnitude of this current cannot be found without making

assumptions of the density distribution in the magnetotail so it is not calculated here. The third and fourth terms in equation 2.75 are only present in the noon-midnight meridian plane if the protons become unmagnetized in the INS. The third term is dependent on excess positive or negative charge and the cross product between the dawn to dusk electric field and the magnetic field unit vector. This current is only present in the INS in the noon-midnight meridian plane if the protons are not responding to the magnetic field due to being unmagnetized while the electrons remain convective drifting. The fourth term is in the direction of the dawn to dusk electric field, which is the positive y-direction, and describes the current of the unmagnetized protons. Therefore, the currents produced by the third and fourth terms in equation 2.75 will be supported if it can be shown that there is an INS region where the protons are unmagnetized in the stretched magnetic field model that was presented in the previous chapter. This analysis is done in Section 4.3. The unmagnetized protons will also support the second term in equation 2.75 because as they are accelerated dawnward in the INS (Lyons and Speiser, 1982), the second term in equation 2.75 says the protons will drift anti-earthward due to the pressure gradient. Therefore, the proton reservoir will be enhanced. Overall, the summation of the currents produced by the four terms in equation 2.75 should be consistent with the current found by calculating the curl of the stretched magnetic field model. In terms of the analysis presented in this chapter, the direction of the curl of the stretched magnetic field model should be consistent with the direction of the curvature current produced by the electrons.

This section calculates the total time-independent current density by finding the curl of the magnetic field. It is found by calculating the cross product in equation 4.3, which gives

$$\vec{\nabla} \times \vec{B} = \begin{vmatrix} \hat{x} & \hat{y} & \hat{z} \\ \frac{1}{a}\frac{\delta}{\delta X} & \frac{1}{a}\frac{\delta}{\delta Y} & \frac{1}{a}\frac{\delta}{\delta Z} \\ B_x & B_y & B_z \end{vmatrix} \tag{4.4}$$

$$= \frac{1}{a}\left(\left(\frac{\delta B_z}{\delta Y} - \frac{\delta B_y}{\delta Z}\right)\hat{x} + \left(\frac{\delta B_x}{\delta Z} - \frac{\delta B_z}{\delta X}\right)\hat{y} + \left(\frac{\delta B_y}{\delta X} - \frac{\delta B_x}{\delta Y}\right)\hat{z}\right).$$

The solution for the noon-midnight meridian plane should not contain any derivatives with respect to Y or the derivatives of the y-component since the y-component has no effect in this plane. The following four derivatives in the above equation are zero (see Appendix G for proof):

$$\frac{\delta B_z}{\delta Y}(X,0,Z) = 0\,, \tag{4.5a}$$

$$\frac{\delta B_y}{\delta Z}(X,0,Z) = 0\,, \tag{4.5b}$$

$$\frac{\delta B_y}{\delta X}(X,0,Z) = 0\,, \tag{4.5c}$$

and

$$\frac{\delta B_x}{\delta Y}(X,0,Z) = 0\,. \tag{4.5d}$$

Therefore, the solution of equation 4.4 in the noon-midnight meridian plane is

$$\vec{\nabla} \times \vec{B} = \frac{1}{a}\left(\frac{\delta B_x}{\delta Z} - \frac{\delta B_z}{\delta X}\right)\hat{y}\,. \tag{4.6}$$

Inserting the above equation into equation 4.3 gives the total time-independent current density for the stretched magnetic field in the noon-midnight meridian plane as

$$\vec{J} = \frac{1}{a\mu_0}\left(\frac{\delta B_x}{\delta Z} - \frac{\delta B_z}{\delta X}\right)\hat{y}\,. \tag{4.7}$$

The necessary derivatives are calculated in Appendix G. Therefore, the direction and value of the current density vector can be found at any point in the noon-midnight meridian plane.

The overall current produced by the stretched magnetic field is purely in the y-direction in the noon-midnight meridian plane. Figure 4.1 shows the sense of this y-current in the magnetotail. There is a large area of westward current centered on the x-axis that corresponds to the NS and a large area of eastward drift that corresponds to the DZN. This is what is physically expected in the magnetotail, as discussed in Chapter 2. The eastward current in the DZN and the westward current in the NS are essential elements of a current loop in the northern half of the magnetotail. Similarly, there is a current loop in the southern half of the magnetotail with an eastward current in the DZS and a westward current in the NS. This creates the double current vortex system presented in Chapter 2. Therefore, the stretched magnetic field model presented in Chapter 3 that was created entirely based on the geometry of the field lines is consistent with a double vortex current system in the magnetotail.

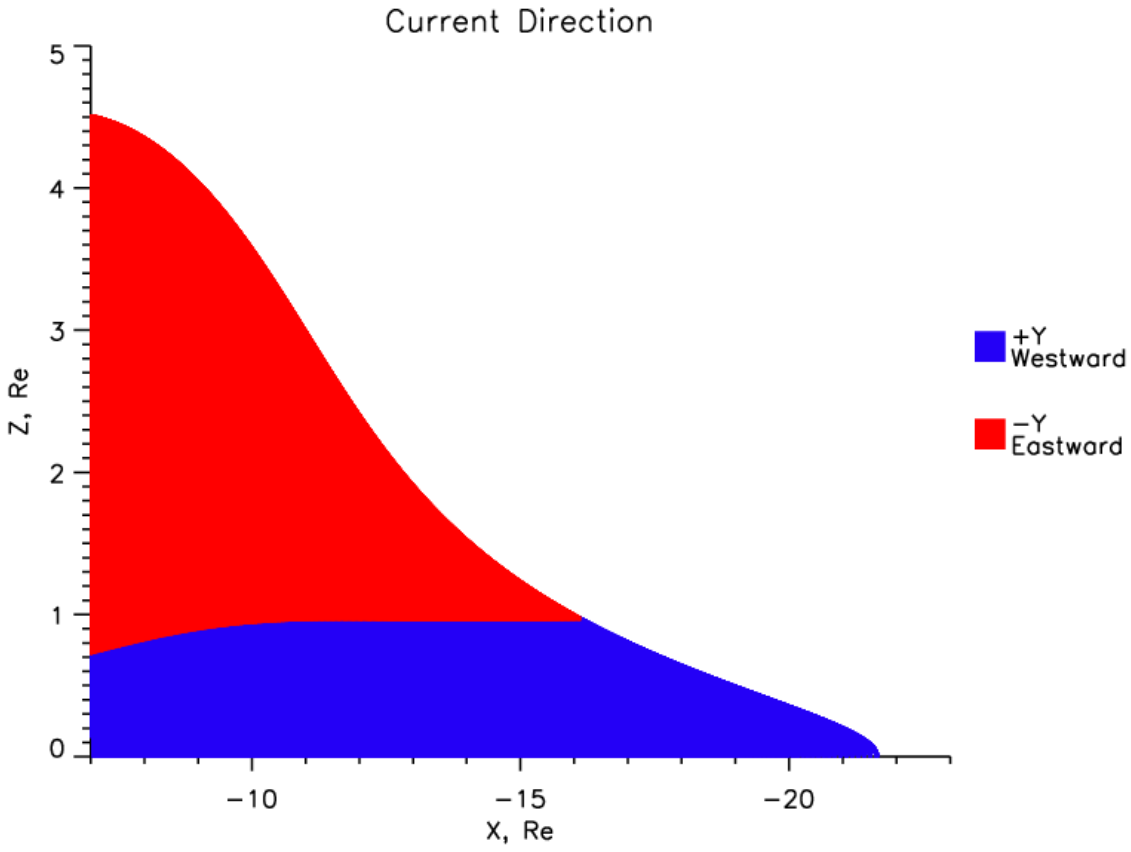

Figure 4.1 The direction of the current in the noon-midnight meridian plane derived from the time-independent form of Maxwell's fourth equation is westward in the NS and eastward in the DZN.

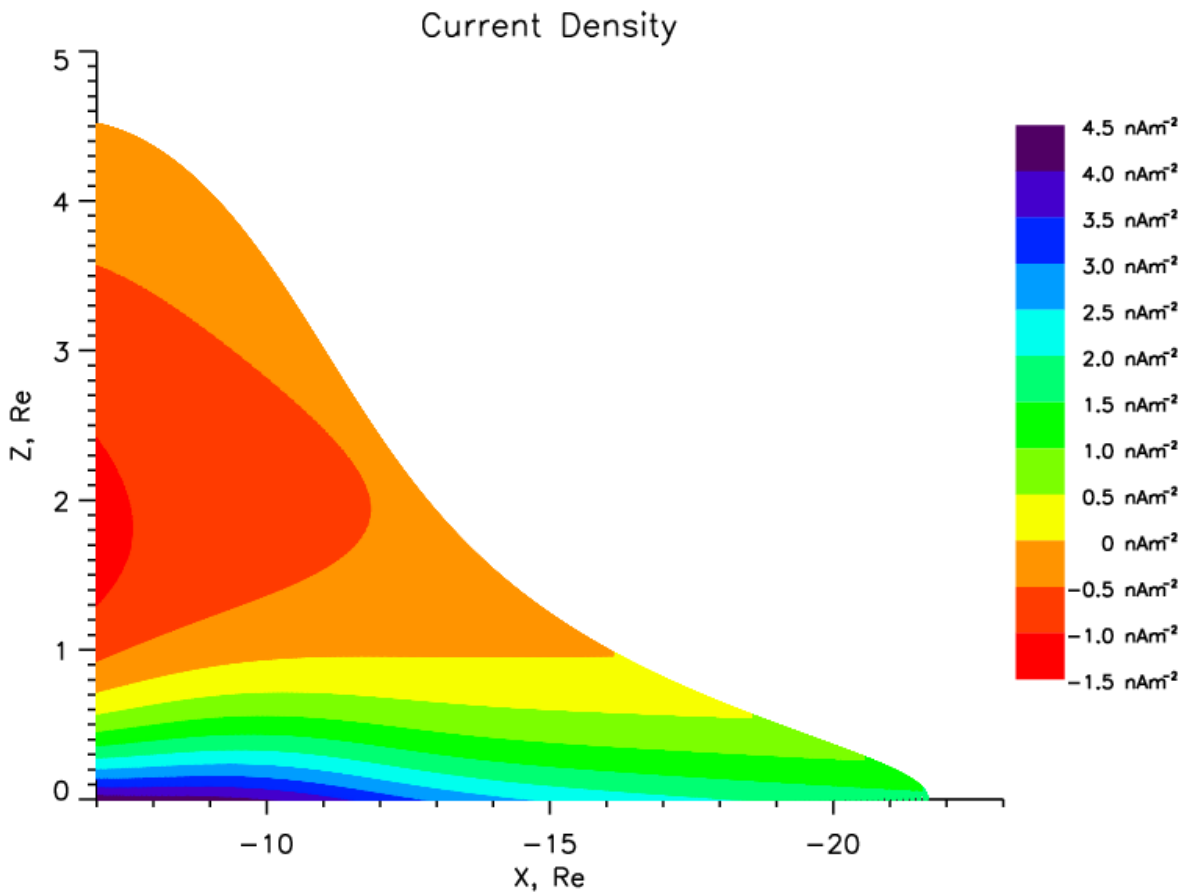

Figure 4.2 The value of the current density in the noon-midnight meridian plane derived from the time-independent form of Maxwell's fourth equation.

The value of the current density can also be found using equation 4.7. Figure 4.2 shows the value of the current density in the magnetotail. There is a very intense positive current density in the INS, indicating there is a very intense westward current in this region. There is a weaker positive current density in the ONS and a weaker negative current density in the DZN. This means that there are weaker currents in these regions compared to the INS. The INS current density is around 4.5 times more intense than the DZN current density. The intense current in the INS is physically expected. As stated in Chapter 2, the main contributors for the current in the magnetotail are the curvature current of the anisotropic electrons and the current due to the unmagnetized protons in the INS. Both the unmagnetized protons and the electrons create a westward current in the INS. Clearly, this maximizes where the curvature is greatest, and that occurs in the earthward part of the SPS where the deep minimum in the magnetic field occurs.

The particle pressure is also highest at this location, which leads to a more intense current, as seen in Figure 4.2. If the current density is integrated over the area shown in Figure 4.2, then there will be an overall westward current. This is physically expected as the current in the NS is not just the current contained in the SPS, it also contains a portion of the crosstail current. Thus, Figure 4.2 does not represent a closed system, but just a slice of the magnetosphere convection. Also, this intense current in the INS can be a key factor in the onset of the substorm. Figure 4.2 shows that the most intense current occurs in the INS at greater than $X = -12$. This corresponds to the location of the VNENL, which is where the first stretched field line reconnects to trigger substorm onset. The intense current at this location provides the necessary conditions for antiparallel reconnection through the Kelvin-Helmholtz instability, which was described in Section 2.3.2. Thus, the stretched magnetic field model that was presented in Chapter 3 inherently supports the magnetotail model that was presented in Chapter 2. The current produced by this magnetic field model found using Ampere's law supports the physical processes that are necessary for substorm onset generation in the near-Earth magnetotail SPS region. Other physical parameters can be found using the stretched magnetic field model that was presented in Chapter 3. This includes the pitch angle and gyroradius of a charged particle as well as the current direction due to specific terms in the overall current formula that was derived in Chapter 2. These parameters are analyzed in the following sections.

4.2 Pitch Angle of Charged Particles in the Magnetotail

Section 2.6.4 briefly described the pitch angle of a particle. In this section, the spectrums of pitch angles in the magnetotail are found. A particle's pitch angle can be found as a particle moves along a field line by using the first adiabatic invariant (equation 2.77). The first adiabatic invariant can be expanded by inserting the definition of the perpendicular energy, which is given in equation 2.82. This expands the first adiabatic invariant to

$$\mu = \frac{mv^2 \sin^2 \alpha}{2B} = \text{constant}. \tag{4.8}$$

Along a magnetic field line, the mass and speed of a particle will stay constant. Therefore, equating the magnetic moment at two points along a magnetic field line gives

$$\frac{mv^2\sin^2\alpha_1}{2B_1} = \frac{mv^2\sin^2\alpha_2}{2B_2}\ , \tag{4.9a}$$

which simplifies to

$$\frac{\sin^2\alpha_1}{B_1} = \frac{\sin^2\alpha_2}{B_2}\ . \tag{4.9b}$$

As briefly mentioned in Chapter 2, there are two important points concerning pitch angle along a field line. The first point is the equator. This location will have the lowest pitch angle value because it corresponds to the lowest magnetic field value. The second point is the mirror point. This location is where the particle has a 90° pitch angle. It will reverse its direction of motion at this point and continue traveling along the field line. By using equation 4.9b, the pitch angle everywhere along a field line can be found if the pitch angle is defined at one point along the field line. Typically, the equatorial pitch angle is defined. Therefore, equation 4.9b changes to

$$\frac{\sin^2\alpha}{B} = \frac{\sin^2\alpha_0}{B_0} \tag{4.10}$$

where α_0 represents the equatorial pitch angle and B_0 represents the equatorial magnetic field magnitude. Solving for the pitch angle gives

$$\alpha = \sin^{-1}\left(\sin\alpha_0\sqrt{\frac{B}{B_0}}\right)\ . \tag{4.11}$$

Now the pitch angle can be found at any point along a magnetic field line.

A range of equatorial pitch angles was used to find the path of charged particles in the magnetotail. An equatorial pitch angle was set for every field line in the magnetotail and then the pitch angles along the field line were calculated using equation 4.11. The range of equatorial pitch angles was chosen from 5° to 80°. A solution for a 0° pitch angle was not calculated because the pitch angle will remain zero as the particle travels along the field line and the particle will be absorbed by the ionosphere. A solution for a 90° pitch angle was not calculated because the particle will remain at just one spot at the equator.

In the magnetotail, the electrons have an anisotropic distribution at the low pitch angle end of the spectrum. The lowest equatorial pitch angle value that was used in these calculations was 5°. Therefore, this solution will be used to represent the path of the anisotropic electrons. This solution is shown below in Figure 4.3. The pitch angle remains below 30° in the majority of the stretched region of the magnetotail. This implies that the motion of the electrons is more parallel than perpendicular to the magnetic field vector in this SPS region, which is in agreement with the expectations from the second adiabatic invariant that were presented in Chapter 2.

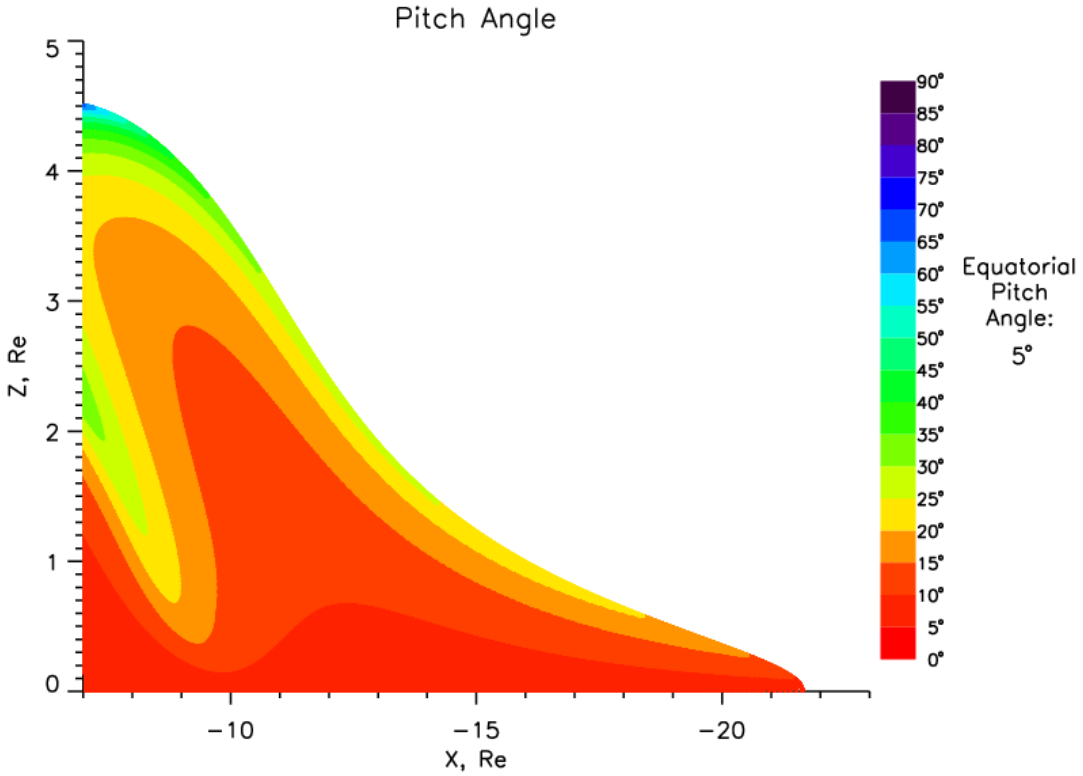

Figure 4.3 Pitch angle spectrum for an equatorial pitch angle of 5°.

The protons in the magnetotail have an isotropic distribution. This means that protons have equatorial pitch angles ranging from 0° to 90°. The pitch angle spectrum for an equatorial pitch angle of 10° is shown below in Figure 4.4. The mirror point location of the charged particles begins to appear in the stretched portion of the field line.

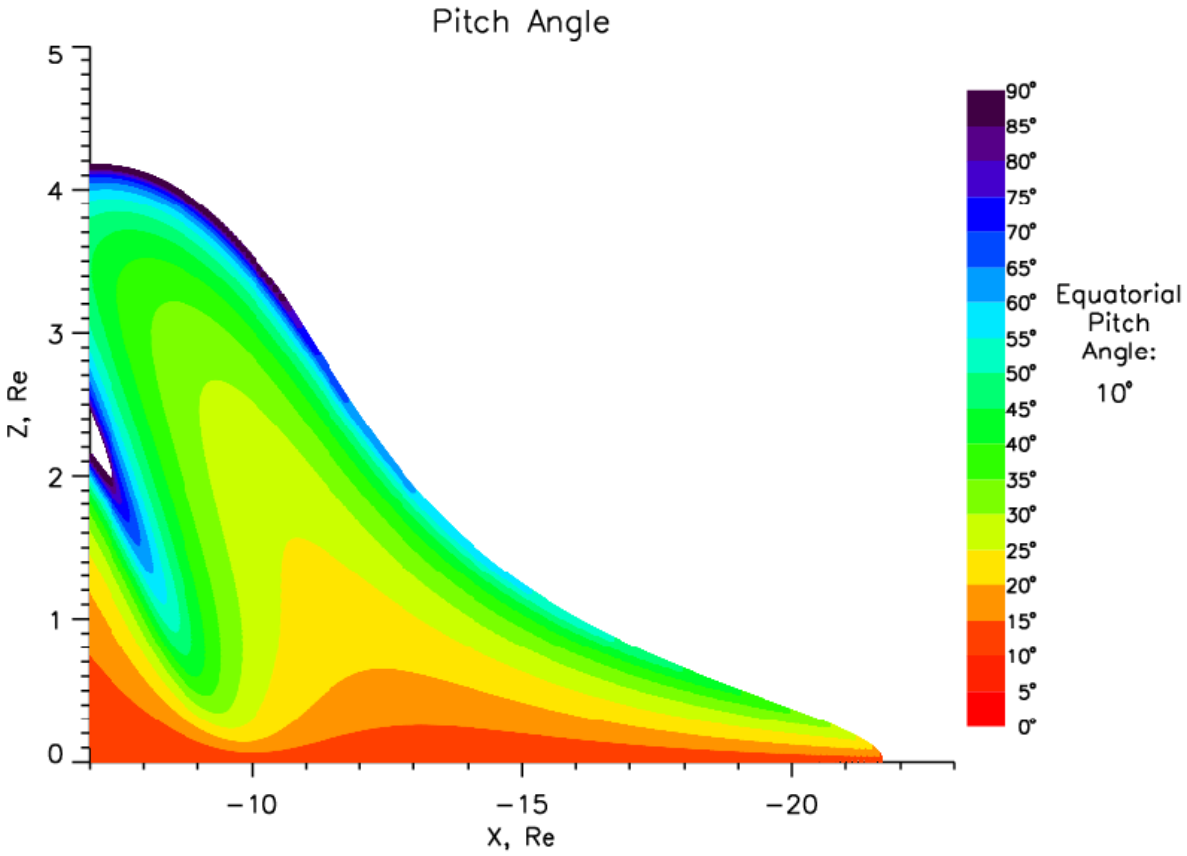

Figure 4.4 Pitch angle spectrum for an equatorial pitch angle of 10°.

As the equatorial pitch angle increases, the mirror point location moves closer to the equatorial plane. The pitch angle spectrum for an equatorial pitch angle of 40° is shown in Figure 4.5. At this point, the particle is mainly bouncing close to the equatorial plane. For greater equatorial pitch angles, the path of the charged particles becomes shorter and shorter until it stays in the equatorial plane. Therefore, the proton motion in the magnetotail varies greatly from bouncing in and out of the SPS to just staying close to the equatorial plane. The pitch angle is needed to calculate the gyroradius of the particles. This is done in the next section.

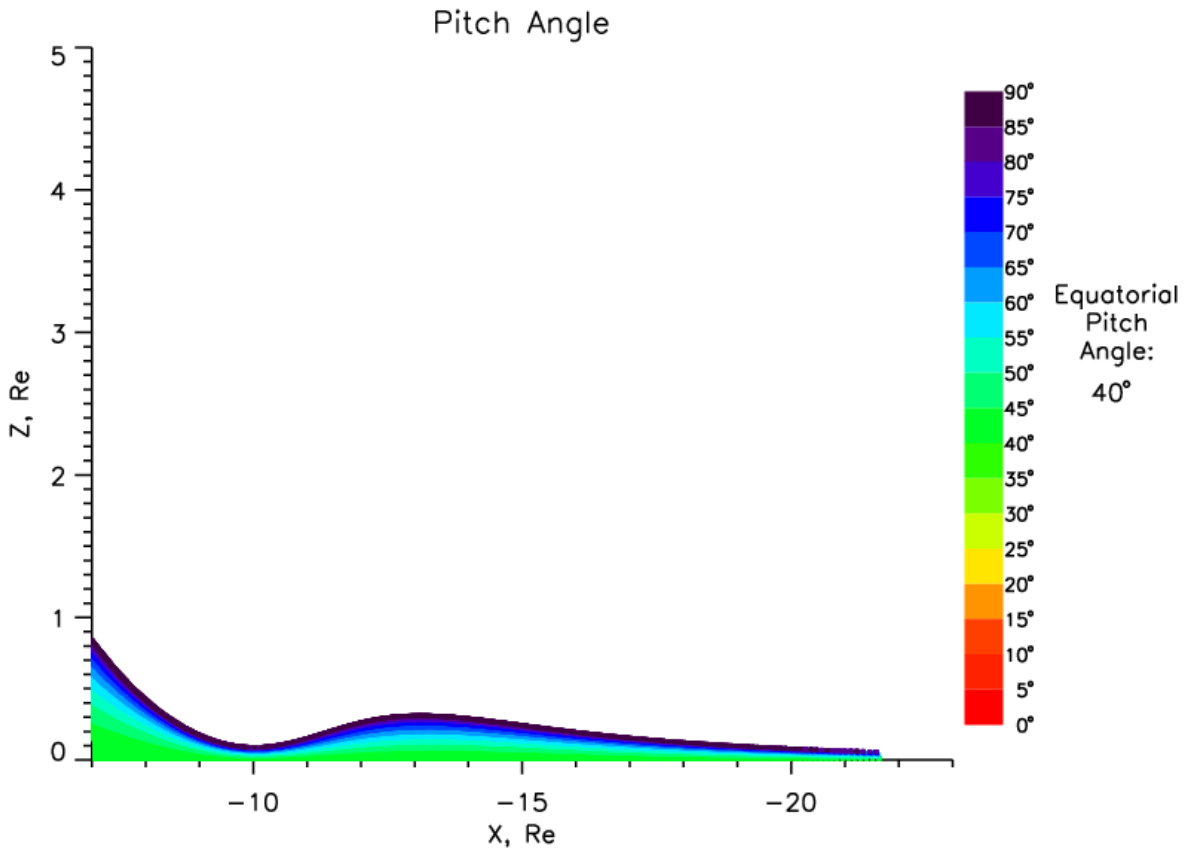

Figure 4.5 Pitch angle spectrum for an equatorial pitch angle of 40°.

4.3 Gyroradius and Unmagnetized Proton Regions

Section 2.6.4 also briefly discussed the gyroradius of a charged particle. It is given in equation 2.76. Defining the gyroradius relative to the radius of the Earth and expanding the perpendicular speed into the total speed and the pitch angle gives

$$R_g = \frac{r_g}{a} = \frac{mv\sin\alpha}{aqB}. \tag{4.12}$$

The speed of a particle can be found if the energy is known. The total energy is given as

$$W = \frac{1}{2}mv^2. \tag{4.13}$$

Solving for the total speed gives

$$v = \sqrt{\frac{2W}{m}} \, . \tag{4.14}$$

Inserting the above equation into equation 4.12 gives the relative gyroradius as

$$R_g = \frac{\sqrt{2mW}\sin\alpha}{aqB} \, . \tag{4.15}$$

In the magnetotail, the protons become unmagnetized in the INS, while the electrons remain magnetized because they have much smaller mass. The above formula can be used to find and confirm the areas in the magnetotail where the protons become unmagnetized. Defining the above equation specifically for a proton gives

$$R_g = \frac{\sqrt{2m_pW}\sin\alpha}{aeB} \, . \tag{4.16}$$

The pitch angle can be found using the method presented in the previous section. Therefore, the gyroradius of a charged particle can be found if a value for the total energy and the equatorial pitch angle are defined.

As stated in Chapter 2, the protons become unmagnetized in the central region of the NS. This splits the NS into two regions: INS and ONS. The protons are unmagnetized in the INS and magnetized in the ONS. The protons become unmagnetized because of the reversal of the x-component of the magnetic field at the center of the NS ($Z = 0$). If the proton is located so the center of its gyration is within one gyroradius of $Z = 0$, then it will be forced to change its gyration sense as it crosses the x-axis, leading to "serpentine" orbits (Speiser, 1965). As seen in equation 4.16, the gyroradius of a proton is dependent on the total energy and equatorial pitch angle of the proton. These two parameters vary from particle to particle so the boundary between the INS and ONS will also vary from particle to particle. This boundary is much more

fluid than the boundary between the NS and the DZs. However, Lyons and Speiser (1982) completed a simulation of the acceleration of the unmagnetized ions in the central region of the NS. They used two different widths for the INS: 1000 km and 5000 km. Their simulations showed that the energy gained by the unmagnetized protons as they accelerate did not vary between the different INS widths. Therefore, an overall definite boundary between the INS and ONS is not necessary because the protons will gain the same amount of energy as they accelerate in the INS even if the width of the INS changes.

The region where the proton becomes unmagnetized can be found mathematically through simple vector manipulation. The vectors that will be used are depicted in Figure 4.6. Inherently, the magnetic field vector and gyroradius vector are perpendicular to each other. The magnetic field line can be split into a summation of linear line segments. The line segment vector $\vec{L}$ can be defined as

$$\vec{L} = (X - X_0)\hat{x} + (Z - Z_0)\hat{z} \tag{4.17}$$

since it is located between the points (X_0, Z_0) and (X, Z) as seen in Figure 4.6. The point (X_0, Z_0) represents the ending point of the previous line segment and is the beginning point of the new line segment. The point (X, Z) represents the ending point of the new line segment and the current location of the center of the particle's gyration. The gyroradius vector can be defined as

$$\vec{R}_g = \left(X_g - X\right)\hat{x} + \left(Z_g - Z\right)\hat{z} \tag{4.18}$$

since it is located between the points (X, Z) and $\left(X_g, Z_g\right)$ as seen in Figure 4.6. The point $\left(X_g, Z_g\right)$ represents the actual location of the particle as it gyrates. The value of Z_g needs to be found to see if the gyroradius vector crosses the x-axis, which causes the protons to become unmagnetized.

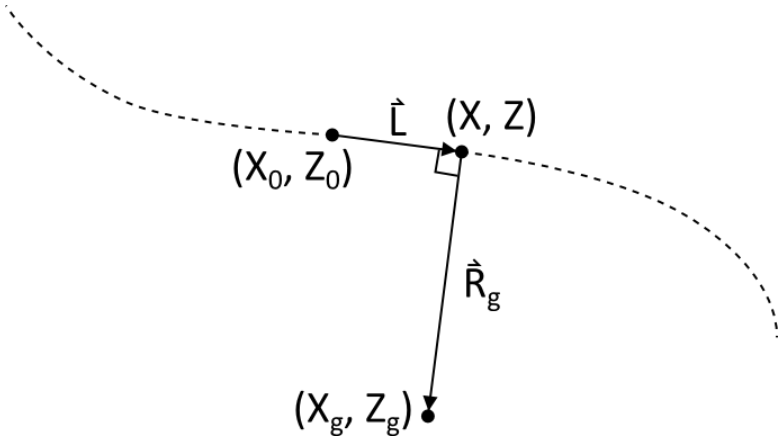

Figure 4.6 Depiction of vectors $\vec{L}$ and $\vec{R}_g$ that will be used in order to find the regions in the magnetotail where the protons become unmagnetized.

Since these two vectors are perpendicular to each other, the dot product between them will be zero. Mathematically, this is given as

$$\vec{L}\cdot\vec{R}_g = \left((X-X_0)\hat{x}+(Z-Z_0)\hat{z}\right)\cdot\left(\left(X_g-X\right)\hat{x}+\left(Z_g-Z\right)\hat{z}\right) \\ = (X-X_0)\left(X_g-X\right)+(Z-Z_0)\left(Z_g-Z\right)=0\,. \tag{4.19}$$

Solving for the x-component of the gyroradius vector gives

$$\left(X_g-X\right) = -\frac{(Z-Z_0)\left(Z_g-Z\right)}{(X-X_0)}\,. \tag{4.20}$$

Another equation is needed in order to find the value of Z_g. The magnitude of the gyroradius can be used, which is given as

$$R_g = \sqrt{\left(X_g-X\right)^2+\left(Z_g-Z\right)^2}\,. \tag{4.21}$$

Inserting equation 4.20 into the above equation gives

$$R_g = \sqrt{\frac{(Z - Z_0)^2 \left(Z_g - Z\right)^2}{(X - X_0)^2} + \left(Z_g - Z\right)^2} = \frac{Z_g - Z}{X - X_0}\sqrt{(X - X_0)^2 + (Z - Z_0)^2}\,. \tag{4.22}$$

Solving for Z_g gives

$$Z_g = Z + \frac{R_g (X - X_0)}{\sqrt{(X - X_0)^2 + (Z - Z_0)^2}}\,. \tag{4.23}$$

If the proton is traveling along the northern portion of the magnetic field line and Z_g is below zero, then the proton becomes unmagnetized. Now, the regions where this occurs in the magnetotail can be easily found.

As mentioned previously, in order to calculate the gyroradius, the total energy and equatorial pitch angle of the particle need to be defined. A typical energy for particles in the magnetotail is 1 keV. Protons will gain more energy in the magnetotail, but this is after they become unmagnetized and are accelerated by the Coulomb force in the INS. Therefore, an initial energy of 1 keV for protons will be chosen. The regions in the magnetotail where the protons will be unmagnetized were calculated for equatorial pitch angles from 5° to 80°. Since the gyroradius is dependent on the sine of the pitch angle, the gyroradius will be smaller for smaller pitch angles. Therefore, it is expected that there is only a small region where the ions are unmagnetized for an equatorial pitch angle of 5° and a large region for an equatorial pitch angle of 80°.

The magnetized and unmagnetized regions for a 1 keV proton in the magnetotail with an equatorial pitch angle of 5° are shown in Figure 4.7. The magnetized regions are represented by orange and the unmagnetized regions are represented by purple. Even at this low equatorial pitch angle, there is still a very small region at the deep minimum and the tailend of the INS where the proton becomes unmagnetized.

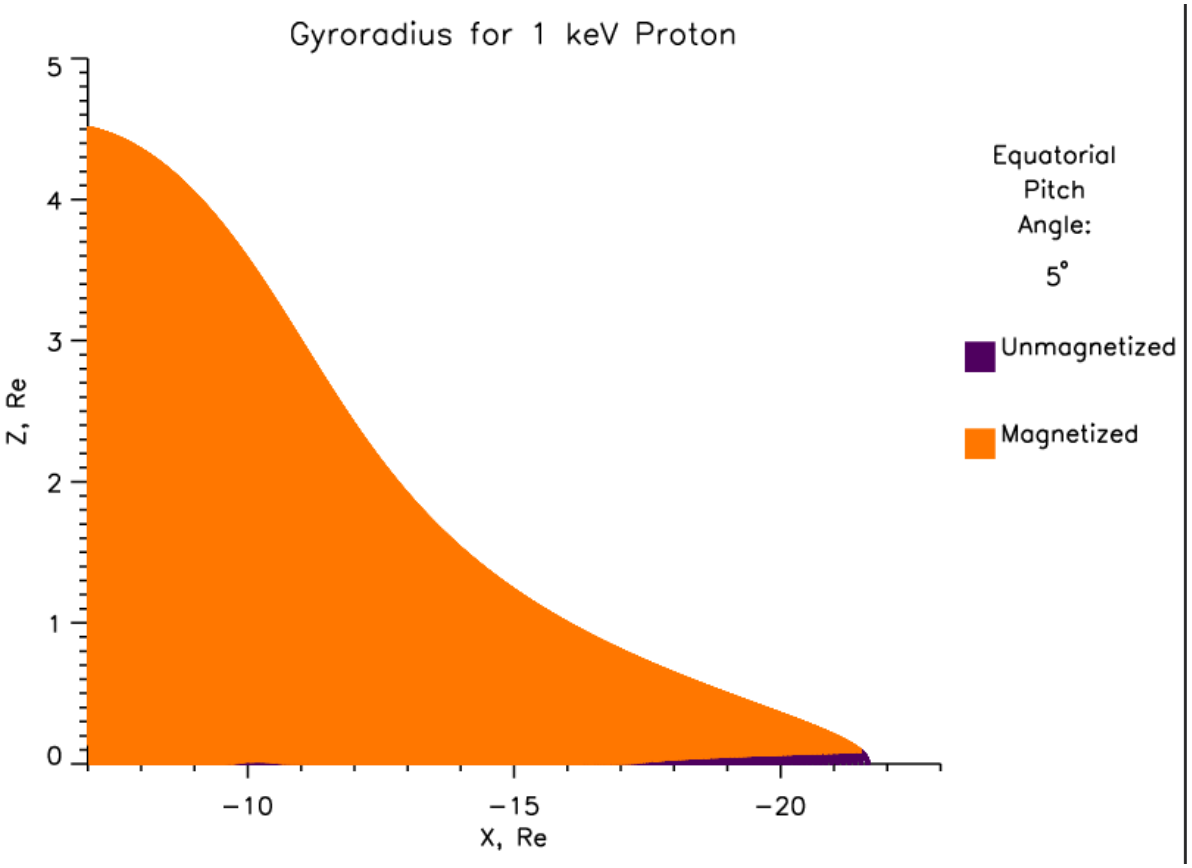

Figure 4.7 Magnetized (orange) and unmagnetized (purple) regions for a 1 keV proton in the magnetotail with an equatorial pitch angle of 5°.

The regions for a 1 keV proton in the magnetotail with an equatorial pitch angle of 30° are shown in Figure 4.8. At this point, the particle is mainly bouncing within the NS. There is one region where the protons are magnetized, which corresponds to the ONS, and a region where the protons are unmagnetized, which corresponds to the INS.

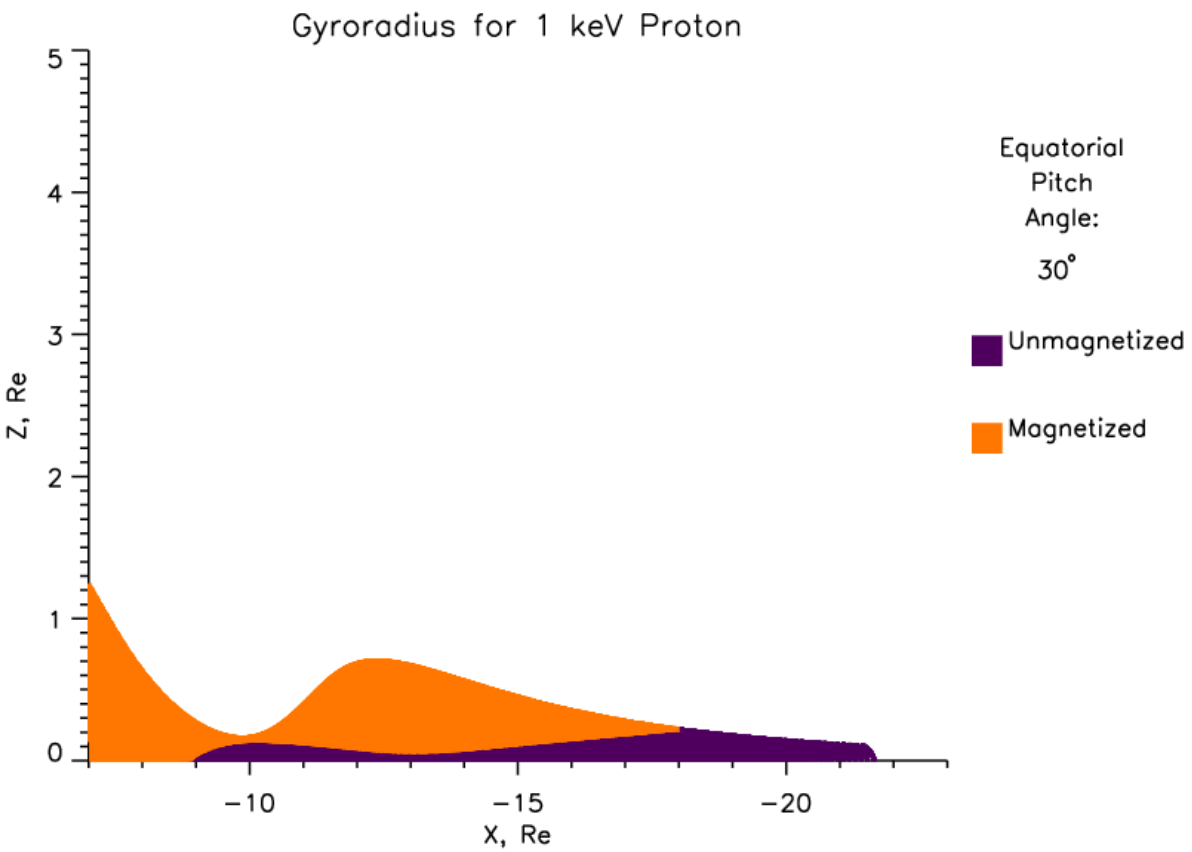

Figure 4.8 Magnetized (orange) and unmagnetized (purple) regions for a 1 keV proton in the magnetotail with an equatorial pitch angle of 30°.

The regions for a 1 keV proton in the magnetotail with an equatorial pitch angle of 60° are shown in Figure 4.9. Protons with this equatorial pitch angle are mainly bouncing within the INS. The protons are essentially unmagnetized throughout the INS, which means that they will not be adiabatic and therefore not follow the adiabatic invariants. According to Lyons and Speiser (1982), once a proton enters the INS, it will be accelerated by the dawn to dusk electric field. It will then either be ejected from the INS and continue normal bounce motion or it will be accelerated to the end of the SPS. The ejected protons have a range of pitch angles, suggesting an isotropic distribution. The electrons remain magnetized in the INS because they have a much smaller gyroradius and therefore will maintain their anisotropic distribution. Thus, the INS is the driving factor in creating an isotropic distribution of protons.

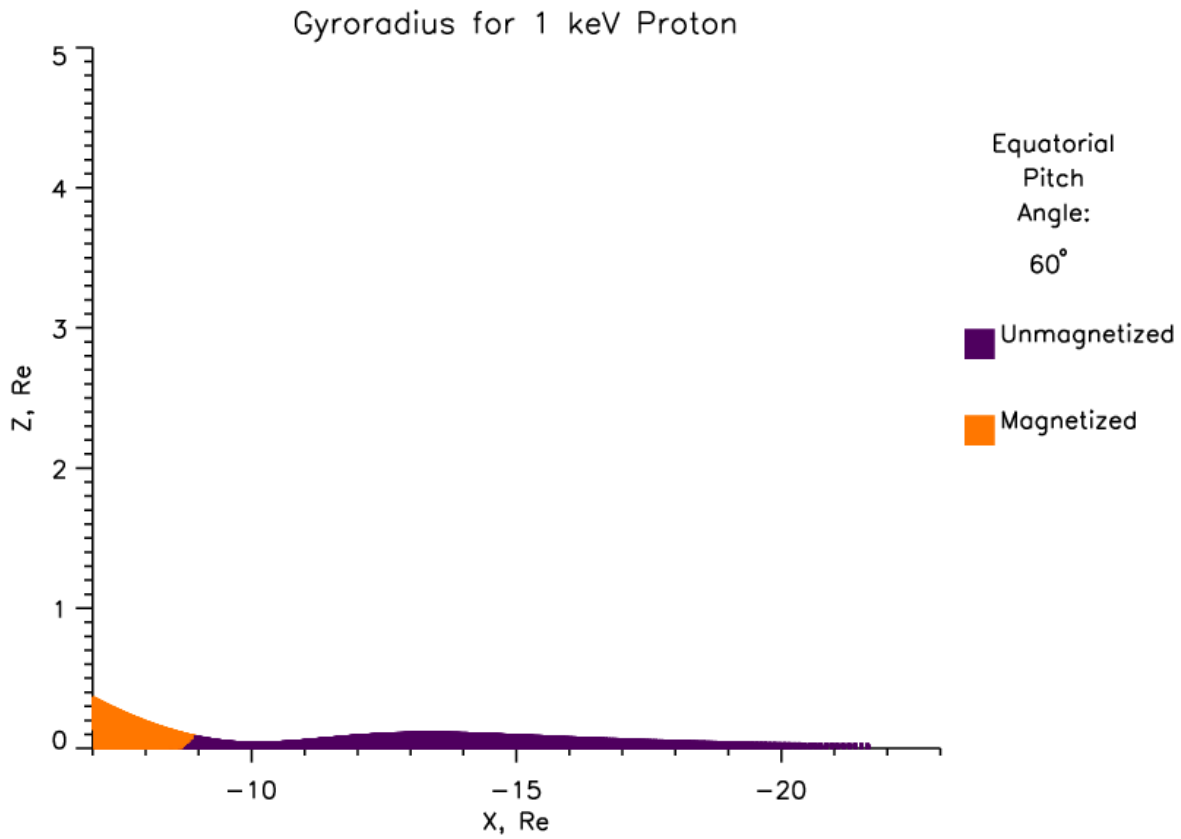

Figure 4.9 Magnetized (orange) and unmagnetized (purple) regions for a 1 keV proton in the magnetotail with an equatorial pitch angle of 60°.

The pitch angle and gyroradius of the charged particles in the magnetotail are useful parameters to understand when trying to analyze the total current in the magnetotail that was derived in Chapter 2. This is done in the next section. Specifically, the direction of the first term in the total current formula is found which describes the curvature current of the electrons.

4.4 Curvature Current of the Electrons

The overall current formula (equation 2.75) contains four terms. The summation of the currents produced by the individual terms will determine the overall current in the magnetotail. The direction of the first term, which is the current due to curvature in the magnetic field line, can be found using the stretched magnetic field model presented in the last chapter. The other three terms in the overall current formula are dependent on other factors than the magnetic field

and therefore cannot be easily calculated without making assumptions. However, the direction of the first current will provide insight into the direction of the overall current because the electron curvature current is the main contributor to the double vortex current system in the magnetotail. If the curvature current direction agrees with the current found in Section 4.1, then the magnetotail model that was presented in Chapter 2 is further supported.

The direction of the first term in equation 2.75 is dependent on the cross product between the magnetic field unit vector and curvature vector. In order to find the direction of this cross product, the curvature vector needs to be found. In Section 2.4.2, the curvature vector was defined in relation to the radius of the osculating circle. However, a more useful definition of the curvature vector is given as (its derivation can be found in Appendix B)

$$\vec{K} = \left(\hat{b} \cdot \vec{\nabla}\right)\hat{b} \,. \tag{4.24}$$

Expanding the vectors in the above equation in terms of their components gives

$$\vec{K} = \left(\left(b_x\hat{x} + b_y\hat{y} + b_z\hat{z}\right) \cdot \left(\frac{1}{a}\frac{\delta}{\delta X}\hat{x} + \frac{1}{a}\frac{\delta}{\delta Y}\hat{y} + \frac{1}{a}\frac{\delta}{\delta Z}\hat{z}\right)\right)\left(b_x\hat{x} + b_y\hat{y} + b_z\hat{z}\right). \tag{4.25}$$

Now the dot product can be evaluated. The result is

$$\vec{K} = \frac{1}{a}\left(b_x\frac{\delta}{\delta X} + b_y\frac{\delta}{\delta Y} + b_z\frac{\delta}{\delta Z}\right)\left(b_x\hat{x} + b_y\hat{y} + b_z\hat{z}\right). \tag{4.26}$$

Multiplying and collecting like terms gives the final result for the curvature vector in three dimensions as

$$\begin{aligned}\vec{K} = \frac{1}{a}\Bigg(&\left(b_x\frac{\delta b_x}{\delta X} + b_y\frac{\delta b_x}{\delta Y} + b_z\frac{\delta b_x}{\delta Z}\right)\hat{x} + \left(b_x\frac{\delta b_y}{\delta X} + b_y\frac{\delta b_y}{\delta Y} + b_z\frac{\delta b_y}{\delta Z}\right)\hat{y} \\ &+ \left(b_x\frac{\delta b_z}{\delta X} + b_y\frac{\delta b_z}{\delta Y} + b_z\frac{\delta b_z}{\delta Z}\right)\hat{z}\Bigg).\end{aligned} \tag{4.27}$$

As stated previously, since the model is only defined in the noon-midnight meridian plane, all terms involving the y-component of the magnetic field or the derivative with respect to Y should be zero. Section 3.3.1 showed that the y-component of the stretched magnetic field is zero in the noon-midnight meridian plane (equations 3.22a and 3.22b). Therefore, any term in equation 4.27 that is multiplied by the y-component of the magnetic field outside of a derivative will be zero in the noon-midnight meridian plane. Thus, the following terms are zero:

$$b_y(X,0,Z)\frac{\delta b_x}{\delta Y} = \frac{B_y(X,0,Z)}{B}\frac{\delta b_x}{\delta Y} = 0\,, \tag{4.28a}$$

$$b_y(X,0,Z)\frac{\delta b_y}{\delta Y} = \frac{B_y(X,0,Z)}{B}\frac{\delta b_y}{\delta Y} = 0\,, \tag{4.28b}$$

and

$$b_y(X,0,Z)\frac{\delta b_z}{\delta Z} = \frac{B_y(X,0,Z)}{B}\frac{\delta b_z}{\delta Z} = 0\,. \tag{4.28c}$$

There are only two terms in equation 4.27 left that contain the y-component of the magnetic field. The first term involves the derivative of the y-component of the magnetic field unit vector with respect to X. The derivative in the term can be expanded as

$$b_x\frac{\delta b_y}{\delta X} = b_x\frac{\delta}{\delta X}\left(\frac{B_y}{B}\right) = b_x\left(\frac{1}{B}\frac{\delta B_y}{\delta X} + B_y\frac{\delta}{\delta X}\left(\frac{1}{B}\right)\right) = 0\,. \tag{4.29}$$

The first term in the above equation is zero because the derivative of the y-component with respect to X is zero in the noon-midnight meridian plane (see Appendix G.2 for proof), and the second term in the above equation is zero because the y-component is outside the derivative. The other term that needs to be calculated involves the derivative of the y-component of the magnetic field unit vector with respect to Z. The derivative in the term can be expanded as

$$b_z \frac{\delta b_y}{\delta Z} = b_z \frac{\delta}{\delta Z}\left(\frac{B_y}{B}\right) = b_z \left(\frac{1}{B}\frac{\delta B_y}{\delta Z} + B_y \frac{\delta}{\delta Z}\left(\frac{1}{B}\right)\right) = 0\,. \tag{4.30}$$

The first term in the above equation is zero because the derivative of the y-component with respect to Z is zero in the noon-midnight meridian plane (see Appendix G.2 for proof), and the second term in the above equation is zero because the y-component is outside the derivative. After removing all terms that are zero in the noon-midnight meridian plane, the curvature vector for the noon-midnight meridian plane is given as

$$\vec{K} = \frac{1}{a}\left(\left(b_x \frac{\delta b_x}{\delta X} + b_z \frac{\delta b_x}{\delta Z}\right)\hat{x} + \left(b_x \frac{\delta b_z}{\delta X} + b_z \frac{\delta b_z}{\delta Z}\right)\hat{z}\right)\,. \tag{4.31}$$

Now the cross product between the magnetic field unit vector and the curvature vector can be found. In the noon-midnight meridian plane, the magnetic field vector only has x and z components. Therefore, the cross product can be easily found and is given as

$$\hat{b} \times \vec{K} = (b_x\hat{x} + b_z\hat{z}) \times (K_x\hat{x} + K_z\hat{z}) = (b_z K_x - b_x K_z)\hat{y}\,. \tag{4.32}$$

Inserting the components for the curvature vector into the above formula gives

$$\hat{b} \times \vec{K} = \frac{1}{a}\left(b_z\left(b_x \frac{\delta b_x}{\delta X} + b_z \frac{\delta b_x}{\delta Z}\right) - b_x\left(b_x \frac{\delta b_z}{\delta X} + b_z \frac{\delta b_z}{\delta Z}\right)\right)\hat{y}\,. \tag{4.33}$$

Expanding the derivatives in the above formula gives

$$\begin{aligned}\hat{b} \times \vec{K} = \frac{1}{a}\Bigg(b_z\Bigg(b_x\left(\frac{1}{B}\frac{\delta B_x}{\delta X} - \frac{B_x}{B^2}\frac{\delta B}{\delta X}\right) + b_z\left(\frac{1}{B}\frac{\delta B_x}{\delta Z} - \frac{B_x}{B^2}\frac{\delta B}{\delta Z}\right)\Bigg) \\ - b_x\left(b_x\left(\frac{1}{B}\frac{\delta B_z}{\delta X} + \frac{B_z}{B^2}\frac{\delta B}{\delta X}\right) + b_z\left(\frac{1}{B}\frac{\delta B_z}{\delta Z} - \frac{B_z}{B^2}\frac{\delta B}{\delta Z}\right)\right)\Bigg)\hat{y}\,,\end{aligned} \tag{4.34}$$

which simplifies to

$$\hat{b} \times \vec{K} = \frac{1}{aB}\left(b_z\left(b_x\frac{\delta B_x}{\delta X} + b_z\frac{\delta B_x}{\delta Z}\right) - b_x\left(b_x\frac{\delta B_z}{\delta X} + b_z\frac{\delta B_z}{\delta Z}\right)\right)\hat{y}\,. \tag{4.35}$$

The necessary derivatives are calculated in Appendix G. Therefore, the direction of the cross product between the magnetic field unit vector and the curvature vector can be found at any point in the noon-midnight meridian plane.

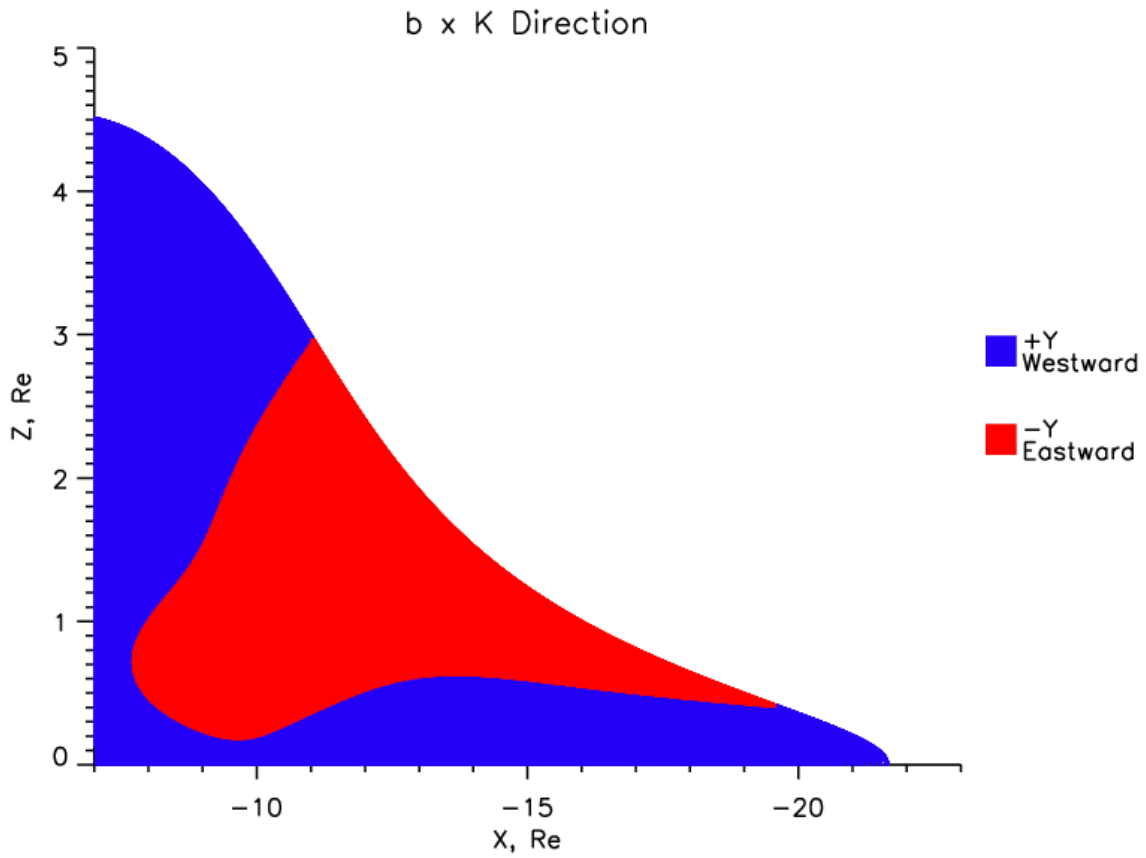

Figure 4.10 The direction of cross product between the magnetic field vector and the curvature vector creates a westward direction that corresponds to the NS and an eastward direction that corresponds to the DZN.

The cross product between the magnetic field vector and the curvature vector is purely in the y-direction. This means that it will produce a result in either the positive y (westward) or

negative y (eastward) direction. The direction of this cross product is shown in Figure 4.10. The colour blue represents the westward direction and the colour red represents the eastward direction. The cross product creates a westward result in a region that corresponds to the NS and an eastward drift in the region that corresponds to the DZN. As stated in Section 2.6, this is what is physically expected for the overall current in the magnetotail.

The electrons carry the current due to curvature in the magnetotail. The direction of this current is not only due to the cross product between the magnetic field vector and the curvature vector but is also due to the difference between twice the parallel energy and the perpendicular energy. As long as this difference produces a positive result, the direction of the current produced by this term will follow what is shown in Figure 4.10. The parallel and perpendicular energy are both dependent on the pitch angle of the particle. The pitch angles that will produce a positive result for this difference can be easily found. First, twice the parallel energy needs to be bigger than the perpendicular energy, which is mathematically given as

$$2W_{\parallel} > W_{\perp} . \tag{4.36}$$

In terms of pitch angle, the parallel and perpendicular energies are defined as

$$W_{\parallel} = \frac{1}{2} m v^2 \cos^2\alpha \tag{4.37a}$$

and

$$W_{\perp} = \frac{1}{2} m v^2 \sin^2\alpha . \tag{4.37b}$$

Inserting these equations into equation 4.36 and cancelling out common terms gives

$$\cos^2\alpha < \frac{1}{2}\sin^2\alpha . \tag{4.38}$$

Solving for α gives the range of pitch angles that will produce a positive result as

$$\alpha < 54.74° . \quad 4.39$$

Therefore, as long as the pitch angle of the particle is under 55°, the curvature current will be as depicted in Figure 4.10. The spectrum of pitch angles for various equatorial pitch angles were calculated in Section 4.2. The spectrum for a low equatorial pitch angle (5°) is shown in Figure 4.3. As can be seen in this figure, the pitch angle never is above 30° in the magnetotail. Therefore, the parallel energy will always be greater than the perpendicular energy for the electrons. Thus, the first term in the overall current formula will create a direction depicted in Figure 4.10, which is what is physically expected.

As stated in Chapter 2, the current in the magnetotail is mainly driven by the curvature current of the electrons and the current due to the unmagnetized protons in the INS. The current due to the unmagnetized protons in the INS enhances the westward current that is already present due to the curvature current of the electrons. Therefore, the current direction shown in Figure 4.10 represents the direction of the total current in the magnetotail as described by the total current equation that was derived in Chapter 2 (equation 2.75). This matches the current direction that was found by analyzing the stretched magnetic field model using Ampere's law and is shown in Figure 4.1. Both figures have a westward current in the NS and an eastward current in the DZN. However, the boundary between the NS and DZN is not the same in both figures but it is close. The NS is bigger in Figure 4.1 than in Figure 4.10. This could imply that the other current terms in the total current formula (equation 2.75) enhance the NS enough to increase its boundaries. Physically, this is a valid statement because both the current due to the cross product between the magnetic field unit vector and the gradient of the perpendicular particle pressure and the current due to the unmagnetized protons enhance the westward current that is present in the NS. Also, the wider NS in the results for the total current could imply that the stretched magnetic field model itself is not correct. Different equations for the stretched magnetic field could produce the expected result. However, in general the current directions presented in Figure 4.1 and Figure 4.10 support the model of the nightside magnetosphere that was presented in Chapter 2.

4.5 Conclusions from Analysis

The stretched magnetic field model presented in the last chapter can be used to calculate parameters in the magnetotail in order to support the magnetotail model that was presented in Chapter 2. The parameters that were calculated in this chapter include the pitch angle and gyroradius at any point in the magnetotail as well as the direction of the first term in the overall current formula along with the overall current direction and current density value. The total current formula was derived in Chapter 2 and the result is given in equation 2.75. It consists of four terms: the curvature current of the anisotropic electrons, the gradient of the perpendicular particle pressure current of the isotropic protons, the convective current due to excess protons or electrons, and the current due to the unmagnetized protons in the INS. The summation of these four currents in the magnetotail will produce the double vortex current system that was presented in Section 2.6.4. In the noon-midnight meridian plane, the double vortex current system is composed of a westward current in the NS and an eastward current in the DZs. The current can be calculated from the stretched magnetic field model that was presented in the previous chapter by using two different methods. First, Ampere's law states that the curl of a magnetic field equals the total current density. Therefore, the current produced by the stretched magnetic field model can be directly found. Second, the direction of the current produced by the individual terms in equation 2.75 can be found and the total current will be the summation of these results. Overall, the total current found using Ampere's law and the total current found by summing the results from the four terms in equation 2.75 should equal each other and follow the double vortex current system that was proposed in Chapter 2.

Figure 4.1 shows the direction of the total current in the magnetotail that was derived from Ampere's law. There is a westward current in the NS and an eastward current in the DZN, which supports the double vortex current system. The stretched magnetic field model was created to have the stretched field line shape that was proposed in Section 2.3.1. Therefore, the results presented in Figure 4.1 show that the stretched field line shape that has four inflection points creates a double vortex system in the magnetotail. Figure 4.2 shows the value of the total current density in the magnetotail that was derived from Ampere's law. It shows a very strong westward current density in the INS, a weak westward current density in the ONS, and a weak

eastward current density in the DZN. The INS current density is approximately 4.5 times more intense than the current density in the DZN. This supports the magnetotail model that was presented in Chapter 2 because the main contributors for the current in the magnetotail are the curvature current of the anisotropic electrons and the current due to the unmagnetized protons in the INS. Both of these currents are expected to have a westward current in the INS, so the strong westward current density seen in Figure 4.2 is physically expected. The strongest current density in the INS occurs at $X > -12$ according to Figure 4.2. This corresponds to where the field lines have the most curvature, the most earthward stretched field lines. An intense current is needed at this area to facilitate antiparallel reconnection through the Kelvin-Helmholtz instability. Therefore, the strong current density in the INS at $X > -12$ seen in Figure 4.2 supports the magnetotail model that was presented in Chapter 2. Overall, the stretched magnetic field model that was presented in Chapter 3 inherently supports the magnetotail model that was presented in Chapter 2 from analyzing the currents produced by this magnetic field using Ampere's law.

In order to analyze the direction of the current produced by the individual terms in the overall current formula (equation 2.75), the pitch angle and gyroradius of a particle need to be analyzed first. A particle's pitch angle can be found by using the first adiabatic invariant if an equatorial pitch angle value is set. The pitch angle spectrum for a low equatorial pitch angle ($\alpha_0 = 5°$) remains below 30° in the majority of the stretched region of the magnetotail (see Figure 4.3). This figure supports the motion of the anisotropic electrons being more parallel than perpendicular to the magnetic field vector as discussed in Section 2.6.4. The protons are assumed to be isotropic in the magnetotail so they will have equatorial pitch angles ranging from 0° to 90°. For higher equatorial pitch angle values, the mirror point location appears in the stretched region of the magnetotail and moves closer to the equatorial plane as the equatorial pitch angle increases (see Figure 4.4 and Figure 4.5). Overall, the pitch angle analysis shows that the electron motion stays mainly parallel to the magnetic field in the stretched region of the magnetotail and the proton motion varies greatly from bouncing in and out of the SPS to just staying close to the equatorial plane.

However, this does not represent the true motion of the protons. The NS is split into two regions: INS and ONS. In the INS, the protons are unmagnetized whereas in the ONS, the

protons are magnetized. The area where the protons are unmagnetized can be found by analyzing the gyroradii of the protons. The boundary between the INS and ONS is fluid because the gyroradius of a particle is dependent on its total energy and equatorial pitch angle, which changes from particle to particle. However, Lyons and Speiser (1982) show that the amount of energy gained by the proton as it accelerates in the INS is not dependent on the width of the INS. Therefore, an overall definite boundary between the INS and ONS is not necessary. For a proton with 1 keV of total energy, a region where it will be unmagnetized is present for every equatorial pitch angle. For an equatorial pitch angle of 5°, there are two regions where the proton will become unmagnetized (see Figure 4.7). The two regions are the deep minimum of the magnetic field (earthward end of INS) and the tailend of the NS. For an equatorial pitch angle of 30°, there is an obvious INS and ONS region (see Figure 4.8). For an equatorial pitch angle of 60°, the motion of the particle is completely within the INS (see Figure 4.9). The protons are essentially unmagnetized in the INS so they do not follow the adiabatic invariants. However, once the proton enters the INS it will either be accelerated to the end of the SPS or be ejected out of the INS at some point and continue bouncing (Lyons and Speiser, 1982). The ejected particles have a range of pitch angles, which create an isotropic distribution for the protons. Therefore, the INS is a very important region in the magnetotail. It creates unmagnetized protons that accelerate due to the Coulomb force and enhance the westward current. Overall, there will always be a region where a proton becomes unmagnetized, so the NS will always be split into an INS and ONS region even if the boundary between the regions varies from particle to particle.

The first term in the overall current formula (equation 2.75) describes the curvature current of the anisotropic electrons. The direction of this current is dependent on the cross product between the magnetic field unit vector and the curvature vector as well as the difference between the parallel and perpendicular pressure of the particle. The cross product has a westward direction in the NS and an eastward direction in the DZN (see Figure 4.10). The difference between the parallel and perpendicular energies of the anisotropic electrons will be positive as long as the pitch angle is less than 55°. For an equatorial pitch angle of 5°, the pitch angle of a particle remains below 30° for the majority of the stretched region of the magnetotail (see Figure 4.3). Therefore, the difference between the parallel and perpendicular energies of the

anisotropic electrons will remain positive in the stretched region of the magnetotail. Thus, the direction of the curvature current will correspond to that shown in Figure 4.10.

The direction of the first term in the overall current formula (equation 2.75) is the only one that could be calculated directly from the stretched magnetic field model that was presented in the previous chapter. The direction of the gradient of the perpendicular particle pressure current (second term in equation 2.75) and the convective current (third term in equation 2.75) could not be calculated without making assumptions concerning the density distribution in the magnetotail. The direction of the current due to the unmagnetized protons is in the direction of the dawn to dusk electric field, which is the westward direction. From the gyroradius analysis, it was shown that the protons will become unmagnetized in the magnetotail dividing the NS into an INS and ONS region. The current due to the unmagnetized protons is evident in Figure 4.2 due to the enhanced current density in the INS region. Comparing Figure 4.1 and Figure 4.10, it can clearly be seen that the total current in the magnetotail and the curvature current of the anisotropic electrons are very similar. Both figures show a westward current in the NS and an eastward current in the DZN. However, the boundary between the NS and DZN is close but not the same in both figures. The NS is bigger in Figure 4.1 than in Figure 4.10. This could imply that other terms in the overall current equation (equation 2.75) enhance the NS current, which causes the NS to become bigger. Specifically, the gradient of the perpendicular particle pressure current that will be carried by the isotropic protons can potentially enhance the NS current as it is expected to produce a westward current in the magnetotail as shown in Section 2.6.2. The thicker NS could also imply that the equations for the stretched magnetic field are incorrect and different equations could provide the expected result. Overall, the current presented in Figure 4.1 and Figure 4.10 agree with each other, which shows that the direction of the total current density agrees with the direction of the curvature current of the anisotropic electrons. Also, these results agree with the double vortex current system that was presented in Chapter 2. Therefore, the results found in this chapter using the stretched magnetic field model presented in the last chapter fully support the magnetotail model that was presented in Chapter 2, namely that the geometry of the stretched magnetic field lines leads to a double vortex current system in the magnetotail.

Chapter 5

Alternative Solution to Divergence Problem

According to Maxwell's equations, the divergence of a magnetic field must equal zero. In Section 3.3, this was accomplished by solving for a y-component of the stretched magnetic field that would force the divergence of the three dimensional magnetic field to be zero. As was shown in Section 3.4, the y-component that was found did not end up being entirely physical. If the limit was taken in either the positive or negative y-direction, the y-component of the magnetic field would have a definite answer, instead of zero as expected. However, since the model will only be used in the noon-midnight meridian plane where the y-component has no effect, the stretched magnetic field equations were deemed physical for the purposes of this thesis. Over the course of this Masters research program, another solution was attempted to fix the divergence of the stretched magnetic field model. This solution involved adding the gradient of a scalar correction potential ϕ to the model magnetic field, forcing the divergence of the total field to be zero. This led to a form of Poisson's equation for ϕ. In order to solve Poisson's equation, a spherical harmonic expansion was used. However, many problems were encountered when numerically trying to solve the equation using Mathematica. In the end, it was decided that, with the readily available computer system, it was too time consuming to find an accurate solution using this method. Also, at a conference, it was suggested that this solution assumes the correction potential does not contribute any currents and therefore does not represent the most general solution. However, the initial stretched magnetic field model does account for the currents present in the magnetotail; therefore, it is assumed that the correction scalar potential can lead to zero divergence without contributing any more currents. Even though a solution was not found using this method, a large amount of time was spent attempting this Poisson solution of the zero divergence problem. Therefore, this chapter will present this method and the problems that were encountered.

5.1 Derivation of General Poisson Solution

Section 3.2 describes a set of equations that were designed to represent the stretched magnetic field in the noon-midnight meridian plane (equations 3.4a-3.4c). Maxwell's equations state that the divergence of a magnetic field must be zero. Divergence is inherently a three dimensional entity. Therefore, as was done in Section 3.3, the model equations need to be defined in three dimensions (see equation 3.11a and 3.11b). As was shown in Section 3.3, these equations are not divergence free, which is mathematically represented as

$$\vec{\nabla} \cdot \vec{B}_{model} \neq 0 \,. \tag{5.1}$$

One method to fix this is by adding a component to the model magnetic field in order to force the divergence to be zero. The added component is chosen to be the gradient of a correction potential ϕ. Therefore, the total magnetic field is given as

$$\vec{B}_{total} = \vec{B}_{model} + \vec{\nabla}\phi \,. \tag{5.2}$$

The correction potential will not contribute to any currents in the system. This can be easily shown by using Maxwell's fourth equation, which is given in equation 4.3. Inserting the total magnetic field (equation 5.2) into Maxwell's fourth equation gives

$$\vec{\nabla} \times \vec{B}_{total} = \vec{\nabla} \times \left(\vec{B}_{model} + \vec{\nabla}\phi\right) = \vec{\nabla} \times \vec{B}_{model} + \vec{\nabla} \times \vec{\nabla}\phi = \vec{\nabla} \times \vec{B}_{model} = \mu_0 \vec{J} \,. \tag{5.3}$$

Thus, the correction potential will not contribute to any currents in the system. The divergence of the magnetic field is given by Maxwell's second equation, which is given in equation 3.9. Inserting the total magnetic field (equation 5.2) into Maxwell's second equation gives

$$\vec{\nabla} \cdot \vec{B}_{total} = \vec{\nabla} \cdot \vec{B}_{model} + \nabla^2\phi \,. \tag{5.4}$$

Setting the above equation to zero and rearranging gives Poisson's equation with the divergence of the model magnetic field acting as the source term, which is mathematically represented as

$$\nabla^2\phi = -\vec{\nabla}\cdot\vec{B}_{model}\,. \tag{5.5}$$

In electrodynamics, Poisson's equation appears when either describing the electric potential for electric fields or vector potential for magnetic fields. It arises through manipulation of Maxwell's equations. For the electric potential, Poisson's equation takes the form of (Griffiths, page 83)

$$\nabla^2 V = -\frac{\rho}{\epsilon_0} \tag{5.6}$$

where ρ is the charge density. The solution of the above equation is typically given as (Griffiths, page 84)

$$V(r,\theta,\varphi) = \frac{1}{4\pi\epsilon_0}\int \frac{\rho(r',\theta',\varphi')}{|\vec{r}-\vec{r}'|}\,d\tau' \tag{5.7}$$

where the vector $\vec{r}$ represents the radius to the field point or the location where the potential is to be calculated and the vector $\vec{r}'$ represents the radius to the source point or where the electric charge is located. For the vector potential, Poisson's equation takes the form of (Griffiths, page 235)

$$\nabla^2\vec{A} = -\mu_0\vec{J}\,. \tag{5.8}$$

The solution of the above equation is typically given as (Griffiths, page 235)

$$\vec{A}(r,\theta,\varphi) = \frac{\mu_0}{4\pi}\int \frac{\vec{J}(r',\theta',\varphi')}{|\vec{r}-\vec{r}'|}\,d\tau'\,. \tag{5.9}$$

Therefore, by following the solutions outlined above, the solution to equation 5.5 will be

$$\phi(r,\theta,\varphi) = \frac{1}{4\pi}\int \frac{\vec{\nabla}\cdot\vec{B}_{model}(r',\theta',\varphi')}{|\vec{r}-\vec{r}'|}d\tau' \ . \tag{5.10}$$

The denominator in equation 5.10 will cause a singular point when $\vec{r} = \vec{r}'$. In order to get a useable solution, the denominator can be expanded in terms of Legendre polynomials to avoid the case where $\vec{r} = \vec{r}'$. The first case is where $\vec{r} > \vec{r}'$. The denominator can be expanded to (Di Bartolo, page 37)

$$\frac{1}{|\vec{r}-\vec{r}'|} = \sum_{l=0}^{\infty}\frac{(r')^l}{r^{l+1}}P_l(\cos\theta) \tag{5.11}$$

where $P_l(\cos\theta)$ represents the Legendre polynomial function in unprimed coordinates. The second case is where $\vec{r} < \vec{r}'$. The denominator can be expanded to (Di Bartolo, page 37)

$$\frac{1}{|\vec{r}-\vec{r}'|} = \sum_{l=0}^{\infty}\frac{r^l}{(r')^{l+1}}P_l(\cos\theta)\ . \tag{5.12}$$

Legendre polynomials are defined in terms of spherical harmonics by (Di Bartolo, page 40)

$$P_l(\cos\theta) = \frac{4\pi}{2l+1}\sum_{m=-l}^{l}Y_{lm}^*(\theta',\varphi')Y_{lm}(\theta,\varphi) \tag{5.13}$$

where $Y_{lm}(\theta,\varphi)$ represents the spherical harmonic function in unprimed coordinates and $Y_{lm}^*(\theta',\varphi')$ represents the complex conjugate of the spherical harmonic function in primed coordinates. Thus, equation 5.11 and equation 5.12 can be expanded to

$$\frac{1}{|\vec{r}-\vec{r}'|} = 4\pi\sum_{l=0}^{\infty}\left(\frac{1}{2l+1}\right)\frac{(r')^l}{r^{l+1}}\sum_{m=-l}^{l}Y_{lm}^*(\theta',\varphi')Y_{lm}(\theta,\varphi) \ \text{ for } \vec{r} > \vec{r}' \tag{5.14a}$$

and

$$\frac{1}{|\vec{r}-\vec{r}'|} = 4\pi \sum_{l=0}^{\infty} \left(\frac{1}{2l+1}\right) \frac{r^l}{(r')^{l+1}} \sum_{m=-l}^{l} Y_{lm}^*(\theta', \varphi') Y_{lm}(\theta, \varphi) \text{ for } \vec{r} < \vec{r}' \,. \tag{5.14b}$$

The above equations can then be inserted into equation 5.10. In order to account for different ranges of the above equations, the integral in equation 5.10 can be split into two integrals. The first integral will represent the range where $\vec{r}$ is greater than $\vec{r}'$ and, thus, will have the integration bounds in r' from 0 to r when describing all space. The second integral will represent the range where $\vec{r}$ is less than $\vec{r}'$ and, thus, will have the integration bounds in r' from r to ∞ when describing all space. Therefore, equation 5.10 becomes

$$\phi(r, \theta, \varphi) = \sum_{l=0}^{\infty} \frac{1}{2l+1} \sum_{m=-l}^{l} Y_{lm}(\theta, \varphi) \left(\frac{c_{lm}(r)}{r^{l+1}} + r^l d_{lm}(r) \right) \tag{5.15}$$

where $c_{lm}(r)$ and $d_{lm}(r)$ contain the integrals over the primed coordinates. Mathematically, in terms of integration over all space, they are given by

$$c_{lm}(r) = \int_0^r \int_0^{\pi} \int_0^{2\pi} \vec{\nabla} \cdot \vec{B}_{model}(r', \theta', \varphi') Y_{lm}^*(\theta', \varphi') (r')^{l+2} \sin\theta' \, dr' d\theta' d\varphi' \tag{5.16a}$$

and

$$d_{lm}(r) = \int_r^{\infty} \int_0^{\pi} \int_0^{2\pi} \vec{\nabla} \cdot \vec{B}_{model}(r', \theta', \varphi') Y_{lm}^*(\theta', \varphi') \frac{(r')^2}{(r')^{l+1}} \sin\theta' \, dr' d\theta' d\varphi' \,. \tag{5.16b}$$

The volumes over which the above two terms are integrated are shown in Figure 5.1 with the integration volume for c_{lm} represented by the colour yellow and the integration volume for d_{lm} represented by the colour green.

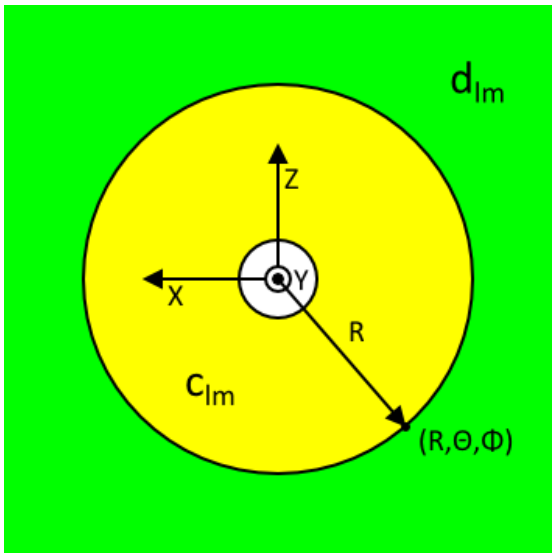

Figure 5.1 Integration volume for c_{lm} (yellow) is everything within a sphere with radius R. Integration volume for d_{lm} (green) is everything outside a sphere with radius R.

5.2 Poisson Solution for Stretched Magnetic Field Model

5.2.1 Coordinate Systems

Before the specific solution of Poisson's equation for the stretched magnetic field model can be discussed, two coordinate systems need to be defined: relative spherical coordinates and relative cylindrical coordinates. Like relative Cartesian coordinates, these systems are spherical and cylindrical coordinates relative to the radius of the Earth. Relative spherical coordinates are represented by the variables (R, Θ, Φ). They are defined as

$$(R, \Theta, \Phi) = \left(\frac{r}{a}, \theta, \varphi\right) . \tag{5.17}$$

The solution to Poisson's equation involves a volume integral. In spherical coordinates, the volume integral is given as

$$d\tau = r^2 \sin\theta \, dr d\theta d\varphi . \tag{5.18}$$

Converting to relative spherical coordinates (conversions are shown in Appendix E.2), the volume integral in relative spherical coordinates is given by

$$d\tau = a^3 R^2 \sin\Theta \, dR d\Theta d\Phi \, . \tag{5.19}$$

Typically, cylindrical coordinates are defined with the z-axis representing the axis of the cylinder. However, as will be discussed in the next subsection, cylindrical coordinates with the x-axis representing the axis of the cylinder will be far more useful for this analysis. The cylindrical coordinates that will be used are given by the variables (s, γ, x) with s representing the radius of the cylinder, γ representing the angle in the y-z plane relative to the negative z-axis, and x representing the axis of the cylinder. Their definitions in terms of Cartesian coordinates are given as

$$(s, \gamma, x) = \left(\sqrt{y^2 + z^2}, \tan^{-1}\left(-\frac{y}{z}\right), x\right) \, . \tag{5.20}$$

Relative cylindrical coordinates are represented by the variables (S, Γ, X). Relative cylindrical coordinates are cylindrical coordinates relative to the radius of the Earth. Mathematically, they are defined as

$$(S, \Gamma, X) = \left(\frac{s}{a}, \gamma, \frac{x}{a}\right) \, . \tag{5.21}$$

The volume integral defined in cylindrical coordinates is given as

$$d\tau = s ds d\gamma dx \, . \tag{5.22}$$

Converting to relative spherical coordinates (conversions are shown in Appendix E.3), the volume integral in relative cylindrical coordinates is given as.

$$d\tau = a^3 S dS d\Gamma dX \, . \tag{5.23}$$

5.2.2 Integration Bounds for Stretched Magnetic Field Model

The stretched magnetic field exists in a confined region in the magnetotail. The divergence of the model magnetic field is only valid in the region where the stretched magnetic field exists. Therefore, the integration bounds in equations 5.16a and 5.16b need to reflect the region where the stretched magnetic field exists, not all space. It would be very difficult to exactly portray the region where the stretched magnetic field exists in the magnetotail in the integration bounds. Therefore, it is assumed that the stretched magnetic field is confined to a cylinder along the negative x-axis that has a radius of five Earth radii. The value of five Earth radii was chosen based on Figure 3.2. As seen in that figure, the maximum height of the stretched field lines is just under five Earth radii. A cylinder was chosen because it simplifies the integration bounds as cylindrical coordinates can be used. It is also assumed that the region from the Earth out to $X = 5\mathrm{R_E}$ is divergence free. This is assumed because the plasmasphere mainly occupies this area, which consists of dipole field lines, and the stretched field lines are very dipole like in this area, which should then already have zero divergence. The volumes over which the c_{lm} and d_{lm} terms are integrated in context to the model magnetic field are depicted in Figure 5.2.

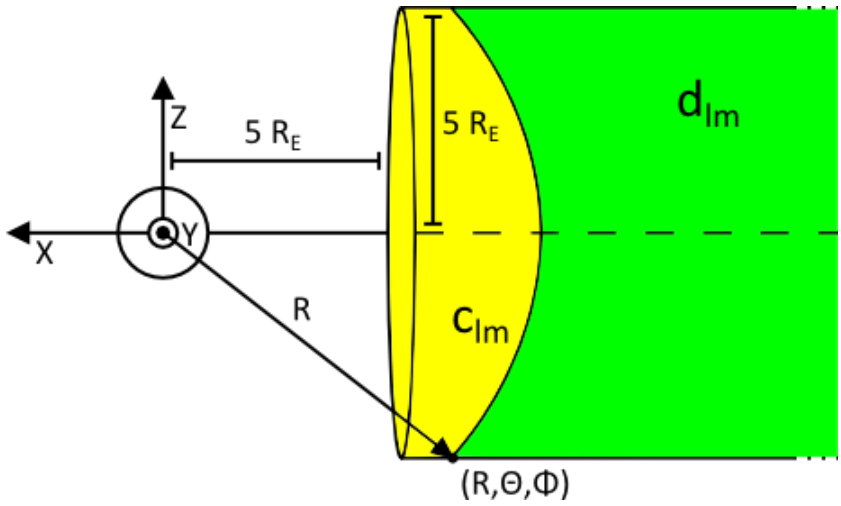

Figure 5.2 Integration volume for c_{lm} (yellow) for the stretched magnetic field model is the intersection between a cylinder along the negative x-axis and a sphere of radius R. Integration volume for d_{lm} (green) for the stretched magnetic field model is the intersection between a cylinder along the negative x-axis and the space outside of a sphere of radius R.

Mathematically, the above integration volume can be found by using a combination of relative spherical and relative cylindrical coordinates. The c_{lm} integration volume represents a cylinder with a rounded end. The cylinder can be represented by relative cylindrical coordinates and the rounded end can be represented by relative spherical coordinates. The location on the negative x-axis where the cylinder ends and the spherical section begins can be found using basic trigonometry. The situation is depicted in Figure 5.3. A triangle is formed between a vector with length R and the edge of the cylinder. Using Pythagoras' theorem, the location on the negative x-axis of the transition is given as

$$R^2 = X^2 + 0^2 + 5^2 = X^2 + 25 \tag{5.24a}$$

and solving for X gives

$$X = -\sqrt{R^2 - 25}\,. \tag{5.24b}$$

The negative solution was chosen because the SPS is centered along the negative x-axis. Now the integration bounds can be found for the cylindrical parts of both the c_{lm} and d_{lm} terms.

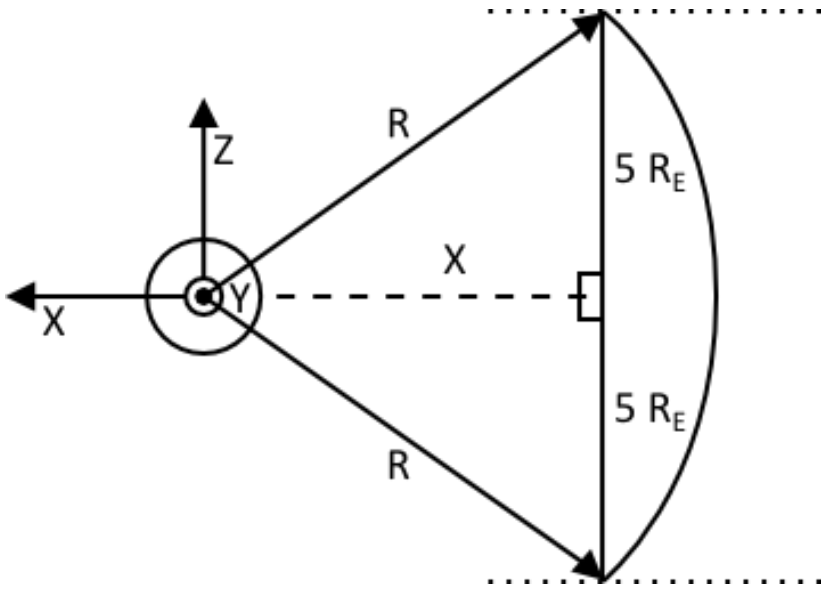

Figure 5.3 Location on the x-axis where the integral volume transitions between a cylinder and a portion of a sphere can be found using the triangle shown here.

For c_{lm}, the cylinder starts at $X = -5$ and ends at the derived location (equation 5.24b). Also, the radius of the cylinder is defined to be 5 R_E. Therefore, the integration bounds for the cylindrical portion of the integration volume are given as

$$0 \leq S' \leq 5\,, \tag{5.25a}$$

$$0 \leq \Gamma' \leq 2\pi\,, \tag{5.25b}$$

and

$$-\sqrt{R^2 - 25} \leq X' \leq -5\,. \tag{5.25c}$$

For d_{lm}, the cylinder starts at the derived location (equation 5.24b) and extends to the end of the SPS. The location will be assumed to be at the DTNL or where the first stretched field line is created. As stated in Section 2.3.2, the first stretched field line is created approximately 100 Earth radii away from the Earth. Therefore, the integration bounds for the cylindrical portion of the integration volume are given as

$$0 \leq S' \leq 5\,, \tag{5.26a}$$

$$0 \leq \Gamma' \leq 2\pi\,, \tag{5.26b}$$

and

$$-100 \leq X' \leq -\sqrt{R^2 - 25}\,. \tag{5.26c}$$

The integration bounds for the spherical portion of c_{lm} and d_{lm} will be the same with the spherical solution added to the cylindrical solution in the c_{lm} case and the spherical solution subtracted from the cylindrical solution in the d_{lm} case. The integration bounds can be found by analyzing the intersection between a plane and a sphere. In this case, the plane is at the intersection between the cylinder and the sphere (equation 5.24b) and the sphere has a radius of

R. The range of R' will be from the plane out to the radius R. The value of R' along the plane can simply be found using the conversion between relative Cartesian coordinates and relative spherical coordinates. Inserting the conversion for X to relative spherical coordinates into equation 5.24b gives

$$R'_{min} \sin\Theta' \cos\Phi' = -\sqrt{R^2 - 25}\,. \tag{5.27}$$

Solving for R'_{min} gives the lower integration bound for R' as

$$R'_{min} = -\frac{\sqrt{R^2 - 25}}{\sin\Theta' \cos\Phi'}\,. \tag{5.28}$$

Therefore, the integration bounds for R' are given as

$$-\frac{\sqrt{R^2 - 25}}{\sin\Theta' \cos\Phi'} \leq R' \leq R\,. \tag{5.29}$$

The integration bounds for Φ' can be found by analyzing the intersection between the sphere and the plane. Mathematically, the intersection can be found by using the definition of a radius. This is given as

$$R^2 = X^2 + Y^2 + Z^2\,. \tag{5.30}$$

Inserting equation 5.24b in place of X and the conversions to relative spherical coordinates in place of Y and Z in the above equation gives

$$R^2 = R^2 - 25 + R^2 \sin^2\Theta' \sin^2\Phi' + R^2 \cos^2\Theta'\,. \tag{5.31}$$

Rearranging and solving for Φ' gives

$$\Phi' = \sin^{-1}\left(\frac{\sqrt{25 - R^2\cos^2\Theta'}}{R\sin\Theta'}\right). \tag{5.32}$$

The arcsine in the above formula will either provide a positive or negative solution. Therefore, the integration bounds need to account for the correct quadrant. The SPS is centered on the negative x-axis. This corresponds to a Φ' value of π. Therefore, the integration bounds for Φ' are given as

$$\pi - \sin^{-1}\left(\frac{\sqrt{25 - R^2\cos^2\Theta'}}{R\sin\Theta'}\right) \leq \Phi' \leq \pi + \sin^{-1}\left(\frac{\sqrt{25 - R^2\cos^2\Theta'}}{R\sin\Theta'}\right). \tag{5.33}$$

The integration bounds for Θ' can be found by using trigonometry. The situation used is shown in Figure 5.4. Using trigonometry, the angle α is given as

$$\alpha = \sin^{-1}\left(\frac{5}{R}\right). \tag{5.34}$$

Therefore, the integration bounds for Θ' are given as

$$\frac{\pi}{2} - \sin^{-1}\left(\frac{5}{R}\right) \leq \Theta' \leq \frac{\pi}{2} + \sin^{-1}\left(\frac{5}{R}\right). \tag{5.35}$$

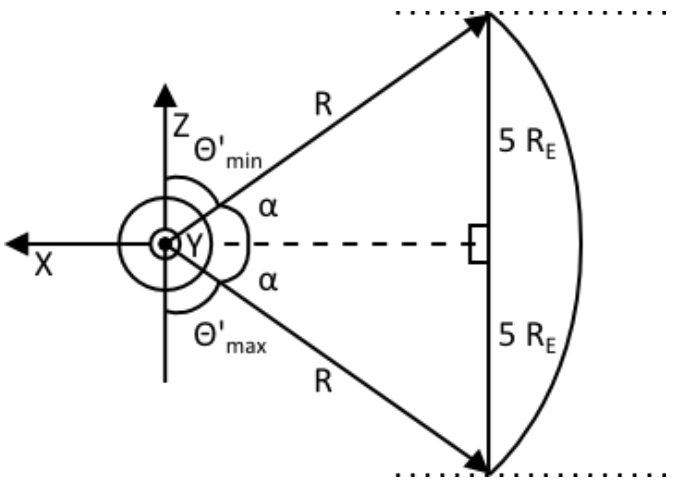

Figure 5.4 Integration bounds for Θ' can be found by using the above triangle.

5.2.3 Poisson Solution

Using the integration bounds found in the last paragraphs (equations 5.25a-5.25c, equations 5.26a-5.26c, equation 5.29, equation 5.33, and equation 5.35), the solution for Poisson's equation for the stretched magnetic field model is given as

$$\phi(R,\Theta,\Phi) = a^2 \sum_{l=0}^{\infty} \frac{1}{2l+1} \sum_{m=-l}^{l} Y_{lm}(\Theta,\Phi)\left(\frac{c_{lm,cyl}(R)}{R^{l+1}} + \frac{c_{lm,sph}(R)}{R^{l+1}} + R^l d_{lm,cyl}(R) - R^l d_{lm,sph}(R)\right) \tag{5.36}$$

where

$$c_{lm,cyl}(R) = \int_0^5 \int_0^{2\pi} \int_{-\sqrt{R^2-25}}^{-5} \vec{\nabla}\cdot\vec{B}_{model}(S',\Gamma',Z') \, Y_{lm}^*\left(\tan^{-1}\left(\frac{\sqrt{(X')^2+(S')^2}}{-S'\cos\Gamma'}\right), \tan^{-1}\left(\frac{S'\sin\Gamma'}{X'}\right)\right)((X')^2+(S')^2)^{l/2} S' dS' d\Gamma' dX' , \tag{5.37a}$$

$$c_{lm,sph}(R) = \int_{\frac{\pi}{2}-\sin^{-1}\left(\frac{5}{R}\right)}^{\frac{\pi}{2}+\sin^{-1}\left(\frac{5}{R}\right)} \int_{\pi-\sin^{-1}\left(\frac{\sqrt{25-R^2\cos^2\Theta'}}{R\sin\Theta'}\right)}^{\pi+\sin^{-1}\left(\frac{\sqrt{25-R^2\cos^2\Theta'}}{R\sin\Theta'}\right)} \int_{-\frac{\sqrt{R^2-25}}{\sin\Theta'\cos\Phi'}}^{R} \vec{\nabla}\cdot\vec{B}_{model}(R',\Theta',\Phi') \, Y_{lm}^*(\Theta',\Phi')(R')^{l+2}\sin\Theta' \, d\Theta' d\Phi' dR' , \tag{5.37b}$$

$$d_{lm,cyl}(R) = \int_0^5 \int_0^{2\pi} \int_{-100}^{-\sqrt{R^2-25}} \vec{\nabla}\cdot\vec{B}_{model}(S',\Gamma',Z') \, Y_{lm}^*\left(\tan^{-1}\left(\frac{\sqrt{(X')^2+(S')^2}}{-S'\cos\Gamma'}\right), \tan^{-1}\left(\frac{S'\sin\Gamma'}{X'}\right)\right)\frac{1}{((X')^2+(S')^2)^{\frac{l+1}{2}}} S' dS' d\Gamma' dX' , \tag{5.37c}$$

and

5.37d

$$d_{lm,spherical}(R) = \int_{\frac{\pi}{2}-\sin^{-1}\left(\frac{5}{R}\right)}^{\frac{\pi}{2}+\sin^{-1}\left(\frac{5}{R}\right)} \int_{\pi-\sin^{-1}\left(\frac{\sqrt{25-R^2\cos^2\Theta'}}{R\sin\Theta'}\right)}^{\pi+\sin^{-1}\left(\frac{\sqrt{25-R^2\cos^2\Theta'}}{R\sin\Theta'}\right)} \int_{-\frac{\sqrt{R^2-25}}{\sin\Theta'\cos\Phi'}}^{R} \vec{\nabla}\cdot\vec{B}_{model}(R',\Theta',\Phi')$$
$$Y_{lm}^{*}(\Theta',\Phi')\frac{1}{(R')^{l+1}}\sin\Theta'\,d\Theta'd\Phi'dR' .$$

The components of the divergence of the stretched magnetic field model were calculated in Section 3.3.1 (equation 3.16 and equation 3.18). Adding together the results from the x and z components gives the total divergence in relative Cartesian coordinates as

$$\vec{\nabla}\cdot\vec{B}_{model}(X,Y,Z) = -\frac{3ZB_{eq,s}}{a(X^2+Y^2+Z^2)^{\frac{5}{2}}}e^{\frac{X}{\Delta X_D}}\left(\frac{-X^2+4Y^2-Z^2}{X^2+Y^2+Z^2}+\frac{X}{\Delta X_D}\right) \quad 5.38$$
$$+\frac{ZX_{extra}(-X^2+Y^2+Z^2)}{a(X^2+Y^2+Z^2)^2}e^{-Z}+\frac{2ZZ_{extra}}{aZ_{scale}}e^{\left(-\frac{(X-X_{min})^2}{X_{scale}}-Y^2-\frac{Z^2}{Z_{scale}}\right)} .$$

This needs to be converted to both relative cylindrical and relative spherical coordinates. The conversion to relative cylindrical coordinates is shown in Appendix I.1 with the result being

$$\vec{\nabla}\cdot\vec{B}_{model}(S,\Gamma,X)$$
$$=\frac{3S\cos\Gamma\,B_{eq,s}}{a(X^2+S^2)^{\frac{5}{2}}}e^{\frac{X}{\Delta X_D}}\left(\frac{-X^2+5S^2\sin^2\Gamma-S^2}{X^2+S^2}+\frac{X}{\Delta X_D}\right) \quad 5.39$$
$$+\frac{S\cos\Gamma\,X_{extra}(-X^2+S^2)}{a(X^2+S^2)^2}e^{S\cos\Gamma}$$
$$-\frac{2S\cos\Gamma\,Z_{extra}}{aZ_{scale}}e^{\left(-\frac{(X-X_{min})^2}{X_{scale}}-S^2\sin^2\Gamma-\frac{S^2\cos^2\Gamma}{Z_{scale}}\right)} .$$

The conversion to relative spherical coordinates is shown in Appendix I.2 with the result being

$$\vec{\nabla}\cdot\vec{B}_{model}(R,\Theta,\Phi) \tag{5.40}$$
$$= -\frac{3\cos\Theta\, B_{eq,s}}{aR^4}\, e^{\frac{R\sin\Theta\cos\Phi}{\Delta X_D}}\left(-1+5\sin^2\Theta\sin^2\Phi+\frac{R\sin\Theta\sin\Phi}{\Delta X_D}\right)$$
$$-\frac{\cos\Theta\, X_{extra}\left(1-2\sin^2\Theta\cos^2\Phi\right)}{aR}\, e^{-R\cos\Theta}$$
$$+\frac{2R\cos\Theta\, Z_{extra}}{aZ_{scale}}\, e^{\left(-\frac{(R\sin\Theta\cos\Phi-X_{min})^2}{X_{scale}}-R^2\sin^2\Theta\sin^2\Phi-\frac{R^2\cos^2\Theta}{Z_{scale}}\right)}.$$

Now all components are known and a solution for the correction potential can be attempted. The results of the attempt are discussed in the next section as well as the problems that arose.

5.3 Results and Problems

As shown in equations 5.38, 5.39, and 5.40, the divergence of the stretched magnetic field model contains three terms. They will be labeled term 1, 2, and 3 respectively. Also, the solution for the correction potential (equation 5.28) can be split into four separate sums based on the four functions that are added together. Therefore, if the three terms in the divergence are taken into account, the correction potential contains 12 separate sums. Since these are infinite sums, it is best to analyze each sum separately in order to find the convergence value. Table 5.1 summarizes the results from using Mathematica to find a convergence value for each part of the correction potential at the point $(-8, 0, 0.5)$. As can be seen in the below table, it was not possible to find the value of the correction potential, due to two problems. First, a value for five of the sums could not be found because not enough terms of the sum could be calculated. All of these sums involved cylindrical coordinates. Therefore, Mathematica could not compute many terms of these sums due to the conversion between spherical and cylindrical coordinates in the spherical harmonics term. The program could not handle higher orders of the spherical harmonics defined with this conversion. Second, two of the sums started to diverge at high orders of l. Both sums started to converge, as expected, but then rapidly started to diverge. It is most likely that this does not represent the actual value of the sum, but shows that the computational limits of the program have been breached and that it cannot accurately calculate

values anymore. The other sum terms converged, some quicker than others, and values are listed in the table below.

Table 5.1 Summary of results for each term in equation 5.28 for the point $(-8, 0, 0.5)$

	$\vec{\nabla} \cdot \vec{B}_{model}$ **Term 1**	$\vec{\nabla} \cdot \vec{B}_{model}$ **Term 2**	$\vec{\nabla} \cdot \vec{B}_{model}$ **Term 3**
$c_{lm,cyl}$	• Could only compute up to $l = 11$ • Could make a guess on value but with large error • 1.00×10^{-2}Tm	• Could only compute up to $l = 3$ • Not enough information to determine value	• Could only compute up to $l = 3$ • Not enough information to determine value
$c_{lm,sph}$	• Computed up to $l = 35$ • 9.60×10^{-3}Tm	• Computed up to $l = 55$ • 2.67×10^{-3}Tm	• Computed up to $l = 65$ • 9.44×10^{-3}Tm
$d_{lm,cyl}$	• Could only compute up to $l = 11$ • Not enough information to determine value	• Could only compute up to $l = 3$ • Not enough information to determine value	• Could only compute up to $l = 3$ • Not enough information to determine value
$d_{lm,sph}$	• Computed up to $l = 35$ • -4.03×10^{-2}Tm	• Computed up to $l = 65$ • Solution started to plateau around $l = 50$ but then started to diverge • $+\infty$?	• Computed up to $l = 65$ • Solution started to plateau around $l = 50$ but then started to diverge • $+\infty$?

In order to make this a viable solution to the divergence of the magnetic field problem, the correction potential needs to be calculated at every point of a fine grid in the magnetotail. The gradient of the correction needs to be numerically found so that it can then be added to the stretched magnetic field model to create an overall divergence free magnetic field. However, this solution is not possible using the method outlined in this chapter. First of all, a value for the correction potential could not be calculated at a single point using Mathematica. Therefore, another platform should be chosen and/or the integration bounds should be redefined. Also, it

was very time consuming to calculate the 12 sums needed for just one point. If a fine grid of points is needed, it would take a very long time to calculate all of those points. Therefore, another platform that is faster is highly recommended as well as the use of super computing system such as Westgrid. The next chapter will mention other methods that were not attempted in this thesis for creating a divergence free magnetic field.

5.4 Summary

During the course of this Masters project, a second method for creating a divergence free magnetic field was attempted. It included adding the gradient of a correction potential to the model magnetic field. Maxwell's second equation is used to find the divergence of the total magnetic field. Solving for the correction potential gives a solution that is in the form of Poisson's equation. A spherical harmonic expansion was used in order to find a solution for the correction potential. The solution involves an infinite sum with two constants that are found by either integrating over the region inside a sphere of radius R or outside a sphere of radius R. Integration bounds for the solution are set to define the region where the SPS exists. They consist of the intersection between a sphere of radius R and a cylinder that is centered along the negative x-axis. A value for the correction potential was attempted at the point $(-8, 0, 0.5)$. However, a value could not be found because a solution could be found for all of the terms that needed to be calculated. Either summation terms could not be calculated past a certain point or the solution would start to converge but then diverge after many sum terms have been calculated. Both of these issues are most likely due to computational problems with Mathematica. Also, the amount of time that it took to calculate a solution at just this one point was very long. If a fine grid is needed to have a divergence free magnetic field model, then this solution will not be feasible. A new platform to calculate these equations is needed as well as access to more computing power would be recommended if this solution is attempted again. Alternative solutions to producing a divergence free magnetic field are discussed in the next chapter.

Chapter 6

Summary, Conclusions, and Suggestions for Further Work

6.1 Summary and Conclusions

6.1.1 Model of the Nightside Magnetosphere

In this thesis, a model of the nightside magnetosphere was presented that contained four regions: plasmasphere, PS, magnetic lobes, and the LLBLs. The PS is split into three regions based on the shape of the closed field lines. The three regions are the DPS, TPS, and SPS. In the DPS, the closed field lines are quasi-dipolar in shape; in the TPS, the closed field lines are transitioning between dipole and stretched shape; and in the SPS, the closed field lines are stretched in shape. The SPS is further split into three regions based on the direction of the current in that region. The three regions are two DZs surrounding a central NS. There is an eastward current in the DZs and a westward current in the NS. This creates an overall current system in the SPS of a double solenoid with the current flowing eastward in the DZs and then closing westward in the NS, as seen in Figure 2.21. The NS is also split into two regions: INS and ONS. The protons are "unmagnetized" in the INS and magnetized in the ONS. The electrons remain magnetized in both the INS and the ONS. As shown by Lyons and Speiser (1982) in a single-particle model of the INS, the INS region leads to strong energization of the protons and this also has serious implication about the current system in the INS. A flow chart of all the regions in the nightside magnetosphere model presented in this thesis is given in Figure 6.1.

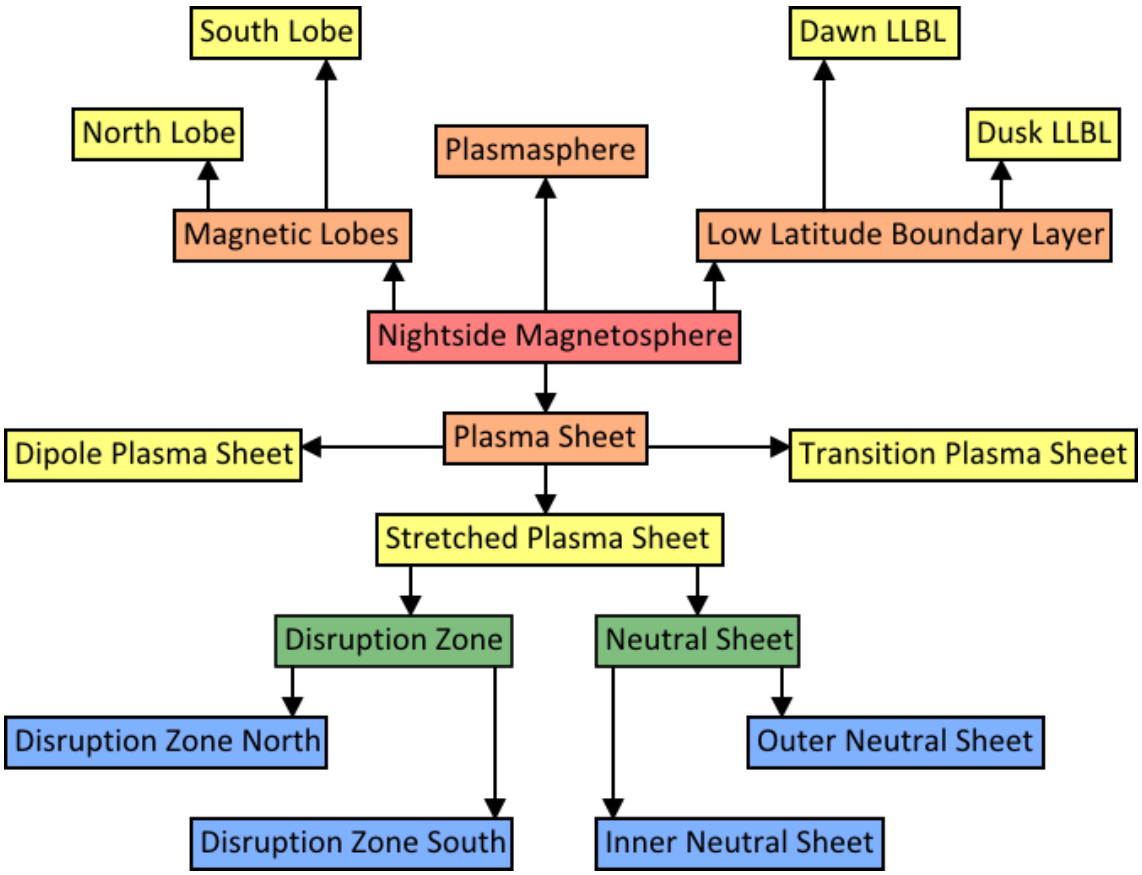

Figure 6.1 The nightside magnetosphere model presented in this thesis contains four major regions: magnetic lobes, plasmasphere, LLBL, and PS; the magnetic lobes are split into the north and south lobes; the LLBLs are split into the dawn and dusk LLBL; the PS is split into the DPS, TPS, and SPS; the SPS is split into the DZs and the NS; the NS is split into the DZN and DZS; and the NS is split into the INS and ONS.

6.1.2 Shape of the Stretched Field Lines

The shape of the closed stretched field lines leads to the double vortex current system in the magnetotail. The stretched field lines have four inflection points, which represents a change in the sense of curvature. The regions of convex curvature comprise the DZs and the central region of concave curvature comprises the NS. This shape is proposed for the stretched field lines for two reasons. Firstly, the stretched field lines need to drape over the plasmasphere in order to facilitate antiparallel reconnection. Secondly, the convective drift causes the plasma to drift towards the NS, which creates inflection points in the field lines. As the NS fills with

plasma, the particle pressure rises, causing the magnetic pressure to fall. A deep minimum in the magnetic field forms in the center of the NS. The deep minimum enhances the curvature in the field lines, especially at the earthward edge of the NS. The double current loops formed in the magnetotail also support the stretching of the magnetic field lines as they create a magnetic field that will enhance the stretching. Furthermore, Shen et al. (2003) showed from Cluster measurements that the curvature sense changes in the SPS, which fully supports the stretched field lines shape used in this thesis.

6.1.3 Role of Stretched Field Lines in Substorms

The growth and decay of the SPS is intimately related to the lifespan of a substorm. The growth phase of the substorm consists of the closed stretched field lines being created through antiparallel reconnection between two open magnetic field lines in the magnetic lobes. The stretched field lines then move earthward and thin down in the NS region over the course of the growth phase. The onset phase occurs when the most earthward stretched field line reconnects, sending plasma down to the ionosphere. The reconnection of the closed stretched field lines also creates a plasmoid, a ball of magnetic field, which is trapped in the SPS, completely independent from the Earth. Each subsequent stretched field line reconnects until there are no more closed stretched field lines left in the SPS. Since the plasmoid is then not confined by the closed field lines in the SPS anymore, it is free to travel away from the Earth. This signifies the beginning of the recovery phase of the substorm, after which the whole substorm process can be repeated.

6.1.4 Double Vortex Current System

The first current system present in the SPS is the double vortex current system. It consists of an eastward current in the DZs that closes westward in the NS. Each term in the overall current formula (equation 2.75) plays a different role in creating this current system. The first term in equation 2.75 is dependent on the curvature vector and the difference between the parallel and perpendicular pressure. This current is carried by the electrons because they will have an anisotropic pressure distribution centered on low pitch angles. Therefore, the electrons

will have a much higher parallel pressure than perpendicular pressure. The protons have an isotropic distribution. Therefore, the protons will not contribute any current due to the first term in equation 2.75 because the overall difference between the parallel and perpendicular pressure of the protons will be zero. The expected direction of this current in the magnetotail is shown in Figure 2.14. It has a westward direction in the NS and an eastward direction in the DZs, which supports the double vortex current system. The second term in equation 2.75 is dependent on the gradient of the perpendicular particle pressure. This current will mainly be carried by the isotropic protons, because the electrons do not have a very high perpendicular pressure. The expected direction of this current in the magnetotail is shown in Figure 2.16. It has a westward direction in both the NS and DZs. Therefore, this current will enhance the westward curvature current of the electrons in the ONS and slightly dampen the eastward curvature current of the electrons in the DZs. The third term in equation 2.75 is the current due to the convective drift. The convective drift will only produce a current when there are either excess protons or electrons in a region. In terms of the double vortex current system, the convective current closes the current loops in the double vortex current system. The last term in equation 2.75 is due to the unmagnetized protons in the INS. Since these protons are unmagnetized, they do not respond to the magnetic field. However, they are pushed by the Coulomb force due to the dawn to dusk electric field present in the magnetotail. This creates a westward current that enhances the westward current produced by the electrons in the INS. These four terms create a double vortex current system in the magnetotail where there is a westward current in the INS and ONS and an eastward current in the DZs, as seen in Figure 2.21.

6.1.5 Neutral Sheet Field-Aligned Current System

The second current system present in the SPS is the NS FAC system. It is an important current system during substorms, which is beyond the scope of this thesis, but it is a direct consequence of the geometry of the field lines in the SPS so it is mentioned here. The electrons remain magnetized in the INS while the protons do not. Therefore, the electrons will convectively drift earthward while the unmagnetized protons will not. This creates an electron reservoir at the earthward end of the INS and a proton reservoir at the opposite end of the INS. Also, the earthward drifting electrons will create an anti-earthward current in the INS. This is

the generator current for the FAC system. The proton reservoir will map down to higher latitudes in the ionosphere through a downward FAC; the electron reservoir will map down to lower latitudes in the ionosphere through an upward FAC. The system closes in the ionosphere through an equatorward Pedersen current where energy can be dissipated through Joule heating. This FAC system creates the pre-onset electron auroral arc that is a critical element in the growth phase of substorms.

6.1.6 Model of the Stretched Magnetic Field

In order to verify that the specific geometry of the stretched field lines outlined in this thesis creates a double vortex current system, a model of the stretched magnetic field was created. The shape of the field lines from this model is shown in Figure 3.2. The model contains three parts of the magnetotail: plasmasphere, TPS, and SPS. As seen in Figure 3.2, the plasmasphere has field lines that have a dipolar shape. The TPS has field lines that are slightly stretched dipolar shapes that have no inflection points. The SPS has field lines that are very stretched and have four inflection points. The length of the stretched field lines is much larger than the length of the field lines in the plasmasphere and TPS. The field line that would have intersected the x-axis at -12 if it was dipolar in shape stretches all the way to -21.8. This supports the anisotropic distribution of the electrons because they will gain a significant amount of parallel energy rather than perpendicular energy as the field lines move closer to the Earth according to the second adiabatic invariant. The four inflection points in the stretched field lines act as surface boundaries between the different regions in the SPS. The regions of convex curvature compose the DZs and the central region of concave curvature composes the NS. The inflection points provide a mathematical basis for defining these regions in the magnetotail.

The stretched magnetic field model was created by defining an x and z component for the stretched magnetic field. The x and z component each contain two terms. The first term in both components contained the dipole field term multiplied by an exponential decay in the negative x direction. This caused the dipole field to decay farther away from the Earth in order to allow for the stretching terms, which are the second terms in each component, to take over. The stretching is accomplished in the x-component by having a maximum. The maximum creates the elongated

portion that is basically parallel to the x-axis of the field line. The stretching is accomplished in the z-component by having a minimum, specifically the deep minimum in the magnetic field that was discussed in Section 2.6.2. The minimum occurs in the center of the NS and creates the intense curvature in the most earthward closed stretched field lines. The y-component did not need to be created by the model as it is only defined in the noon-midnight meridian plane; the y-component has no effect on the field line shape in this plane.

6.1.7 Physical Tests for the Model of the Stretched Magnetic Field

After the model was created, it underwent two physical tests. The first test is if the model magnetic field has zero divergence. This could not be tested unless there was a y-component of the stretched magnetic field. The divergence equation was used to solve for a y-component that would automatically make the divergence of the model zero. The second physical test are the limits at infinity. The Earth's magnetic field is zero at an infinite distance away from the Earth. The stretched magnetic field model needs to reflect this. All limits are found to be zero except for the limit of the y-component at positive or negative infinity in the y-direction. The solution was a finite value instead of zero. However, since the model is only used in the context of the noon-midnight meridian plane, the stretched magnetic field model is deemed physical. The y-component has no effect on this plane. Now, the stretched magnetic field equations can be used to find different parameters in the magnetotail.

6.1.8 Total Current from Model of the Stretched Magnetic Field Using Ampere's Law

According to Ampere's law, the current that is directly created from a magnetic field can easily be found. This was done for the stretched magnetic field model and the direction of the resulting current was given in Figure 4.1 and the current density value was given in Figure 4.2. The total time-independent current represents the summation of the current due to free charges and the magnetization current. As derived in Section 2.5.3, this results in a total current equation (equation 2.75) that contains four terms. The total current produced by these four terms is shown

in Figure 4.1 and Figure 4.2. As seen in Figure 4.1, the total current is westward in the NS and eastward in the DZN. This supports the double vortex current system that was presented in Chapter 2. Since this current was found using a model that was based entirely on the shape of the field lines, it can be concluded that the stretched field lines that have inflection points lead to a double vortex current system in the magnetotail. As seen in Figure 4.2, the total current density is strongly westward in the INS, weakly westward in the ONS, and weakly eastward in the DZN. Therefore, there are much weaker currents in the ONS and DZN than in the INS (INS current is approximately 4.5 times more intense than the current in the DZN). This supports the magnetotail model presented in Chapter 2 because the main contributors for the current are the curvature current of the anisotropic electrons and current due to the unmagnetized protons in the INS. Both of these currents are expected to be westward in the INS so a strong current is necessary. Also, the unmagnetized protons gain energy as they drift in the INS so the strength of the current will increase over time. According to Figure 4.2, the strongest current occurs at $X > -12$. This corresponds to the location of the deep minimum in the magnetic field and is where the stretched field lines have the most intense curvature. An intense current is needed at this location for antiparallel reconnection through the Kelvin-Helmholtz instability at the VNENL. Overall, the stretched magnetic field model that was presented in Chapter 3 inherently supports the magnetotail model that was presented in Chapter 2. The current produced by this magnetic field model found using Ampere's law supports the physical processes that are necessary for substorm onset generation in the near-Earth magnetotail SPS region.

6.1.9 Charged Particle's Pitch Angle Using Model of the Stretched Magnetic Field

Other parameters that were calculated using the stretched magnetic field model include the pitch angle and gyroradius of the charged particles. A particle's pitch angle in the magnetotail can be found by using the first adiabatic invariant if an equatorial pitch angle is defined. The pitch angle results show the path of the charged particles in the magnetotail. The electrons will have a low equatorial pitch angle because of their anisotropic distribution. The path for a 5° equatorial pitch angle is shown in Figure 3.3. For this equatorial pitch angle, the pitch angle remains below 30° in the majority of the stretched region of the magnetotail. Therefore, the motion of the electrons will be more parallel than perpendicular, which shows the

importance of the second adiabatic invariant for these particles. As the equatorial pitch angle increases, the mirror point moves closer to the equatorial plane. Figure 4.4 shows for an equatorial pitch angle of 10°. The mirror point becomes present in the stretched portion of the magnetotail. For an equatorial pitch angle of 40° (Figure 4.5), the particle is bouncing within the NS in the equatorial plane. Overall, the electron motion stays mainly parallel to the magnetic field in the stretched region of the magnetotail and the proton motion varies greatly from bouncing in and out of the SPS to just staying close to the equatorial plane. However, this is not the true path of the protons in the SPS. As mentioned previously, the protons become unmagnetized in the INS or center of the NS. This changes the path of the protons in the SPS and will be discussed in the following subsection.

6.1.10 Unmagnetized Regions in the SPS Using Model of the Stretched Magnetic Field

The gyroradius of a proton can be used to find the area where it becomes unmagnetized in the SPS. As mentioned previously, the NS is split into two regions: INS and ONS. The boundary between the INS and ONS is fluid because the gyroradius of a particle is dependent on its total energy and equatorial pitch angle. However, Lyons and Speiser (1982) showed that the amount of energy gained by the proton does not depend on the width of the INS. Therefore, an overall definite boundary between the INS and ONS is not necessary. For a proton with 1 keV of total energy, which is a typical value in the magnetotail, a region where it will be unmagnetized is present for every pitch angle. Figure 4.7 shows the unmagnetized regions for a proton with an equatorial pitch angle of 5°. There is an unmagnetized region at the deep minimum ($X > -12$) and at the tail end of the NS. Figure 4.8 shows that for an equatorial pitch angle of 30°, there is a definite INS and ONS region with both spanning the length of the NS. For an equatorial pitch angle of 60° (Figure 4.9), the motion of the proton is completely within the INS. The protons are essentially unmagnetized in the INS, so they do not follow the adiabatic invariants. However, Lyons and Speiser (1982) showed that once the proton enters the INS, it is either accelerated by the Coulomb force to the end of the SPS or it is randomly ejected at some point during its acceleration. The ejected protons have a wide range of pitch angles and

therefore have an isotropic distribution. The electrons have a much smaller gyroradius than the protons so they remain magnetized in the INS and keep their anisotropic distribution. Therefore, the INS is important for two reasons. It enhances the westward current and intensifies it over time as the protons gain energy as they accelerate. As well, it creates the isotropic distribution of the protons outside the INS.

6.1.11 Curvature Current from Electrons Using Model of the Stretched Magnetic Field

The direction of the current produced by the first term in equation 2.75 can be found using only the stretched magnetic field model that was presented in Chapter 3. This current is dependent on the cross product between the magnetic field unit vector and the curvature vector and the difference between the parallel and perpendicular pressure. The cross product produces a westward current in the NS and an eastward current in the DZN, as seen in Figure 4.10. The difference between the parallel and perpendicular pressure will be positive as long as the pitch angle stays below 55°. As seen in Figure 4.3, for an equatorial pitch angle of 5°, the pitch angle remained below 30° for the majority of the stretched region of the magnetotail. Therefore, the difference between the parallel and perpendicular pressures will be positive giving the direction of the current due to the first term in equation 2.75 as what is shown in Figure 4.10. This represents the curvature current of the anisotropic electrons, which is where the majority of the current will be coming from in the magnetotail. Therefore, the total current (Figure 4.1) and the current due to the first term in equation 2.75 (Figure 4.10) should be similar. Comparing the two figures, they are very similar except that the boundary between the DZN and NS is close but not the same in both figures. The NS is bigger in Figure 4.1 than it is in Figure 4.10. This could imply that other terms in equation 2.75 enhance the NS current, making it wider. Specifically, the second term in equation 2.75 is carried by the isotropic protons and has a westward direction in both the DZN and ONS. Therefore, this proton current could enhance the westward current in the ONS and cause the boundary to move farther up in the z-direction. Also, this could imply that the equations for the stretched magnetic field are not correct and need to be changed in order to produce the expected result. Overall, the currents presented in Figure 4.1 and Figure 4.10

support each other as well as the model of the nightside magnetosphere that was presented in Chapter 2. Therefore, the results found using the stretched magnetic field model support the theory of the current systems present in the magnetotail. Namely, closed stretched magnetic field lines with four inflection points create a double vortex current system in the magnetotail.

6.2 Suggestions for Future Work

In order to continue this project, it is important to create a fully physical three dimensional model. As stated before, the current model is only physical in the noon-midnight meridian plane. The unphysical part of the model currently is the y-component. It does not satisfy the limits at negative or positive infinity in the y-direction. A second attempt at creating a divergence free magnetic field involved solving a form of Poisson's equation in order to find a correction potential that would be added to the model magnetic field. However, this attempt failed as some of the infinite sums could not be calculated and others failed to converge. Also, the amount of time that it took to calculate the correction potential for one point makes the solution not feasible for a fine grid of points. Therefore, creating a model with a physical magnetic field is the necessary next step in this project. A physical magnetic field model can be found by defining the magnetic field in a way that is inherently divergence free instead of using the divergence to find the third component that would create a divergence free magnetic field or adding a correction potential to the magnetic field to create a divergence free magnetic field, as was done in this thesis. This can be done in three ways, which are presented in sections 6.2.1, 6.2.2, and 6.2.3.

6.2.1 Method 1: Vector Potential

The first method for creating an inherently divergence free magnetic field is defining the magnetic field in terms of a vector potential. In order to make it divergence free, the Del operator $\vec{\nabla}$ is crossed with the vector potential $\vec{A}$, namely

$$\vec{B} = \vec{\nabla} \times \vec{A} \,. \tag{6.1}$$

The divergence of the above formula is inherently zero, which can easily be shown by

$$\vec{\nabla} \cdot \vec{B} = \vec{\nabla} \cdot \left(\vec{\nabla} \times \vec{A}\right) = 0 \,. \tag{6.2}$$

The above equation is zero because the solution for the term inside of the brackets will be perpendicular to both the Del operator and the magnetic vector potential. The dot product between the Del operator and something that is perpendicular to the Del operator will be zero. Thus, the divergence is zero when the magnetic field is defined in this manner. However, in this case, the main criterion for the design of the magnetic field is the field line shape. Defining the magnetic field in terms of a vector potential does not lead to an intuitive approach for creating a magnetic field with a specific field line shape. This is because the components of the magnetic field are dependent on the subtraction between various spatial derivatives of the magnetic vector potential, which is mathematically represented by

$$B_x = \frac{\delta A_z}{\delta y} - \frac{\delta A_y}{\delta z} \,, \tag{6.3a}$$

$$B_y = \frac{\delta A_x}{\delta z} - \frac{\delta A_z}{\delta x} \,, \tag{6.3b}$$

and

$$B_z = \frac{\delta A_y}{\delta x} - \frac{\delta A_x}{\delta y} \,. \tag{6.3c}$$

It would be difficult to determine how to define the magnetic vector potential in order to create a specific field line shape. However, if successful, a divergence free magnetic field would be obtained.

6.2.2 Method 2: Euler Potentials

The second method of defining a magnetic field that is inherently divergence free is using Euler potentials. This is mathematically represented as

$$\vec{B} = \vec{\nabla}\alpha \times \vec{\nabla}\beta \tag{6.4}$$

where α and β represents "two scalar functions that are conserved along field lines" (Stern, 1967). The above definition of magnetic field is also divergence free. This can be shown using some simple vector identities. First, the divergence of the magnetic field will be taken, which is given as

$$\vec{\nabla} \cdot \vec{B} = \vec{\nabla} \cdot \left(\vec{\nabla}\alpha \times \vec{\nabla}\beta\right). \tag{6.5}$$

The above equation can be simplified using the following vector identity (Huba, page 4):

$$\vec{\nabla} \cdot \left(\vec{A} \times \vec{B}\right) = \vec{B} \cdot \vec{\nabla} \times \vec{A} - \vec{A} \cdot \vec{\nabla} \times \vec{B}\,. \tag{6.6}$$

Therefore, equation 6.5 becomes

$$\vec{\nabla} \cdot \vec{B} = \vec{\nabla}\beta \cdot \left(\vec{\nabla} \times \vec{\nabla}\alpha\right) - \vec{\nabla}\alpha \cdot \left(\vec{\nabla} \times \vec{\nabla}\beta\right) = 0\,. \tag{6.7}$$

The two cross products are zero because the Del operator cannot be perpendicular to itself. Therefore, defining the magnetic field in terms of Euler potentials gives a magnetic field that is inherently divergence free. However, using equation 6.4 to define a magnetic field is not as simple as guessing values for α and β and checking to see what magnetic field shape is created. This would be far too difficult. Instead, a specific field line shape can be defined. Then, equation 6.4 can be manipulated to find a physical magnetic field that fits the field line shape. However, this can only be accomplished numerically. This is not advantageous for the work done with magnetic fields presented in this thesis because multiple derivatives need to be taken

using the magnetic field vector. If only a numerical solution is available for the magnetic field vector, the derivatives will need to be calculated numerically and a degree of error is inherently associated with numerical solutions. Thus, the numerical solution will give an inaccurate solution compared to the exact solution that can be found if equations for the magnetic field were known. For more information on using Euler potentials to define magnetic fields, see Stern (1967).

6.2.3 Method 3: Poloidal and Toroidal Vector Fields

The third method of defining a magnetic field that is inherently divergence free is splitting the magnetic field into its poloidal and toroidal vector fields. The poloidal and toroidal directions relative to each other are shown below in Figure 6.2. The toroidal field is represented by the colour green and the poloidal field is represented by the colour red.

Figure 6.2 The direction of the toroidal and poloidal vector fields relative to each other

If the toroidal field is pointing up out of the page, the poloidal field would exist in the plane perpendicular to the toroidal field, as shown in the above figure. As long as there are no magnetic monopoles, the magnetic field can be represented by the combination of the poloidal and toroidal vector fields (Backus, 1986). Mathematically, this is represented by

$$\vec{B} = \vec{P} + \vec{Q} = \vec{\nabla} \times \left(\vec{r} \times \vec{\nabla} P\right) + \vec{r} \times \vec{\nabla} Q \qquad 6.8$$

where $\vec{P}$ is the poloidal vector field, P is the poloidal scalar, $\vec{Q}$ is the toroidal vector field, and Q is the toroidal scalar. The above equation represents an inherently divergence free magnetic field. This can be easily shown. Taking the divergence of the above equation gives

$$\vec{\nabla} \cdot \vec{B} = \vec{\nabla} \cdot \left(\vec{\nabla} \times \left(\vec{r} \times \vec{\nabla} P\right) + \vec{r} \times \vec{\nabla} Q\right) = \vec{\nabla} \cdot \left(\vec{\nabla} \times \left(\vec{r} \times \vec{\nabla} P\right)\right) + \vec{\nabla} \cdot \left(\vec{r} \times \vec{\nabla} Q\right). \quad 6.9$$

The first term on the right in the above formula is automatically zero because the term inside the brackets will produce a solution that is perpendicular to the Del operator. Therefore, the dot product with that solution and the Del operator will be zero. The second term in the above equation needs to be expanded using the vector identity given in equation 6.6. Thus, the second term in equation 6.9 becomes

$$\vec{\nabla} \cdot \left(\vec{r} \times \vec{\nabla} Q\right) = \vec{\nabla} Q \cdot \vec{\nabla} \times \vec{r} - \vec{r} \cdot \vec{\nabla} \times \vec{\nabla} Q. \quad 6.10$$

The second term in the above formula is automatically zero since the two vectors are parallel to each other. The first term is zero since the cross product between the Del operator and the radius vector is zero. Therefore, the divergence of the magnetic field in terms of the poloidal and toroidal field is zero. Thus, equation 6.8 will produce a physical magnetic field. However, this method has the same problem as defining the magnetic field in terms of Euler potentials. The solution that will be provided using this method can only be numerical. Thus, there will be errors associated with the drift and current calculations. If an exact solution for the magnetic field could be obtained, then there would be no numerical errors. For more details on modeling the magnetic field in terms of its poloidal and toroidal components, see Backus (1986).

Using any of the above three methods, a divergence free magnetic field can be found. If the limit of the magnetic field is also zero at all extremes, then the magnetic field will be physical in three dimensions. This three dimensional physical magnetic field is a crucial next step in continuing this research because it can be used to find current directions in three dimensions.

References

Alekseev, I. I. and V. P. Shabansky (1972), A model of a magnetic field in the geomagnetosphere, *Planetary and Space Science*, 20, 1, 117-133.

Backus, G. (1986), Poloidal and toroidal fields in geomagnetic field modeling, *Reviews of Geophysics*, 24, 1, 75-109.

Baker, D. A. and J. E. Hammel (1965), Experimental studies of penetration of a plasma stream into a transverse magnetic field, *The Physics of Fluids*, 8, 4, 713-722.

Baker, D. N., S. J. Bame, J. Birn, W. C. Feldman, J. T. Gosling, E. W. Hones, Jr., R. D. Zwickl, J. A. Slavin, E. J. Smith, B. T. Tsurutani, and D. G. Sibeck (1984), Direct observations of passages of the distant neutral line (80-140 R_E) following substorm onsets: ISEE-3, *Geophysical Research Letters*, 11, 10, 1042-1045.

Baumjohann, Wolfgang and Rudolf A. Treumann (1997), *Basic Space Plasma Physics*, Imperial College Press, London.

Carpenter, D. L. (1966) Whistler studies of the plasmapause in the magnetosphere, *Journal of Geophysical Research*, 71, 3, 693-709.

Choe, J. Y. and D. B. Beard (1974a), The compressed geomagnetic field as a function of dipole tile, *Planetary and Space Science*, 22, 4, 595-608.

Choe, J. Y. and D. B. Beard (1974b), The near earth magnetic field of the magnetotail current, *Planetary and Space Science*, 22, 4, 609-615.

Choe, J. Y., D. B. Beard, and E. C. Sullivan (1973), Precise calculation of the magnetosphere surface for a tilted dipole, *Planetary and Space Science*, 21, 3, 485-498.

Cowley, S. W. H. (1973), A qualitative study of the reconnection between the Earth's magnetic field and an interplanetary field of arbitrary orientation, *Radio Science*, 8, 11, 903-913.

Cowley, S. W. H. (1978), The rffect of pressure anisotropy on the equilibrium structure of magnetic current sheets, *Planetary Space Science*, 26, 1037-1061.

Crooker, N. U., J. G. Lyon, and J. A. Fedder (1998), MHD model merging with IMF B_y: Lobe cells, sunward polar cap convection, and overdrapped lobes, *Journal of Geophysical Research*, 103, A5, 9143-9151.

Di Bartolo, Baldassare (2004), *Classical Theory of Electromagnetism*, World Scientific Publishing Co., Singapore.

Dungey, J. W. (1961), Interplanetary magnetic field and the auroral zones, *Physical Review Letters*, 6, 2, 47-48.

Eastman, T. E., E. W. Hones, Jr., S. J. Bame, and J. R. Asbridge (1976), The magnetosphere boundary layer: site of plasma, momentum and energy transfer from the magnetosheath into the magnetosphere, *Geophysical Research Letters*, 3, 11, 685-688.

Erickson, G. M. (1984), On the cause of X-line formation in the near-Earth plasma sheet: Results of adiabatic convection of plasma-sheet plasma, *Magnetic Reconnection in Space and Laboratory Plasmas,* Ed. Edward W. Hones, Jr., American Geophysical Union, Washington, 296-302.

Finlay, C. C., S. Maus, C. D. Beggan, T. N. Bondar, A. Chambodut, T. A. Chernova, A. Chulliat, V. P. Golovkov, B. Hamilton, M. Hamoudi, R. Holme, G. Hulot, W. Kuang, B. Langlais, V. Lesur, F. J. Lowes, H. Lühr, S. Macmillan, M. Mandea, S. McLean, C. Manoj, M. Menvielle,

I. Michaelis, N. Olsen, J. Rauberg, M. Rother, T. J. Sabaka, A. Tangborn, L. Tøffner-Clausen, E. Thébault, A. W. P. Thomson, I. Wardinski, Z. Wei, and T. I. Zvereva (2010), International Geomagnetic Reference Field: the eleventh generation, *Geophysical Journal International*, 183, 1216-1230.

Galvan, D. A., M. B. Moldwin, B. R. Sandel, and G. Crowley (2010), On the causes of plasmaspheric rotation variability: IMAGE EUV observations, *Journal of Geophysical Research*, 115, A01214, doi:10.1029/2009JA014321.

Griffiths, David J. (1999), *Introduction to Electrodynamics*, Pearson Addison Wesley, New Jersey.

Haerendel, G. (2010), Equatorward moving arcs and substorm onset, *Journal of Geophysical Research*, 115, A07212, doi:10.1029/2009JA015117.

Harris, E. G. (1962), On a plasma sheath separating regions of oppositely directed magnetic field, *Il Nuovo Cimento*, 23, 1, 115-121.

Hau, L.-N, R. A. Wolf, G.-H Voigt, and C. C. Wu (1989), Steady state magnetic field configurations for the earth's magnetotail, *Journal of Geophysical Research*, 94, A2, 1303-1316.

Hilmer, R. V. and G.-H. Voigt (1995), A magnetospheric magnetic field model with flexible current systems drive by independent physical parameters, *Journal of Geophysical Research*, 100, A4, 5613-5626.

Hones, E. W., Jr. (1963), Motion of charged particles trapped in the earth's magnetosphere, *Journal of Geophysical Research*, 68, 5, 1209-1219.

Hones, E. W., Jr. (1984), Plasma sheet behavior during substorms, *Magnetic Reconnection in Space and Laboratory Plasmas,* Ed. Edward W. Hones, Jr., American Geophysical Union, Washington, 178-184.

Hones, E. W., Jr., J. R. Asbridge, S. J. Bame, M. D. Montgomery, S. Singer, and S.-I. Akasofu (1972), Measurements of magnetotail plasma flow made with Vela 4B, *Journal of Geophysical Research*, 77, 28, 5503-5522.

Huba, J. D. (2011), *NRL Plasma Formulary*, Naval Research Laboratory, Washington, DC.

Jordan, C. E. (1994), Empirical models of the magnetospheric magnetic field, *Reviews of Geophysics*, 32, 2, 139-157.

Kabin, K., E. Spanswick, R. Rankin, E. Donovan, and J. C. Samson (2011), Modeling the relationship between substorm dipolarization and dispersionless injection, *Journal of Geophysical Research*, 116, A04201, doi:10.1029/2010JA015736.

Kivelson, Margaret G. and Christopher T. Russell (1995), *Introduction to Space Physics*, Cambridge University Press, New York.

Lee, L. C., S. Wang, and C. Q. Wei (1988), Streaming sausage, kink and tearing instabilities in a current sheet with applications to the earth's magnetotail, *Journal of Geophysical Research*, 93, A7, 7354-7365.

Lopez, R. E. and D. N. Baker (1994), Evidence for particle acceleration during magnetospheric substorms, *The Astrophysical Journal Supplement Series*, 90, 531-539.

Lu, G., N. A. Tsyganenko, A. T. Y. Lui, H. J. Singer, T. Nagai, and S. Kokubun (1999), Modeling of time-evolving magnetic fields during substorms, *Journal of Geophysical Research*, 104, A6, 12327-12337.

Lyons, L. R. and T. W. Speiser (1982), Evidence for current sheet acceleration in the geomagnetic tail, *Journal of Geophysical Research*, 87, A4, 2276-2286.

Luhmann, J. G. and L. M. Friesen (1979), A simple model of the magnetosphere, *Journal of Geophysical Research*, 84, A8, 4405-4408.

McPherron, R. L., C. T. Russell, and M. P. Aubry (1973), Satellite studies of magnetospheric substorms on August 15, 1968 9. Phenomenological model for substorms, *Journal of Geophysical Research*, 78, 16, 3131-3149.

Mead, G. D. (1964), Deformation of the geomagnetic field by the solar wind, *Journal of Geophysical Research*, 67, 7, 1181-1195.

Mead, G. D. and D. H. Fairfield (1975), A quantitative magnetospheric model derived from spacecraft magnetometer data, *Journal of Geophysical Research*, 80, 4, 523-534.

Miller, J. (2013), Solar magnetic reconnection seen in detail, *Physics Today*, 66, 9, 12-13.

Mitchell, D. G., D. J. Williams, C. Y. Huang, L. A. Frank, and C. T. Russell (1990), Current carriers in the near-earth cross-tail current sheet during substorm growth phase, *Geophysical Research Letters*, 17, 5, 583-586.

Moldwin, M. B. and W. J. Hughes (1992), Multi-satellite observations of plasmoids: IMP 8 and ISEE 3, *Geophysical Research Letters*, 19, 11, 1081-1084.

Nakagawa, T. and A. Nishida (1989), Southward magnetic field in the neutral sheet produced by wavy motions propagating in the dawn-dusk direction, *Geophysical Research Letters*, 16, 11, 1265-1268.

Ness, N. F. (1969), The geomagnetic tail, *Reviews of Geophysics*, 7, 1-2, 97-127.

Olson, W. P. (1974), A model of the distributed magnetospheric currents, *Journal of Geophysical Research*, 79, 25, 3731-3778.

Olson, W. P. and K. A. Pfitzer (1974), A quantitative model of the magnetospheric magnetic field, *Journal of Geophysical Research*, 79, 25, 3739-3748.

Olson, W. P. and K. A. Pfitzer (1977), *Magnetospheric magnetic modeling, annual scientific report*, McDonnell Douglas Astronautics Co., Huntington Beach, CA, USA, AD-A-037492.

Olson, W. P. and K. A. Pfitzer (1982), A dynamic model of the magnetospheric magnetic and electric fields for July 29, 1977, *Journal of Geophysical Research*, 87, A8, 5943-5948.

Parks, George K. (2004), *Physics of Space Plasmas An Introduction Second Edition*, Westview Press, Boulder, Colorado.

Pulkkinen, T. I., D. N. Baker, D. G. Mitchell, R. L. McPerron, C. Y. Huang, and L. A. Frank (1994), Thin current sheets in the magnetotail during substorms: CDAW 6 revisited, *Journal of Geophysical Research*, 99, A4, 5793-5803.

Pulkkinen, T. I., D. N. Baker, D. H. Fairfield, R. J. Pellinen, J. S. Murphree, R. D. Elphinstone, R. L. McPherron, J. F. Fennell, R. E. Lopez, and T. Nagai (1991), Modeling the growth phase of a substorm using the Tsyganenko model and multi-spacecraft observations: CDAW-9, *Geophysical Research Letters*, 18, 11, 1963-1966.

Pulkkinen, T. I., D. N. Baker, R. J. Pellinen, J. Büchner, H. E. J. Koskinen, R. E. Lopez, R. L. Dyson, and L. A. Frank (1992), Particle scattering and current sheet stability in the geomagnetic tail during the substorm growth phase, *Journal of Geophysical Research*, 97, A12, 19283-19297.

Roederer, J. G. (1969), Quantitative models of the magnetosphere, *Reviews of Geophysics*, 7, 1-2, 77-96.

Saito, M. H., L.-N. Hau, C.-C. Hung, Y.-T. Lai, and Y.-C. Chou (2010), Spatial profile of magnetic field in the near-Earth plasma sheet prior to depolarization by THEMIS: Feature of minimum B, *Geophysical Research Letters*, 37, L08106, doi:10.1029/2010GL042813.

Shen, C., X. Li, M. Dunlop, Z. X. Liu, A. Balogh, D. N. Baker, M. Hapgood, and X. Wang (2003), Analyses on the geometrical structure of magnetic field in the current sheet based on cluster measurements, *Journal of Geophysical Research*, 108, A5, 1168, doi:10.1029/2002JA009612.

Sitnov, M. I., N. A. Tsyganenko, A. Y. Ukhorskiy, and P. C. Brandt (2008), Dynamical data-based modeling of the storm-time geomagnetic field with enhanced spatial resolution, *Journal of Geophysical Research*, 113, A07218, doi:10.1029/2007JA013003.

Sofko, G. J., K. A. McWilliams, and C. R. Bryant (2013), The substorm current wedge and midnight sector partial ring current near substorm onset: A synthesis based on a magnetotail magnetic field geometry model, *Advances in Polar Science*, 24, 1, 32-41.

Speiser, T. W. (1965), Particle trajectories in model current sheets 1. Analytical solutions, *Journal of Geophysical Research*, 70, 17, 4219-4226.

Speiser, T. W. (1967), Particle trajectories in model current sheets 2. Applications to auroras using a geomagnetic tail model, *Journal of Geophysical Research*, 72, 15, 3919-3932.

Stern, D. (1967), Geomagnetic euler potentials, *Journal of Geophysical Research,* 72, 15, 3995-4005.

Sugiura, M. and D. J. Poros (1973), A magnetospheric field model incorporating the OGO 3 and 5 magnetic field observations, *Planetary and Space Science*, 21, 10, 1763-1773.

Taylor, H. E. and E. W. Hones Jr. (1965), Adiabatic motion of auroral particles in a model of the electric and magnetic fields surrounding the Earth, *Journal of Geophysical Research*, 70, 15, 3605-3628.

Thomas, G. R., D. M. Willis, and R. J. Pratt (1974), Simplified representations of the magnetopause boundary surface for a quantitative model of the magnetosphere, *Journal of Atmospheric and Terrestrial Physics*, 36, 6, 1037-1044.

Tóth, G., I. V. Sokolov, T. I. Gombosi, D. R. Chesney, C. R. Clauer, D. L. De Zeeuw, K. C. Hansen, K. J. Kane, W. B. Manchester, R. C. Oehmke, K. G. Powell, A. J. Ridley, I. I. Roussev, Q. F. Stout, O. Volberg, R. A. Wolf, S. Sazykin, A. Chang, B. Yu, and J. Kóta (2005), Space Weather Modeling Framework: A new tool for the space science community, *Journal of Geophysical Research*, 110, A12226, doi:10.1029/2005JA011126.

Tsyganenko, N. A. (1987), Global quantitative models of the geomagnetic field in the cislunar magnetosphere for different disturbance levels, *Planetary and Space Science*, 35, 11, 1347-1358.

Tsyganenko, N. A. (1989), A magnetospheric magnetic field model with a warped tail current sheet, *Planetary and Space Science*, 37, 1, 5-20.

Tsyganenko, N. A. (1995), Modeling the Earth's magnetospheric magnetic field confined within a realistic magnetopause, *Journal of Geophysical Research*, 100, A4, 5599-5612.

Tsyganenko, N. A. (1996), Effects of the solar wind conditions on the global magnetospheric configuration as deduced from data-based field models, *European Space Agency Special Publication*, ESA SP-389, 181-185.

Tsyganenko, N. Z. (2002a), A model of the near magnetosphere with a dawn-dusk asymmetry 1. Mathematical structure, *Journal of Geophysical Research*, 107, A8, 1179, doi:10.1029/2001JA000219.

Tsyganenko, N. A. (2002b), A model of the near magnetosphere with a dawn-dusk asymmetry 2. Parameterization and fitting to observations, *Journal of Geophysical Research*, 107, A8, 1176, doi:10.1029/2001JA000220.

Tsyganenko, N. A. and A. V. Vsmanov (1982), Determination of the magnetospheric current system parameters and development of experimental geomagnetic field models based on data from IMP and HEOS satellites, *Planetary and Space Science*, 30, 10, 985-998.

Tsyganenko, N. A. and M. I. Sitnov (2005), Modeling the dynamics of the inner magnetosphere during strong geomagnetic storms, *Journal of Geophysical Research*, 110, A03208, doi:10.1029/2007JA012260.

Tsyganenko, N. A. and M. I. Sitnov (2007), Magnetospheric configurations from a high-resolution data-based magnetic field model, *Journal of Geophysical Research*, 112, A06225, doi:10.1029/2007JA12260.

Tsyganenko, N. A., H. J. Singer, and J. C. Kasper (2003), Storm-time distortion of the inner magnetosphere: How severe can it get?, *Journal of Geophysical Research*, 108, A5, 1209, doi:10.1029/2002JA009808.

Tsyganenko, N. A. (1990), Quantitative models of the magnetospheric magnetic field: methods and results, *Space Science Reviews*, 54, 75-186.

Vasyliunas, V. M. (1981), Plasma dheet fynamics: effects on, and feedback from, the polar ionosphere, *Exploration of the Polar Upper Atmosphere*, 64, 229-244.

Voigt, G. H. (1972), A three dimensional analytical magnetospheric model with defined magnetopause, *Zeitschrift fuer Geophysik*, 38, 2, 319-346.

Walker, R. J. (1976), An evaluation of recent quantitative magnetospheric magnetic field models, *Reviews of Geophysics and Space Physics*, 14, 3, 411-427.

Wanliss, J. A., J. C. Samson, and E. Friedrich (2000), On the use of photometer data to map dynamics of the magnetotail current sheet during substorm growth phase, *Journal of Geophysical Research*, 105, A12, 27673-27684.

Watanabe, M. and G. J. Sofko (2008), Synthesis of various ionospheric convection patterns for IMF B_y-dominated periods: Split crescent cells, exchange cells, and theta aurora formation, *Journal of Geophysical Research*, 113, A09218, doi:10.1029/2007JA012868.

Watanabe, M. and G. J. Sofko (2009a), Role of interchange reconnection in convection at small interplanetary magnetic field clock angles and in transpolar arc motion, *Journal of Geophysical Research*, 114, A01209, doi:10.1029/2008JA013426.

Watanabe, M. and G. J. Sofko (2009b), Dayside four-sheet field-aligned current system during IMF B_y-dominated periods, *Journal of Geophysical Research*, 114, A03208, doi:10.1029/2008JA0136815.

Watanabe, M., G. J. Sofko, K. Kabin, R. Rankin, A. J. Ridley, C. R. Clauer, and T. I. Gombosi (2007), Origin of the interhemispheric potential mismatch of merging cells for interplanetary magnetic field B_y-dominated periods, *Journal of Geophysical Research*, 112, A10205, doi:10.1029/2006JA012179.

Watanabe, M., M. Pinnock, A. S. Rodger, N. Sato, H. Yamagishi, A. S. Yukimatu, R. A. Greenwald, J.-P. Villain, and M. R. Hairston (1998), Localized activation of the distant tail neutral line just prior to substorm onsets, *Journal of Geophysical Research*, 103, A8, 17651-17669.

Williams, D. J. and G. D. Mead (1965), Nightside magnetosphere configuration as obtained from trapped electrons at 1100 kilometers, *Journal of Geophysical Research*, 70, 13, 3017-3029.

Williams, D. J., D. G. Mitchell, C. Y. Huang, L. A. Frank, and C. T Russell (1990), Particle acceleration during substorm growth and onset, *Geophysical Research Letters*, 17, 5, 587-590.

Willis, D. M. and R. J. Pratt (1972), A quantitative model of the geomagnetic tail, *Journal of Atmospheric and Terrestrial Physics*, 34, 12, 1955-1976.

Zhou, X. and B. T. Tsurutani (2001), Interplanetary shock triggering of nightside geomagnetic activity: Substorms, pseudobreakups, and quiescent events, *Journal of Geophysical Research*, 106, A9, 18957-18967.

Appendices

A. Calculation of the Maximum Height of the Plasmasphere in the Z Direction

The equation for the field lines of Earth's dipole magnetic field is given by (Kivelson and Russell, page 166)

$$r = L\sin^2\theta \qquad \text{A.1}$$

where L represents how many Earth radii away from the Earth that the field line intersects with the equatorial plane. Using this result and the dipole field equations in relative Cartesian coordinates in the noon-midnight meridian plane (equations 3.3a – 3.3c), the maximum height of the plasmasphere in the z direction can be calculated.

The maximum height in the *z* direction of the dipole field lines in the plasmasphere will occur when the z-component of the magnetic field is zero because the field line will be completely in the *x*-direction. This is mathematically represented as

$$\frac{(X^2 - 2Z^2)B_{eq,s}}{(X^2 + Z^2)^{5/2}} = 0\,, \qquad \text{A.2a}$$

which simplifies to

$$X^2 - 2Z^2 = 0\,. \qquad \text{A.2b}$$

Solving for X gives the result of

$$X = \sqrt{2}Z\,. \tag{A.3}$$

The above equation gives a relation between X and Z when the z-component of the magnetic field is zero. However, this does not help when wanting to know the height of a specific field line. Thus, the equation for the field lines of the Earth's dipole magnetic field is needed. First, it needs to be converted to relative Cartesian coordinates. This is accomplished by first converting to Cartesian coordinates using the following relations:

$$r = \sqrt{x^2 + y^2 + z^2} \tag{A.4a}$$

and

$$\sin\theta = \frac{\sqrt{x^2 + y^2}}{\sqrt{x^2 + y^2 + z^2}}\,. \tag{A.4b}$$

Inserting these conversions into equation A.1 gives the field line formula in Cartesian coordinates as

$$\sqrt{x^2 + y^2 + z^2} = La\frac{x^2 + y^2}{x^2 + y^2 + z^2}\,, \tag{A.5a}$$

which simplifies to

$$(x^2 + y^2 + z^2)^{3/2} = La(x^2 + y^2)\,. \tag{A.5b}$$

Converting to relative Cartesian coordinates (equation 3.2) gives

$$(a^2X^2 + a^2Y^2 + a^2Z^2)^{3/2} = La(a^2X^2 + a^2Y^2)\,, \tag{A.6a}$$

which simplifies to

$$(X^2 + Y^2 + Z^2)^{3/2} = L(X^2 + Y^2)\,. \qquad \text{A.6b}$$

Now, the dipole field line equation can be found for the noon-midnight meridian plane by setting Y to zero giving:

$$(X^2 + Z^2)^{3/2} = LX^2 \qquad \text{A.7}$$

Inserting equation A.3 into the above equation gives

$$(2Z^2 + Z^2)^{3/2} = 2LZ^2\,, \qquad \text{A.8a}$$

which simplifies to

$$3^{3/2}Z^3 = 2LZ^2\,. \qquad \text{A.8b}$$

Solving for Z gives the final result as

$$Z = \frac{2L}{3^{3/2}}\,. \qquad \text{A.9}$$

Therefore, for any field line with a value L, the maximum height in the *z*-direction of the dipole field lines can be found by using the above equation. For a plasmasphere with the plasmapause being at around five Earth radii in the equatorial plane, the maximum height in the *z*-direction will be

$$Z = \frac{2 \times 5}{3^{3/2}} = 1.92 \approx 2\,. \qquad \text{A.10}$$

Thus, the maximum height in the z-direction will be approximately two Earth radii.

B. Curvature Vector for a Magnetic Field

Section 2.4.2 (equation 2.16) gives a definition of the curvature vector in terms of the radius of the osculating circle. A cartoon of the curvature vector for a magnetic field is shown below in Figure B.1.

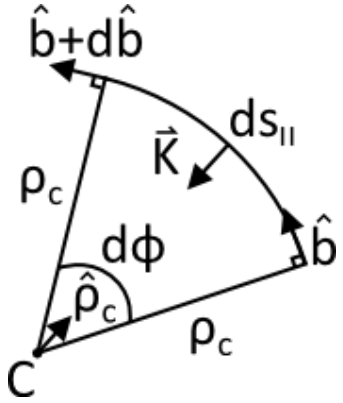

Figure B.1 Variables defined along a curvy magnetic field line including the radius of the osculating circle, curvature vector, and magnetic field vector.

The arc length $ds_{\|}$ can be found by using the formula for the definition of a radian, which is given as

$$ds_{\|} = r d\varphi \,. \tag{B.1}$$

Rearranging the equation for the radius of the osculating circle gives

$$r = \frac{ds_{\|}}{d\varphi} \,. \tag{B.2}$$

Inserting the above equation into equation 2.16 gives a new definition for the curvature vector as

$$\vec{K} = -\frac{d\varphi}{ds_{\|}}\hat{r} = \frac{d\varphi}{ds_{\|}}\hat{K} \,. \tag{B.3}$$

Now, this derivative needs to be defined specifically for a magnetic field.

The vector $d\hat{b}$ can be found using vector subtraction. This is shown below in Figure B.2.

Figure B.2 Direction of $d\hat{b}$ found through vector subtraction.

From comparing the two figures presented in this appendix, it can be concluded that the direction of $d\hat{b}$ is the same as the direction of the curvature vector. Therefore, the direction of the derivative of the magnetic field with respect to φ will also have the same direction as the curvature vector because $d\hat{b}$ will determine the direction of the derivative. Therefore, the definition of the curvature vector can be changed to

$$\vec{K} = \frac{d\varphi}{ds_{\parallel}}\frac{d\hat{b}}{d\varphi} = \frac{d\hat{b}}{ds_{\parallel}} . \qquad \text{B.4}$$

Now, this derivative needs to be defined specifically for a magnetic field.

The magnetic unit vector defined in Cartesian coordinates in two dimensions is given as

$$\hat{b} = \cos\varphi\,\hat{x} + \sin\varphi\,\hat{y} . \qquad \text{B.5}$$

Taking the derivative of the magnetic unit vector with respect to φ gives the result of

$$\frac{d\hat{b}}{d\varphi} = -\sin\varphi\,\hat{x} + \cos\varphi\,\hat{y} . \qquad \text{B.6}$$

Taking the dot product between these two vectors gives

$$\hat{b} \cdot \frac{d\hat{b}}{d\varphi} = (\cos\varphi\,\hat{x} + \sin\varphi\,\hat{y}) \cdot (-\sin\varphi\,\hat{x} + \cos\varphi\,\hat{y}) \qquad \text{B.7}$$

$$= -\cos\varphi\sin\varphi + \cos\varphi\sin\varphi = 0\ .$$

Therefore, these two unit vectors are perpendicular to each other. Since the curvature vector is in the same direction as the $d\hat{b}$ unit vector, the curvature is perpendicular to the magnetic field. In general, a vector can be defined as either parallel to the magnetic field ($\hat{b}$) or perpendicular to the magnetic field ($\vec{K}$). For example, the Del operator represents derivatives with respect to space. Therefore, it can be split into derivatives that are parallel to the magnetic field and derivatives that are perpendicular to the magnetic field, which is mathematically given as

$$\vec{\nabla} = \hat{b}\frac{d}{ds_{\parallel}} + \vec{K}\frac{d}{ds_{\perp}}\ . \qquad \text{B.8}$$

The first term in the above equation represents the derivative in space that is parallel to the magnetic field and the second term represents the derivative in space that is perpendicular to the magnetic field. As shown in equation B.4, the curvature vector is dependent on the derivative in space that is parallel to the magnetic field. Therefore, only the first term in equation B.8 is wanted. A simple dot product will isolate the first term in equation B.8 giving

$$\hat{b} \cdot \vec{\nabla} = \hat{b} \cdot \left(\hat{b}\frac{d}{ds_{\parallel}} + \vec{K}\frac{d}{ds_{\perp}}\right) = \frac{d}{ds_{\parallel}}\ . \qquad \text{B.9}$$

Thus, the final result for the curvature vector is simply given by

$$\vec{K} = \frac{d\hat{b}}{ds_{\parallel}} = \frac{d}{ds_{\parallel}}(\hat{b}) = (\hat{b} \cdot \vec{\nabla})\hat{b}\ . \qquad \text{B.10}$$

C. Proof of Relation between Curvature Vector and Magnetic Field Unit Vector

As was derived in the previous appendix, the curvature vector can be defined in terms of the Del operator and the magnetic field unit vector (equation B.10). The relation can be defined in an alternate way using the following vector identity (Huba, page 4):

$$\vec{\nabla}(\vec{A}\cdot\vec{B}) = \vec{A}\times(\vec{\nabla}\times\vec{B}) + \vec{B}\times(\vec{\nabla}\times\vec{A}) + (\vec{A}\cdot\vec{\nabla})\vec{B} + (\vec{B}\cdot\vec{\nabla})\vec{A}\,. \tag{C.1}$$

Inserting the magnetic field unit vector in place of both $\vec{A}$ and $\vec{B}$ in the above equation gives:

$$\vec{\nabla}(\hat{b}\cdot\hat{b}) = 2\hat{b}\times(\vec{\nabla}\times\hat{b}) + 2(\hat{b}\cdot\vec{\nabla})\hat{b}\,, \tag{C.2a}$$

which simplifies to

$$\frac{\vec{\nabla}(b^2)}{2} = \hat{b}\times(\vec{\nabla}\times\hat{b}) + (\hat{b}\cdot\vec{\nabla})\hat{b}\,. \tag{C.2b}$$

The magnitude of a unit vector is one. Therefore, the right hand side of the above equation is zero. After rearranging the above equation, the result is

$$(\hat{b}\cdot\vec{\nabla})\hat{b} = -\hat{b}\times(\vec{\nabla}\times\hat{b}) = (\vec{\nabla}\times\hat{b})\times\hat{b}\,. \tag{C.3}$$

Inserting the above equation into equation B.10 gives a new definition of the curvature vector as

$$\vec{K} = (\vec{\nabla}\times\hat{b})\times\hat{b}\,. \tag{C.4}$$

Now, if the cross product is taken between the magnetic field unit vector and the curvature vector, the result is

$$\hat{b} \times \vec{K} = \hat{b} \times \left((\vec{\nabla} \times \hat{b}) \times \hat{b} \right). \quad \text{C.5}$$

The cross product of the left hand side in the above equation can be expanded using the following vector identity (Huba, page 4):

$$\vec{A} \times (\vec{B} \times \vec{C}) = (\vec{A} \cdot \vec{C})\vec{B} - (\vec{A} \cdot \vec{B})\vec{C}. \quad \text{C.6}$$

This changes equation C.5 to

$$\hat{b} \times \vec{K} = (\hat{b} \cdot \hat{b})\vec{\nabla} \times \hat{b} - \left(\hat{b} \cdot (\vec{\nabla} \times \hat{b}) \right) \hat{b}. \quad \text{C.7}$$

The dot product in the second term in the above equation will be zero because the result of the cross product between the Del operator and the magnetic field unit vector will be perpendicular to the magnetic field unit vector. Therefore, the above equation simplifies to

$$\hat{b} \times \vec{K} = (b^2)\vec{\nabla} \times \hat{b}. \quad \text{C.8}$$

Once again, the magnitude of a unit vector is one. Therefore, the above equation simplifies to the final result of

$$\hat{b} \times \vec{K} = \vec{\nabla} \times \hat{b}. \quad \text{C.9}$$

D. Derivation of Relation between Energy and Pressure

In order to find the relation between energy and pressure, some basic physical relations need to be defined. From statistical mechanics, every degree of freedom a particle has is associated with thermal energy $E_{thermal}$ mathematically given as

$$E_{thermal} = \frac{1}{2} f k_b T \qquad \text{D.1}$$

where f is the degrees of freedom, k_B is Boltzmann's constant, and T is the temperature. Assuming a free particle, energy conservation gives the kinetic energy W of the particle equaling the thermal energy of the particle, which is mathematically given as

$$W = \frac{1}{2} f k_B T \, . \qquad \text{D.2}$$

This relation will prove useful later in the derivation.

Now that energy has been defined, it needs to be related to pressure. This is done by manipulating the ideal gas law, which is given as

$$p = n k_B T \, . \qquad \text{D.3}$$

Rearranging equation D.2 gives

$$k_B T = \frac{2W}{f} \, . \qquad \text{D.4}$$

The above equation can be inserted into equation D.3 to give a relation between pressure and kinetic energy as

$$p = \frac{2nW}{f} \, . \qquad \text{D.5}$$

Now, the relation between parallel and perpendicular energies and pressures can be found using the above formula.

In order to use equation I.5 to find the relation between the parallel energy and parallel pressure, the degrees of freedom needs to be assessed. Physically, there is only one degree of freedom that is associated with being parallel to the magnetic field vector. Therefore, equation D.5 defined specifically for the parallel energy and parallel pressure gives the result of

$$p_{\parallel} = 2nW_{\parallel} \, . \qquad \text{D.6}$$

The degrees of freedom also need to be found for the perpendicular case. In a three dimensional situation, if there is one degree of freedom that is parallel to the magnetic field vector, then there are two degrees of freedom that are perpendicular to the magnetic field. For example, if the magnetic field vector is purely in the z direction, then both the x and y directions would be perpendicular to the magnetic field vector. Therefore, equation D.5 defined specifically for the perpendicular energy and perpendicular pressure gives the result of

$$p_{\perp} = nW_{\perp} \, . \qquad \text{D.7}$$

E. Integrals and Derivatives for Relative Coordinates

E.1 Relative Cartesian Coordinates

Derivatives using Cartesian coordinates can be changed to derivatives using relative Cartesian coordinates by the following relations:

$$\frac{\delta}{\delta x} = \frac{\delta}{\delta(aX)} = \frac{1}{a}\frac{\delta}{\delta X} \, , \qquad \text{E.1a}$$

$$\frac{\delta}{\delta y} = \frac{\delta}{\delta(aY)} = \frac{1}{a}\frac{\delta}{\delta Y} \, , \qquad \text{E.1b}$$

and

$$\frac{\delta}{\delta z} = \frac{\delta}{\delta(aZ)} = \frac{1}{a}\frac{\delta}{\delta Z} \,. \qquad \text{E.1c}$$

Integrals using Cartesian coordinates can be changed to integrals using relative Cartesian coordinates by the following relations:

$$dx = d(aX) = adX \,, \qquad \text{E.2a}$$

$$dy = d(aY) = adY \,, \qquad \text{E.2b}$$

and

$$dz = d(aZ) = adZ \,. \qquad \text{E.2c}$$

E.2 Relative Spherical Coordinates

Integrals using spherical coordinates can be changed to integrals using relative spherical coordinates by the following relations:

$$dr = d(aR) = adR \,, \qquad \text{E.3a}$$

$$d\theta = d\Theta \,, \qquad \text{E.3b}$$

and

$$d\varphi = d\Phi \,. \qquad \text{E.3c}$$

E.3 Relative Cylindrical Coordinates

Integrals using cylindrical coordinates can be changed to integrals using relative cylindrical coordinates by the following relations:

$$ds = d(aS) = adS\,, \tag{E.4a}$$

$$d\gamma = d\Gamma\,, \tag{E.4b}$$

and

$$dx = d(aX) = adX\,. \tag{E.4c}$$

F. Derivation of Maxima for Second Term in X-Component of Stretched Magnetic Field

F.1 Derivation for Maximum in X direction

The maximum in the X direction can be found by taking the derivative of the second term in the x-component of the stretched magnetic field (equation 3.5) with respect to X and equating it to zero giving

$$\frac{1}{a}\frac{\delta}{\delta X}\left(-\frac{XZ}{X^2+Z^2}X_{extra}e^{-Z}\right) = \frac{\delta}{\delta X}\left(-\frac{XZ}{X^2+Z^2}X_{extra}e^{-Z}\right) = 0\,. \tag{F.1}$$

Taking the derivative with respect to X gives

$$-\frac{Z}{X_{max}^2+Z^2}X_{extra}e^{-Z}+\frac{2X_{max}^2Z}{(X_{max}^2+Z^2)^2}X_{extra}e^{-Z}=0\,. \tag{F.2}$$

Simplifying gives

$$-1+\frac{2X_{max}^2}{X_{max}^2+Z^2}=-X_{max}^2+Z^2+2X_{max}^2=0\,. \tag{F.3}$$

Solving for X_{max} gives the final result of

$$X_{max}=\pm Z\,. \tag{F.4}$$

F.2 Derivation for Maximum in Z direction

The maximum in the Z direction can be found by taking the derivative of the second term in the z-component of the stretched magnetic field (equation 3.8) with respect to Z and setting it to zero gives

$$\frac{1}{a}\frac{\delta}{\delta Z}\left(-\frac{XZ}{X^2+Z^2}X_{extra}e^{-Z}\right)=\frac{\delta}{\delta Z}\left(-\frac{XZ}{X^2+Z^2}X_{extra}e^{-Z}\right)=0\,. \tag{F.5}$$

Taking the derivative with respect to Z gives

$$-\frac{X}{X^2+Z_{max}^2}X_{extra}e^{-Z}+\frac{2XZ_{max}^2}{(X^2+Z_{max}^2)^2}X_{extra}e^{-Z}+\frac{XZ}{X^2+Z_{max}^2}X_{extra}e^{-Z}=0\,. \tag{F.6}$$

Simplifying gives

$$-1+\frac{2Z_{max}^2}{X^2+Z_{max}^2}+Z_{max}=0\,. \tag{F.7}$$

Rearranging gives the final result as

$$Z_{max}^3 + Z_{max}^2 + X^2 Z_{max} - X^2 = 0\,. \qquad \text{F.8}$$

G. Derivatives of the Stretched Magnetic Field

G.1 X-Component

The x-component of the stretched magnetic field is given in equation 3.20a. Taking the derivative with respect to X gives

$$\frac{\delta B_x}{\delta X} = -3ZB_{eq,s}\frac{\delta}{\delta X}\left(\frac{X}{(X^2+Y^2+Z^2)^{5/2}}e^{\frac{X}{\Delta X_D}}\right) - ZX_{extra}e^{-Z}\frac{\delta}{\delta X}\left(\frac{X}{X^2+Y^2+Z^2}\right). \qquad \text{G.1}$$

Computing the derivatives and simplifying gives

$$\frac{\delta B_x}{\delta X} = -\frac{3ZB_{eq.s}}{(X^2+Y^2+Z^2)^{5/2}}e^{\frac{X}{\Delta X_D}}\left(\frac{-4X^2+Y^2+Z^2}{X^2+Y^2+Z^2}+\frac{X}{\Delta X_D}\right) - \frac{Z(-X^2+Y^2+Z^2)}{(X^2+Y^2+Z^2)^2}X_{extra}e^{-Z}\,. \qquad \text{G.2}$$

Setting Y to zero gives the result for the noon-midnight meridian plane as

$$\frac{\delta B_x}{\delta X}(X,0,Z) = -\frac{3ZB_{eq,s}}{(X^2+Z^2)^{5/2}}e^{\frac{X}{\Delta X_D}}\left(\frac{-4X^2+Z^2}{X^2+Z^2}+\frac{X}{\Delta X_D}\right) - \frac{Z(-X^2+Z^2)}{(X^2+Z^2)^2}X_{extra}e^{-Z}. \qquad \text{G.3}$$

Taking the derivative of the x-component of the stretched magnetic field with respect to Y gives

$$\frac{\delta B_x}{\delta Y} = -3XZB_{eq,s}e^{\frac{X}{\Delta X_D}}\frac{\delta}{\delta Y}\left(\frac{1}{(X^2+Y^2+Z^2)^{5/2}}\right) - XZX_{extra}e^{-Z}\frac{\delta}{\delta Y}\left(\frac{1}{X^2+Y^2+Z^2}\right). \quad \text{G.4}$$

Computing the derivatives and simplifying gives

$$\frac{\delta B_x}{\delta Y} = \frac{15XYZB_{eq,s}}{(X^2+Y^2+Z^2)^{7/2}}e^{\frac{X}{\Delta X_D}} + \frac{2XYZ}{(X^2+Y^2+Z^2)^2}X_{extra}e^{-Z}. \quad \text{G.5}$$

Setting Y to zero gives the result for the noon-midnight meridian plane as

$$\frac{\delta B_x}{\delta Y}(X,0,Z) = 0. \quad \text{G.6}$$

Taking the derivative of the x-component of the stretched magnetic field with respect to Z gives

$$\frac{\delta B_x}{\delta Z} = -3XB_{eq,s}e^{\frac{X}{\Delta X_D}}\frac{\delta}{\delta Z}\left(\frac{Z}{(X^2+Y^2+Z^2)^{5/2}}\right) - XX_{extra}\frac{\delta}{\delta Z}\left(\frac{Ze^{-Z}}{X^2+Y^2+Z^2}\right). \quad \text{G.7}$$

Computing the derivatives and simplifying gives

$$\frac{\delta B_x}{\delta Z} = -\frac{3XB_{eq,s}(X^2+Y^2-4Z^2)}{(X^2+Y^2+Z^2)^{7/2}}e^{\frac{X}{\Delta X_D}} - \frac{X}{X^2+Y^2+Z^2}X_{extra}e^{-Z}\left(\frac{X^2+Y^2-Z^2}{X^2+Y^2+Z^2}-Z\right). \quad \text{G.8}$$

Setting Y to zero gives the result for the noon-midnight meridian plane as

$$\frac{\delta B_x}{\delta Z}(X,0,Z) = -\frac{3XB_{eq,s}(X^2-4Z^2)}{(X^2+Z^2)^{7/2}}e^{\frac{X}{\Delta X_D}} - \frac{X}{X^2+Z^2}X_{extra}e^{-Z}\left(\frac{X^2-Z^2}{X^2+Z^2}-Z\right). \quad \text{G.9}$$

G.2 Y-Component

The y-component of the stretched magnetic field is given in equation 3.20b. Taking the derivative with respect to X gives

$$\frac{\delta B_y}{\delta X} = -3YZB_{eq,s}\frac{\delta}{\delta X}\left(\frac{e^{\frac{X}{\Delta X_D}}}{(X^2+Y^2+Z^2)^{\frac{5}{2}}}\right) \tag{G.10}$$
$$+\frac{YZB_{eq,s}}{\Delta X_D}\frac{\delta}{\delta X}\left(\frac{X(3X^2+2Y^2+3Z^2)e^{\frac{X}{\Delta X_D}}}{(X^2+Z^2)^2(X^2+Y^2+Z^2)^{\frac{3}{2}}}\right)$$
$$-YZX_{extra}e^{-Z}\frac{\delta}{\delta X}\left(\frac{X^2}{(X^2+Z^2)(X^2+Y^2+Z^2)}\right)$$
$$+Z^3X_{extra}e^{-Z}\frac{\delta}{\delta X}\left(\frac{1}{(X^2+Z^2)^{3/2}}\tan^{-1}\left(\frac{Y}{\sqrt{X^2+Z^2}}\right)\right)$$

$$-\frac{2Z}{Z_{scale}}Z_{extra}e^{-\frac{Z^2}{Z_{scale}}}\mathrm{erf}(Y)\frac{\delta}{\delta X}\left(e^{-\frac{(X-X_{min})^2}{X_{scale}}}\right).$$

Computing the derivatives and simplifying gives

$$\frac{\delta B_y}{\delta X} = -\frac{3YZB_{eq,s}}{(X^2+Y^2+Z^2)^{5/2}}e^{\frac{X}{\Delta X_D}}\left(\frac{1}{\Delta X_D}-\frac{5X}{X^2+Y^2+Z^2}\right) \tag{G.11}$$
$$+\frac{YZB_{eq,s}}{\Delta X_D(X^2+Z^2)^2(X^2+Y^2+Z^2)^{3/2}}e^{\frac{X}{\Delta X_D}}\left(9X^2+2Y^2+3Z^2\right.$$
$$+\frac{X(3X^2+2Y^2+3Z^2)}{\Delta X_D}-\frac{4X^2(3X^2+2Y^2+3Z^2)}{X^2+Z^2}$$
$$\left.-\frac{3X^2(3X^2+2Y^2+3Z^2)}{X^2+Y^2+Z^2}\right)$$
$$-\frac{2XYZ}{(X^2+Z^2)(X^2+Y^2+Z^2)}X_{extra}e^{-Z}\left(1-\frac{X^2}{X^2+Z^2}-\frac{X^2}{X^2+Y^2+Z^2}\right)$$

$$-\frac{XZ^3}{(X^2+Z^2)^2}X_{extra}e^{-Z}\left(\frac{3}{\sqrt{X^2+Z^2}}\tan^{-1}\left(\frac{Y}{\sqrt{X^2+Z^2}}\right)+\frac{Y}{X^2+Y^2+Z^2}\right)$$
$$+\frac{4Z(X-X_{min})}{X_{scale}Z_{scale}}Z_{extra}e^{\left(-\frac{(X-X_{min})^2}{X_{scale}}-\frac{Z^2}{Z_{scale}}\right)}\mathrm{erf}(0)\,.$$

Setting Y to zero gives the result for the noon-midnight meridian plane as

$$\frac{\delta B_y}{\delta X}(X,0,Z)=0\,. \qquad \text{G.12}$$

Taking the derivative of the y-component with respect to Y gives

$$\frac{\delta B_y}{\delta Y}=-3ZB_{eq,s}e^{\frac{X}{\Delta X_D}}\frac{\delta}{\delta Y}\left(\frac{Y}{(X^2+Y^2+Z^2)^{5/2}}\right) \qquad \text{G.13}$$
$$+\frac{XZB_{eq,s}}{\Delta X_D(X^2+Z^2)^2}e^{\frac{X}{\Delta X_D}}\frac{\delta}{\delta Y}\left(\frac{Y(3X^2+2Y^2+3Z^2)}{(X^2+Y^2+Z^2)^{3/2}}\right)$$
$$-\frac{X^2Z}{X^2+Z^2}X_{extra}e^{-Z}\frac{\delta}{\delta Y}\left(\frac{Y}{X^2+Y^2+Z^2}\right)$$
$$+\frac{Z^3}{(X^2+Z^2)^{3/2}}X_{extra}e^{-Z}\frac{\delta}{\delta Y}\left(\tan^{-1}\left(\frac{Y}{\sqrt{X^2+Z^2}}\right)\right)$$
$$-\frac{2Z}{Z_{scale}}Z_{extra}e^{\left(-\frac{(X-X_{min})^2}{X_{scale}}-\frac{Z^2}{Z_{scale}}\right)}\frac{\delta}{\delta Y}\left(\mathrm{erf}(Y)\right)\,.$$

Calculating the derivatives and simplifying gives

$$\frac{\delta B_y}{\delta Y}=-\frac{3ZB_{eq,s}(X^2-4Y^2+Z^2)}{(X^2+Y^2+Z^2)^{5/2}}e^{\frac{X}{\Delta X_D}} \qquad \text{G.14}$$
$$+\frac{XZB_{eq,s}}{\Delta X_D(X^2+Z^2)^2(X^2+Y^2+Z^2)^{3/2}}e^{\frac{X}{\Delta X_D}}\left(3X^2+6Y^2+3Z^2\right.$$
$$\left.-\frac{3Y^2(3X^2+2Y^2+3Z^2)}{X^2+Y^2+Z^2}\right)-\frac{X^2Z(X^2-Y^2+Z^2)}{(X^2+Z^2)(X^2+Y^2+Z^2)^2}X_{extra}e^{-Z}$$
$$+\frac{Z^3}{(X^2+Z^2)(X^2+Y^2+Z^2)}X_{extra}e^{-Z}-\frac{2Z}{Z_{sca;e}}Z_{extra}e^{\left(-\frac{(X-X_{min})^2}{X_{scale}}-Y^2-\frac{Z^2}{Z_{scale}}\right)}\,.$$

The noon-midnight meridian plane solution is not needed for this thesis.

Taking the derivative of the y-component with respect to Z gives

$$\frac{\delta B_y}{\delta Z} = -3YB_{eq,s}e^{\frac{X}{\Delta X_D}}\frac{\delta}{\delta Z}\left(\frac{Z}{(X^2+Y^2+Z^2)^{5/2}}\right) + \frac{XYB_{eq,s}}{\Delta X_D}e^{\frac{X}{\Delta X_D}}\frac{\delta}{\delta Z}\left(\frac{Z(3X^2+2Y^2+3Z^2)}{(X^2+Z^2)^2(X^2+Y^2+Z^2)^{3/2}}\right) - X^2YX_{extra}\frac{\delta}{\delta Z}\left(\frac{Ze^{-Z}}{(X^2+Z^2)(X^2+Y^2+Z^2)}\right) + X_{extra}\frac{\delta}{\delta Z}\left(\frac{Z^3e^{-Z}}{(X^2+Z^2)^{3/2}}\tan^{-1}\left(\frac{Y}{\sqrt{X^2+Z^2}}\right)\right) - \frac{2}{Z_{scale}}Z_{extra}e^{-\frac{(X-X_{min})^2}{X_{scale}}}\text{erf}(Y)\frac{\delta}{\delta Z}\left(Ze^{-\frac{Z^2}{Z_{scale}}}\right). \quad \text{G.15}$$

Computing the derivatives and simplifying gives

$$\frac{\delta B_y}{\delta Z} = -\frac{3YB_{eq,s}(X^2+Y^2-4Z^2)}{(X^2+Y^2+Z^2)^{5/2}} + \frac{XYB_{eq,s}}{\Delta X_D(X^2+Z^2)^2(X^2+Y^2+Z^2)^{3/2}}e^{\frac{X}{\Delta X_D}}\left(3X^2+2Y^2+9Z^2 - \frac{4Z^2(3X^2+2Y^2+3Z^2)}{X^2+Z^2} - \frac{3Z^2(3X^2+2Y^2+3Z^2)}{X^2+Y^2+Z^2}\right) - \frac{X^2Y}{(X^2+Z^2)(X^2+Y^2+Z^2)}X_{extra}e^{-Z}\left(1-Z-\frac{2Z^2}{X^2+Z^2} - \frac{2Z^2}{X^2+Y^2+Z^2}\right) + \frac{Z^2}{(X^2+Z^2)^{3/2}}X_{extra}e^{-Z}\left(3\tan^{-1}\left(\frac{Y}{\sqrt{X^2+Z^2}}\right) - Z\tan^{-1}\left(\frac{Y}{\sqrt{X^2+Z^2}}\right) - \frac{3Z^2}{X^2+Z^2}\tan^{-1}\left(\frac{Y}{\sqrt{X^2+Z^2}}\right) - \frac{YZ^2}{\sqrt{X^2+Z^2}(X^2+Y^2+Z^2)}\right) \quad \text{G.16}$$

$$-\frac{2Z_{extra}}{Z_{scale}}\left(1-\frac{2Z^2}{Z_{scale}}\right)e^{\left(-\frac{(X-X_{min})^2}{X_{scale}}-\frac{Z^2}{Z_{scale}}\right)}\mathrm{erf}(Y)\,.$$

Setting Y to zero gives the result for the noon-midnight meridian plane as

$$\frac{\delta B_y}{\delta Z}(X,0,Z)=0\,. \qquad \text{G.17}$$

G.3 Z-Component

The z-component of the stretched magnetic field is given in equation 3.20c. Taking the derivative with respect to X gives

$$\frac{\delta B_z}{\delta X}=B_{eq,s}\frac{\delta}{\delta X}\left(\frac{(X^2+Y^2-2Z^2)}{(X^2+Y^2+Z^2)^{5/2}}e^{\frac{X}{\Delta X_D}}\right)-Z_{extra}e^{\left(-Y^2-\frac{Z^2}{Z_{scale}}\right)}\frac{\delta}{\delta X}\left(e^{-\frac{(X-X_{min})^2}{X_{scale}}}\right). \qquad \text{G.18}$$

Calculating the derivatives and simplifying gives

$$\frac{\delta B_z}{\delta X}=\frac{B_{eq,s}}{(X^2+Y^2+Z^2)^{5/2}}e^{\frac{X}{\Delta X_D}}\left(2X+\frac{X^2+Y^2-2Z^2}{\Delta X_D}-\frac{5X(X^2+Y^2-2Z^2)}{X^2+Y^2+Z^2}\right) \qquad \text{G.19}$$
$$+\frac{2(X-X_{min})}{X_{scale}}Z_{extra}e^{\left(-\frac{(X-X_{min})^2}{X_{scale}}-Y^2-\frac{Z^2}{Z_{scale}}\right)}.$$

Setting Y to zero gives the result for the noon-midnight meridian plane as

$$\frac{\delta B_z}{\delta X}(X,0,Z)=\frac{B_{eq,s}}{(X^2+Z^2)^{5/2}}e^{\frac{X}{\Delta X_D}}\left(\frac{3X(-X^2+4Z^2)}{X^2+Z^2}+\frac{X^2-2Z^2}{\Delta X_D}\right) \qquad \text{G.20}$$
$$+\frac{2(X-X_{min})}{X_{scale}}Z_{extra}e^{\left(-\frac{(X-X_{min})^2}{X_{scale}}-\frac{Z^2}{Z_{scale}}\right)}.$$

Taking the derivative of the z-component with respect to Y gives

$$\frac{\delta B_z}{\delta Y} = B_{eq,s} e^{\frac{X}{\Delta X_D}} \frac{\delta}{\delta Y}\left(\frac{X^2+Y^2-2Z^2}{(X^2+Y^2+Z^2)^{5/2}}\right) - Z_{extra} e^{\left(-\frac{(X-X_{min})^2}{X_{scale}} - \frac{Z^2}{Z_{scale}}\right)} \frac{\delta}{\delta Y}\left(e^{-Y^2}\right). \quad \text{G.21}$$

Calculating the derivatives and simplifying gives

$$\frac{\delta B_z}{\delta Y} = \frac{Y B_{eq,s}}{(X^2+Y^2+Z^2)^{5/2}} e^{\frac{X}{\Delta X_D}}\left(2 - \frac{5(X^2+Y^2-2Z^2)}{X^2+Y^2+Z^2}\right) + 2Y Z_{extra} e^{\left(-\frac{(X-X_{min})^2}{X_{scale}} - Y^2 - \frac{Z^2}{Z_{scale}}\right)}. \quad \text{G.22}$$

Setting Y to zero gives the result for the noon-midnight meridian plane as

$$\frac{\delta B_z}{\delta Y}(X,0,Z) = 0. \quad \text{G.23}$$

Taking the derivative of the z-component with respect to Z gives

$$\frac{\delta B_z}{\delta Z} = B_{eq,s} e^{\frac{X}{\Delta X_D}} \frac{\delta}{\delta Z}\left(\frac{X^2+Y^2-2Z^2}{(X^2+Y^2+Z^2)^{5/2}}\right) - Z_{extra} e^{\left(-\frac{(X-X_{min})^2}{X_{scale}} - Y^2\right)} \frac{\delta}{\delta Z}\left(e^{-\frac{Z^2}{Z_{scale}}}\right). \quad \text{G.24}$$

Calculating the derivatives and simplifying gives

$$\frac{\delta B_z}{\delta Z} = -\frac{3Z B_{eq,s}(3X^2+3Y^2-2Z^2)}{(X^2+Y^2+Z^2)^{7/2}} e^{\frac{X}{\Delta X_D}} + \frac{2Z}{Z_{scale}} Z_{extra} e^{\left(-\frac{(X-X_{min})^2}{X_{scale}} - Y^2 - \frac{Z^2}{Z_{scale}}\right)}. \quad \text{G.25}$$

Setting Y to zero gives the result for the noon-midnight meridian plane as

$$\frac{\delta B_z}{\delta Z}(X,0,Z) = -\frac{3Z B_{eq,s}(3X^2-2Z^2)}{(X^2+Z^2)^{7/2}} e^{\frac{X}{\Delta X_D}} + \frac{2Z}{Z_{scale}} Z_{extra} e^{\left(-\frac{(X-X_{min})^2}{X_{scale}} - \frac{Z^2}{Z_{scale}}\right)}. \quad \text{G.26}$$

H. Limits of the Stretched Magnetic Field at Infinity

H.1 Limit of Negative Infinity in the X direction

The x-component of the stretched magnetic field (equation 3.20a) can be rearranged to

$$B_x = -\frac{3ZB_{eq,s}}{\left(1+\frac{Y^2}{X^2}+\frac{Z^2}{X^2}\right)^{5/2}}\left(\frac{1}{X^4}\right)e^{\frac{X}{\Delta X_D}} - \frac{Z}{1+\frac{Y^2}{X^2}+\frac{Z^2}{X^2}}\left(\frac{1}{X}\right)X_{extra}e^{-Z}\,. \tag{H.1}$$

Taking the limit as X approaches negative infinity gives

$$\lim_{X\to-\infty} B_x = -\frac{3ZB_{eq,s}}{(1+0+0)^{5/2}}(0)(0) - \frac{Z}{1+0+0}(0)X_{extra}e^{-Z} = 0\,, \tag{H.2}$$

which is what is physically expected.

The y-component of the stretched magnetic field (equation 3.20b) can be rearranged to

$$\begin{aligned} B_y = &-\frac{3YZB_{eq,s}}{\left(1+\frac{Y^2}{X^2}+\frac{Z^2}{X^2}\right)^{5/2}}\left(\frac{1}{X^5}\right)e^{\frac{X}{\Delta X_D}} + \frac{YZ\left(3+\frac{2Y^2}{X^2}+\frac{3Z^2}{X^2}\right)B_{eq,s}}{\Delta X_D\left(1+\frac{Z^2}{X^2}\right)^2\left(1+\frac{Y^2}{X^2}+\frac{Z^2}{X^2}\right)^{3/2}}\left(\frac{1}{X^4}\right)e^{\Delta X_D} \\ &- \frac{YZ}{\left(1+\frac{Z^2}{X^2}\right)\left(1+\frac{Y^2}{X^2}+\frac{Z^2}{X^2}\right)}\left(\frac{1}{X^2}\right)X_{extra}e^{-Z} \\ &+ \frac{Z^3}{\left(1+\frac{Z^2}{X^2}\right)^{3/2}}\tan^{-1}\left(\frac{Y}{\sqrt{1+\frac{Z^2}{X^2}}}\left(\frac{1}{X}\right)\right)X_{extra}e^{-Z} \\ &- \frac{2Z}{Z_{scale}}Z_{extra}e^{\left(-X^2\left(\frac{\left(1-\frac{X_{min}}{X}\right)^2}{X_{scale}}+\frac{Z^2}{Z_{scale}X^2}\right)\right)}\mathrm{erf}(Y)\,. \end{aligned} \tag{H.3}$$

Taking the limit as X approaches negative infinity gives

$$\lim_{X\to-\infty} B_y = -\frac{3YZB_{eq,s}}{(1+0+0)^{5/2}}(0)(0) + \frac{YZ(3+0+0)B_{eq,s}}{\Delta X_D(1+0)^2(1+0+0)^{3/2}}(0)(0) - \frac{YZ}{(1+0)(1+0+0)}(0)X_{extra}e^{-Z} + \frac{Z^3}{(1+0)^{3/2}}(0)X_{extra}e^{-Z} - \frac{2Z}{Z_{scale}}Z_{extra}(0)\text{erf}(Y) = 0\,, \tag{H.4}$$

which is what is physically expected.

The z-component of the stretched magnetic field (equation 3.20c) can be rearranged to

$$B_z = \frac{\left(1+\frac{Y^2}{X^2}-\frac{2Z^2}{X^2}\right)B_{eq,s}}{\left(1+\frac{Y^2}{X^2}+\frac{Z^2}{X^2}\right)^{5/2}}\left(\frac{1}{X^3}\right)e^{\frac{X}{\Delta X_D}} - Z_{extra}e^{\left(-X^2\left(\frac{\left(1-\frac{X_{min}}{X}\right)^2}{X_{scale}}+\frac{Z^2}{Z_{scale}X^2}\right)\right)}\,. \tag{H.5}$$

Taking the limit as X approaches negative infinity gives

$$\lim_{X\to-\infty} B_z = \frac{(1+0-0)B_{eq,s}}{(1+0+0)^{5/2}}(0)(0) - Z_{extra}(0) = 0\,, \tag{H.6}$$

which is what is physically expected.

H.2 Limit of Positive/Negative Infinity in the Y Direction

The x-component of the stretched magnetic field (equation 3.20a) can be rearranged to

$$B_x = -\frac{3XZB_{eq,s}}{\left(\frac{X^2}{Y^2}+1+\frac{Z^2}{Y^2}\right)^{5/2}}\left(\frac{1}{Y^5}\right)e^{\frac{X}{\Delta X_D}} - \frac{XZ}{\frac{X^2}{Y^2}+1+\frac{Z^2}{Y^2}}\left(\frac{1}{Y^2}\right)X_{extra}e^{-Z}\,. \tag{H.7}$$

Taking the limit as Y approaches positive/negative infinity gives

$$\lim_{Y\to\pm\infty} B_x = -\frac{3XZB_{eq,s}}{(0+1+0)^{5/2}}(0)e^{\frac{X}{\Delta X_D}} - \frac{XZ}{0+1+0}(0)X_{extra}e^{-Z} = 0\,, \tag{H.8}$$

which is what is physically expected.

The y-component of the stretched magnetic field (equation 3.20b) can be rearranged to

$$\begin{aligned} B_y = &-\frac{3ZB_{eq,s}}{\left(\frac{X^2}{Y^2}+1+\frac{Z^2}{Y^2}\right)^{\frac{5}{2}}}\left(\frac{1}{Y^4}\right)e^{\frac{X}{\Delta X_D}} + \frac{XZ\left(\frac{3X^2}{Y^2}+2+\frac{3Z^2}{Y^2}\right)B_{eq,s}}{\Delta X_D(X^2+Z^2)^2\left(\frac{X^2}{Y^2}+1+\frac{Z^2}{Y^2}\right)^{\frac{3}{2}}}e^{\frac{X}{\Delta X_D}} \\ &-\frac{X^2Z}{(X^2+Z^2)\left(\frac{X^2}{Y^2}+1+\frac{Z^2}{Y^2}\right)}\left(\frac{1}{Y}\right)X_{extra}e^{-Z} \\ &+\frac{Z^3}{(X^2+Z^2)^{\frac{3}{2}}}\tan^{-1}\left(\frac{Y}{\sqrt{X^2+Z^2}}\right)X_{extra}e^{-Z} \\ &-\frac{2Z}{Z_{scale}}Z_{extra}e^{\left(-\frac{(X-X_{min})^2}{X_{scale}}-\frac{Z^2}{Z_{scale}}\right)}\mathrm{erf}(Y)\,. \end{aligned} \tag{H.9}$$

Taking the limit as Y approaches positive/negative infinity gives

$$\begin{aligned} \lim_{Y\to\pm\infty} B_y = &-\frac{3ZB_{eq,s}}{(0+1+0)^{5/2}}(0)e^{\frac{X}{\Delta X_D}} + \frac{XZ(0+2+0)B_{eq,s}}{\Delta X_D(X^2+Z^2)^2(0+1+0)^{3/2}}e^{\frac{X}{\Delta X_D}} \\ &-\frac{X^2Z}{(X^2+Z^2)(0+1+0)}(0)X_{extra}e^{-Z} \\ &+\frac{Z^3}{(X^2+Z^2)^{3/2}}\tan^{-1}(\pm\infty)X_{extra}e^{-Z} \end{aligned} \tag{H.10a}$$

$$-\frac{2Z}{Z_{scale}}Z_{extra}e^{\left(-\frac{(X-X_{min})^2}{X_{scale}}-\frac{Z^2}{Z_{scale}}\right)}\text{erf}(\pm\infty)\,,$$

which simplifies to

$$\lim_{Y\to\pm\infty}B_y=\frac{2XZB_{eq,s}}{\Delta X_D(X^2+Z^2)^2}e^{\frac{X}{\Delta X_D}}\pm\frac{\pi Z^3}{2(X^2+Z^2)^{3/2}}X_{extra}e^{-Z} \qquad \text{H.10b}$$
$$-\frac{\sqrt{\pi}Z}{Z_{scale}}Z_{extra}e^{\left(-\frac{(X-X_{min})^2}{X_{scale}}-\frac{Z^2}{Z_{scale}}\right)}.$$

The limit of the y-component in the positive or negative infinity direction in Y produces a finite result. This is not what is physically expected. However, if a limit is then taken at negative infinity in the X direction or positive infinity in the Z direction, a physical solution of zero is achieved. This can be easily shown by first rearranging equation H.10b to

$$\lim_{Y\to\pm\infty}B_y=\frac{2ZB_{eq,s}}{\Delta X_D\left(1+\frac{Z^2}{X^2}\right)^2}\left(\frac{1}{X^3}\right)e^{\frac{X}{\Delta X_D}}\pm\frac{\pi Z^3}{2\left(1+\frac{Z^2}{X^2}\right)^{3/2}}\left(\frac{1}{X^3}\right)X_{extra}e^{-Z} \qquad \text{H.11}$$
$$-\frac{\sqrt{\pi}Z}{Z_{scale}}Z_{extra}e^{\left(-X^2\left(\frac{(X-X_{min})^2}{X_{scale}}+\frac{Z^2}{Z_{scale}}\right)\right)}.$$

Taking the limit as X approaches negative infinity gives

$$\lim_{X\to-\infty}\lim_{Y\to\pm\infty}B_y=\frac{2ZB_{eq,s}}{\Delta X_D(1+0)^2}(0)(0)\pm\frac{\pi Z^3}{2(1+0)^{3/2}}(0)X_{extra}e^{-Z}-\frac{\sqrt{\pi}Z}{Z_{scale}}Z_{extra}(0) \qquad \text{H.12}$$
$$=0\,,$$

which is what is physically expected. In order to take the limit in the Z direction, equation H.10b can be rearranged to

$$\lim_{Y\to\pm\infty} B_y = \frac{2XB_{eq,s}}{\Delta X_D\left(\frac{X^2}{Z^2}+1\right)^2}\left(\frac{1}{Z^3}\right)e^{\frac{X}{\Delta X_D}} \pm \frac{\pi}{2\left(\frac{X^2}{Z^2}+1\right)^{3/2}}X_{extra}e^{-Z} - \frac{\sqrt{\pi}Z}{Z_{scale}}Z_{extra}e^{\left(-Z^2\left(\frac{(X-X_{min})^2}{X_{scale}Z^2}+\frac{1}{Z_{scale}}\right)\right)}. \quad \text{H.13}$$

Taking the limit as Z approaches positive infinity gives

$$\lim_{Z\to\infty}\lim_{Y\to\pm\infty} B_y = \frac{2XB_{eq,s}}{\Delta X_D(0+1)^2}(0)e^{\frac{X}{\Delta X_D}} \pm \frac{\pi}{2(0+1)^{3/2}}X_{extra}(0) - \frac{\sqrt{\pi}(\infty)}{Z_{scale}}Z_{extra}(0) = 0\,, \quad \text{H.14}$$

which is what is physically expected. The third term in equation H.14 is found to be zero by using L'Hôpital's rule, which is given as

$$\lim_{x\to c}\frac{f(x)}{g(x)} = \lim_{x\to c}\frac{f'(x)}{g'(x)}\,. \quad \text{H.15}$$

Applying this rule to the third term in equation H.14 gives

$$\lim_{Z\to\infty}\frac{Z}{e^{Z^2}} = \lim_{Z\to\infty}\frac{1}{2Ze^{Z^2}} = 0\,. \quad \text{H.16}$$

Therefore, the limit of the y-component of the stretched magnetic field in the positive/negative infinity produces a finite result, but if a limit is then taken in either the X or the Z direction, a physical result of zero is obtained.

The z-component of the stretched magnetic field (equation 3.20c) can be rearranged to

$$B_z = \frac{\left(\frac{X^2}{Y^2} + 1 - \frac{2Z^2}{Y^2}\right) B_{eq,s}}{\left(\frac{X^2}{Y^2} + 1 + \frac{Z^2}{Y^2}\right)^{5/2}} \left(\frac{1}{Y^3}\right) e^{\frac{X}{\Delta X_D}} - Z_{extra} e^{\left(-Y^2\left(\frac{(X-X_{min})^2}{X_{scale}Y^2} + 1 + \frac{Z^2}{Z_{scale}Y^2}\right)\right)} . \quad \text{H.17}$$

Taking the limit as Y approaches positive/negative infinity gives

$$\lim_{Y \to \pm\infty} B_z = \frac{(0 + 1 - 0) B_{eq,s}}{(0 + 1 + 0)^{5/2}} (0) e^{\frac{X}{\Delta X_D}} - Z_{extra}(0) = 0 , \quad \text{H.18}$$

which is what is physically expected.

H.3 Limit of Positive Infinity in the Z Direction

The x-component of the stretched magnetic field (equation 3.20a) can be rearranged to

$$B_x = -\frac{3XB_{eq,s}}{\left(\frac{X^2}{Z^2} + \frac{Y^2}{Z^2} + 1\right)^{5/2}} \left(\frac{1}{Z^4}\right) e^{\frac{X}{\Delta X_D}} - \frac{X}{\frac{X^2}{Z^2} + \frac{Y^2}{Z^2} + 1} \left(\frac{1}{Z}\right) X_{extra} e^{-Z} . \quad \text{H.19}$$

Taking the limit as Z approaches positive infinity gives

$$\lim_{Z \to \infty} B_x = -\frac{3XB_{eq,s}}{(0 + 0 + 1)^{5/2}} (0) e^{\frac{X}{\Delta X_D}} - \frac{X}{0 + 0 + 1} (0) X_{extra}(0) = 0 , \quad \text{H.20}$$

which is what is physically expected.

The y-component of the stretched magnetic field (equation 3.20b) can be rearranged to

$$B_y = -\frac{3YB_{eq,s}}{\left(\frac{X^2}{Z^2}+\frac{Y^2}{Z^2}+1\right)^{5/2}}\left(\frac{1}{Z^4}\right)e^{\frac{X}{\Delta X_D}} + \frac{XY\left(\frac{3X^2}{Z^2}+\frac{2Y^2}{Z^2}+3\right)B_{eq,s}}{\Delta X_D\left(\frac{X^2}{Z^2}+1\right)^2\left(\frac{X^2}{Z^2}+\frac{Y^2}{Z^2}+1\right)^{3/2}}\left(\frac{1}{Z^4}\right)e^{\frac{X}{\Delta X_D}}$$
$$-\frac{X^2Y}{\left(\frac{X^2}{Z^2}+1\right)\left(\frac{X^2}{Z^2}+\frac{Y^2}{Z^2}+1\right)}\left(\frac{1}{Z^3}\right)X_{extra}e^{-Z}$$
$$+\frac{1}{\left(\frac{X^2}{Z^2}+1\right)^{3/2}}\tan^{-1}\left(\frac{Y}{\sqrt{\frac{X^2}{Z^2}+1}}\left(\frac{1}{Z}\right)\right)X_{extra}e^{-Z}$$
$$-\frac{2Z}{Z_{scale}}Z_{extra}e^{\left(-Z^2\left(\frac{(X-X_{min})^2}{X_{scale}Z^2}+\frac{1}{Z_{scale}}\right)\right)}\mathrm{erf}(Y)\,. \qquad \text{H.21}$$

Taking the limit as Z approaches positive infinity gives

$$\lim_{Z\to\infty} B_y = -\frac{3YB_{eq,s}}{(0+0+1)^{\frac{5}{2}}}(0)e^{\frac{X}{\Delta X_D}} + \frac{XY(0+0+3)B_{eq,s}}{\Delta X_D(0+1)^2(0+0+1)^{\frac{3}{2}}}(0)e^{\frac{X}{\Delta X_D}} \qquad \text{H.22a}$$
$$-\frac{X^2Y}{(0+1)(0+0+1)}(0)X_{extra}(0) + \frac{1}{(0+1)^{\frac{3}{2}}}(0)X_{extra}(0)$$
$$-\frac{2(\infty)}{Z_{scale}}Z_{extra}(0)\mathrm{erf}(Y)\,,$$

which can be simplified to

$$\lim_{Z\to\infty} B_y = 0\,. \qquad \text{H.22b}$$

This is what is physically expected. The last term in equation H.22a is zero due to L'Hôpital's rule (see equation H.16).

The z-component of the stretched magnetic field (equation 3.20c) can be rearranged to

$$B_z = \frac{\left(\frac{X^2}{Z^2} + \frac{Y^2}{Z^2} - 2\right) B_{eq,s}}{\left(\frac{X^2}{Z^2} + \frac{X^2}{Z^2} + 1\right)^{5/2}} \left(\frac{1}{Z^3}\right) e^{\frac{X}{\Delta X_D}} - Z_{extra} e^{\left(-Z^2\left(\frac{(X-X_{min})^2}{X_{scale} Z^2} + \frac{Y^2}{Z^2} + \frac{1}{Z_{scale}}\right)\right)} . \quad \text{H.23}$$

Taking the limit as Z approaches positive infinity gives

$$\lim_{Z \to \infty} B_z = \frac{(0 + 0 - 2) B_{eq,s}}{(0 + 0 + 1)^{5/2}} (0) e^{\frac{X}{\Delta X_D}} - Z_{extra}(0) = 0 , \quad \text{H.24}$$

which is what is physically expected.

I. Conversion of Divergence of Stretched Magnetic Field Model

I.1 Conversion to Relative Cylindrical Coordinates

The conversions between relative Cartesian coordinates and relative cylindrical coordinates are given as

$$X = X , \quad \text{I.1a}$$

$$Y = S \sin \Gamma , \quad \text{I.1b}$$

$$Z = -S \cos \Gamma , \quad \text{I.1c}$$

and

$$S = \sqrt{Y^2 + Z^2} . \quad \text{I.1d}$$

Inserting these conversions into equation 5.38 and simplifying gives the result of

$$\vec{\nabla}\cdot\vec{B}_{model}(S,\Gamma,X)$$
$$= \frac{3S\cos\Gamma\, B_{eq,s}}{a(X^2+S^2)^{\frac{5}{2}}} e^{\frac{X}{\Delta X_D}}\left(\frac{-X^2+5S^2\sin^2\Gamma-S^2}{X^2+S^2}+\frac{X}{\Delta X_D}\right)$$
$$+\frac{S\cos\Gamma\, X_{extra}(-X^2+S^2)}{a(X^2+S^2)^2} e^{S\cos\Gamma}$$
$$-\frac{2S\cos\Gamma\, Z_{extra}}{aZ_{scale}} e^{\left(-\frac{(X-X_{min})^2}{X_{scale}}-S^2\sin^2\Gamma-\frac{S^2\cos^2\Gamma}{Z_{scale}}\right)}. \quad \text{I.2}$$

I.2 Conversion to Relative Spherical Coordinates

The conversions between relative Cartesian coordinates and relative spherical coordinates are given as:

$$X = R\sin\Theta\cos\Phi\,, \quad \text{I.3a}$$

$$Y = R\sin\Theta\sin\Phi\,, \quad \text{I.3b}$$

$$Z = R\cos\Theta\,, \quad \text{I.3c}$$

and

$$R = \sqrt{X^2+Y^2+Z^2}\,. \quad \text{I.3d}$$

Inserting these conversions into equation 5.38 and simplifying gives the result of

I.4

$$\vec{\nabla}\cdot\vec{B}_{model}(R,\Theta,\Phi)$$
$$= -\frac{3\cos\Theta\, B_{eq,s}}{aR^4} e^{\frac{R\sin\Theta\cos\Phi}{\Delta X_D}}\left(-1+5\sin^2\Theta\sin^2\Phi+\frac{R\sin\Theta\sin\Phi}{\Delta X_D}\right)$$
$$-\frac{\cos\Theta\, X_{extra}\left(1-2\sin^2\Theta\cos^2\Phi\right)}{aR} e^{-R\cos\Theta}$$

$$+\frac{2R\cos\Theta\, Z_{extra}}{aZ_{scale}}e^{\left(-\frac{(R\sin\Theta\cos\Phi-X_{min})^2}{X_{scale}}-R^2\sin^2\Theta\sin^2\Phi-\frac{R^2\cos^2\Theta}{Z_{scale}}\right)}.$$